

A Critical Assessment of the Finite Element Method for
Calculating Magnetic Fields in Electron Optics

A Thesis Submitted for the Degree
of
Doctor of Philosophy
in
The University of Aston in Birmingham
by
Khadija Basher Mohamed Tahir

November, 1985

Department of Mathematics and Physics

DEDICATION

TO MY HUSBAND AHMED
AND MY CHILDREN MEDIA

LAWEEN

SOLEEN

A CRITICAL ASSESSMENT OF THE FINITE ELEMENT METHOD
FOR CALCULATING MAGNETIC FIELDS IN ELECTRON OPTICS

A THESIS FOR THE DEGREE OF DOCTOR OF PHILOSOPHY

BY

KHADIJA BASHER MOHAMED TAHIR

SUMMARY

The present investigation is concerned with the determination of the magnetic field distribution in magnetic electron lenses by means of the finite element method. A critical comparison is made of the available finite element computer programs. Necessary modifications have been made in certain programs, useful comments and general data format were written for two recently developed programs.

Special attention has been paid to those factors that affect the efficiency of the finite element method in computer aided design of magnetic electron lenses. These include the correct choice of boundary conditions. Another important factor investigated is the influence of mesh layout for the subsequent finite element calculations.

By recomputing several examples of lenses found in the literature, discrepancies of up to 30% were reduced, resulting in excellent agreement with the associated experimental results, simply by rearranging the mesh layout in a more convenient way. Through a more systematic application of the finite element method, several misleading conclusions to be found in the literature were detected. Some of these conclusions arose from the finite element method itself, as previously mentioned. Other misleading conclusions were also discovered that were not due to the finite element method but to design errors in the lens itself.

A study has been made of the errors in lens design including the inadequate thickness of iron shrouds etc.

KEYWORDS

Finite element method, magnetic lenses, magnetic field distribution, computer aided design, single pole lens, double pole lens.

ACKNOWLEDGEMENTS

I am most grateful to Professor T. Mulvey, for his most valuable supervision and advice throughout this work.

I also would like to thank Mrs. B. Lencová of the Institute of Scientific Instruments, Czechosl. Acad. Sci. for providing her computer program and other valuable information.

I would like to record my appreciation of the useful discussions I had with Dr. S. Al-Hilly and Dr. H. Nasr at the early stages of this work.

My thanks are due to my colleagues, Mrs. I. Al-Nakeshli, Mrs. H.C. Yin and Mr. A.S. Alamir for their cooperation during our research work.

I also wish to thank all the University staff in the Physics Department, Computer Centre and Library for their help and kindness.

I am most grateful to the Gulf Organisation for Industrial Consulting of Doha; in particular to its Secretary General, Dr. A. Al-Moajil and the data bank staff for the use of their computing facilities at the early stages of this study.

My special thanks are due to Mr. S. Rahman and his wife Dr. S. Saied for all their help and kindness during my stay in Birmingham for this study.

I am grateful to my husband for his patience and encouragement throughout this work. Had it not been for his support this work would not have been done.

I also wish to thank Mrs. Maria Jones and Miss Janet Hadley for their help in typing this thesis.

Last but not least, I wish to record my deep affection and thanks for my parents who put me onto the path of learning.

CONTENTS

	<u>Page</u>
Summary	
Acknowledgements	
Contents	1
List of figures	5
List of tables	20
List of symbols	21
1. Introduction	23
1.1 The magnetic electron lens	23
1.2 Forms of magnetic electron lenses	24
1.2.1 Iron-free coils	24
1.2.2 Single polepiece lenses	24
1.2.3 Double polepiece lenses	26
1.2.4 Other lenses including superconducting and miniature lenses	27
1.3 Computer aided design of electron optical systems	27
1.3.1 Field calculations	28
1.3.1.1 The finite difference method (FDM)	28
1.3.1.2 The finite element method (FEM)	29
1.3.1.2.1 The integral finite element method	29
1.3.1.2.2 The differential finite element method	31
1.3.2 Electron trajectories	33
1.3.3 Imaging properties and aberrations	34
1.4 The computer programs used in this work for calculating magnetic field using the finite element method	36
1.4.1 Munro's Programs	36

	<u>Page</u>	
1.4.2	Nasr's Programs	38
1.4.3	Lencová's Program (AMAG)	39
1.5	Application of the finite element method for designing electron magnetic lenses	40
1.5.1	Aims of the present work	41
1.5.2	Difficulties in using finite element programs	41
1.5.3	Possible misleading conclusions in the design of magnetic lenses	41
1.5.4	Elimination of difficulties encountered in finite element programs	46
2.	Computer Programs for Calculating Magnetic Fields	47
2.1	The basic theory	47
2.1.1	The differential finite element method	53
2.1.1.1	Munro's programs	53
2.1.1.1.1	Munro's program for unsaturated magnetic lenses (M12)	53
2.1.1.1.2	Munro's program for saturated magnetic lenses (M13)	56
2.1.1.2	Nasr's programs	58
2.1.1.2.1	Nasr's improved vector potential program VPLIN for magnetic structures under linear conditions	59
2.1.1.2.2	Nasr's improved vector potential program under non-linear conditions (VPSAT)	63
2.1.1.3	Lencová's Program (AMAG)	66

	<u>Page</u>
2.2	69
Axial flux density distribution due to the current windings in the coil by Biot-Savart Law	
3.	72
Input data and output results of computer programs for calculating magnetic field distribution	
3.1	72
Introduction	
3.2	72
Data preparation	
3.2.1	74
Data preparation for Munro's programs	
3.2.1.1	74
Program M12	
3.2.1.2	75
Program M13	
3.2.2	75
Data preparation for Nasr's Programs	
3.2.2.1	75
Program VPLIN	
3.2.2.2	76
Program VPSAT	
3.2.3	76
Data preparation for Lencová's Program AMAG	
3.4	76
Comparison of the output results of computer programs used in calculation of magnetic field distribution	
3.4.1	77
Asymmetrical lens under linear condition	
3.4.2	77
Symmetrical lens under linear condition	
3.4.3	80
Asymmetrical lens under non-linear condition	
3.4.4	83
Symmetrical lens under non-linear condition	
3.5	86
Computer core store and time required for running each program	
3.6	87
Graphic outputs	
4.	97
Difficulties with the Finite Element Method	
4.1	97
General difficulties	
4.2	97
Factors Affecting the Accuracy of the FEM	

	<u>Page</u>	
4.2.1	The effect of mesh distribution	98
4.2.2	The effect of mesh numbers	110
4.2.3	The polepiece shape effect	112
4.2.4	The boundary effects	115
4.3	Faults and misinterpretations in lens design	121
4.3.1	External leakage due to insufficient magnetic circuit (shroud) thickness	121
4.3.2	Influence of coil size and position	132
4.4	Systematic investigation on possible lens designs	136
4.4.1	Important parameters of double pole lenses	136
4.4.2	Important parameters in single pole lenses	138
4.4.2.1	Comparison of B_{Fe} -H curves for single-pole lenses	143
4.4.3	Effect of current density in lens windings	148
5.	Conclusions and discussion	152
	References	162
	Appendices	A1
	1. Tables	A1
	2. Program Biot	A16
	3. Program VPLIN	A18
	4. Program VPSAT	A35
	5. Program AMAG	A65

LIST OF FIGURES

<u>Figure</u>	<u>Title</u>	<u>Page</u>
1.1	Single polepiece lens	24
1.2	Double polepiece lens: (a) symmetrical, (b) asymmetrical	26
1.3	Typical magnetisation curve for soft iron	37
2.1	Subdivision of quadrilaterals into finite elements (a) one possible way, (b) alternative way, (c) combination of (a) and (b) for better accuracy	49
2.2	Boundary loss in a magnetic lens	51
2.3	Triangular finite element. The vertices numbered counter clockwise, $A(z,r)$ is the vector potential assumed to vary linearly with z and r .	54
2.4	A node 0 in contact with twelve right-angled, overlapping, triangular finite elements	55
2.5	Rectangular single polepiece lens with mesh distributions in Z and R directions and two inner boundaries, ZLB and ZRB to be used in Nasr's programs for further runs	60
2.6	RUN: 2, mesh size 25 x 25, from $Z = -75$ MM to $Z = -25$ MM	62
2.7	RUN: 3, mesh size 25 x 25, from $Z = -25$ MM to $Z = 5$ MM	62
2.8	RUN: 4, mesh size 25 x 25, from $Z = 5$ MM to $Z = 100$ MM	62

<u>Figure</u>	<u>Title</u>	<u>Page</u>
2.9	Axial flux density distribution for rectangular single pole lens under linear conditions, excitation given 10000 A-t with thin coil (4 x 48 mm ²), (ooo) using Munro's (M12) program (25 x 25 meshes), (x x) using Nasr's (VPLIN) program (25 x 25 meshes) 4 runs	64
2.10	Relation between the relative permeability (μ_r) of magnetic material and the flux density B	65
2.11	Axial flux density $B_c(z)$ from a coil of rectangular cross-section at a point P on the axis	71
3.1	Rectangular single polepiece test lens with mesh distribution in Z and R directions and two inner boundaries, ZLB and ZRB, to be used in Nasr's programs. The regions for Runs 1, 2, 3 and 4 are also shown in the figure.	78
3.2	Comparison between the output results of axial flux density distribution (B_T) shown above of the single pole test lens shown in figure 3.1 with same mesh distribution and mesh number (25,25) M12, Vplin and AMAG give the same results, while Vplin with 4-runs gives a smoother curve but the same peak value. AMAG with the larger number of meshes (69 x 90) gives a much lower peak and smoother curve (since the number of meshes increased in both Z and R directions) this boundary condition give a boundary loss in excitation. This loss had been overcome by	79

<u>Figure</u>	<u>Title</u>	<u>Page</u>
	surrounding the open boundary by 5mm thick high permeability iron sheet	
3.3a	Quarter section of rectangular double pole test lens to be used as data for Munro and Nasr's programs showing boundary and mesh distribution in Z and R direction and two inner boundaries ZLB and ZRB to be used in Nasr's programs for further runs	81
3.3b	Quarter section of rectangular double pole test lens showing the boundary and mesh distribution in Z and R direction, to be used as data for Lencova's AMAG program	81
3.4	The axial flux density distribution of the rectangular double pole (test) lens under linear conditions using xxx (27 * 44) meshes for M12, VPLIN, AMAG and(●●●)using 67*90 meshes for AMAG. Note there is no difference in the output result of M12 VPLIN and AMAG when same number of meshes (27 * 44) is used while there is improvement in peak value when more meshes are used.	82
3.5	Axial flux density distribution of spherical single pole lens. Excitation of 10000 A-t. With coil of 598 mm ² . (Munro, Nasr and AMAG programs). Note the improvement at Z = -34 and Z = 0 with AMAG program with 66 x 90 meshes (i.e. the unusual shape of the flux distribution improved)	84

<u>Figure</u>	<u>Title</u>	<u>Page</u>
3.6	Axial flux density distribution of lens shown in figure (3.5). (1) Excitation of 10,000 A-t (2) Excitation of 100,000 A-t. (Munro, Nasr and AMAG programs)	85
3.7	The axial flux density distribution of the rectangular double polepiece test lens under non linear conditions (the magnetic circuit is very large to show the field distribution inside it). The lens excitation 10,000 A-t, with short solenoid (6 x 60 mm ²). Different programs are used	88
3.8	The axial flux density distribution of rectangular double polepiece test lens shown in (fig. 3.7) under non-linear conditions. Excitation of 100,000 A-t. With coil of (6 x 60 mm ²). Munro, Nasr and AMAG programs are used. Note the difference in the field behaviour inside the magnetic circuit, between M13, Vpsat and AMAG programs and the improvement with more meshes	89
3.9	Distribution of flux lines throughout the magnetic circuit of Al-Khashab's (1983) spherical single pole lens, recomputed with original magnetic circuit. Note the excessive external leakage. Lens excitation 10 ⁵ A-t. X Plotting error	90

<u>Figure</u>	<u>Title</u>	<u>Page</u>
3.10	Distribution of flux lines throughout the magnetic circuit of the lens shown in figure 3.9 but redesigned with a thicker magnetic circuit leading to reduced external leakage field.	90
3.11	AMAG IJ graphic output of Al-Khashab's (1983) spherical single pole lens recomputed with original magnetic circuit; the output shows the distribution of the materials in the mesh (0 = vacuum, 1 = iron, 3 = coil)	92
3.12	AMAG IJ graphic output for mapping iron flux density of the lens in figure 3.11. Note the iron flux density is very high at the magnetic circuit	93
3.13	AMAG IJ graphic output of the distribution of materials in the mesh for Al-Khashab's spherical single pole lens but redesigned with thicker magnetic circuit (shrouds) to reduce external leakage	94
3.14	AMAG IJ graphic output map of iron flux density of the lens in figure 3.13 (thicker shrouds). Note the higher flux density in the polepiece region. Note also how the iron flux density is reduced in the shrouds.	95
4.1	Munro's (1975) double pole lens (quarter section) with original mesh distribution. This figure shows that the meshes are concentrated at the polepiece gap region and	99

<u>Figure</u>	<u>Title</u>	<u>Page</u>
	insufficient number of meshes defining the polepiece profile and coil winding	
4.2	New mesh distribution for figure (4.1). The number of radial meshes defining the polepiece profile and coil winding increased keeping the original distribution of the other parts constant	99
4.3	Two axial field distribution for Munro's lens note the different in the B_m value when the mesh arrangement is slightly changed.	99
4.4	Cleaver's (1978) double pole lens (quarter section only) lens with high permeability shroud and permendure polepieces ($S_g = 10\text{mm}$, $D = 5\text{mm}$)	101
4.5	New mesh distribution for Cleaver's (1978) lens. It can be noticed that the mesh distribution is changing gradually, and special attention has been paid to define the polepiece profile	101
4.6	The axial field distribution for Cleaver's lens, shown in figure (4.4). (1) Cleaver's results (2) Results obtained according to the new mesh arrangement shown in Figure (4.5), (3) Computation results using steps method	103
4.7	the axial field distribution for Cleaver's lens (figure 4.4) under saturation condition ($\mathcal{O} \times 10^4 \text{ A-t}$) showing (1) Cleaver's results (2) results obtained in this study according to the mesh arrangement shown in Figure (4.5)	104

<u>Figure</u>	<u>Title</u>	<u>Page</u>
4.8	Recalculated axial field distribution for Christofides (1982) lens (Hermes II) at different excitations using optimised mesh distribution and the same number of mesh points	106
4.9	Axial field distribution for Christofides lens (figure 4.8). Comparison between experimentally determined, computed values of Christofides and recomputed values in this study	108
4.10a	Comparison between the total field B_T at the peak (1) experimental (2) calculated by Christofides (1982) (3) calculated by present author	109
4.10b	Comparison between (1) B_{Fe} at the peak experimental and (2) B_T -coil calculated by Christofides and (3) by the present author	109
4.11	Spherical single pole lens under linear condition. Excitation of 10 000 A.t. Coil of $26 \times 23 \text{ mm}^2$. (Munro, Nasr and AMAG programs) Note the improvement at $Z = -34$ and $Z = 0$ with AMAG program with 66×90 meshes, i.e. the unusual field shape	111
4.12	Variation of the peak axial flux density value with the reciprocal of the mesh number $1/n$. 1) in double pole lens using arbitrary mesh arrangement. 2) in single pole lens with convenient mesh arrangement. It can be noticed in the figure that in the first case	113

<u>Figure</u>	<u>Title</u>	<u>Page</u>
	when the mesh arrangement is not correct there is higher error and it is improving with larger number of meshes. While in second case the error is low and the change is small with increasing the number of meshes	
4.13	Symmetrical double polepiece of constant gap width ($S_g = 10\text{mm}$) with different polepiece taper angle θ . Permeability $\mu_r = 5 \times 10^4$ Exciting coil placed between the polepieces	114
4.14	Axial flux density distribution of lenses shown in figure (4.13). Lenses excited by a flat thin coil under linear condition. Same mesh distribution and number was used.	114
4.15	Simple asymmetrical test lens consisting of a coil and an iron ring. The figure shows an outer boundary, mesh point numbers and two inner boundaries for use with the VPLIN program	116
4.16	The total axial flux density distribution computed with (25x25) meshes using M12, VPLIN, AMAG. ■ The total axial field distribution using AMAG (51x96) meshes on the asymmetrical test lens shown in figure 4.15 $S/D_m = 0.033$. Using the different boundary setting. The first boundary setting at -60 and 75mm cause 8% loss in excitation when either 25, 25 or 51, 96 meshes are used. The second and correct boundary reduce the boundary loss in excitation to within 1%.	118

<u>Figure</u>	<u>Title</u>	<u>Page</u>
	The flux values near the boundary will be affected while the peak value will stand for either mesh number the same as it was for first boundary.	
4.17	The axial field distribution . 1.B(z) coil calculated with Biot Savart program with infinite boundary 2.B(z) coil calculated with AMAG program using finite boundary (80mm) 3.B(z) for coil + iron rings with AMAG program using finite boundary (80mm) and finally 4 B(z) for mini ring lens after surrounding the coil + iron rings with (A) 8mm thick iron casing and (B) (32, 28mm) thick iron casing.	119
4.18	Axial flux density distribution in mini ring lens shown in Figure 4.17 under non linear condition 1. (ooo) with thin iron casing 8mm 2. (ooo) with thicker iron casing (32 from side and 28 from up) to prevent leakage. Note: The difference between 1 and 2 is due to both boundary loss (7.4%) and leakage flux which have effect in the peak value equal to (8%) loss in 1. 3. (ooo) the axial flux density distribution of iron free coil computed as in previous cases 1 and 2 with 71*73 meshes using AMAG program. 4 (ooo) the axial flux density distribution of iron free coil calculated by Biot Savart law, the difference between 3 and 4 due to boundary loss is (14%) in 3.	120

<u>Figure</u>	<u>Title</u>	<u>Page</u>
4.19	<p>Recalculation axial field distributions of the Al-Khashab's (1983) lens. i.e. Spherical single pole lens with coil surrounding the polepiece.</p> <p>$D_2/D_1 = 1.88, S/D_m = 0.347,$</p> <p>$S = 26\text{mm}.$ Note: Appreciable external leakage occurs at excitations higher than 16445 A-t, i.e. at B_{pf} higher than 1.5 Tesla.</p>	122
4.20	<p>Variation of axial field distribution with excitation for spherical single pole lens shown above, with larger iron circuit than in figure 4.19. The external leakage occur at excitation higher than 200,000 A-t. i.e. pole face flux density (B_{pf}) higher than 4 Tesla.</p>	124
4.21	<p>Axial flux density distribution for spherical single pole lens shown above at different lens excitation using $(26 \times 23\text{mm}^2)$ coil surrounding the polepiece lens. (-24 to 2mm) after making the iron circuit large enough to prevent external leakage</p>	125
4.22	<p>The total axial flux density distribution and the B_{Fe} values (B_T, B_{Fe}) at the pole face tip of spherical single pole lens shown in Figure 4.19 at different lens excitation. (Calculated for four different thicknesses (1-4) of the lens shell).</p> <p><u>Note</u> The value of both B_T and B_{Fe} at the pole face increase with increasing shell thickness.</p>	126

<u>Figure</u>	<u>Title</u>	<u>Page</u>
4.23	Recalculation of the variation of axial field distribution with lens excitation using the original magnetic circuit (A) Christofides' (1982) zero bore lens Hermes). The external flux leakage is indicated at B_{pf} higher than 1.5 Tesla	128
4.24	Variation of axial field distribution with lens excitation. Same lens of figure (4.23) recomputed with thicker magnetic circuit (B) designed to reduce external leakage	129
4.25	Variation of B_T and B_{Fe} at pole face with lens excitation for (A) original magnetic circuit; (B) thicker magnetic circuit see Figure (4.23) and Figure (4.24). B coil at pf is shown for reference.	130
4.26	Axial flux density distribution of the rectangular double pole (test) lens shown above after surrounding the boundary with (5mm) high permeability iron sheet to overcome boundary loss in excitation (ooo for long solenoid (b) and xxx for short solenoid (a)). Note the external flux leakage which is larger in case of coil (b).	131
4.27a	Axial flux density distribution in rectangular double pole lens at different lens excitations with thin coil ($D_2/D_1 = 31$, $S/D_m = 0.094$) the coil position -3 to 3mm. The shrouds are very large (70mm, 50mm), i.e. there is no leakage up to (9) Tesla at the peak	133

<u>Figure</u>	<u>Title</u>	<u>Page</u>
4.27b	Axial flux density distribution for double pole test lens shown using sufficient shrouds (70,50mm) (i.e. no leakage) with solenoid ($D_2/D_1 = 1.107$, $S/D_m = 0.508$) at different lens excitations	134
4.28a	Rectangular double pole test lens with thin magnetic circuit (A) and thick magnetic circuit (B). The lens exciting coils a and b have the same cross section.	135
4.28b	Variation of B_{Fe} at pole face with magnetic field strength (H) of double polepiece test lens shown above. 1 (xxx) B_{Fe} value at pf when the lens excited by coil (a) (short solenoid) using magnetic circuit thickness 15 mm. (A) 2. (●●●) B_{Fe} values when the lens excited by coil (b) using previous magnetic circuit (A). 3 (ooo) B_{Fe} values when the lens is excited with coil (b) using thicker magnetic circuit (B). Note: the change of B_{Fe} value for coil (b) when the magnetic circuit is thicker in 3	135
4.29	Recalculation of the axial flux density distribution for Al-Khashab(1983) spherical single pole lens at different lens excitations using coil of $S/D_m = 0.019$, $D_2/D_1 = 12.89$, $S = 1\text{mm}$. Note the external leakage problems appear at 13×10^4 A-t, i.e. at Bpf 6.35 Tesla	137

<u>Figure</u>	<u>Title</u>	<u>Page</u>
4.30	(1) Variation of the magnetization of the polepiece tip and (2) the variation of the half-width of rectangular double polepiece test lens as a function of magnetic field strength (H) excited: with b (●—●—●) long solenoid coil; a (○—○—○) short solenoid coil	139
4.31	For coil position a - d as a function B_{Fe} at the pole face p_f and the axial field half width (d_h) with coil positions lens excitation in a spherical single pole lens. Full diagram shown in figure (4.21)	141
4.32	(1) Variation of the magnetization of polepiece tip and (2) the variation of the half-width of spherical single pole lens as a function of the lens excitation by thin coil ($D_2/D_1 = 9.8, S/D_m = 0.0185$) a (○—○—○) thin coil position (-0.5 to 0.5mm), b (●—●—●) thin coil position (0.5 to 1.5mm), c (x—x—x) thick coil surrounding the polepiece	142
4.33	Variation of (1) B_{Fe} values at p_f and (2) half width with lens excitation of spherical single pole lens excited with different S/D_m coils placed at same distance from the pole face	144
4.34	Axial flux density distribution for spherical single pole lens at different lens excitation with coil ($D_2/D_1 = 1.88, S/D_m = 0.347$). The	146

<u>Figure</u>	<u>Title</u>	<u>Page</u>
	lens is improved by very large shrouds and shielding from the open side (6 mm), $\frac{D_{in}}{D_{out}} = 0$ (Vanishingly small bore).	
4.35	Variation of the B_{Fe} value at pf tip, as function of field strength (H A/m), with coil size and position, for the redesigned spherical single polepiece lens, shown in figure (4.34)	147
4.36	Comparison between the axial flux density distribution (keeping the current density constant) of rectangular double pole piece lens shown in figure (4.27a): excited with (1) short solenoid placed in the gap between the two polepieces (2) combination of short solenoid placed in the gap and two coils (of total area = 360mm^2) as shown above. Note the cross-section of lens. (2) is half of lens (1). There is no significant difference in peak flux value or the half width between two cases	149
4.37	Comparison between the axial flux density distribution (keeping the current density constant) of the spherical single pole lens shown in figure (4.34) excited with (1) a coil ($D_2/D_1 = 24$, $S/D_m = 0.26$, $S = 13$ mm placed outside the pole face (solid line) (2) a combination of a thick coil surrounding the polepiece and a thin coil of the same cross section placed outside the	150

<u>Figure</u>	<u>Title</u>	<u>Page</u>
	polepiece (dotted line). Note the cross-section of lens (2) is half that of lens (1). Case 2 has a slightly lower peak and lower half-width than case 1	
5.1	Contribution (B_{coil}) of the exciting coil and of the iron (B_{Fe}) to the total axial flux density B_T in the single polepiece lens shown in Fig. 2.5.	160
	<u>Note</u> The positive and negative parts of the B_{Fe} curve balance within 1% indicating low computational error.	
5.2	The variation of Cs with the current density for four different double pole lenses at 2000 KV at $Z = 0$ mode, log/log scale. Lens 1 as shown above (quarter section) is a rectangular double pole test lens computed with $S_g/D = \infty$ and $S_g/D = 2$ (dashed line). Lens 2 is similar to lens 1, but with smaller axial pole piece radius with $S_g/D = \infty$. Lens 3 is a spherical double pole lens $S_g/D = 2$.	161

LIST OF TABLES

<u>Table</u>	<u>Title</u>	<u>Page</u>
1.1	Magnetisation curve for soft iron (Munro 1971)	37
2.1	A typical relation between the relative permeability and the flux density of a magnetic material (Nasr 1981)	65
3.1	General format of the data for program M12	A2
3.2	General format of the data for program M13	A4
3.3	General format of the data for program VPLIN	A7
3.4	General format of the data for program VPSAT	A10
3.5	General format of the data for program AMAG	A13
3.6	The computer core store and time required for compilation and running each program and the number of iteration required under saturation condition	87

LIST OF SYMBOLS

A	Magnetic vector potential
A_{θ}	Azimatal component of magnetic vector potential
Area	Area of triangle
A-t	Ampere turns
B	Magnetic flux density
B_C	B (coil) axial flux density at any point due to the coil windings
B_{Fe}	B (iron) axial flux density at any point due to the magnetization of the iron
B_r	Radial component of magnetic flux density
B_z	Axial component of magnetic flux density
$B_T, B(z)$	Total axial flux density $B_T = B_C + B_{Fe}$
B_{pf}	The axial magnetic flux density at the pole face
B_{max}	Peak value of the axial magnetic flux density
C_C	Chromatic aberration coefficient
C_S	Spherical aberration coefficient
Det	Determinant in triangle = 2 x Area
D_{in}, D	Inner diameter of the lens bore
D_m	Mean diameter of the coil windings $D_m = (D_1 + D_2)/2$
D_{out}	Outer diameter of the lens polepiece
D_1	Inner diameter of the coil
D_2	Outer diameter of the coil
d_h	Half-width of the axial magnetic flux density distribution
e	Electron charge
E	Energy functional
H	Magnetic strength (A/m)
H_C	Magnetic strength due to electric currents

H_m	Magnetic strength due to magnetic material
m	Mass of the electron
M	Magnetization of magnetic material
M_o	Magnification $M_o = \frac{\alpha_o}{\alpha_i}$ where α_o and α_i are the convergence angles of the trajectory at Z_o and Z_i
NI	Excitation of the lens (A-t)
$NI/vr^{1/2}$	Excitation parameter
L	Lens outer diameter (mm)
R	Polepiece axial radius
\ddot{r}	Radial acceleration
s, S	Coil width
S_g	Gap width of the double pole
V_r	Relativistically corrected accelerating voltage $V_r = V (1+0.978 \times 10^{-6}V)$ where V is the applied accelerating voltage of electrons
W	Stored magnetic energy per unit volume
\ddot{z}	Axial acceleration
η	Electron charge to mass ratio e/m
μ	Permeability of the magnetic material $\mu = \mu_o \mu_r$
μ_r	Relative permeability of the magnetic material
μ_d	The differential permeability $\mu_d = \frac{\partial B}{\partial H} / \mu_o$
μ_o	Permeability of free space ($4 \pi \times 10^{-7}$ Henry/m)
χ	Magnetic susceptibility
ϕ	Magnetic flux
σ	Current density in the lens coil
$\dot{\theta}$	Angular velocity

CHAPTER ONE

INTRODUCTION

1.1 The Magnetic Electron Lens

Busch (1926) was the first to explain the theory of focusing electrons by means of rotationally symmetric magnetic fields in a way analogous to the focusing of light beams by glass lenses. A magnetic electron lens can be defined as an axially symmetric magnetic field which can be described by its axial flux density $B(z)$. The simplest lens is an axially symmetric iron-free coil but most magnetic lenses usually consist of double polepiece lenses or more recently a single polepiece. The arrangement of lenses can be either "symmetrical" or "asymmetrical" depending on the design of their respective magnetic circuits. A lens is symmetrical when a plane of symmetry $Z=0$ exists so that $B(z) = B(-z)$. This is achieved when both polepiece bores have the same diameter. When the two bore diameters D_{in1} and D_{in2} differ from each other, the lenses are asymmetric. One common reason for constructing asymmetric lenses is the need for providing access for introducing the specimen. Thus the bore is made larger for this reason. However, the specimen may also be introduced sideways through the polepiece gap. There is no need, in this case, to make one bore wider than the other.

Distinction is also made between "saturated" and "unsaturated" lenses. A lens is considered unsaturated if the axial flux density distribution B_z created by a coil with I ampere-turns is proportional to I .

1.2 Forms of Magnetic Electron Lenses

Many kinds of magnetic lenses have been devised and investigated by different research workers. The most commonly known are:

1.2.1 Iron-free Coils

The simplest form of an iron-free magnetic lens is a solenoid consisting of either a wire or tape wound around a non-magnetic core. Basset and Mulvey (1969) have shown that this kind of lens has an appreciably lower spherical aberration. The well-known Biot-Savart Law is used in calculating the axial flux density for these lenses.

Marai (1977) surveyed the iron-free lenses and showed that optimum designs for them do in fact exist.

1.2.2 Single Polepiece Lenses

Figure 1.1 shows a single polepiece lens converging a beam of

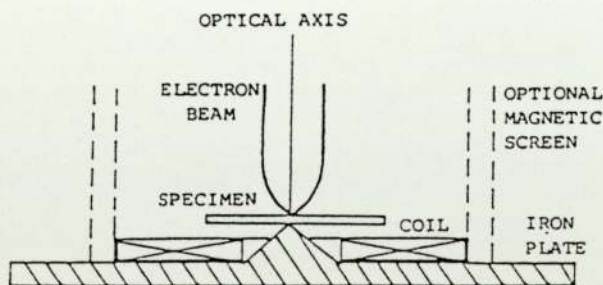


Fig. 1.1 Single polepiece lens

electrons onto a solid specimen. The lens consists, essentially, of a narrow flat coil winding placed over a single polepiece. The axial flux density distribution is asymmetrical and is created outside the

lens structure. The peak position of the field is located a few millimeters from the poleface (snout). This provides more space for manipulating the specimen as well as reducing the effects, of any imperfections in the iron circuit or the coil, on the lens properties.

Due to the highly asymmetrical field distribution characteristics, the focal properties of single polepiece lenses differ appreciably from those of conventional double polepiece lenses. The increased axial flux density at the tip of the polepiece as well as the reduced half-width of the field distribution lead to lower aberrations.

A single polepiece lens may be used as an objective lens in TEM and STEM (Mulvey, 1974). The asymmetrical field distribution gives the possibility of using it in two different modes of operation. In a projector lens, Marai and Mulvey (1976) have shown that the lens has a lower distortion coefficient by a factor of about 2.5 when the polepiece of the lens is facing the incoming electron beam (preferred direction), than when it is used facing the screen (non-preferred direction). Al Hilly (1982), has demonstrated the advantages of this in the correction of distortions in the electron microscope. Hill and Smith (1982) used the single pole lens as a scanning electron microscopy objective.

Mulvey (1982) has reviewed the present stage of iron polepiece lenses development with particular emphasis on improved imaging achieved in transmission electron microscopes when using a single polepiece lens as projector lens plus another single polepiece lens as spiral distortion corrector.

1.2.3 Double Polepiece Lenses

Double polepiece lenses are more commonly used than single polepiece lenses. Figure 1.2 illustrates a typical configuration of double polepiece systems which can be either symmetric or asymmetric.

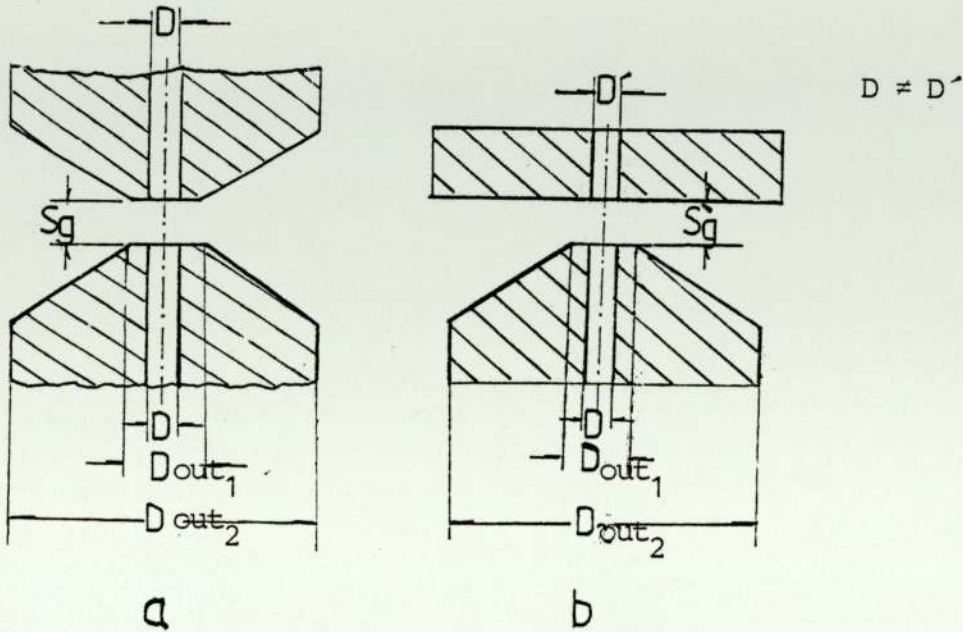


Fig. 1.2 Double polepiece lens (a) Symmetrical (b) Asymmetrical

In the symmetrical system, two identical pairs of truncated cones are separated by a gap of width S_g which allows the electron beam to pass. In the asymmetric system one of the truncated cones is replaced by a flat extended polepiece, which is usually part of one of the lens casing flanges. The magnetic field of a double polepiece is non-uniform near the lens axis, where the axial hole is located. This gives rise to the refractive action of the lens. The ratio of gap width to inner diameter (S_g/D) determines the lens properties.

Mulvey and Wallington (1969) have published a comprehensive review of double polepiece lenses. The unique properties of asymmetrical double polepiece lenses were discussed by Yanaka and Watanabe (1966).

1.2.4 Other Lenses including Superconducting and Miniature Lenses

Recent advances in electron microscopy have led to the introduction of unconventional and miniaturised lenses. The most interesting of these are the superconducting lenses the origin of which goes back to the late fifties when the discovery of high field superconductors stimulated research in their main attractions which are electromagnetic stability, compact construction and high magnetic field gradients (Lefranc, Knapek and Dietrich, 1982).

Miniature lenses were developed at the University of Aston in Birmingham by Mulvey and his collaborators. One form of these is the highly compact coil with forced cooling (Mulvey and Newman, 1972), which seems to be on the brink of being introduced into commercial electron optical instrument design on a larger scale (Riecke, 1982). Another, 'rotation-free', magnetic electron lens doublet of high magnification is described by Juma and Mulvey (1978). This lens is some two orders of magnitude smaller in volume and weight than those of a comparable conventional lens unit.

1.3 Computer Aided Design of Electron Optical Systems

Digital computers are extensively used in designing electron optical systems. Computer utilisation is particularly needed in the following three steps. (i) Field Calculations, (ii) determination of electron trajectories and (iii) determination of imaging properties and aberrations. In this study emphasis will be made in the field calculations.

1.3.1 Field Calculations

A number of methods are available for computing the electric or magnetic fields from given initial or boundary conditions. The most common of these methods, used in computer aided design, are the finite difference and the finite element methods. These methods are based on the well known mathematical technique of finding approximate numerical solutions for analytically unsolvable differential equations. This involves replacement of a continuous partial differential equation by a system of ordinary linear equations which are solved by standard mathematical techniques.

1.3.1.1 The Finite Difference Method (FDM)

In the finite difference method (FDM) the entire region of the problem is covered by a discrete mesh network.

Mesh formulae in the finite difference method can be derived using either a Taylor series or the integral method, both of which are well explained in the mathematical literature ((Ames, 1969), (Forsythe et al., 1960) and (Varga, 1962)).

Kasper and Lenz (1980), have suggested that better accuracies can be achieved for a given number of meshes using the finite difference method, especially for axial field distributions than is possible with the differential finite element method.

There is no suitable general program for calculating magnetic and electric fields by the finite difference method. This makes a comparison between the finite difference and other numerical methods

such as the finite element method very difficult. Denegri et al. (1976) developed a finite difference method that employs a similar mesh distribution to that of differential finite element method, but the method has not yet been fully implemented.

1.3.1.2 The Finite Element Method (FEM)

The finite difference method becomes very complicated when the material coefficients are discontinuous e.g. at the interface conditions like those for the magnetic field at surface of yokes with finite permeability. For the computation of such fields, the finite element method (FEM) is more convenient. The FEM uses triangular mesh grids instead of rectangular ones used in FDM. The FEM was applied, originally, in structural and electrical engineering (Zienkiewicz and Cheung, 1965).

1.3.1.2.1 The Integral Finite Element Method

Newman et al. (1972) applied the finite element method in its integral form to the computation of magnetic field strength. Division into finite elements is carried out for the magnetic material only. The magnetisation is assumed constant over each element. The field strength (H_C) due to the current in the windings is found directly from Biot-Savart Law,

$$H_C = \frac{1}{4} \frac{\int \underline{J} \times \underline{r}}{r^3} dv \quad (1.1)$$

\underline{J} is the current density in the coil windings and v is the volume of the coil windings.

The field (H_m) due to magnetisation in the iron elements is given by,

$$H_m = \frac{1}{4\pi} \text{grad} \int \frac{M \cdot r}{r^3} dv \quad (1.2)$$

where M is the magnetisation at each element and is given by,

$$M = (\mu_r - 1) H = \chi H \quad (1.3)$$

where $\chi = \mu_r - 1 =$ susceptibility of the magnetic material

Magnetisation (M) is given in terms of the flux density as follows,

$$M = \frac{B}{\mu_0} \left(1 - \frac{1}{\mu_r}\right) \quad (1.4)$$

where $B = \mu_r \mu_0 H$

Also the total field strength H is given by,

$$H = H_c + H_m \quad (1.5)$$

substituting for H_m from equation 1.2

$$H = H_c - \frac{1}{4\pi} \text{grad} \int \frac{M \cdot r}{r^3} dv \quad (1.6)$$

If the magnetic material is divided into N finite elements we get N similar equations which have the general form

$$H_i = H_{ci} + \sum_{j=1}^N K_{ij} \chi_j H_j, \text{ where } i = 1, 2, \dots, N \quad (1.7)$$

and K_{ij} are factors that depend on the field points geometry. Since each element of the coefficient K_{ij} will have two components, 2N simultaneous equations are generated for N finite elements. If (χ_j) the susceptibility of the j^{th} element were known, the equation

equation could be solved directly to obtain the two components of (H) which are H_{ix} and H_{iy} . If X_j values are not known, then an iteration process must be used in which the initial values of X_j are assumed. Then the equations are adjusted using a table of X/H values and the process is repeated until a prescribed degree of convergence is achieved. This will depend on the number of iron elements which are involved and the degree of saturation. The two components of magnetisation M_x and M_y are calculated from the field strength components H_{ix} and H_{iy} and the field H_m due to the iron is calculated at any point from equation (1.2) and added to the field H_c from the coil windings to give the total field H.

Calculation of Axial Flux Density Distribution

The total axial flux density distribution $B(z)$ of a magnetic lens, at any point on the axis, is a function of the current in the coil windings and the known magnetisation value M_z in the iron elements.

$$\text{So} \quad B(z) = B_c + B_{Fe} \quad (1.8)$$

where B_c is the axial flux density due to the coil windings, B_{Fe} is the axial flux density due to the magnetisation in the iron elements.

1.3.1.2.2 The Differential Finite Element Method

Munro introduced the FEM to electron optics (Munro, 1971). He used the FEM in its differential form to design a set of programs to calculate the flux density in all parts of the lens including parts where it would be difficult to measure the flux density experimentally. Munro's programs are popular with research workers, in the field of electromagnetic field calculations, due to

availability of a very clear manual (Munro, 1975) containing all the necessary information about the programs as well as prints of the original programs.

Munro's programs reduced the efforts needed in construction and experimental testing of the trial lenses to a minimum. With the help of these programs the shape of the polepiece and other parts of the magnetic circuit can be easily changed in order to reach a satisfactory design for the specific application of the lens.

The differential finite element method is convenient for structures with different permeability since the permeability of the magnetic material is specified at all parts of the structure, while in other methods like the finite difference method, it is often difficult to satisfy boundary conditions, e.g. between the coil, free space and magnetic circuit. The finite element method used by Munro is most convenient for dealing with saturation conditions where μ_r has to be calculated for each element in each iteration process. This method can be used also for calculating the field distribution in superconducting lenses. The superconducting material is simply characterised by relative permeability $\mu_r = 0$.

Mulvey and Nasr (1980a) pointed out that the finite element method, used in Munro's programs, can be limited by the fact that the vector potential at the boundary has to be set to zero. Nasr maintained that this cannot be true unless there was an infinite radius or when the flux $\phi = 0$. This will make Munro's programs work well and with high accuracy for conventional magnetic electron lenses. For open structures or other types of magnetic lenses, e.g. single polepiece lenses, there will be boundary losses in the excitation. This is elaborated further in Chapter 2. Nasr reduced the effect of this

developing Munro's programs into a set of improved vector potential programs, which made the increase in the number of meshes used possible, taking into account the computer store requirement.

Lencová (1984) designed a new program which is based on differential finite elements like the previous programs. Lencová's program deals with both linear and non-linear computations. A very large number of mesh points can be used by this program up to 6500 points, including the points on the boundary with $A = 0$.

Details of all the above programs are explained in later sections.

1.3.2 Electron Trajectories

Electron trajectories in magnetic lenses can be defined in the simple form of three equations, given by Goddard and Klemperer (1944).

$$\dot{z} = - \left(\frac{e}{m}\right)^2 A \frac{dA}{dz} \quad (1.9)$$

$$\dot{r} = - \left(\frac{e}{m}\right)^2 A \frac{dA}{dr} \quad (1.10)$$

$$\dot{\theta} = - \frac{e}{m} \frac{A}{r} \quad (1.11)$$

The essential features of these equations are their linearity in which first order derivatives \dot{z} , \dot{r} do not appear.

To calculate the electron trajectories, the values of $\frac{dA}{dr}$ and $\frac{dA}{dz}$ are calculated from the variation of the vector potential A over each quadrilateral given by Munro (1975) or Nasr (1981). Al Hilly (1982) has elaborated the inputting of these values into a special program to

arrive at trajectory path calculations. Modifications of Nasr's program and combination with Al Hilly's work lead to a general program for trajectory calculations.

1.3.3 Imaging Properties and Aberrations

If an electron passing through a magnetic electron lens forms a perfect image, then this image is called 'Gaussian' and the corresponding electrons are called Gaussian rays or Gaussian trajectories. The Gaussian path is described by the paraxial equation

$$r'' + \frac{\eta}{8V_r} B^2 r = 0 \quad (1.12)$$

where V_r is the relativistic accelerating voltage. B is the axial flux density and η is the charge to mass ratio of the electron.

Departure from Gaussian images are called aberrations which are expressed in terms of coefficients. A number of aberrations can affect the functioning of magnetic electron lenses. The importance of each depend on the magnetic lens function.

Aberrations, in magnetic electron lenses, are generally of two types. Those which are due to the electrons travelling far from the lens axis or along paths that are inclined at a steep slope to it, are known as geometrical aberrations; the most important of which are spherical aberrations and distortions. On the other hand, aberrations caused by wavelength spread of the incident beam are known as chromatic aberrations. These aberrations arise due to the variations in the accelerating voltage or fluctuations in the current. Energy loss in the specimen can also cause aberrations.

Various numerical methods are available for calculating the aberration coefficients of electron lenses. Munro (1975) computed the spherical and chromatic aberration coefficients, by using Simpson's rule to evaluate the aberration integrals

$$C_s = \frac{\eta}{128V_r} \int_{z_0}^{z_i} \left(\frac{3\eta}{V_r} B^4 r_\alpha^4 + 8B'^2 r_\alpha^4 - 8B^2 r_\alpha^2 r_\alpha'^2 \right) dz \quad (1.13)$$

$$C_c = \frac{\eta}{8V_r} \int_{z_0}^{z_i} B^2 r_\alpha^2 dz \quad (1.14)$$

where $r_\alpha(z)$ is the solution of the paraxial ray equation with initial conditions $r_\alpha(z_0) = 0$ and $r_\alpha'(z_0) = 1$ if the aberration coefficients are referred to z_0 or $r_\alpha(z_i) = 0$ and $r_\alpha'(z_i) = -1$ if the aberration coefficients are referred to z_i . For low or high magnification conditions, the magnification is calculated from the formula $M_0 = \frac{\alpha_0}{\alpha_i}$ where α_0 and α_i are the convergence angles of the trajectory at z_0 and z_i respectively.

The paraxial electron trajectories are computed, using a fourth-order Runge-Kutta formula to solve the paraxial ray equation (Eq. 1.12). Marai (1977) developed an asymptotic program for the calculation of distortion coefficients which was restricted to parallel incoming rays. However, Munro and Marai's programs can determine the aberration coefficients for one lens field distribution only, which render them inconvenient for calculating multi-lens systems.

1.4 The Computer Programs used for Calculating Magnetic Field using the Finite Element Method

All the programs used in this work are based on the finite element method and the same basic theory. This is elaborated in Chapter 2. However, these programs are different in their capacity and the input data and output result formats as explained in Chapter 3, which deals with data preparation for each program for both linear and saturated cases. Extensive comments are presented in several programs as part of this work.

1.4.1 Munro's Programs

Two programs are available in Munro's Manual (Munro 1975). First the M12 program is designed for dealing with unsaturated magnetic lenses (linear conditions), where the magnetic material has constant permeability. A set of linear equations in terms of vector potential coefficients is obtained and the matrix equation is solved by Gaussian elimination.

The second program M13 is for saturated magnetic lenses (non-linear condition), where the magnetic material permeability varies with the flux density. Here the data input allows for the magnetisation curve (Figure 1.3) in the form of tables of H and B of each magnetic material (Table 1.1). A set of non-linear equations in terms of vector potential coefficients similar to the linear case equation is obtained and solved by Newton-Raphson iteration, and the resulting matrix is solved by Gaussian elimination.

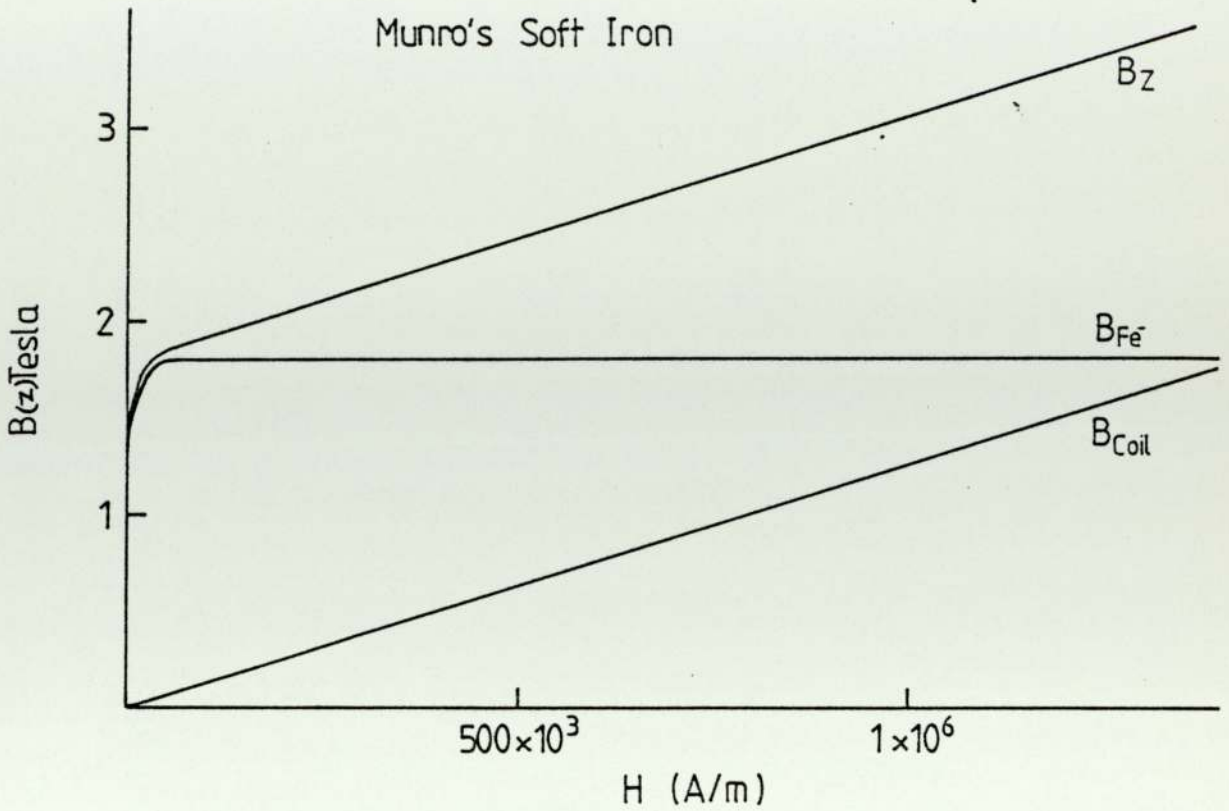


Figure 1.3 Typical magnetisation curve for soft iron.

TABLE 1.1 MAGNETISATION CURVE FOR SOFT IRON (Munro 1975)

50.0	0.400
100.0	0.680
150.0	0.880
200.0	1.020
344.0	1.224
560.0	1.282
807.7	1.325
1040.1	1.351
1344.1	1.377
2720.0	1.442
4716.6	1.500
8880.8	1.589
11124.9	1.623
15613.1	1.679
27509.9	1.790
44157.6	1.840
60940.5	1.866
77421.0	1.898
92469.1	1.919
106713.4	1.937
156847.3	2.000
236424.8	2.100
395579.8	2.300
634312.3	2.600
873044.8	2.900
1032199.8	3.100

1.4.2 Nasr's Programs

Nasr developed his programs for calculating magnetic fields during his research work at the University of Aston in Birmingham. The theoretical bases for these programs are fully explained in his PhD Thesis (Nasr, 1981). However, no manuals, similar to those developed by Munro (1975) are available on Nasr's programs. These programs were mostly stored at the University of Aston in Birmingham computers without instructions or comments. As part of this study, Nasr's programs have been explained and modified in some instances, in co-operation with the author. As a result, Nasr's programs are available now in a form similar to those of Munro.

Two programs were developed by Nasr, the first designated VPLIN deals with field calculations throughout the magnetic circuits of unsaturated (linear) magnetic lenses. Nasr's VPLIN like Munro's M12 program, assumes the magnetic circuit has constant and finite permeability. The main advantage of the VPLIN program over the M12 program is that with the former it is possible to use more meshes than is possible with the later, utilising the same or marginally higher computer memory store. This is achieved by introducing two inner boundaries which divide the lens into selected areas. This yields a better overall field distribution than is possible with M12 program. This, however, requires more computer time. This subject is explained further in both Chapters 2 and 3.

The second program developed by Nasr is called the VPSAT. This deals with saturated magnetic lenses like Munro's M13, and the basic difference, recognised by applying this program and M13 to several

designs, was the extra number of meshes this program enables us to use in the axial direction. The comparison is shown in Chapter 3.

The VPSAT program, after some modifications carried out in cooperation with Nasr, can deal with both linear and saturated lenses under all conditions and can substitute for M12 and M13 as well as VPLIN. This together with the possibility of using a higher number of meshes, for the same memory size, are advantages of this program. Copies of both VPLIN and VPSAT programs are included with the appendices.

1.4.3 Lencová's Program (AMAG)

Lencová (1984) devised her program (AMAG) in Fortran 4 at the Institute of Scientific Instruments, Czechoslovakia. Aston University was supplied with a copy of this program, as part of scientific exchange between the two institutions. The program was adapted to Fortran 77 and compiled in the Harris 800 system by the help of University electron microscopy group (Mrs. I. Al-Nakeshli and Mrs. H.C. Yin). Comments were provided on the program and a copy is included in the appendices.

AMAG is based on the same theory but utilises different algorithms from the previous programs, for both linear and saturation cases, it uses the Cholesky decomposition method combined with the conjugate gradient method (or the preconditioned conjugate gradient method) of Mejerink and Van der Vorst, (Lencová 1984) for solving the linear equations.

Several applications of the AMAG program were made and a full description of it is given in Chapter 2. Chapter 3 gives the data preparation and comparison between the output results of this program and the previous ones.

1.5 Application of the Finite Element Method for Designing
Electron Magnetic Lenses

The finite element method has been the base for most electron magnetic lens design work, since Munro introduced this method to electron optics (Munro, 1973). Designers were motivated to use this method since experimental methods take more time and effort. Literature reviews show that finite element programs are dominant in magnetic lens design work. This situation is acceptable if the method is used in moderation i.e. not with blind faith. Unfortunately this is not the case in much of the published work. This situation was, perhaps, natural. At the beginning, when any new scientific method is invented or a new application of an established method is devised, the authors tend to point out the advantages of their inventions and, whether consciously or unconsciously, gloss over the difficulties and limitations. This is what seems to have happened to the application of the finite element method to magnetic lens design. Mulvey and Nasr (1980a) pointed out some of the limitations of this method. Nasr concentrated on the boundary loss in excitation and overcame this problem to some extent by improving Munro's programs so that more meshes can be used. Nasr believed that the main source of problems was the boundary setting. In the present work, limitations in Nasr's programs were also discovered. Lencová's program has the added advantage of high capacity and ease of application. The user, however, is likely to encounter some difficulties similar to those of the previous programs, if he is not aware of the inherent limitations of these programs.

A comparison is made in chapter 3 between the three programs under both linear and non-linear conditions. The programs were applied to

the design of the same electron magnetic lens and the same number of meshes were used. The difference between the results was recorded in terms of computer time, memory size and the output results as well as the number of iterations performed in case of the non-linear programs.

1.5.1 Aims of the present work

A major objective of the present investigation is to throw light on the various factors that affect the accuracy of the finite element method, when applied to electromagnetic field calculations. The aim was not to invent new magnetic electron lens designs (although this was partly done in some instances) but to review and comment on the available programs. By applying these programs to some existing designs, it was hoped to detect possible design problems and point out any misleading conclusions drawn in the literature. Chapter 4, for example, pinpoints the main difficulties associated with these programs. The improvements made in several existing designs and the relevant conclusions are also presented.

1.5.2 Difficulties in using finite element programs

This study agrees with previous work about the boundary problems, in both open and partially open structures. However during the course of this work it was found that boundary problems arise in closed structures at high excitation (saturation condition) i.e. in saturated conventional, and double pole lenses. This is shown in Chapter 4.

Computation work carried out in this study indicated that changing the mesh distribution of the data may significantly change the overall

results. This effect was found to be more pronounced in non-cylindrical and sharp angle pole face profiles. To show this effect a lens of known field distribution was chosen. Since in unsaturated symmetrical double polepiece lenses, the maximum flux density B_{\max} at the centre of the air gap is known, for a given gap S_g and axial bore diameter D , according to the following equation see (Mulvey and Wallington, 1969):

$$B_{\max} = \frac{\mu_0 NI}{L} \quad \text{(Fert and Durandean equation) assuming very high } \mu_r \quad (1.15)$$

$$\text{where } L = \sqrt{S_g^2 + 0.45D^2}$$

Equation (1.15) was applied to Munro's symmetrical double polepiece lens shown in chapter 4. It was discovered that Munro's computed value was 3.6% higher than the value calculated from Eq. 1.15.

By rearranging the mesh distribution in the radial direction, increasing the meshes defining the pole face profile and using more meshes for defining the coil region, the computed value came into good agreement with the expected value.

The second difficulty associated with the finite element method is the number of meshes to be used. Nasr attributed the improvements, obtained through his programs, to the increased mesh numbers. This study proved Nasr's hypothesis to be true to some extent. However, Nasr's programs use more meshes in the axial direction only, by increasing the number of runs performed. The number of meshes in both axial and radial directions cannot be increased. This fact can limit the advantages of Nasr's programs especially for complicated designs where more meshes are necessary in both directions.

To show the effect of the number of meshes used a rectangular single polepiece lens was computed with the above mentioned three programs i.e. Munro's, Nasr's 4 run program and Lencová's. Results are presented in chapter 3.

Another important practical factor is the thickness of the iron casing (i.e. the lens shroud), especially under saturation conditions. This study has indicated that some of the published results of lens designs indicate that these designs had boundary problems and in addition the thickness of the iron casing was quite inadequate. This is discussed further in Chapter 4.

The boundary loss in excitation and also the leakage effect was also studied in double pole lenses, with solenoid or other thick coils. A rectangular double pole lens was designed to illustrate this effect.

The leakage effect manifests itself also in the external lens flux. Chapter 4 includes plots of these lines throughout the magnetic circuit of single pole lenses. A computer graphics program, designed by Munro (1975) and referred to as M31, was utilised in these evaluations. Lencová's AMAG program produce several graphic outputs which show the material distribution on the mesh, and the flux density distribution in the magnetic circuit.

The shielding (surrounding the lens by magnetic material of infinitely high permeability) is another important factor, in connection with the application of the finite element method in lens design to minimise the boundary problems. This factor is important if good accuracy is desired in the design. This study has indicated that the shielding is not important in double pole lenses under linear condition, since the

double poles actually act as a shielding. On the other hand, both boundary problems and leakage effect is significant in double pole lenses under saturation conditions (i.e. at high excitation). The boundary and shielding is very important to minimise boundary problems with reasonable computer core size in open structures like single pole lenses, iron free lenses, and simple coils with iron rings under both linear and saturation condition while for a double pole lens this study proved it is effective under saturation condition only. Examples of this effect are shown in chapter 4.

1.5.3 Possible misleading conclusions in the design of magnetic lenses

As mentioned earlier, faults in a lens design caused by any of the previously mentioned factors may lead to false conclusions and misleading judgments. This is especially likely to happen if the computer programs are relied upon unduly for comparing two or more configurations for the purpose of choosing the best design. Examples of such conclusions are mentioned in chapter 4, e.g. Cleaver's double pole lens (Cleaver 1978); Cleaver's computation gave 8.4% higher value for maximum flux density in the gap than the value expected from equation (1.15), under linear conditions.

Al-Khashab (1983) has carried out a study about the best size and position of the coil, concluding that thinner coils were better than thicker ones for magnetisation behaviour of the polepiece. This study has shown these conclusions to be erroneous, since there were two serious problems in these lenses, due to both boundary loss in excitation and leakage problems affecting the performance of the lens, as discussed in Chapter 4.

Another investigation was made at Aston University on lenses designed by Christofides. These lenses are designated Hermes, Hermes II and Hermes III. The computed values of peak axial flux density of Hermes II were 26% higher than the experimentally measured values (Christofides' 1982). The discrepancy between the computed and measured distributions were explained by Christofides in terms of the "inherent errors" in the computer program M13, "experimental errors" caused by the finite size of the Hall probe, and finally possible variations between the magnetisation properties of the magnetic material (Swedish iron) used in the experimental lens and those of the soft iron assumed in computing. Christofides thesis shows these discrepancies for both the total field at the peak and the iron contribution (B_{Fe}) to the peak value. Since the mesh data used by Christofides were not reported in his thesis, the lens was recomputed with the same dimensions and with a convenient mesh distribution using limited mesh numbers (25,50) and large mesh numbers (54,100). It was found that, for example, at 10800 A-t. Hermes II gave a peak in very good agreement with the experimental results. Another fact worth mentioning is that for higher excitations boundary problems arise and the iron casing is inadequate. In a further calculation by the present author, with correct boundary and a redesigned iron casing the loss in excitation due to boundary and leakage effects disappeared. In Christofides original computations of the flux density distribution, at excitations higher than 16000 A-t., three sources of error were at work i.e. the inadequate mesh layout which gave high peak value, insufficient boundary which caused loss in excitation and insufficient iron casing thickness which gave inadequate flux distribution.

1.5.4 Elimination of difficulties encountered in finite element programs

Throughout this work, application of all the available programs was made initially with a limited number of meshes, then with progressively larger numbers so that comparisons could be made at every stage of the calculation. The effect of each of the previously mentioned factors was studied separately and several lenses were used including single and double polepieces, iron-free lenses, coils with rings as well as symmetrical ring lenses. Sufficient information was gained from these applications to outline a method taking into consideration all the above mentioned factors, for designing electron magnetic lenses by the finite element programs. The method starts by setting the correct boundary and a suitable mesh layout, as outlined in this study. This method proved its usefulness in pinpointing and rectifying certain errors in lens design.

CHAPTER TWO

COMPUTER PROGRAMS FOR CALCULATING MAGNETIC FIELDS

2.1 The Basic Theory

The energy functional E for a rotationally symmetric circuits, can be expressed as (Munro 1971, Nasr 1981, Lencová 1984),

$$E = 2 \pi \int \int_{\text{Total Area}} (W - JA) r \, dr \, dz \quad (2.1)$$

Where

$$W = \int_0^B \underline{H} \cdot d\underline{B} = \frac{1}{\mu_0} \int_0^B \frac{B}{\mu_r} \, dB \quad (2.2)$$

where $A(r,z)$ is the angular component of the vector potential, $A=0$ at the lens axis and at infinity. $J(r,z)$ describes the distribution of the current density in the excitation coil.

The flux density B is given by

$$B = \sqrt{\left(\frac{\partial A}{\partial r}\right)^2 + \left(\frac{\partial A}{\partial z}\right)^2}$$
$$B_r = -\frac{\partial A}{\partial z} \quad (2.3)$$

$$\text{and } B_z = \frac{1}{r} \frac{\partial(rA)}{\partial r}$$

The field intensity $H = B / \mu_r \mu_0$ where μ_r is the relative permeability which can, in the magnetic material, depend on the value of the flux density. For non-linear magnetic material, W is given by equation 2.2.

If H is a linear function of B, it holds that,

$$W = \frac{B^2}{\mu_0 \mu_{r0}} \quad (2.4)$$

where W is the stored magnetic energy per unit volume, i.e. the work per unit volume required to produce a final magnetic flux density B. μ_{r0} is the relative permeability from the beginning of the magnetization curve. $\mu_{r0} = 1$ in non-magnetic parts.

Integration of equation (2.1) should be over an infinite area. But for magnetically shielded lenses, the boundary with $A=0$ can be put close to the lens. For axially symmetric problems equation 2.1 becomes

$$E = 2 \pi \iint_{\text{Total Area}} \left(\frac{B^2}{2 \mu_0 \mu_r} - JA \right) r \, dz \, dr \quad (2.5)$$

It can also be shown (Munro 1971) that the minimization of equation (2.5) is equivalent to solving the three sets of equations, given by,

$$\begin{aligned} \underline{B} &= \text{curl } \underline{A} \\ \underline{H} &= \frac{1}{\mu} \underline{B} \end{aligned} \quad (2.6)$$

$$\text{curl } \underline{H} = \underline{J}$$

which the vector potential \underline{A} (x,y,z) is required to satisfy at every point within a surface S. Hence:

$$E = 2 \pi \iint_{\text{Total Area}} \left(\frac{1}{2 \mu_0 \mu_r} \text{curl } \underline{A} \cdot \text{curl } \underline{A} - \underline{J} \cdot \underline{A} \right) r \, dz \, dr \quad (2.7)$$

In the case of rotationally-symmetric magnetic lenses, the only components of \underline{A} and \underline{J} which are non-zero are the circumferential components A_θ and J_θ . In this case equation (2.7) can be rewritten as:

$$E = \iint_{\text{Total Area}} \left\{ \frac{1}{2\mu_0\mu_r} \left[\left(\frac{\partial A_\theta}{\partial z} \right)^2 + \left(\frac{\partial A_\theta}{\partial r} + \frac{A_\theta}{r} \right)^2 \right] - J_\theta A_\theta \right\} 2\pi r dr dz \quad (2.8)$$

The minimization of equation (2.8) can be carried out by the finite element method. The magnetic structure, including the current carrying coil, the magnetic material and the space around it, as defined by the outer boundary (for which the vector potential A must be known and is equal to 0 at infinity, is divided into a grid of quadrilaterals. Each quadrilateral is divided, in turn, into two triangles. This can be done in two alternative ways as shown in figures 2.1a and 2.1b. In each case the vertices of six triangular elements meet at a lattice. Combination of arrangements 2.1a and 2.1b, as shown in 2.1c, gives twelve triangles in contact with each node, thereby improving the accuracy of calculation.

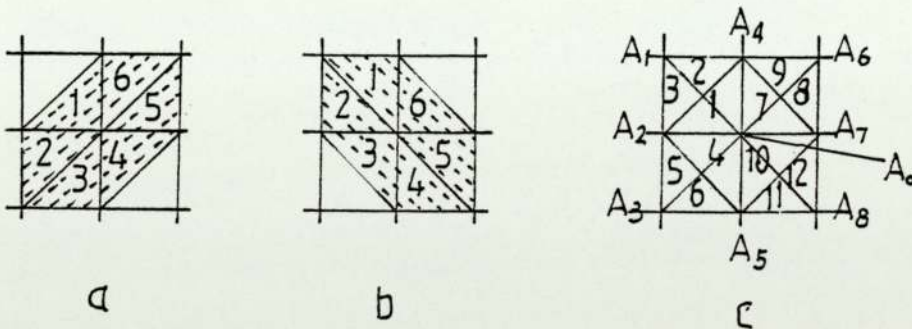


Figure 2.1 Subdivision of quadrilaterals into finite elements
 (a) one possible way, (b) alternative way,
 (c) combination of (a) and (b) for better accuracy

With this arrangement Munro (1973) derived a nine point equation for each node in terms of the vector potentials at the nodes and the eight vector potential values at the other vertices of the triangles in contact with the node, as shown in figure 2.1c. In this case the values of known vector potentials at the boundary are substituted and the equations solved for the unknown vector potentials at each node. This will lead to the determination of the flux density over each element. The flux values can also be calculated and the axial flux density determined from the vector potential values near the axis.

The axial flux density $B(z)$ is given by:

$$B(z) = \frac{z(A_1 r_2^3 - A_2 r_1^3)}{r_1 r_2 (r_2^2 - r_1^2)} \quad (2.9)$$

where A_1 and A_2 are the vector potential at distances r_1 and r_2 from the axis respectively. Eq. (2.9) determines $B(z)$ from the vector potential values on the two lines closest to the axis. According to Lencová (1984), her program AMAG determines $B(z)$ values based on two lines as well as one line. In the latter case $B(z) = \frac{2A_1}{r_1}$

Boundary loss in excitation

The values of the vector potential at the outer boundary must be known so that the finite element equations can be solved for the unknown vector potentials. Because of axial symmetry, the vector potential along the axis is zero ($A=0$). However, the vector potential at the other three boundaries cannot be zero unless they are at infinity. This, in practice, means if the boundary is taken at a far distance and the value of (A) is assumed zero; the results will be reasonably accurate. This, of course, necessitates increased computer memory store.

The boundary problem can be elaborated as follows:

The field strength H is given by,

$$H = \frac{B(z)}{\mu_0 \mu_r} \quad (2.10)$$

For a path (1) that encloses the coil windings,

$$\frac{1}{\mu_0} \int \frac{B(z)}{\mu_r} \cdot dl = NI \quad (2.11)$$

A finite boundary must be specified where $A=0$. Thus the boundary problem arises in the differential finite element method. The boundary loss must be minimised, otherwise the lens excitation calculated by the differential finite element method will be less than the excitation found from the Biot-Savart Law.

Nasr (1981) calculated the boundary loss in excitation as shown in figure (2.2).

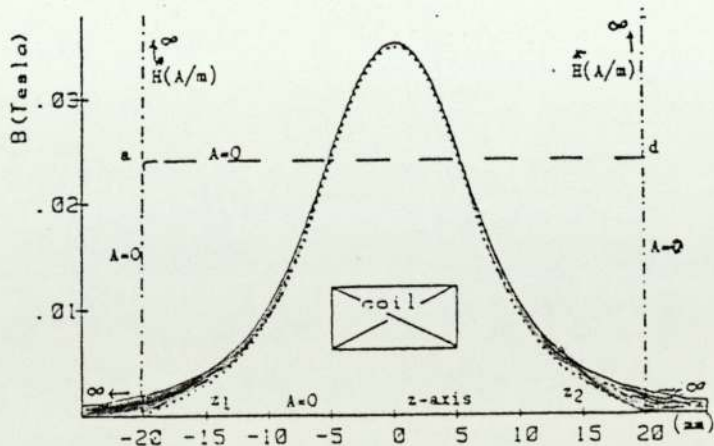


Figure 2.2 Boundary loss in a magnetic lens

The shaded area represents the excitation (lost) from the axial field distribution and transferred to the boundary. The excitation of an iron free coil was calculated with the Biot-Savart Law and the differential finite element method for a finite boundary. The calculations were repeated after surrounding the lens firstly by a superconducting sheet $A=0$ within the specified boundary, and secondly by an iron sheet of infinite permeability. Results showed a boundary loss in the case of the superconducting sheet. But no loss was apparent in the iron sheet case. The boundary loss causes errors in the calculated field which are highest near the boundary. The calculated axial field distribution in the central region of the structure, remote from the finite boundary, has good accuracy.

In the case of closed magnetic circuits, for example in conventional lenses, which were the basis of Munro's research work, the differential finite element method is satisfactory. The case is similar to the case of a lens surrounded with an iron sheet where there is no boundary loss. This study proved that is correct for linear conditions where the magnetic circuit has high relative permeability, and will not apply in saturation conditions.

On the other hand for open circuits, like iron free coils, or partly open circuits, like single-polepiece lenses, the differential finite element method may lead to unacceptable errors in the axial field distribution due to the loss at the boundary. These errors can be avoided or minimised by using computers with very large core stores. However, such computers are not always available, especially for the initial design work of magnetic lenses where research workers need to change data repeatedly and get results quickly. Thus the need arises

for a method which can guarantee reasonable accuracy for magnetic lens design work, using mini or micro computers. Nasr's programs (Nasr, 1981) as will be illustrated later, are designed to cater for such work. These programs give adequately smooth curves for axial field distribution. This guarantees the accuracy of the derivatives.

2.1.1 The differential finite element method

A number of programs are available utilising the differential finite element method for computing the vector potential distribution and flux density distribution of magnetic structures.

2.1.1.1 Munro's programs

Two programs are available in Munro's manuals (Munro, 1975) for calculating the field distribution characteristics namely M12 for the unsaturated magnetic lenses (linear condition), where the magnetic material has constant permeability, and M13 for the saturated magnetic lenses (non-linear condition), where the magnetic material permeability varies with the flux density.

2.1.1.1.1 Munro's program for unsaturated magnetic lenses (M12)

Munro's program M12 computes the vector potential distribution and the flux density distribution throughout the magnetic circuit and coil windings of unsaturated rotationally-symmetric lenses, where the magnetic material has constant permeability. The calculations involve minimising the energy functional represented by equation (2.8).

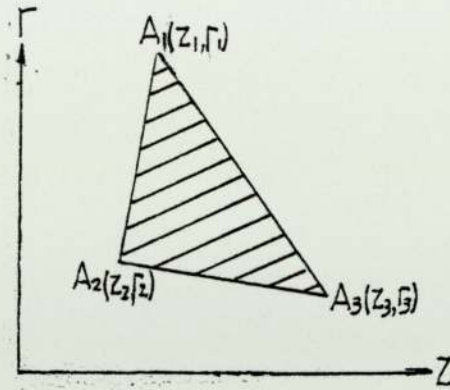


Figure 2.3 Triangular finite element. The vertices numbered counter clockwise, $A(z,r)$ is the vector potential assumed to vary linearly with z and r .

By considering a triangular finite element mesh as shown in figure 2.3 assuming that $A(z,r)$ varies linearly across the triangle, thus the contribution from the triangle to the value of the functional can be put in equation 2.8 if the area of the triangle is sufficiently small. Then the values of A and r at the centroid can represent the triangle. For the functional to be minimized $\frac{\partial \Delta E}{\partial A_i} = 0$. At the three vertices of the triangle represented by figure 2.3, a matrix equation is formed,

$$\frac{\partial \Delta E}{\partial A_i} = [D_{ij}] \cdot [A_j] - [Q_i] \quad (2.12)$$

$$i = 1,2,3; j = 1,2,3$$

Because of symmetry D_{ij} requires the calculation of 6 elements only.

The finite element equations for this program are obtained as follows: Considering 0 as the general node in contact with twelve finite element triangles (figure 2.4), a nodal equation is obtained at point 0 where the value of the vector potential A_0 is affected by the eight neighbouring vector potentials at the other vertices of the twelve triangles in contact.

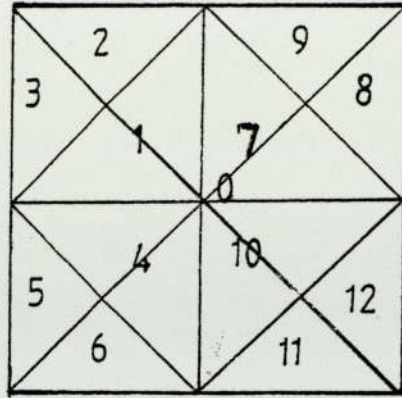


Figure 2.4 A node 0 in contact with twelve right angled, overlapping, triangular finite elements.

At any node (n) the change in energy functional is given as the total change from twelve triangles ($T_1, T_2, T_3, T_4, \dots, T_{12}$) in contact with node n. By expressing this change in functional at node n in matrix form given by equation (2.12) a nine point equation for the node (n) is obtained:

$$P_1 A_{n-1-1} + P_2 A_{n-1} + P_3 A_{n-1+1} + P_4 A_{n-1} + P_5 A_n + P_6 A_{n+1} + P_7 A_{n+1-1} + P_8 A_{n+1} + P_9 A_{n+1+1} = C_n \quad (2.13)$$

$$\text{where } C_n = Q_1 + Q_2 + Q_3 + \dots + Q_{12} \quad (2.14)$$

P_1, P_2, \dots, P_9 are the coefficients of nodal equations for node n which can be expressed in matrix form as follows:

$$N_{eq} \begin{bmatrix} P \end{bmatrix} \begin{matrix} \leftarrow N_{eq} \rightarrow \\ \left\{ \begin{matrix} A_{1+2} \\ \vdots \\ A_{2l-1} \\ A_{2l+1} \\ \vdots \\ A_{1l-1+l} \end{matrix} \right\} \end{matrix} = \begin{matrix} \left\{ \begin{matrix} C_{1+2} \\ \vdots \\ C_{2l-1} \\ C_{2l+1} \\ \vdots \\ C_{1l-1+l} \end{matrix} \right\} \end{matrix} \quad (2.15)$$

where $l = 0$ for asymmetrical problems and $l = 1$ for symmetrical problems.

The matrix equation (2.15) has some important properties:- (a) It is a sparse matrix since each nodal equation can be expressed in terms of the vector potential at the node and the eight neighbouring vector potential values, (b) It has the properties of a banded matrix with half band width equal to I and (c) it is symmetrical about the diagonal. Hence only the coefficients of the banded matrix in the upper triangle of the matrix need be stored. The matrix equation (2.15) is solved by the Gaussian elimination, to give the vector potential at each mesh-point.

The axial flux density distribution is obtained by numerical differentiation of the computed vector potentials at the mesh points near the axis. Flux values throughout the magnetic circuit are obtained at the centre of each finite element by numerical differentiation of the mesh point potentials at the vertices of the element.

M12 program consists of the main program and twelve subroutines. It permits of a maximum mesh size of $JM = 50$ mesh points in the axial direction by $IM = 25$ mesh points in the radial direction. If more than 25×50 mesh points are required then the dimensions of the array variables must be increased accordingly. This requires a larger computer store and more time. Munro found that the execution time is roughly proportional to I^3J and the store required is roughly I^2J .

2.1.1.1.2 Munro's programs for saturated magnetic lenses (M13)

Munro's program (M13) deals with saturated magnetic lenses, in which the lens excitation is so high that non-linear magnetisation curves must be considered. The program is designed to handle magnetic

circuits of up to five different magnetic materials. Data input allows for magnetisation curves in form of tables B and H of each magnetic material as shown in table (1.1). For H values which are lower than those in the table, i.e. those which represent the linear part of the magnetic material, the program assumes that the magnetisation curve has a constant slope. For H values greater than those provided in the data, the curve is assumed to have a constant slope equal to the free space permeability (μ_0).

As in the case of unsaturated magnetic lenses program M12, the saturation program M13 computes the axial flux density. Assuming linear variations of A across a finite element triangle, the values of radial and axial flux density (B_r) and (B_z) and (B) are calculated from equation (2.3). The corresponding values of μ_r and the incremental permeability (μ_{rinc}) are found from the magnetisation characteristics. The finite elements equation for the general node (equation 2.13) applies. Hence a set of nine point non-linear equations are generated at each node. These non-linear equations are solved by the Newton-Raphson iteration, by calculating the matrix equation,

$$(J_{nm}) (\Delta A_m) = E_m. \quad (2.16)$$

where J_{nm} is the Jacobian matrix of the non-linear equations, ΔA_m is the difference in vector potential at the mth node between two consecutive iterations k and k+1 and is given by,

$$(\Delta A_m) = (A_m)^k - (A_m)^{k+1} \quad (2.17)$$

E_m is the matrix of the residuals. ΔA_m is calculated from equation (2.16). After each iteration, the new value of J_{nm} is obtained and

the resulting matrix is solved by Gaussian elimination and a new approximation for the vector potential values is calculated from,

$$(A)^{k+1} = (A^k) + (\Delta A)^k \quad (2.18)$$

This process is repeated until the change in $(\Delta A)^k$ is within a certain accuracy limit.

This program like M12 consists of a main program and extra subroutines to deal with iteration processes. In general for a mesh with J points in the axial direction and I points in the radial direction, the execution time is roughly proportional to NI^3J and the store required is roughly proportional to NI^2J , where N is the number of iterations required to achieve adequate convergence.

2.1.1.2 Nasr's Programs

Nasr's programs were present in Aston University's ICL 1905 computer system, with several trial versions for each program. Unfortunately no manuals and no comments on how the programs functioned were available.

At the early stages of this work, applications of all the available versions were performed to find the best copy. As a result of these applications it was discovered that the saturation program (VPSAT) had not been applied for symmetrical cases, and in case of saturation the program was erroneously repeating the linear procedure. With Nasr's collaboration, several major modifications were made in the main program and in the saturation subroutine. The present VPSAT program, which is now fully documented by the present author, now deals with both symmetrical and asymmetrical lenses as well as linear and saturation conditions.

As part of this study comments were written on both of Nasr's programs, VPLIN and VPSAT. Both programs together with comments are listed in Appendices 3 and 4 for reference purposes.

2.1.1.2.1 Nasr's improved vector potential program VPLIN for magnetic structures under linear conditions

Nasr's program VPLIN, like Munro's program M12, computes the vector potential distribution and the flux density distribution throughout the magnetic circuit and coil windings of unsaturated rotationally symmetric magnetic lenses. The magnetic circuit is assumed to have constant, finite permeability. The algorithm of program VPLIN like that of M12 involves minimising the energy functional represented by equation (2.8). This minimisation is performed numerically using the finite element method. The region to be analysed is divided into small quadrilaterals which are subdivided further into small triangular finite elements, within which the vector potential A is assumed to vary linearly.

There are important differences between Munro's program M12 and Nasr's program VPLIN which make the latter produce results of the same or better accuracies with the same computer core size. This can be explained as follows:

Figure 2.5 shows a rectangular single pole lens. The outer boundary is represented by CDEF.

Both M12 and VPLIN programs assume that the vector potential at the boundaries CF, CD, EF and DE (the axis) is zero. This will naturally affect the results since $A \neq 0$ at CF, CD and EF. The region within

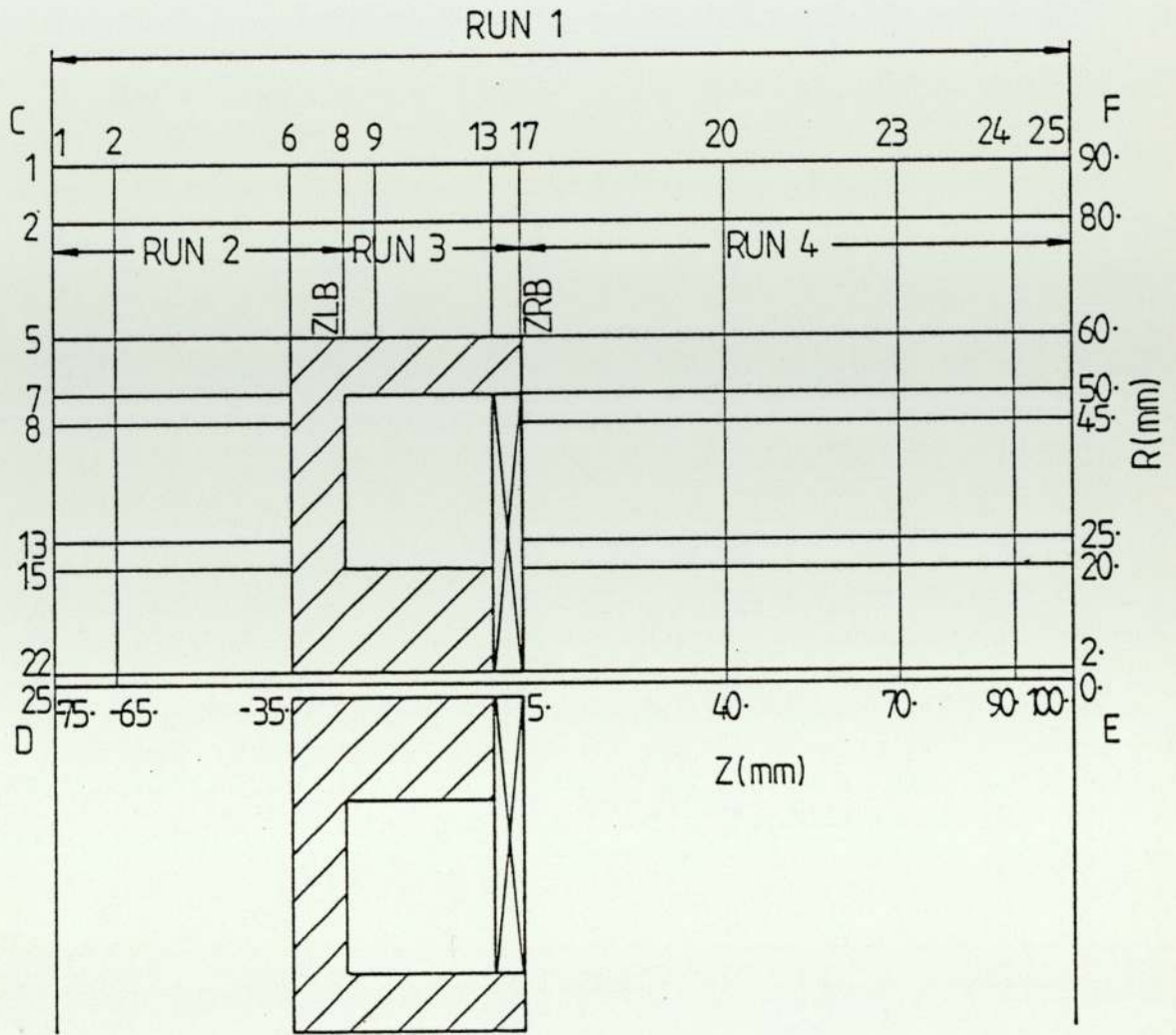


Figure 2.5 Rectangular single polepiece lens with mesh distributions in Z and R directions and two inner boundaries, ZLB and ZRB to be used in Nasr's programs for further runs.

the finite boundary CDEF is divided into a grid of quadrilaterals, which includes the magnetic material, the coil and the free space. Edges of the quadrilateral are chosen perpendicular or parallel to the axis. Major mesh lines define the geometry of the structure and change the mesh size. The programs will subdivide the large quadrilaterals into smaller ones and finally to triangles representing the finite elements.

With M12 program, the only way to improve accuracy is to increase the major mesh line numbers which will increase the computer core requirement. VPLIN program achieves improved accuracy with the same core size by introducing two inner boundaries ZLB and ZRB, remote from the other boundaries CD and FE, so that a finer mesh size is obtained. The inner boundaries ZLB and ZRB divide the structure into three regions which correspond to RUN 2, RUN 3 and RUN 4 calculations on the computer. The whole structure CDEF is used for the first calculation (RUN 1) which will give similar results to those obtained from M12 program if the same mesh line numbers are used. When RUN 1 is completed, the vector potential values along the inner boundaries ZLB and ZRB are saved to be used in subsequent runs.

RUN 2 region, shown in figure 2.6 , has boundaries CD, GH and the axis DH with vector potential values set along them to zero. The right hand side boundary is ZLB with vector potential values saved from RUN 1. The region is divided by mesh lines in both axial and radial directions and the computations are done as for RUN 1.

For RUN 3, shown in figure 2.7 , the vector potential values at the axis HM and boundary GL are set to zero. The values at the left hand

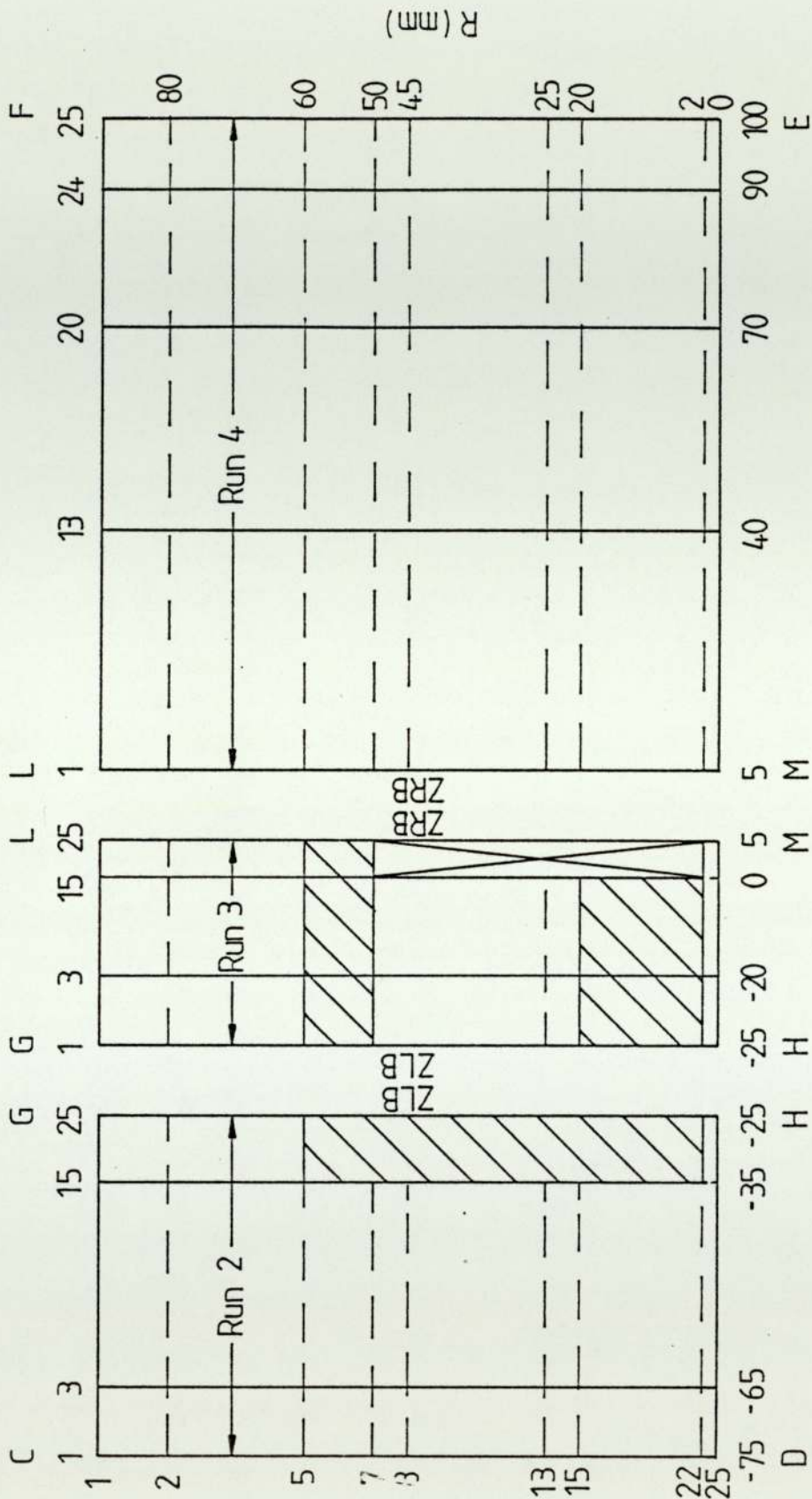


Figure 2.6
Run: 2
Mesh size 25 x 25
From Z = -75mm
To Z = -25mm

Figure 2.7
Run: 3
Mesh size 25 x 25
From Z = -25mm
To Z = 25mm

Figure 2.8
Run: 4
Mesh size 25 x 25
From Z = 25mm
To Z = 100mm

side boundary ZLB and right hand side boundary ZRB are those saved from RUN 1. The region is again divided by mesh lines as explained for RUNS 1 and 2 and the computations are carried out.

For RUN 4, shown in figure 2.8, the left hand side boundary (ZRB) vector potential values are those saved from RUN 1, while the values for boundaries LF, FE and ME (the axis) are set to zero. Division by mesh lines and computations are carried out again.

The three RUNS 2, 3 and 4 yield the final distribution of the vector potential throughout the magnetic lens. These results are more accurate than RUN 1 results, as shown in figure 2.9 .

2.1.1.2.2 Nasr's improved vector potential program under non-linear conditions (VPSAT)

This program, like Munro's program (M13), is based on the minimisation of the energy functional represented by equation (2.1) where W is defined by equation (2.2). However, in addition to minimising the boundary problems associated with Munro's program, there are other differences which will be explained below.

The boundary problems associated with Munro's programs (M12) and (M13) have been explained previously. In order to get accurate results with these programs, the boundaries have to be set at relatively far distances. This requires very large core store.

VPSAT program overcomes the boundary problems, associated with Munro's (M13) program, by locating two inner boundaries in a way similar to (VPLIN) program. The whole structure is used in the first run

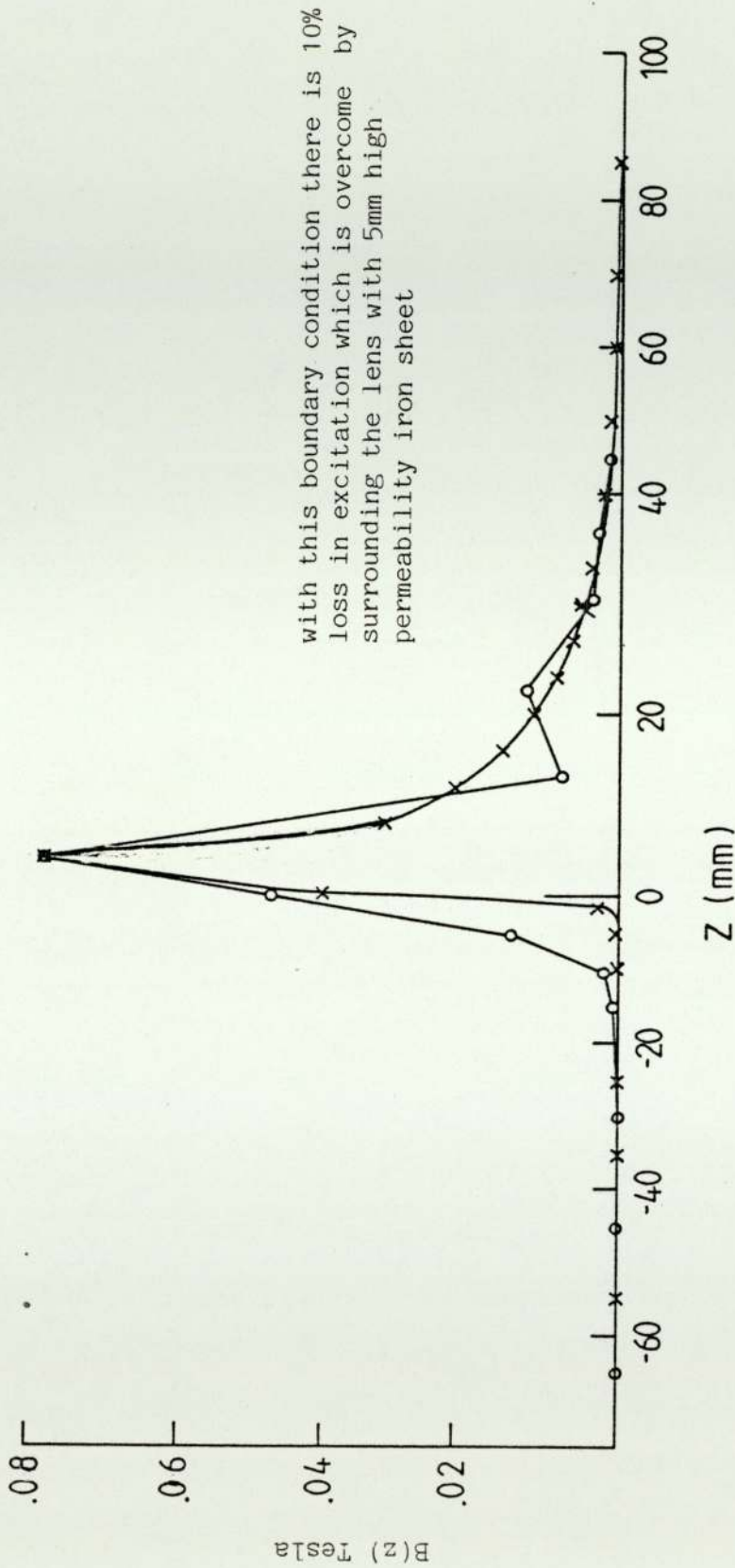


Figure 2.9 Axial flux density distribution for rectangular single pole lens under linear conditions excitation given 1000 A-t with thin coil ($4 \times 4.8 \text{ mm}^2$)
 (O-O-O) using Munro's (M12) program (25 x 25 meshes)
 (x-x-x) using Nasr's (Vplin) program (25 x 25 meshes) 4 runs

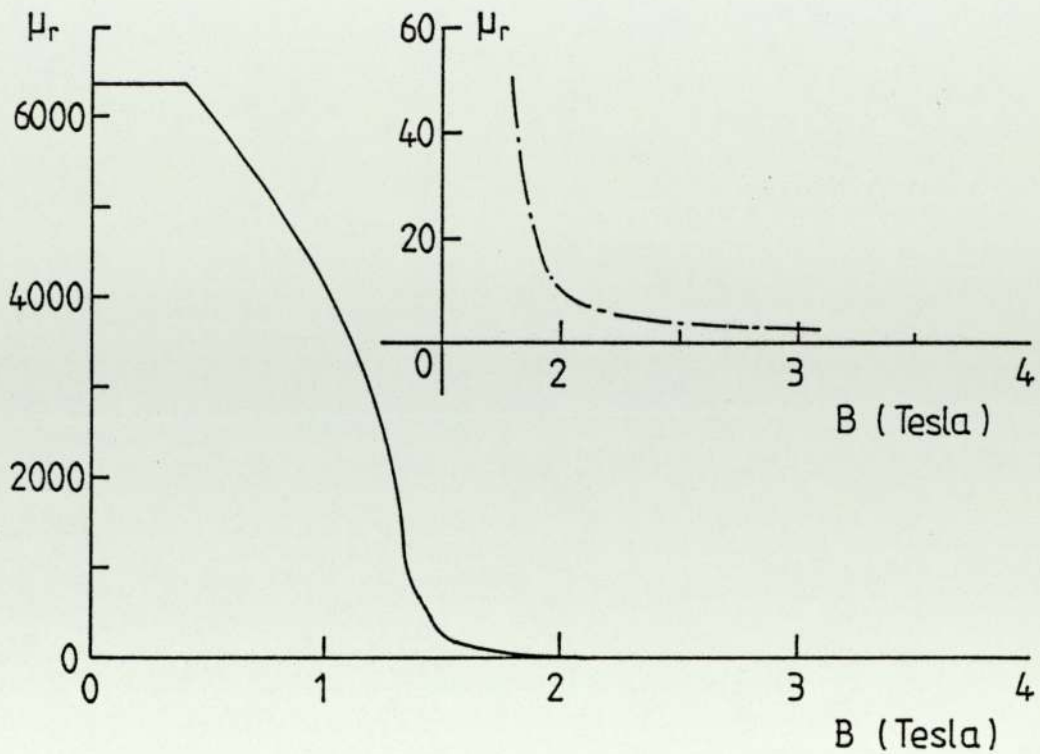


Figure 2.10 Relation between the relative permeability (μ_r) of magnetic material and the flux density B.

TABLE 2.1 A TYPICAL RELATION BETWEEN THE RELATIVE PERMEABILITY AND THE FLUX DENSITY OF A MAGNETIC MATERIAL (Nasr 1981)

.0	6366.2
.4	6366.2
.68	5411.3
.88	4668.5
1.02	4058.
1.224	2831.4
1.325	1735.
1.351	1033.6
1.377	815.3
1.442	521.9
1.5	253.1
1.589	142.4
1.623	116.1
1.679	85.6
1.79	51.8
1.84	33.2
1.866	24.4
1.898	19.5
1.919	16.5
1.937	14.4
2.	10.1
2.1	7.1
2.3	4.6
2.6	3.3
2.9	2.6
3.1	2.4

As in Munro's M13 program, the contribution to the functional at any node (m) comes from the twelve triangles in contact with the node, a set of nine-point non-linear equations are generated at each node of finite element grid, similar to equation (2.13).

These non-linear equations are solved by Newton-Raphson iteration by calculating the matrix equation (2.16). The value of the Jacobian matrix (J_{nm}) and the sum of residuals E_m is calculated by determining the values of B, μ_r and DMU where DMU is the incremental relative permeability and is determined from figure 2.10 or table (2.1). ΔA_m as previously mentioned, is the difference in vector potential at the mth node between the iterations k and k+1 and is calculated from equation (2.17). After each iteration a new value of J_{nm} is obtained and the resulting matrix, like in Munro's (M13), is solved by Gaussian elimination and a new approximation for the vector potential values is calculated according to equation (2.18). This cycle of operations is repeated until the change (ΔA)^k is within a certain accuracy limit.

The VPSAT program can be used for linear cases as well as non-linear ones, i.e. it can substitute for the VPLIN program. This is another advantage of this program as one program, suitable for both linear and non-linear conditions, needs to be stored.

2.1.1.3 Lencová's Program (AMAG)

Lencová's AMAG program has the same theoretical basis as Munro's and Nasr's programs, since it utilises the finite element method for calculating the vector potential and flux density distribution in the magnetic circuit of a rotationally symmetric magnetic electron lens. The stored energy is expressed by equation (2.1). Program AMAG is

arranged in two stages, the first stage deals with the linear approximation with constant iron relative permeability μ_{r0} , which is relative initial permeability. The second step is the non-linear computation of the vector potential. In this stage, account is taken of the dependence of iron permeability on flux density in each part of the magnetic material, as is the case in Munro's M13 and Nasr's VPSAT programs. Additionally program AMAG deals with cases when the magnetic material is on the axis (eg. boreless lenses) by a special subroutine designated 'AMULV'. In this case $B(z)$ value from equation (2.9) will be divided by the relative permeabilities obtained from the magnetisation curves or from the beginning of the magnetisation curve in the linear case i.e. the flux density is determined in an infinitesimally small bore along the axis.

In Lencová's program, as in all the previous finite element programs, the whole area is divided into quadrilaterals which are subdivided into triangles; each small triangle contains only one type of medium (iron, coil or non-magnetic material). The vertices of each triangle are numbered counter-clockwise from 1 to 3 as shown in figure 2.3. Where $A(z,r)$ is a linear function of the r and z coordinates in the triangle; the flux density at each triangle can be evaluated from equation (2.3). If the triangle lies in the magnetic material and a first approximation of the non-linear method is required, the value of the two permeabilities μ_r and μ_d can be determined from the magnetization curve to a linear approximation given by $\mu_r = \mu_d = \mu_{r0}$. Where μ_d is the differential permeability and is given by $\mu_d = \frac{\partial B}{\partial H} / \mu_0$. For the non-linear computation μ_r and μ_d are evaluated from the magnetization curve with the help of the following formulae:



(1) If $BC \leq BM(1, I)$, then $\mu_r = \mu_d = \mu_{ro}$

(2) If $BC > BM(J, I)$ where $J = IH(I)$, then $\mu_d = 1$ and μ_r is defined under 3 below

(3) If $BM(J, I) < BC \leq BM(J + 1, I)$, then

$$\mu_d = \frac{BM(J+1, I) - BM(J, I)}{\mu_o(H(J+1, I) - H(J, I))} \quad (2.19)$$

$$\mu_r = \frac{BC}{\mu_o H(J, I) + (BC - BM(J, I)) / \mu_d} \quad (2.20)$$

where BC and BM are the axial flux density distribution from the computation process and the tables respectively. H is the field strength.

Up to two kinds of iron may be handled (as opposed to five in Munro's program) represented by two magnetization curves, or B/H tables. In the case of saturated lenses the lens excitation may be progressively increased by giving a series of current densities in the coil. For the first step i.e. the lowest coil excitation, the computation of the lens is performed by linear approximation. Then in each non-linear approximation a correction to the vector potential at the mesh nodes is obtained and added to the previous vector potential. A maximum of 7 approximations is allowed for each excitation, typical values being 2 to 3 while in certain cases this was increased to higher than 7 approximations. If the range of the absolute value of these corrections is smaller than 3%, computation is stopped and the results are printed out.

For the next excitation the resulting vector potential from the previous excitation is used. Since in saturation, a 50% increase in

lens excitation will not produce a 50% increase in the flux density, the new starting vector potential will be multiplied by a lower value of $(1 + a)/2$ where a is the ratio of the new and the last excitations.

For the solution of the linear equation (2.18) the AMAG program uses the Cholesky decomposition, combined with the conjugate gradient method (or pre-conditioned conjugate method of Meijerink and Vander Vost (Lencová 1984)).

Program AMAG gives almost the same results for the axial field distribution as Munro and Nasr's programs if the same number and distribution of meshes is used. However, this program deals with several excitations with the same data.

2.2 Axial flux density distribution due to the current windings in the coil by Biot-Savart Law

Nasr (1981), derived the axial flux density B_c at a point P of axial coordinates z due to the current in a circular loop of radius r carrying a current I_c , from Biot-Savart Law. Nasr's (1981) program "Biot" has been used by the present author and listed in Appendix 2 for reference purposes. From Biot-Savart Law,

$$[B_c(z)]_{\text{loop}} = \mu_0 \frac{I_c r^2}{2(r^2 + z^2)^{3/2}} \quad (2.21)$$

For a coil of rectangular cross section and excitation NI ampere turns (Fig. 2.11), B_c becomes,

$$B_C = \frac{\mu_0 \cdot NI}{4A(r_2 - r_1)} [Z_p \ln X_1 - Z_m \ln X_2] \quad (2.22)$$

In this case $A = \frac{1}{2}$ (coil width)

$(r_2 - r_1)$ = the difference between the outer and inner radii

μ_0 = the permeability of free space = $1.256637 \cdot 10^{-6}$

$$Z_p = Z + A$$

where (Z) is the axial distance of the point (p)

$$Z_m = Z - A$$

$$X_1 = \frac{\tan \frac{1}{2} \left(\frac{\pi}{2} + \alpha_1 \right)}{\tan \frac{1}{2} \left(\frac{\pi}{2} + \alpha_0 \right)} \quad (2.23)$$

$$X_2 = \frac{\tan \frac{1}{2} \left(\frac{\pi}{2} + \beta_1 \right)}{\tan \frac{1}{2} \left(\frac{\pi}{2} + \beta_0 \right)} \quad (2.24)$$

$\alpha_1, \alpha_0, \beta_1, \beta_0$ are shown in figure 2.11 .

If the coil dimensions and the excitation are known then $\alpha_1, \alpha_0, \beta_1$ and β_0 can be calculated.

For a coil of arbitrary shape, the field at the axis can be calculated as the contribution of several current loops by dividing the coil into a number of circular elements whose cross-section form a grid of quadrilateral elements. The current for each element is given by,

$$(I_C)_i = (J)_i \cdot (\text{area})_i \quad (2.25)$$

where $(I_C)_i$ = the current in i^{th} element, $(J)_i$ is the current density of the i^{th} element.

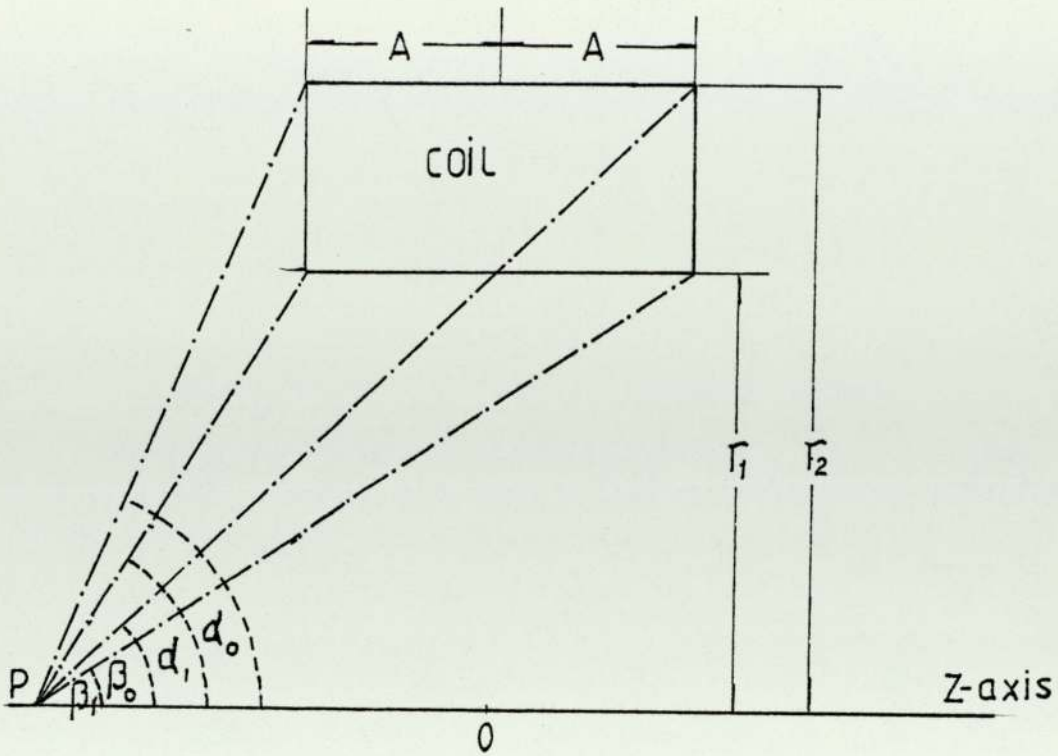


Figure 2.11 Axial flux density $B_C(z)$ from a coil of rectangular cross-section at a point P on the axis

The axial flux density $[B_C]$ at the point P is derived according to equation (2.21).

The total contribution from the coil to the flux density at axial point p is then given by

$$B_C(z) = \sum_i [B_C]_i$$

CHAPTER THREE

INPUT DATA AND OUTPUT RESULTS OF COMPUTER PROGRAMS FOR CALCULATING MAGNETIC FIELD DISTRIBUTION

3.1 Introduction

The first step in the application of computers to magnetic field distribution for lens design is the choice of a convenient program compatible with available computer memory store and time. Once that is done, there are procedures to be followed, in the input data preparation, which are often specific to each program and a full understanding of them will save the user much time and effort. In the following sections, special attention is drawn to the input data and output results of Munro (1975), Nasr (1981) and Lencová's (1984) programs.

3.2 Data Preparation for Munro, Nasr and Lencová's computer programs

This study has shown that the choice of the correct boundary, a good mesh layout and careful mesh distribution are prerequisites of successful computer aided design. To prepare data, for the calculation of the axially symmetric magnetic field distribution in magnetic lenses the lens cross section is shown later for example in figure 3.3a. Symmetrical lenses require only a quarter section, with symmetry plane on the right; asymmetrical lenses require a half cross section as shown in fig. 2.5 since they do not have a plane of symmetry in the middle of the lens.

The next step is to choose a suitable boundary to surround the magnetic circuit, at such a distance that the flux density can be assumed negligibly small at the boundary. This can be done, for example by calculating the axial flux density produced by the coil, directly, from the application of the well known Biot-Savart Law with a suitable computer program, like the one mentioned in section (2.1.2).

The whole region of the magnetic circuit, surrounded by the chosen boundary, is then divided into quadrilaterals in such a way that all the outlines of the magnetic circuit and the coil windings lie along the quadrilateral's edges. It is advisable that these edges are drawn as near as possible parallel to or perpendicular to the lens axis. The axial and radial coordinates, for the mesh points, are written in millimeters with decimal points.

The original, quadrilaterals are subdivided into smaller ones to provide fine mesh which is of utmost importance in finite element analysis. This is performed automatically by the computer, in accordance with the mesh numbers specified.

Careful mesh distribution is required in all parts of the lens, with particular attention for the polepiece gap, region defining the polepiece and the coil windings. However, this should not be done at the expense of the other parts of the lens. The best approach is to change the mesh length gradually and avoid abrupt changes.

Standard R-Z Coordinates are used; $R=0$ on the lens axis. For asymmetrical lenses, the origin of the Z coordinate can be chosen at any convenient position; for symmetrical lenses, the origin is

conveniently chosen at the plane of symmetry. This is the case for the Munro, Nasr, and Lencová programs. Note however in the Lencová program the Z coordinate is considered positive; in the Munro and Nasr program the Z coordinate is considered to be negative (see Figures 3.3a and 3.3b).

Data writing formats are of course specific to each program. Munro, has provided a comprehensive manual on his programs, which give a detailed account of input data formats. A brief description of these is given in the following paragraphs largely for comparison with the other program formats. However, Nasr and Lencová have not yet published similar manuals for their programs. A considerable effort has therefore been made in this thesis to analyse in detail Nasr's program, to correct programming errors and to provide an authoritative manual for future use. In addition Lencová's program, in collaboration with the author, has been adapted for the Harris 800 computer and tested out on critical problems.

3.2.1 Data Preparation for Munro's Programs

Data preparation will vary according to whether the computation is performed for linear or non-linear conditions. Munro's program M12 deals with linear cases (unsaturated magnetic lenses), while program M13 deals with non-linear cases (saturated magnetic lenses).

3.2.1.1 Program M12

Table (3.1) illustrates the general data format for program M12, and gives full explanation of the symbols used.

3.2.1.2 Program M13

Program M13 deals with saturated magnetic lenses, in which the lens excitation is so high that non-linear magnetisation curves of the magnetic material must be taken into consideration. The program can deal with up to five different materials compared with only one in Nasr's program and two in Lencová's. Table (3.2) shows the general data format for this program, with the symbol's explanations.

3.2.2 Data Preparation for Nasr's Programs

Nasr's programs VPLIN and VPSAT as mentioned above had no user manual or operator instructions. Therefore, general formats for data inputs were developed for these programs during the course of this study.

3.2.2.1 Program VPLIN

The essential steps, in the data preparation for Nasr's VPLIN program, are similar to that of Munro's M12 program. However, in case of the VPLIN program, two extra mesh lines are chosen as inner boundaries as explained in section (2.1.1.2.1). These inner boundaries divide the whole data region used for RUN1 into three parts representing RUN2, RUN3 and RUN4, for asymmetrical cases; and into two parts for symmetrical cases representing RUN2 and RUN3. The inner boundaries are chosen from the axial mesh lines i.e. perpendicular to the lens axis.

Table (3.3) illustrates the general data format for program VPLIN, with the symbol's explanations.

3.2.2.2 Program VPSAT

This program was developed, in its general form, to deal with both saturated and unsaturated magnetic lenses. For the saturation case, the non-linear relation between the relative permeability μ_r of the magnetic material and the flux density B (Table 2.1) is introduced in the iteration process.

The general data format, prepared for program VPSAT, is shown in Table (3.4), with the symbol's explanations.

3.2.3 Data Preparation for Lencová's Program AMAG

This program deals with both linear and saturation cases and can compute data of several excitations for the same run.

Through information provided by Mrs Lencová, and after repeated trials at the University of Aston's computers, sufficient experience was gained to draw up a general data format shown in Table (3.5), with the symbol's explanations.

3.4 Comparison of the Output Results of Computer Programs used in Calculation of Magnetic Field Distribution

In order to make a critical comparison of the capability of the above mentioned computer programs, special model lenses were devised for the purpose of revealing any inherent errors in the programs. Data inputs, for all the programs, were compiled with the same boundary conditions, and the same mesh layouts and mesh numbers were used.

The relevant flux density was computed, under non-saturation conditions, with the three programs M12, VPLIN and AMAG. The computation was repeated for the same lenses, under saturation conditions, utilising programs M13, VPSAT and AMAG. Furthermore, both cases of symmetry and asymmetry were considered in each comparison.

3.4.1 Asymmetrical Lens under Linear Condition

The rectangular single polepiece lens shown in figure 3.1 was one of the lenses used for these comparisons. The data was compiled from this lens with the same mesh layouts for the linear programs M12, VPLIN and AMAG according to tables 3.1, 3.3 and 3.5 respectively. In addition to the usual data, program VPLIN requires the inner boundaries to be fixed, as indicated in figure 3.1 .

The output results from the three programs are shown in figure 3.2 which indicates that for the same conditions and mesh layouts i.e. limited computer memory size, programs M12, AMAG as well as VPLIN with only one run produce almost identical results. However the VPLIN program, with four runs, provides for more meshes in the axial direction by introducing the inner boundaries, as explained in section (2.1.1.2.1), with only marginally more memory size. Consequently program VPLIN, produces a smoother curve with better overall results than the other two programs.

3.4.2 Symmetrical Lens under Linear Condition

Figure 3.3a shows the boreless double polepiece test lens (quarter section) designed for comparison purposes. In this figure, the symmetry plane is on the right i.e. the negative quarter is shown.

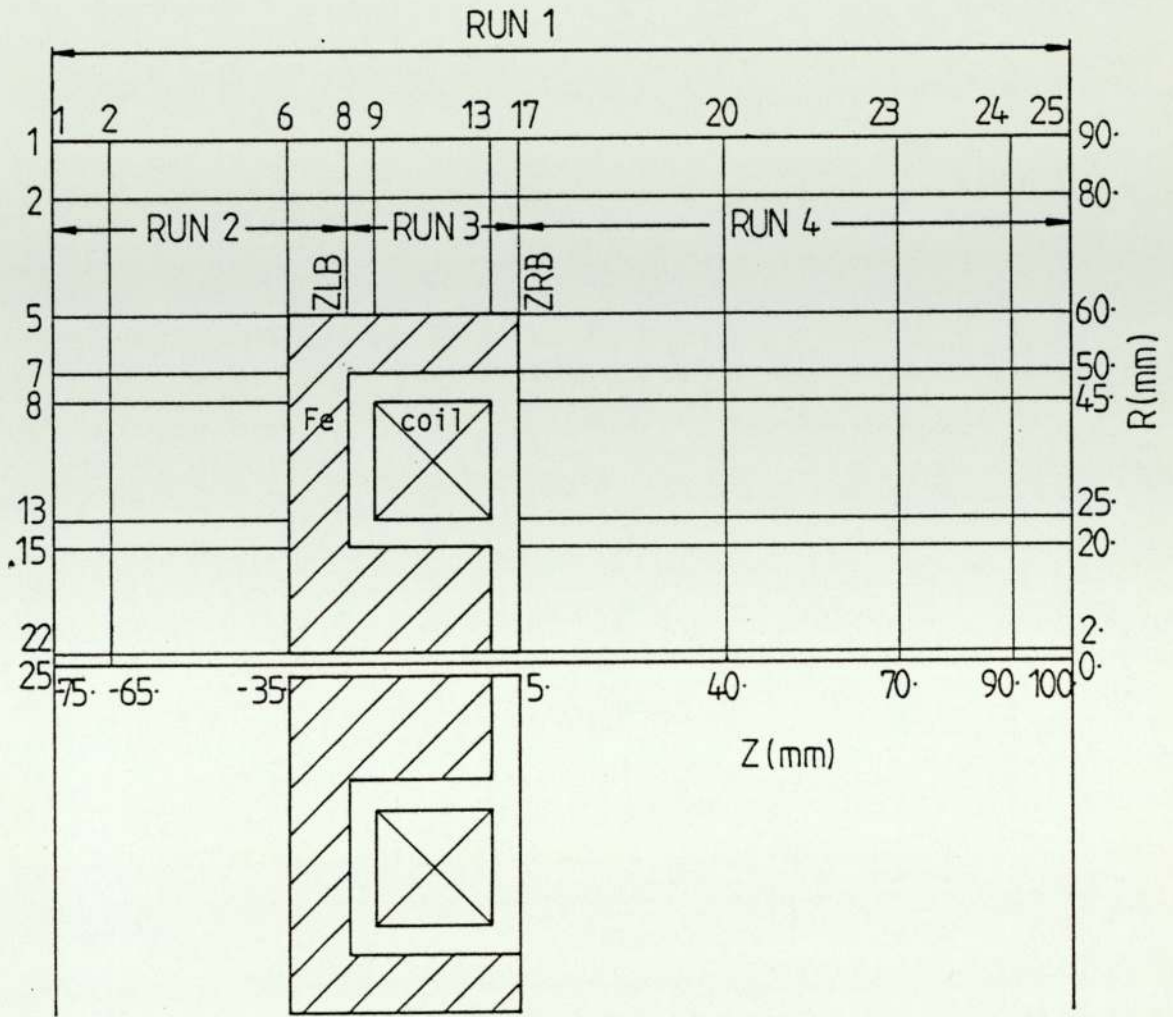
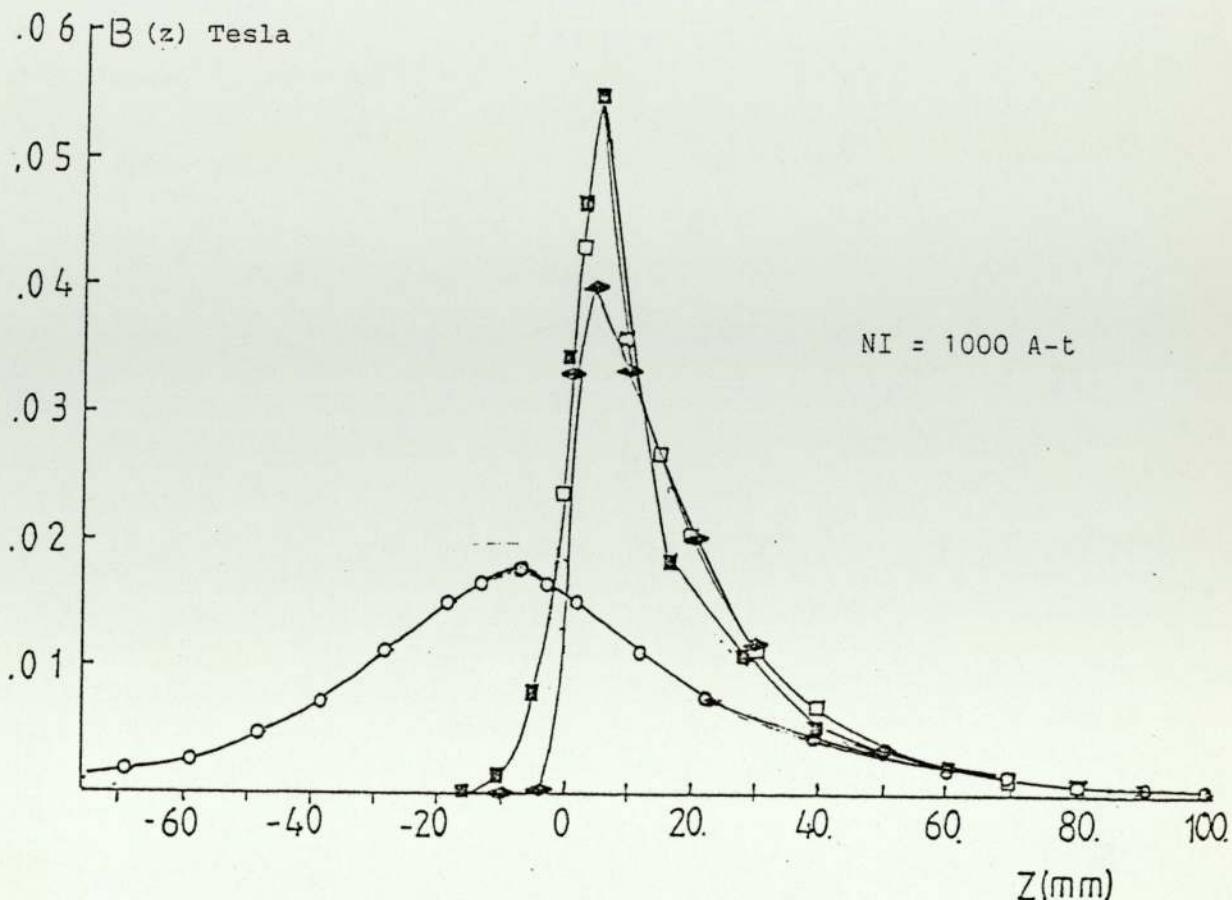


Figure 3.1 Rectangular single polepiece test lens with mesh distribution in Z and R directions and two inner boundaries, ZLB and ZRB, to be used in Nasr's programs.

The Regions for Runs 1, 2, 3 and 4 are also shown in the figure.



- Axial field distribution B_T Calculated with M12, Vplin and AMAG programs (25 x 25) meshes 14.8% loss in NI
- Axial field distribution B_T Calculated with Vplin (25 x 25) 4 runs
- ◆ Axial field distribution B_T Calculated with AMAG (69 x 90) 13.86% loss in NI
- B coil calculated with Biot Savart program

Figure 3.2 Comparison between the output results of axial flux density distribution (B_T) shown above of the single pole test lens shown in figure 3.1 with same mesh distribution and mesh number (25,25) M12, Vplin and AMAG give the same results, while Vplin with 4-runs gives a smoother curve but the same peak value. AMAG with the larger number of meshes (69 x 90) gives a much lower peak and smoother curve (since the number of meshes is increased in both Z and R directions) This boundary condition give a boundary loss in excitation. This loss had been overcome by surrounding the open boundary by 5mm thick high permeability iron sheet.

The boundaries are set just outside the lens, since the two poles can act like boundaries.

The data used for programs M12, VPLIN and AMAG are written according to tables 3.1, 3.3 and 3.5 respectively.

The output results are shown in figure 3.4 . As with the asymmetrical lens, the results obtained for the same mesh layouts with programs M12, AMAG and VPLIN (one run) are identical, while program VPLIN produces a smoother curve (with three runs). The three programs, with more mesh numbers, are expected to produce lower axial peak flux density values which are in better agreement with results predicted from equation (1.15). This was tested with AMAG program.

3.4.3 Asymmetrical Lens under Non-linear Condition

Al-Khashab's spherical single pole lens shown in figure 3.5 was used for the computation of magnetic field distribution under saturation condition. The lens was recomputed with correct boundary and redesigned with thick shrouds, to avoid boundary loss and leakage problems, as explained in section (4.4.1).

The data compiled from this lens, with the same mesh layouts, excitation and boundary conditions for non-linear programs M13, VPSAT and AMAG according to tables 3.2, 3.4 and 3.5 respectively. The corresponding output results are shown in figures 3.5 and 3.6.

The results, obtained from programs M13, VPSAT with only one run and AMAG, are almost identical. Program VPSAT with four runs produced better values, as shown in figure 3.5. This makes program VPSAT and

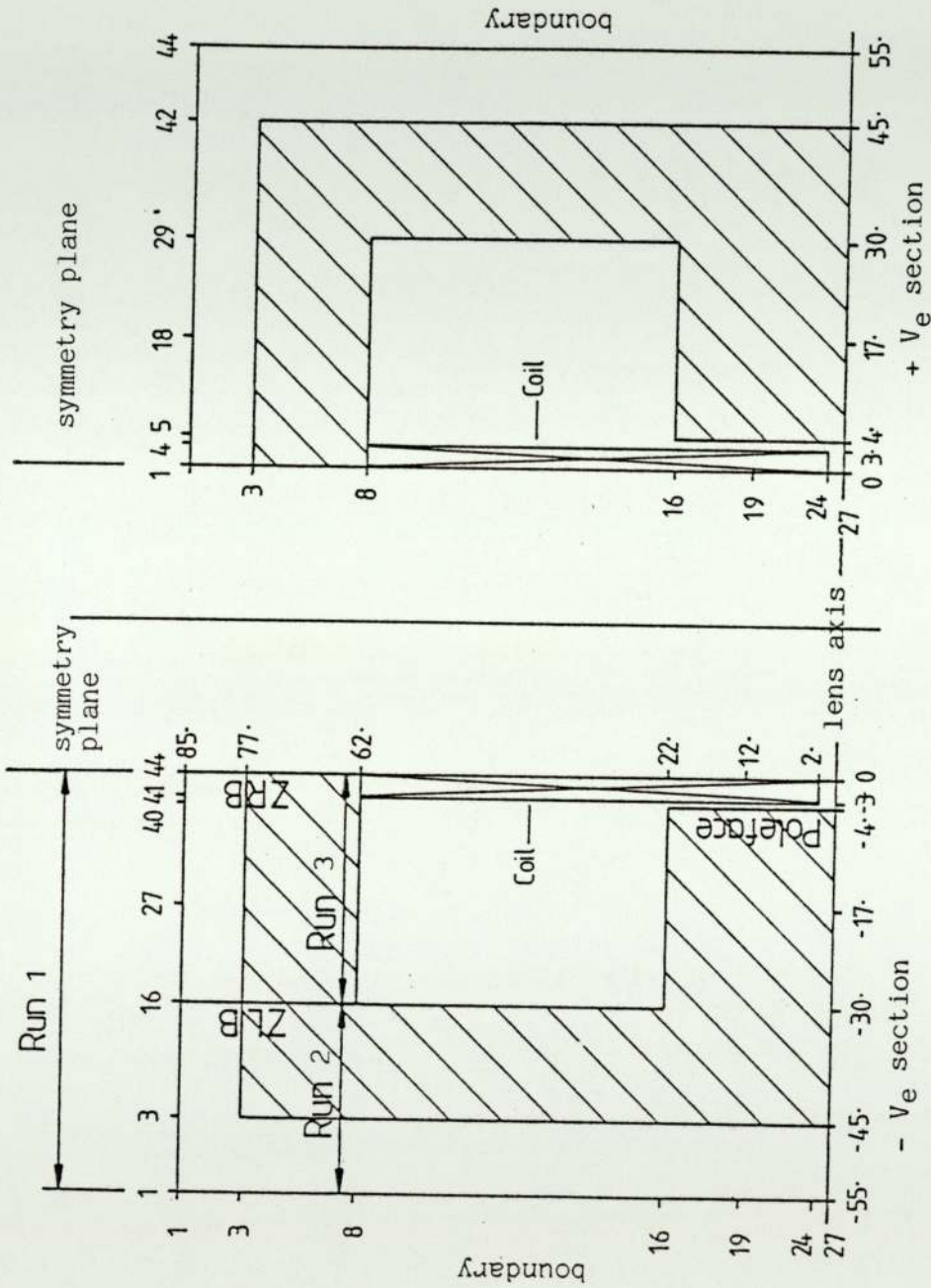


Figure 3.3a

Quarter section of rectangular double pole test lens to be used as data for Munro and Nasr's programs showing boundary and mesh distribution in Z and R direction and twin inner boundaries Z1B and ZRB to be used in Nasr's programs for further runs.

Figure 3.3b

Quarter section of rectangular double pole test lens showing the boundary and mesh distribution in Z and R direction, to be used as data for Lencová's AMAG program.

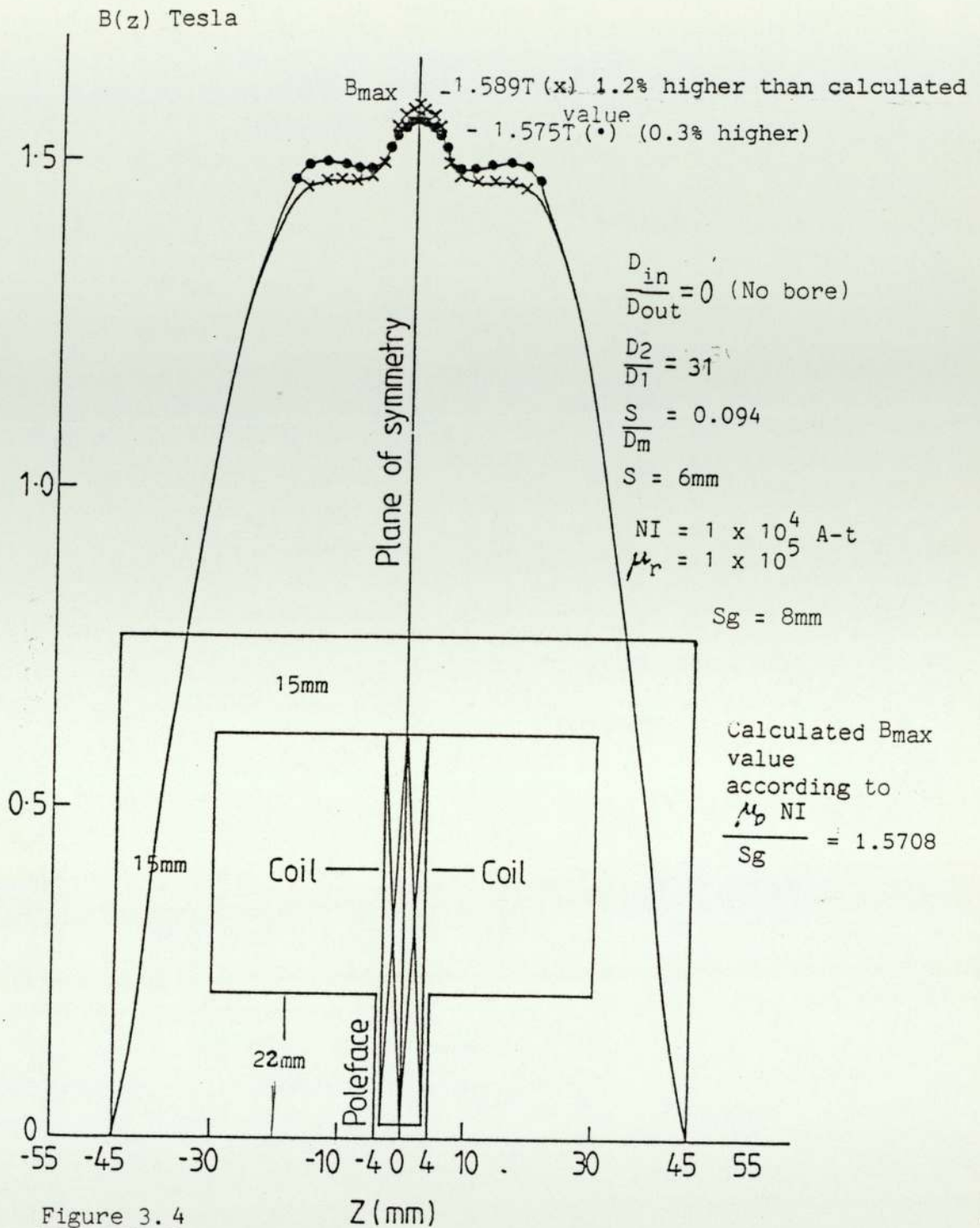


Figure 3.4

The axial flux density distribution of the rectangular double pole (test) lens under linear conditions using xxx (27 * 44) meshes for M12, VPLIN, AMAG and ●●● using 67 * 90 meshes for AMAG.

Note there is no difference in the output result of M12 VPLIN and AMAG when same number of meshes (27 * 44) is used while there is improvement in peak value when more meshes are used.

the corresponding linear program VPLIN more suitable for research laboratories with small store computers where the computer time is not as important as the memory store. Figure 3.6 shows the axial flux density distribution obtained by applying the three programs (M13, VPSAT, AMAG), (1) at given excitations of 1×10^4 A-t and (2) at given excitations of 1×10^5 A-t. A difference in the flux distribution behaviour is noticed inside the iron circuit at (1×10^5 A-t) between both M13, VPSAT and AMAG.

Experience shows that it is advisable for VPSAT program to choose the two inner boundaries remote from the coil region (i.e. remote from the region of high flux density) in asymmetric cases, or exclude the coil region from the final run.

Increasing the number of meshes, other things being equal, is expected to result in better values from all the programs. This was tested with AMAG program only.

3.4.4 Symmetrical Lens under Non-linear Condition

When the rectangular double pole test lens (quarter section) shown in figure 3.3a was used for the symmetrical lens under non-linear condition, it was noticed that the lens had 14% boundary loss in excitation and flux leakage at 1×10^5 A-t. The lens was redesigned with a correct boundary and very thick shrouds to show the behaviour of each program inside the magnetic circuit.

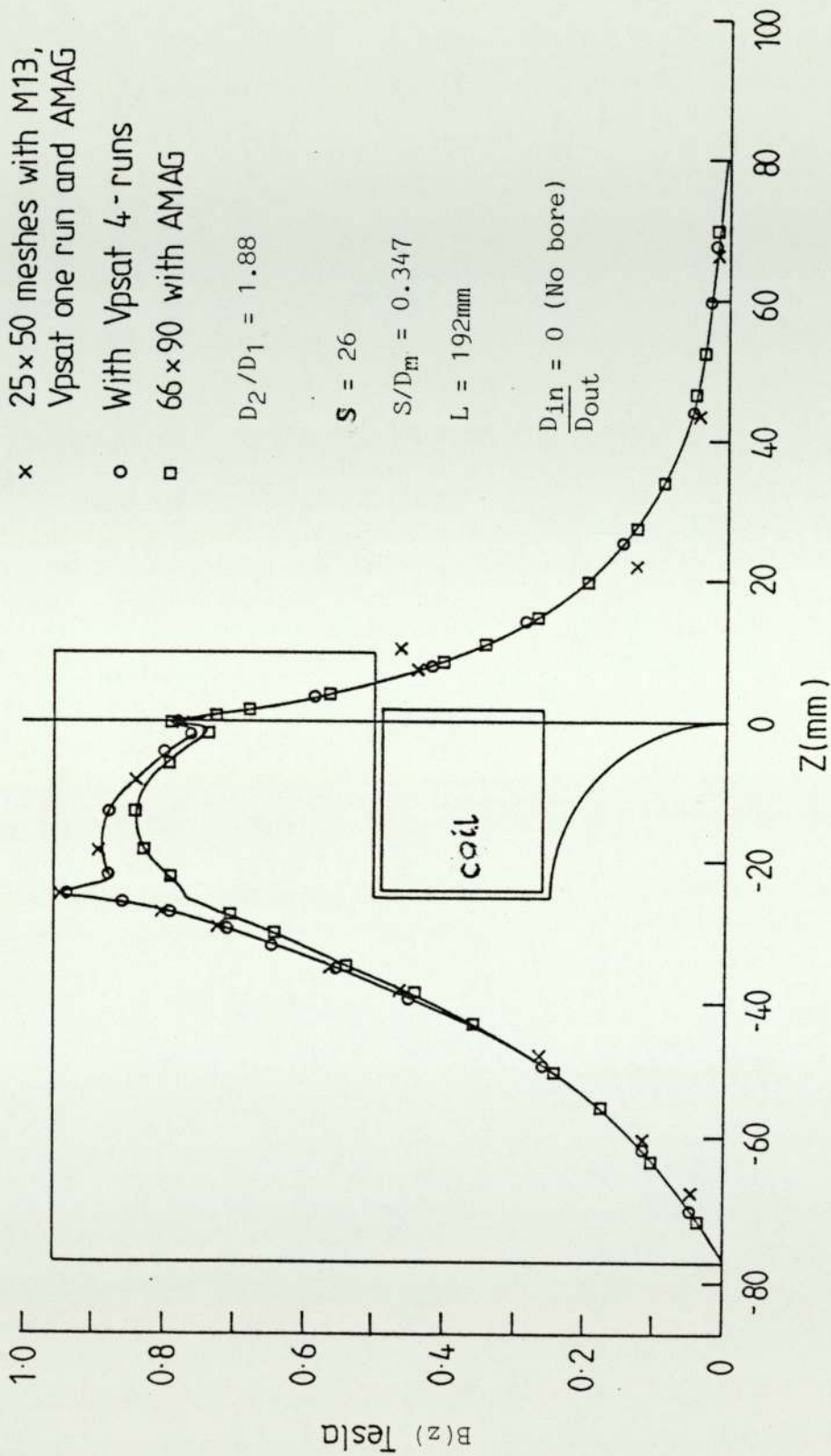


Figure 3.5 Axial flux density distribution of spherical single pole lens. Excitation of 10000 A-t. With coil of 598 mm². (Munro, Nasr and AMAG programs). Note the improvement at Z = -34 and Z = 0 with AMAG program with 66 x 90 meshes. (i.e the unusual shape of the flux distribution improved)

Output results of:

x 25 x 50 M13 and Vpsat one run

• 25 x 50 AMAG

o 60 x 90 AMAG

— Same result for all programs in (1)

Note the difference of the flux values inside the magnetic circuit between the results of M13, Vpsat and AMAG in (2) at 1×10^5 A-t, this difference is not noticed in 1×10^4 A-t in (1)

$$\frac{D_{in}}{D_{out}} = 0 \text{ (no bore)}$$

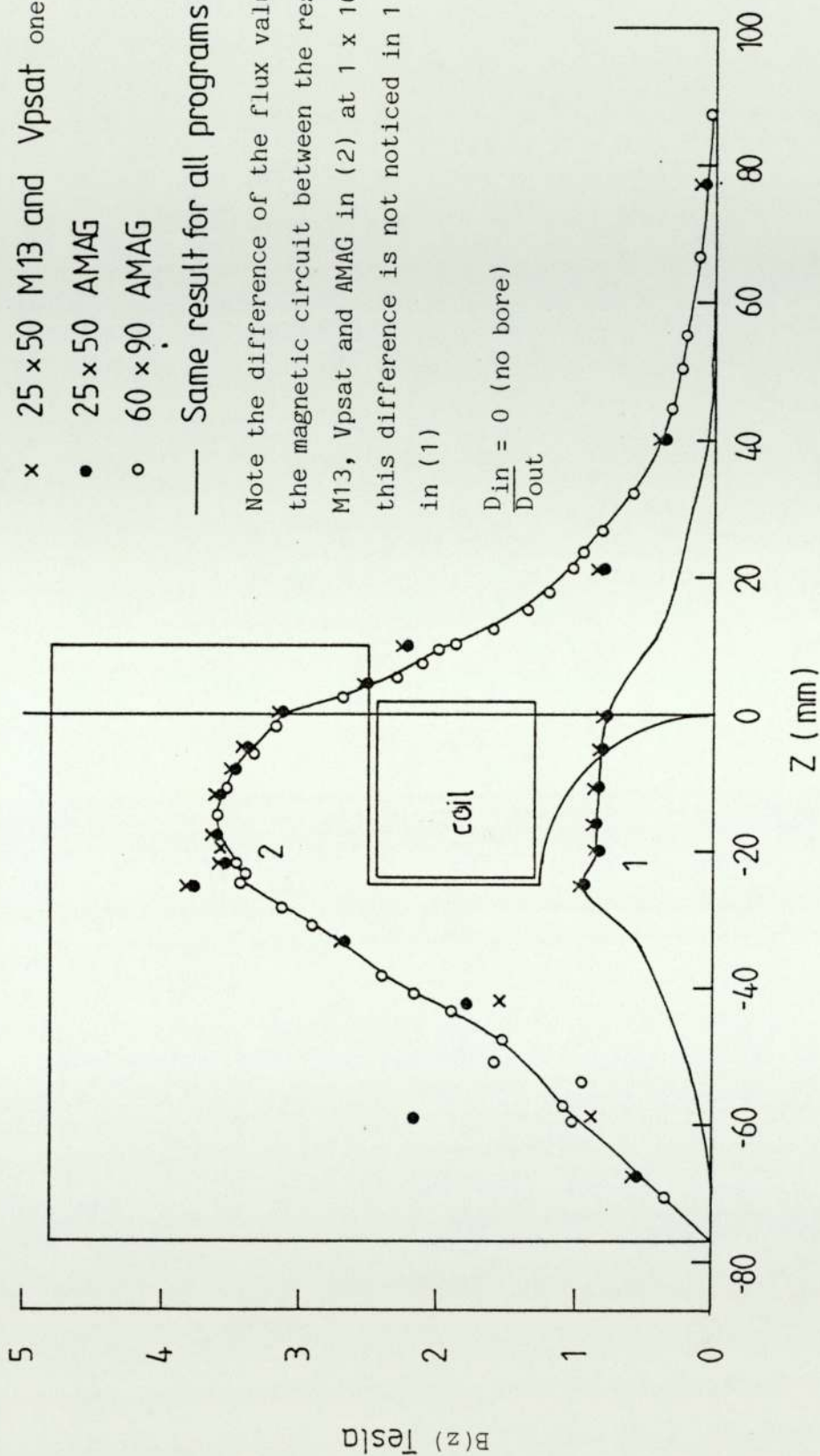


Figure 3.6 Axial flux density distribution of lens shown in figure (3.5).

(1) Excitation of 10,000 A-t. (2) Excitation of 100,000 A-t.

(Munro, Nasr and AMAG programs).

The data used with non-linear programs M13, VPSAT and AMAG were prepared according to tables (3.2), (3.4) and (3.5) respectively, while figures 3.7 and 3.8 indicate the corresponding outputs. It is advisable for VPSAT program data to choose the first inner boundary correctly; avoiding regions of high flux density, such as the regions which are close to the coil winding or the magnetic circuit otherwise wrong field results at that region will be obtained, or as has been advised by Nasr (1981) to exclude the coil region from the final run.

As with the previous cases, results obtained from programs M13, VPSAT with only one run, are almost identical except the field distribution inside the magnetic circuit is different in certain regions as shown in fig. 3.8 at 1×10^5 A-t, while this is not noticed in fig. 3.7 at 1×10^4 A-t. Program VPSAT with three runs produced a smoother curve. Also, increasing the number of meshes, keeping other conditions constant, is expected to result in better results from all the programs. Only AMAG program was tested with more meshes.

3.5 Computer core store and time required for running each program

Compilation of all the above programs has been made in Harris 800, and a critical comparison was not possible between Munro, Nasr and Lencová's program AMAG since the latter is designed originally for large capacity meshes using double procession technique. Table (3.6) shows the comparison.

Table (3.6) The computer core store and time required for compilation and running each program, and the number of iterations required under saturation condition

PROGRAM	COMPUTATION TIME (SECS)	STORE REQUIRED (KILO BYTES)	THE NO. OF MESHES	NO. OF ITERATIONS
M12	8.17	94	27*44	—
VPLIN	28.48	123	27*44	—
AMAG (LIN.)	64.30	236	27*44	—
M13	118.60	104	27*44	14
VPSAT	214.33	144	27*44	14
AMAG (SAT.)	600.24	236	27*44	9

3.6 Graphic Outputs

Figures 3.9 and 3.10 show the graphic outputs of Munro's M31 program.

The method used for this program is that the program finds, by linear interpolation between the computed flux values at points on the finite element mesh, a set of points with the required flux value. The flux line is then plotted by joining these points together with a series of straight-line segments.

To run program M31, data is required specifying the scale of plot and values of the flux lines to be plotted. The program also uses as data the mesh layout and polepiece geometry (as previously set for running program M12, M13 or the first run data from Vplin or VPSAT).

The above mentioned figures show the distribution of flux lines throughout the magnetic circuit for Al-Kashab's(1983) spherical single pole lens recomputed with the original shrouds (magnetic circuit) at an excitation of 10^5 A-t as shown in Figure 3.9. There is noticeable

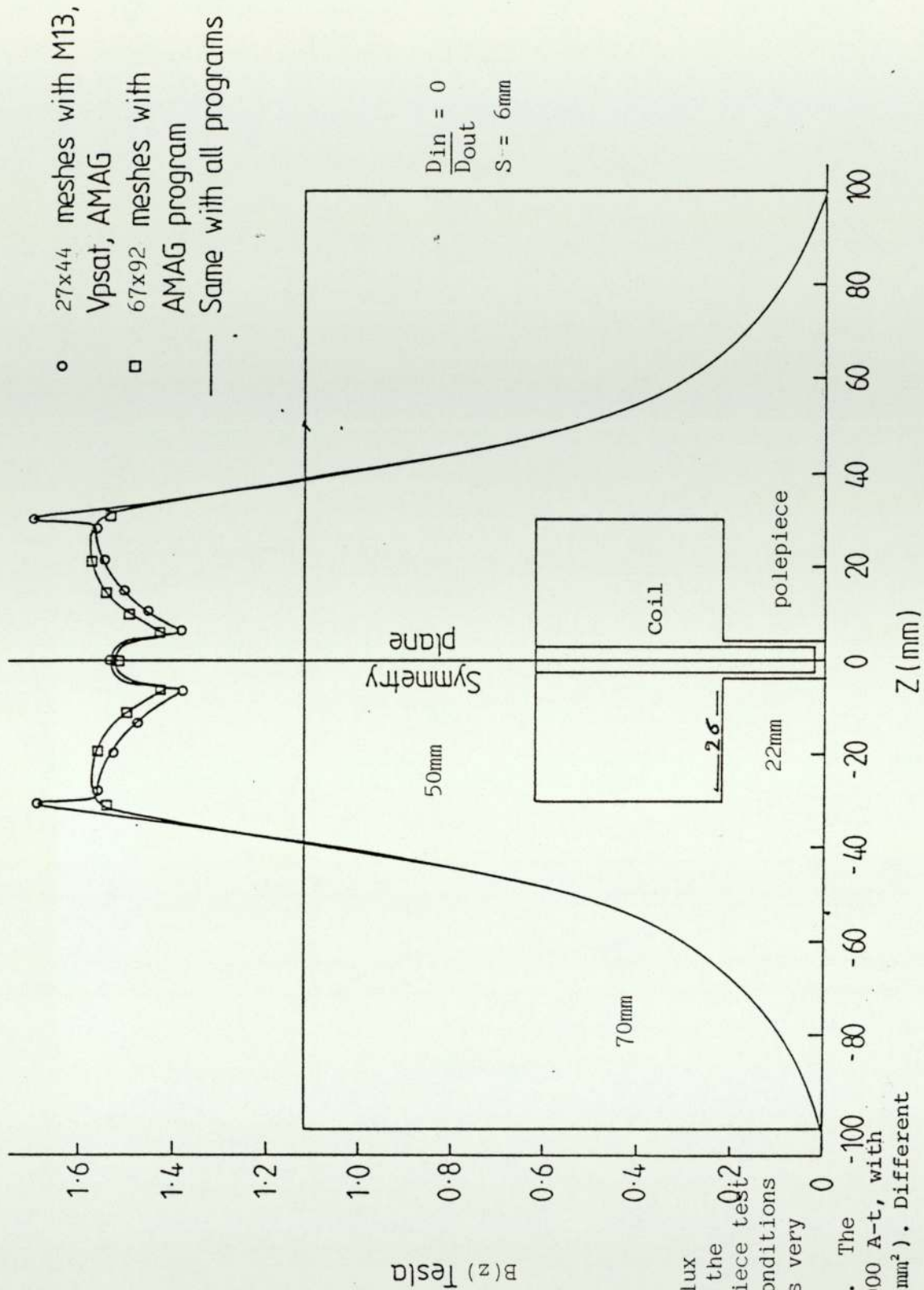


Figure 3.7 The axial flux density distribution of the rectangular double polepiece test lens under non linear conditions (the magnetic circuit is very large to show the field distribution inside it). The lens excitation is 10,000 A-t, with short solenoid ($6 \times 60 \text{ mm}^2$). Different programs are used.

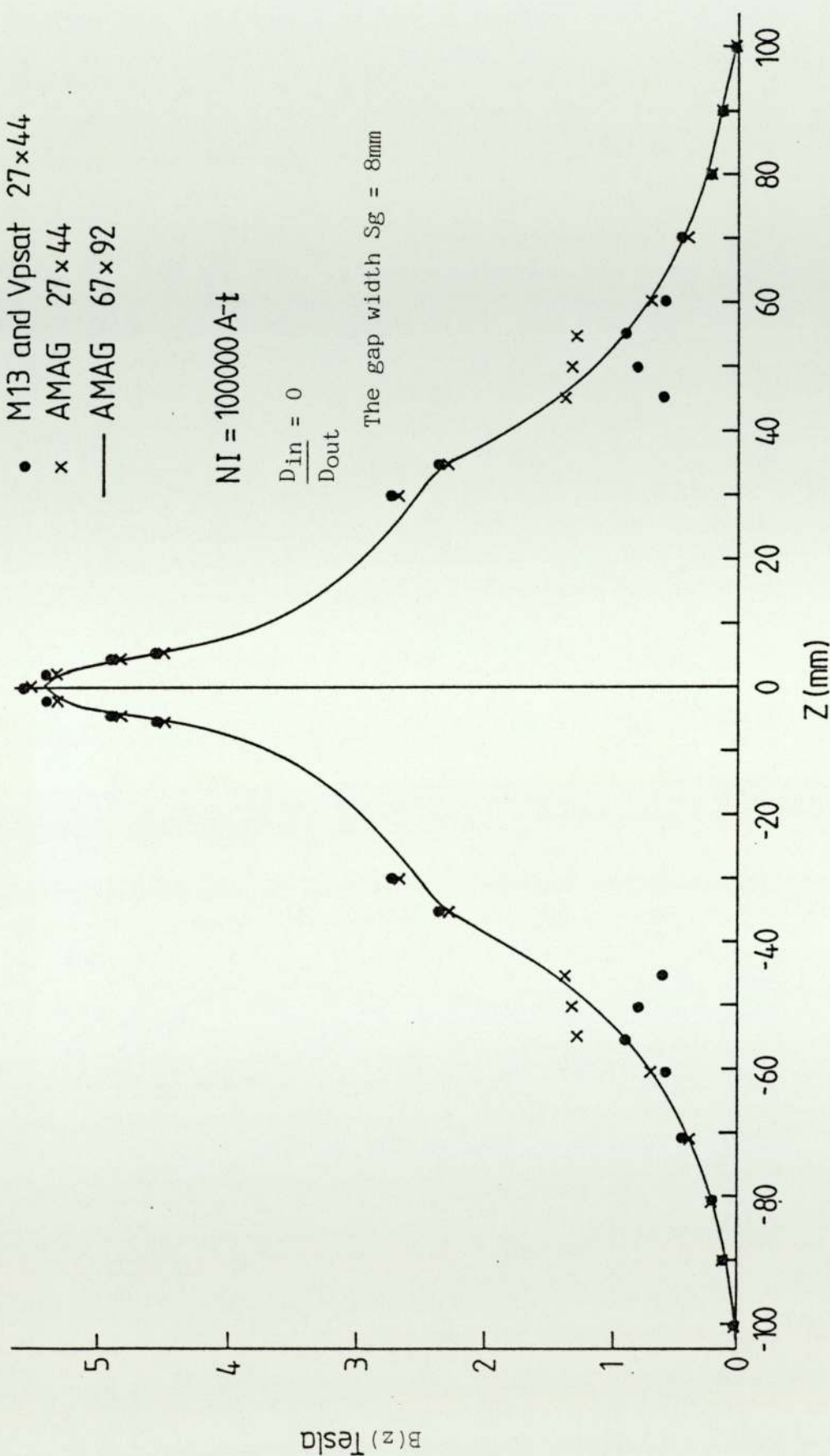


Figure 3.6 The axial flux density distribution of rectangular double polepiece test lens shown in (fig. 3.7) under non-linear conditions. Excitation of 100,000 A-t. With coil of $(6 \times 60\text{mm}^2)$. Munro, Nasr and AMAG programs are used. Note the difference in the field behaviour inside the magnetic circuit, between M13, Vpsat and AMAG programs and the improvement with more meshes.

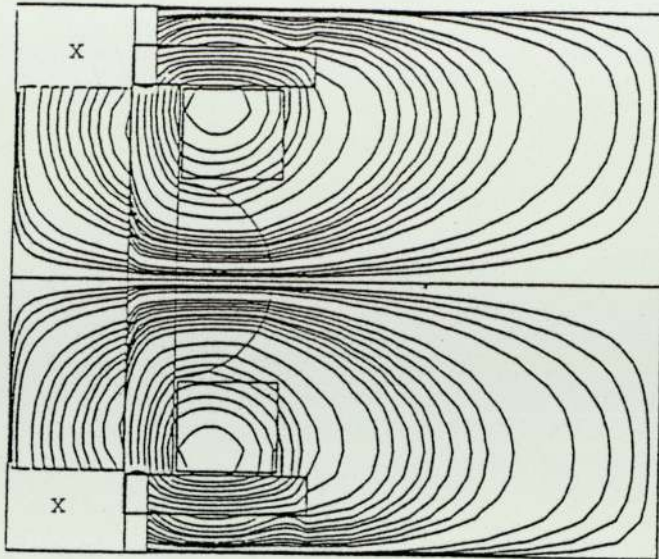


Figure 3.9 Distribution of flux lines throughout the magnetic circuit of Al-Khashab's (1983) spherical single pole lens, recomputed with original magnetic circuit. Note the excessive external leakage. Lens excitation is 10^5 A-t
x plotting error

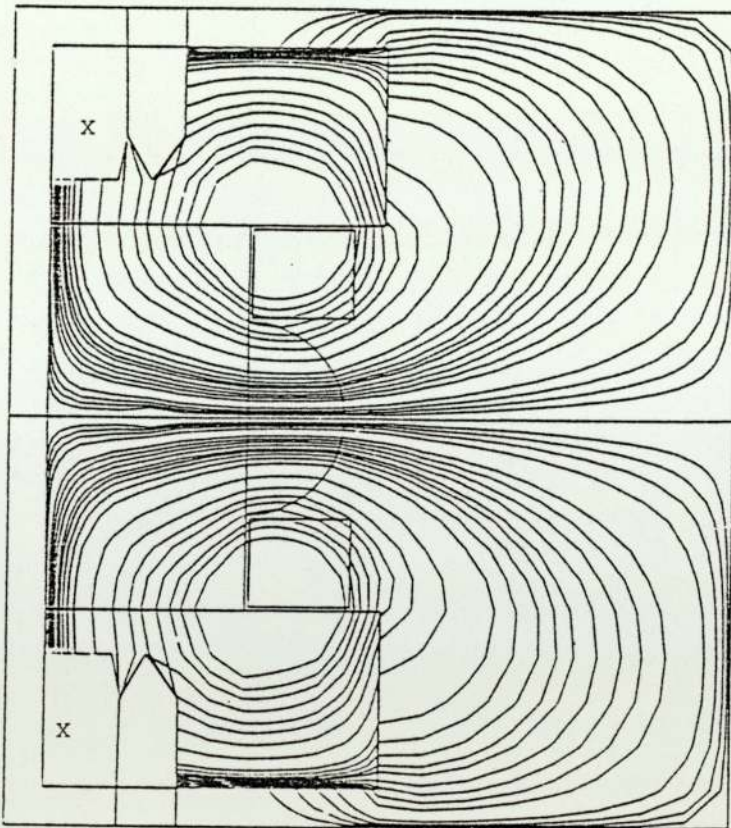


Figure 3.10 Distribution of flux lines throughout the magnetic circuit of the lens shown in figure 3.9 but redesigned with a thicker magnetic circuit leading to reduced external leakage field.

external flux leakage. Figure 3.10 shows how the leakage was reduced by thicker magnetic circuit (shroud) using the same mesh layout and the same excitation.

Figures 3.11, 3.12, 3.13 and 3.14 are graphic outputs for program AMAG. These outputs are given in form of IJ (indices) map, the indices I (in the radial direction) and J (in the axial direction) refer to the lower right-hand corner of the small quadrilateral.

The first map shown in figures 3.11 and 3.13., prints the type of material in each small quadrilateral which are 0 for air, 1 for the magnetic material and 3 for the coil. This map is useful for checking the input data, and checking that the position of each material is in its place.

Figure 3.11 and 3.13 show the distribution of material in the mesh for the recomputed Al-Khashab spherical single pole lens with the original shroud and with a thicker shroud.

Similarly the flux density map shown in figures 3.12 and 3.14 prints the coded value of iron flux density in each small quadrilateral lying in the magnetic material, the flux density is coded into numbers and letters in ascending order from 0 to 9 and A to Z.

The coding table is written below the flux map, as shown in figure 3.12. The iron flux density in the shroud reaches higher than 2.5 Tesla (P) and reaches 2.8 Tesla (S) in certain parts, while the polepiece tip is 2.6 Tesla (Q). Figure 3.14 shows that with the thicker shroud, the iron flux density is reduced in most parts of the

```

** PARAMETERS OF THE MESH: I1= 25, J1= 50, IRZ= 1250
++   OF F.E.M. SYSTEM: I2= 23, J2= 48, IS= 1104
** FURTHER PARAMETERS: MAPMAT= 0, MAPPSI= 0, LISTIR= 0, LISTFD= 0, IDISC= 0

```

***** DISTRIBUTION OF MATERIALS IN MESH

INDEX I	INDEX J									
	5	10	15	20	25	30	35	40	45	50
2	-	0	0	0	0	0	0	0	0	0
3	-	0	0	1	1	1	1	1	1	1
4	-	0	0	1	1	1	1	1	1	1
5	-	0	0	1	1	1	1	1	1	1
6	-	0	0	1	1	1	1	1	1	1
7	-	0	0	1	1	1	1	1	1	1
8	-	0	0	1	1	1	1	1	1	1
9	-	0	0	1	1	1	1	1	1	1
10	-	0	0	1	1	1	1	1	1	1
11	-	0	0	1	1	1	1	1	1	1
12	-	0	0	1	1	1	1	1	1	1
13	-	0	0	1	1	1	1	1	1	1
14	-	0	0	1	1	1	1	1	1	1
15	-	0	0	1	1	1	1	1	1	1
16	-	0	0	1	1	1	1	1	1	1
17	-	0	0	1	1	1	1	1	1	1
18	-	0	0	1	1	1	1	1	1	1
19	-	0	0	1	1	1	1	1	1	1
20	-	0	0	1	1	1	1	1	1	1
21	-	0	0	1	1	1	1	1	1	1
22	-	0	0	1	1	1	1	1	1	1
23	-	0	0	1	1	1	1	1	1	1
24	-	0	0	1	1	1	1	1	1	1
25	-	0	0	1	1	1	1	1	1	1

LINEAR APPROXIMATION

CURRENT DENSITY IN COIL= 1.672E+01 A/MM**2
 AREA OF EXCITATION COIL 598.000 MM**2

Figure 3.11 AMAG IJ graphic output of Al-Khashab's (1983) spherical single pole lens recomputed with original magnetic circuit; the output shows the distribution of the materials in the mesh (0 = vacuum, 1 = iron, 3 = coil)

***** MAP OF IRON FLUX DENSITY (TESLA)

BMAX= 3.3433E+00 TESLA FOR J= 24 AND I= 13
 BMIN= 9.2590E-01 TESLA FOR J= 6 AND I= 0

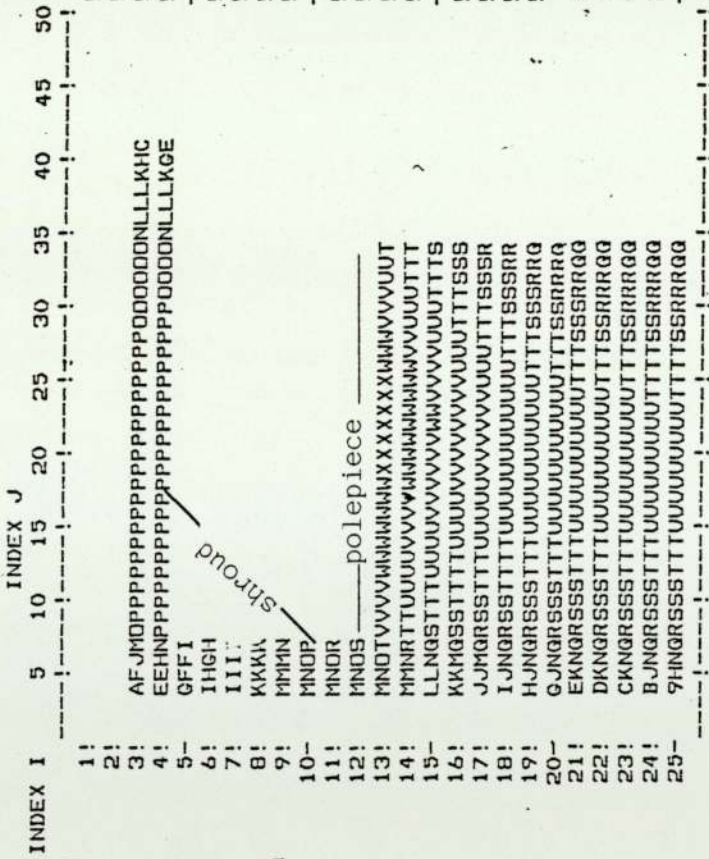


Figure 3.12 AMAG.IJ
 graphic output for
 mapping iron flux
 density of the lens
 in figure 3.11.
 Note the iron flux
 density is very high
 at the magnetic
 circuit

$$NI = 1 \times 10^5 \text{ A-t}$$

$$\frac{D_{in}}{D_{out}} = 0$$

Numbers from 0 to 9 mean iron flux
 density more than zero Tesla and less
 than 1 Tesla
 Letters from A to X mean flux density
 more than 1 Tesla and more than 3.3

Tesla

MEANING OF LETTERS: (Flux density in Tesla)	
'C'	0.00
'4'	0.50
'9'	1.00
'E'	1.50
'J'	2.00
'0'	2.50
'T'	3.00
'0'	0.10
'5'	0.60
'A'	1.10
'F'	1.60
'K'	2.10
'P'	2.60
'U'	3.10
'1'	0.20
'6'	0.70
'B'	1.20
'G'	1.70
'L'	2.20
'Q'	2.70
'V'	3.20
'2'	0.30
'7'	0.80
'C'	1.30
'H'	1.80
'M'	2.30
'R'	2.80
'N'	3.30
'3'	0.40
'8'	0.90
'D'	1.40
'I'	1.90
'N'	2.40
'S'	2.90
'X'	3.40

***** MAP OF IRON FLUX DENSITY (TESLA)

BMAX= 4.0192E+00 TESLA FOR J= 22 AND I= 13
 BMIN= 5.8217E-02 TESLA FOR J= 3 AND I= 24

INDEX J

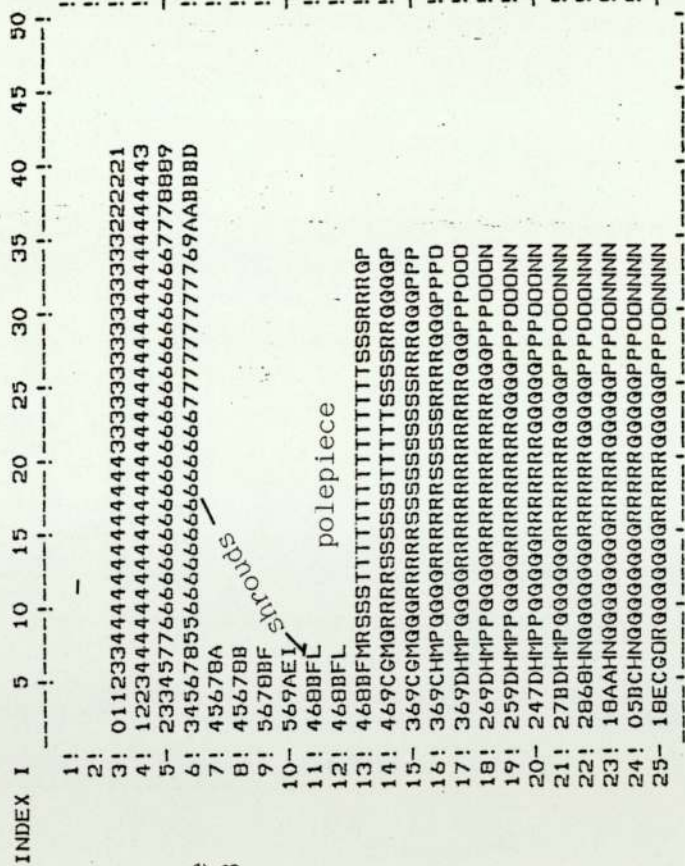


Figure 3.14

AMAG IJ graphic output map of iron flux density of the lens in figure 3.13 (thicker shrouds). Note the higher flux density in the polepiece region. Note also how the iron flux density is reduced in the shrouds.

$$NI = 10^5 \text{ A-t}$$

$$\frac{D_{in}}{D_{out}} = 0$$

Numbers 0 to 9 mean iron flux density more than 0 Tesla and less than 1.34 Tesla

Letters A to T mean iron flux density more than 1.34 Tesla to flux density of more than 3.89 Tesla

MEANING OF LETTERS: (Flux density in Tesla)

'C'	0.00	<'0'<	0.13	<'1'<	0.27	<'2'<	0.40	<'3'<	0.54	<'4'<
'4'<	0.67	<'5'<	0.80	<'6'<	0.94	<'7'<	1.07	<'8'<	1.21	<'9'<
'9'<	1.34	<'A'<	1.47	<'B'<	1.61	<'C'<	1.74	<'D'<	1.88	<'E'<
'E'<	2.01	<'F'<	2.14	<'G'<	2.28	<'H'<	2.41	<'I'<	2.55	<'J'<
'J'<	2.68	<'K'<	2.81	<'L'<	2.99	<'M'<	3.08	<'N'<	3.22	<'O'<
'O'<	3.35	<'P'<	3.48	<'Q'<	3.62	<'R'<	3.75	<'S'<	3.89	<'T'<

shroud to a value between 0.13 Tesla (O) and 1.7 Tesla (D), while in the polepiece tip it is increased to 3.08 tesla (N). The iron flux density map is also very useful to detect the IJ position of B_{\max} .

In figure 3.12 B_{\max} is equal to 3.34 Tesla (X) while in figure 3.14 B_{\max} is equal to 3.89 Tesla (T).

This study is showing that both M31 graphic output and AMAG maps can be used in complementary basis since in the first case the plots are related to r and z coordinates, therefore they give the actual polepiece shape and give a general idea about flux behaviour, while in the second case the maps are related to IJ indices and give more specific and quantitative information about the iron flux density (keeping in mind that this useful information can be obtained even in the absence of plotting facilities).

CHAPTER FOUR

DIFFICULTIES WITH THE FINITE ELEMENT METHOD

CALCULATIONS

4.1 General difficulties

During the course of this study, it was possible to pinpoint some common errors in computer aided magnetic lens design. These errors can be, generally, classified under two different headings; the first can be ascribed to factors inherent in the finite element method itself, while the second is related to factors inherent in the process of lens design which has, in some instances, led research workers into erroneous conclusions.

4.2 Factors Affecting the Accuracy of the FEM

Previous research workers have drawn attention to some of the limitation of FEM, when applied to magnetic field calculations. Thus Hill and Smith (1980) have pointed out that, for a single pole lens, the mesh layout is critical. They showed that for the same lens geometry, different mesh layouts give widely varying results for the same excitation.

Craven and Scott (1985) have also shown that large discrepancies in optical properties may be caused by what appear to be small variations in the axial field calculation, due to inherent limitations of Munro's programs. These errors are almost certainly due to the use of an unfavourable mesh distribution.

The effects of the boundary and mesh numbers were also discussed by Nasr (1981). Nasr minimised the boundary problems associated with the FEM programs designed earlier by Munro (1971). Nasr attributed the improvements, obtained through his improved programs, to the increased mesh numbers used. However, as explained earlier in section 2.1.1.2.1, Nasr's programs use more meshes in the axial direction only. This study has shown that the boundary effect is greater in open structures like iron free coils and partially open structures, like single pole lenses under linear conditions. However the boundary effect is not serious in conventional double pole lenses under linear condition, since the magnetic circuit has high permeability under linear condition and $A=0$ outside the magnetic circuit.

Under saturation condition the boundary setting is important in all cases i.e. even in double pole lenses, since the external leakage flux can be often high under saturation conditions. If this is the case, setting the boundary too close to the iron casing may cause boundary loss in excitation.

4.2.1 The Effect of Mesh Distribution

To show specifically the effect of mesh distribution, a lens of known field distribution, shown in Figure 4.1, was chosen. This lens is an unsaturated symmetrical double polepiece lens. The maximum flux density, B_m , at the centre of the air gap S_g , separating the parallel faces of the two polepieces is given by equation (1.15).

When equation (1.15) was applied to Munro's double pole lens (quarter section) shown in figure 4.1, ($S_g = 10$ mm, $D = 10$ mm), B_m was 0.0500 Tesla at 480 A-t. Munro (1975) has computed B_m according to the mesh

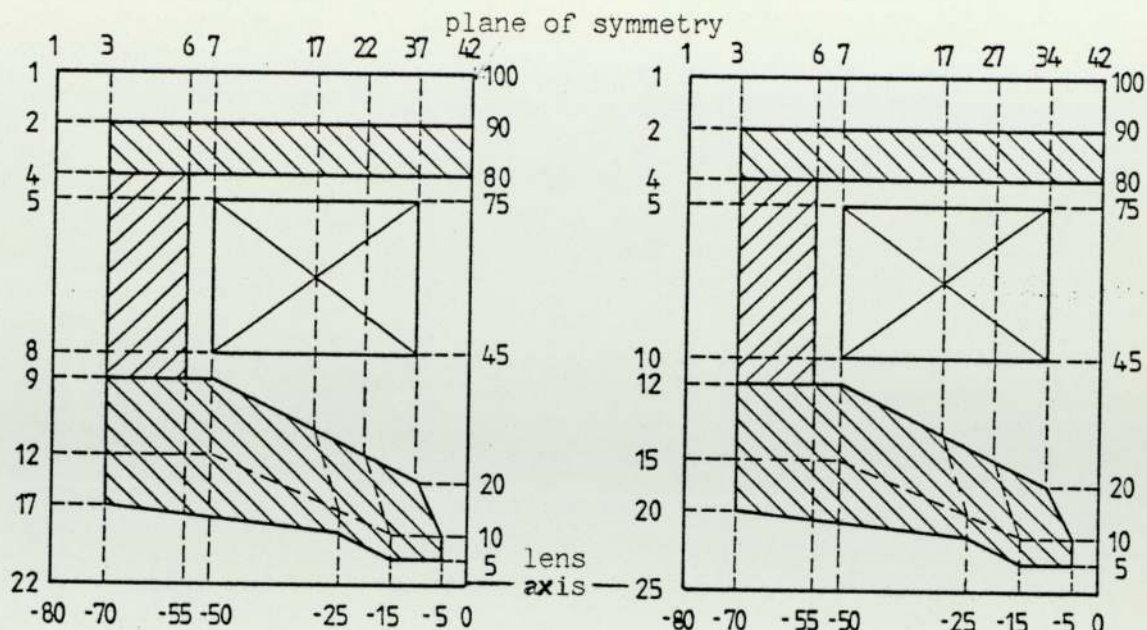


Figure 4.1 Munro's (1975) double pole lens (quarter section) with original mesh distribution. This figure shows that the meshes are concentrated at the pole-
 B_z (T)

Figure 4.2 New mesh distribution for figure (4.1). The number of radial meshes defining the pole piece profile and coil winding increased keeping the original distribution of the other parts constant

1. Munro's results
 $(B_m = 0.0519T)$
2. Results according to the mesh arrangement of figure (4.2)
 $(B_m = 0.0501T)$

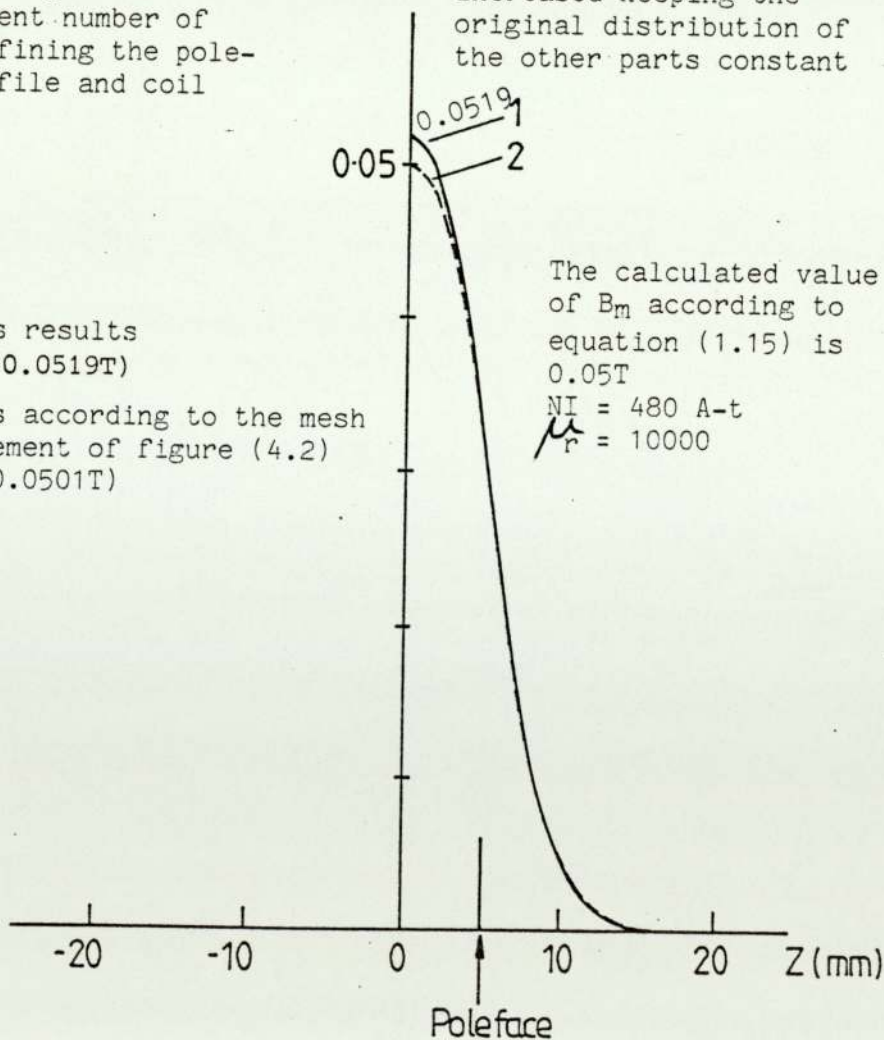


Figure 4.3 Two axial field distribution for Munro's lens note the difference in the B_m value when the mesh arrangement is slightly changed.

distribution shown in the figure and obtained a result of 0.0519 Tesla which is about 3.6% higher. A further step, taken in this study, was to rearrange the mesh distribution of Munro's lens in the R direction and Z direction as shown in figure 4.2. When B_m was recomputed, according to the new mesh arrangement, a result of 0.0501 Tesla was obtained which is in agreement with the value obtained from equation (1.15).

The results of the axial field computations for the two cases are shown in figure 4.3 i.e. that of Munro's original mesh distribution as well as the new mesh arrangement suggested in this study. Notice the effect of the mesh distribution is shown in the maximum flux density in the gap between the two poles only.

The same procedure was applied to the symmetrical double polepiece lens designed by Cleaver (1978). This lens, shown in figure (4.4), (quarter section) has an air gap S_g of 10 mm, an axial bore diameter D of 5 mm and is excited by a solenoid. Cleaver used Munro's programs for computing the lens field distribution under both saturation and non-saturation conditions. The mesh distribution used for the computations is, unfortunately, not indicated in Cleaver's published results. The B_m value obtained by Cleaver, under non-saturation conditions at 10^4 A-t was 1.29 Tesla which is 8.4% higher than the value of 1.19 Tesla calculated from equation (1.15). The computations were repeated, in this study, at the same excitation and according to the mesh distribution shown in figure 4.5. The same program used by Cleaver was applied. The B_m value thus obtained was 1.20 Tesla which is only 0.8% higher than the calculated value. Thus the error was reduced to an almost negligible amount, by using a convenient mesh distribution.

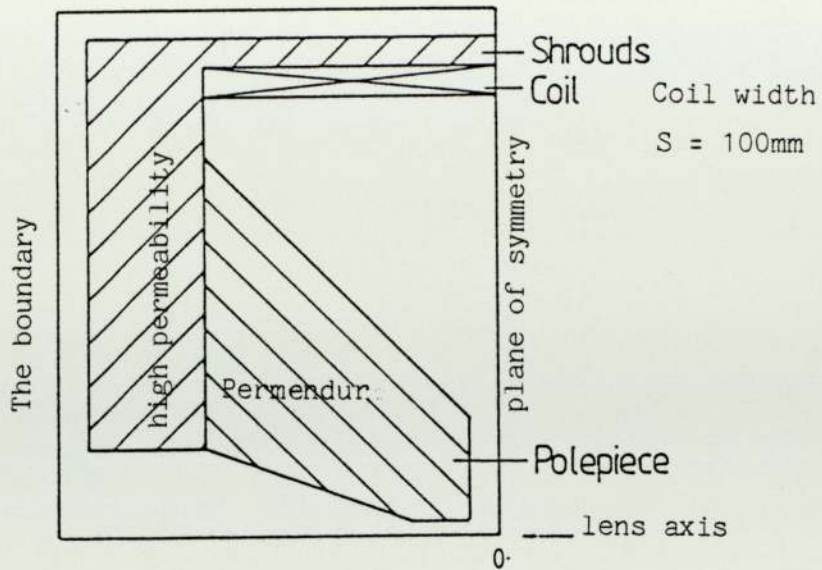


Figure 4.4
Cleaver's (1978) double pole lens (quarter section only) lens with high permeability shroud and permendur polepieces ($S_g = 10\text{mm}$, $D = 5\text{mm}$)

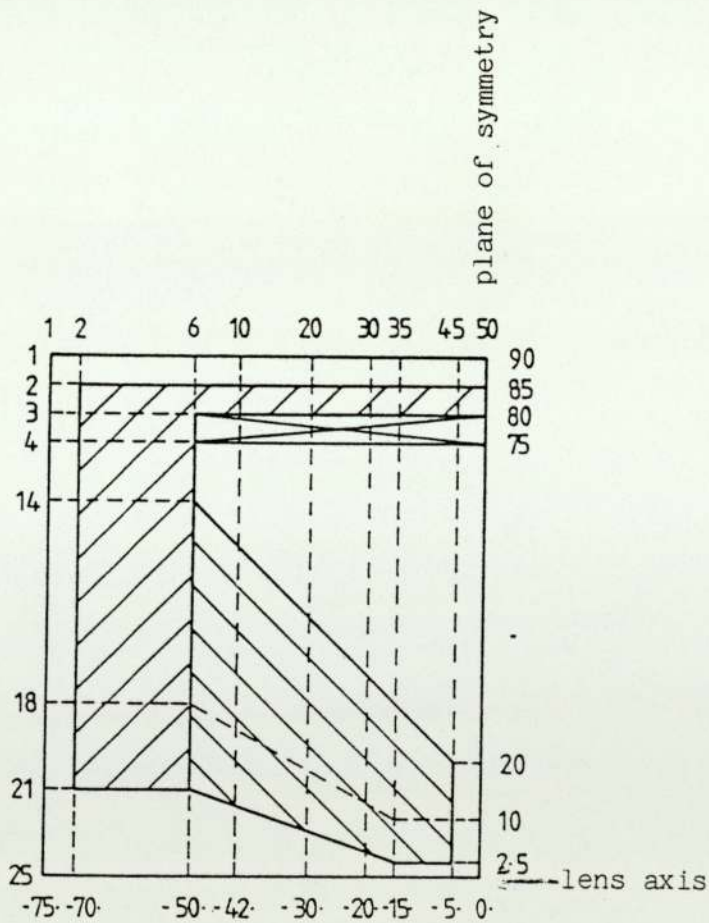


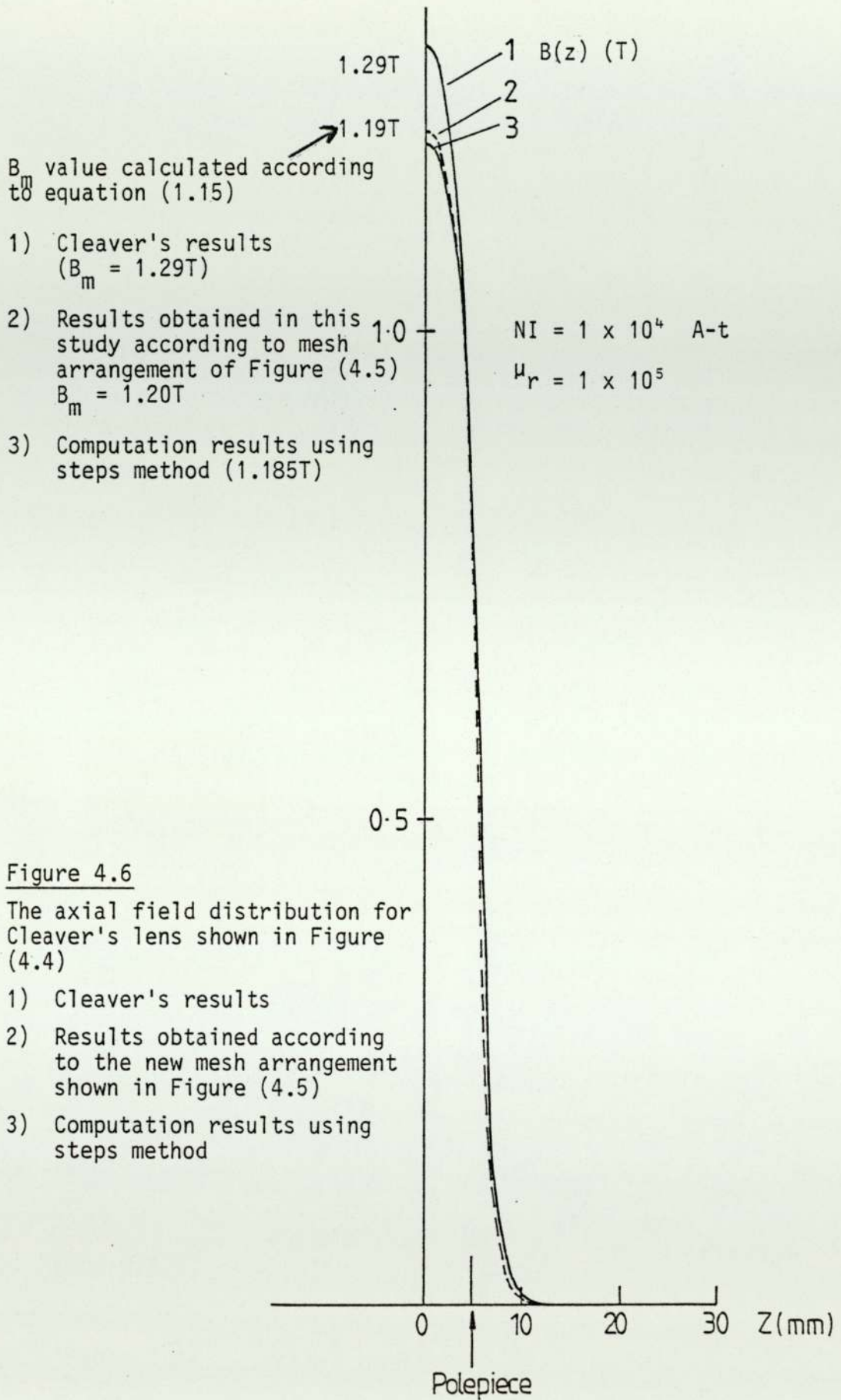
Figure 4.5
New mesh distribution for Cleaver's (1978) lens. It can be noticed that the mesh distribution is changing gradually, and special attention has been paid to define the polepiece profile

Figure 4.6 indicates the axial field distribution computed by Cleaver and that computed for the same lens, but according to the mesh distribution suggested in this study. It can be noticed in figure 4.6 that the mesh distribution have effect on the B_m value at the gap while there is not significant effect in other regions.

The above two examples, of field calculations under non-saturation conditions, indicate that the distribution of the meshes, apart from their numbers, have a significant effect on the computed flux density at the peak region. To obtain high accuracy, the mesh length should change gradually. Abrupt changing of the mesh length should be avoided, bearing in mind that more mesh points are needed near the two polepieces.

The errors detected in the Munro and Cleaver's computations referred to above are due to their mesh arrangements, because meshes have been concentrated at the polepiece region, at the expense of other lens parts.

The effect of the mesh arrangement, on field calculations under saturation conditions, was also studied. Cleaver's lens, shown in figure 4.4 was again utilised for this purpose. The lens has a shroud of very high permeability, as suggested by Cleaver. Figure 4.7 shows the axial field distribution results, computed at 90×10^3 A-t using Munro's saturation program. Cleaver's results, using the same computer program, are also shown. In the non-critical region, outside the air gap region, there is excellent agreement. However in the critical air region the difference between the two sets of results is obvious. Thus B_m is 3.58 according to Cleaver's computation which



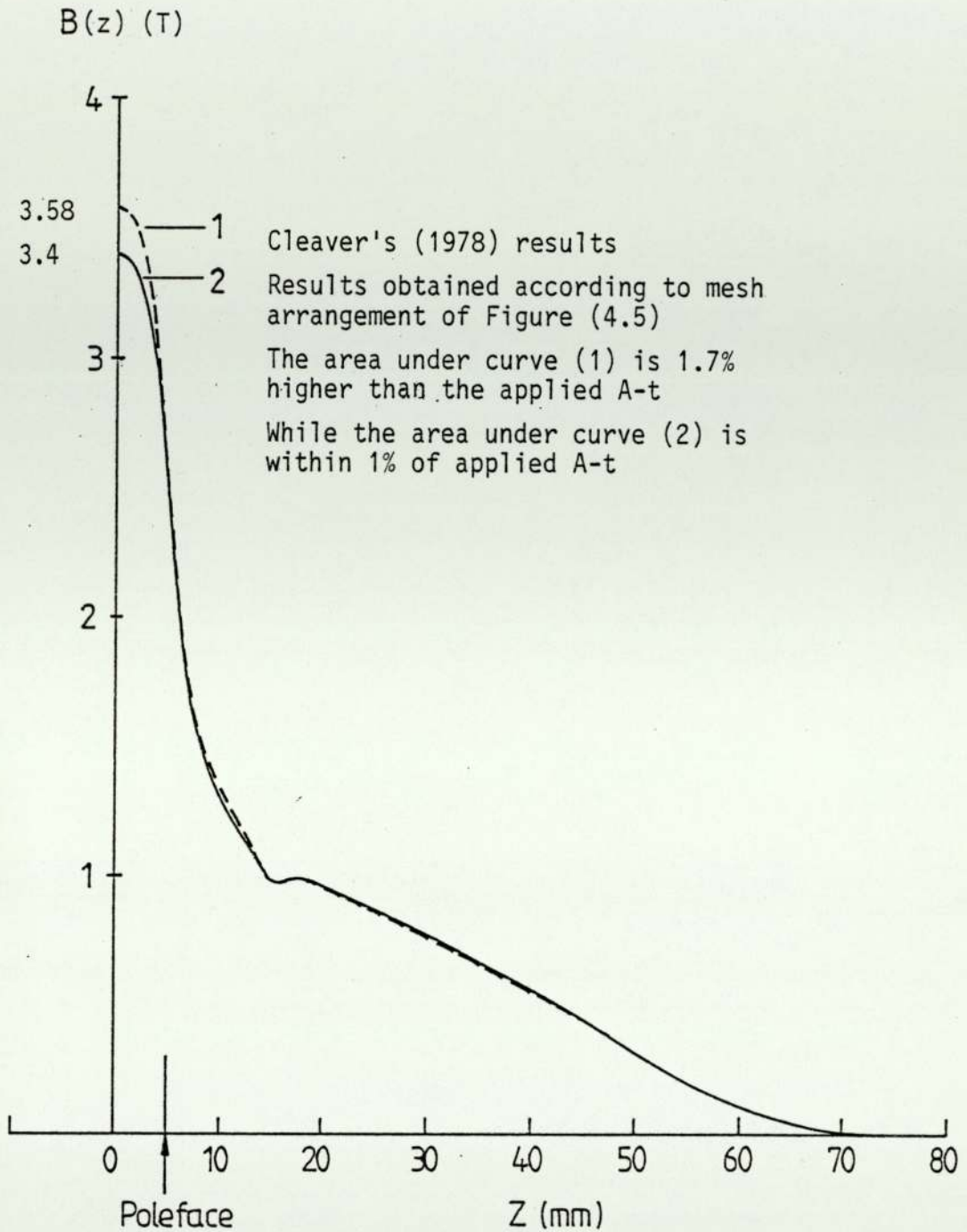


Figure 4.7

The axial field distribution for Cleaver's lens (Figure 4.4) under saturation condition (9×10^4 A-t) showing (1) Cleaver's results (2) results obtained in this study according to the mesh arrangement shown in Figure (4.5)

is about 5.4% higher than the B_m value of 3.4 Tesla computed from the mesh distribution shown in figure 4.5. When the computation was carried out using step method (changing the polepiece shape into an artificial shape which will give rectangular meshes), the results were in a good agreement with the results obtained in this study.

The area under Cleaver's axial field distribution curve is 1.7% higher than the corresponding $A-t$ applied, while the area under the new mesh arrangement curve is within 1% of $A-t$ applied, i.e. the main influence is in the B_m value in the gap region.

Another example of the mesh distribution effect on magnetic field calculations, under saturation conditions, was revealed in Christofides' (1982) single pole lens shown in figure 4.8.

According to Christofides' (1982), the peak axial flux density of the lens, computed by Munro's saturation program M13, is 26% higher than the experimentally measured value. Christofides in his thesis thought that Munro's program had some "inherent inaccuracies" and these, combined with "possible experimental errors, caused by the finite size of the Hall probe as well as possible variations between the magnetic properties of the material used in the experimental lens (Swedish iron) and the soft iron assumed in computing", have caused the large discrepancy between the experimental and computed values.

This study has shown that Christofides' postulations were not correct and his experimental results are in fact compatible with computations, correctly carried out, by Munro's program M13. The problem had arisen, purely and simply, from the inadequate mesh layout used by Christofides. When a convenient mesh layout was used, results are

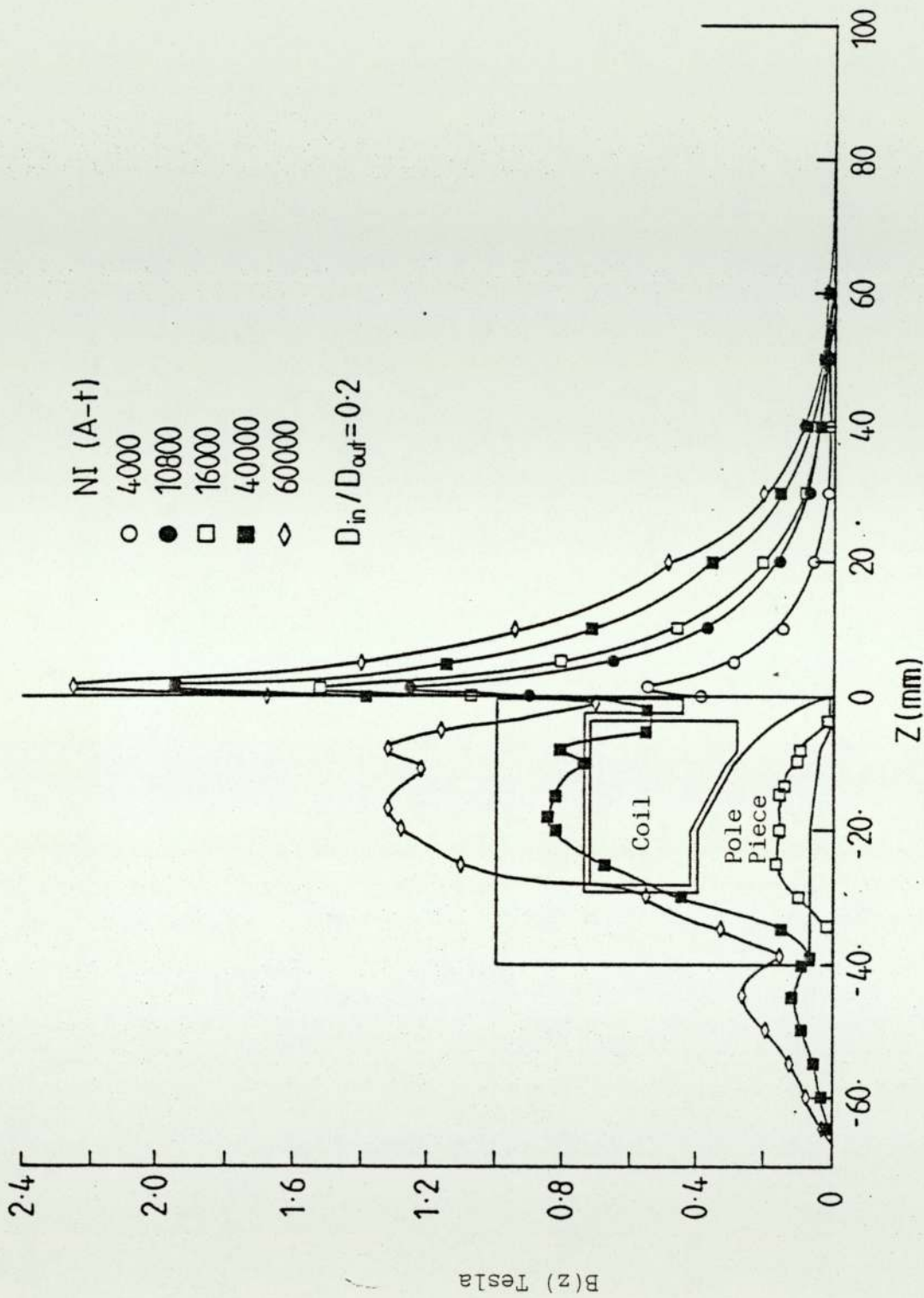


Figure 4.8 Recalculated axial field distribution for Christofides (1982) lens (Hermes II) at different excitations using optimised mesh distribution and the same number of mesh points

shown in figure 4.8 the computed peak flux density value was in very good agreement with the experimental results as shown in figure 4.9 .

The effect of mesh layout on calculated results is also clear in figures (4.10a and 4.10b) which shows, for the same number of mesh points, but different mesh arrangements the total (B_T) axial field distribution and that due to iron magnetisation B_{Fe} at different lens excitations. Figure 4.10a shows the experimental values for the total field B_T , and those calculated by Christofides (1982) and by the present author. The differences between the experimental and Christofides computed values are clear, while the values computed from this study are in a good agreement with Christofides experimental values. Figure 4.10b shows a comparison between B_{Fe} (experimental) and ($B_T - B_{Coil}$) calculated by Christofides and by the present author. The calculations by the present author are in excellent agreement with experimental values. This indicates strongly that Christofides used an unsuitable mesh arrangement and probably assumed that the choice of mesh was not a significant parameter. The computation was carried out in this study with M13 program, 25, 50 meshes and with AMAG program, 32, 70 meshes and finally with AMAG, 54, 100; the results were in good agreement in the three cases.

It therefore is advisable to pay sufficient attention to the mesh distribution especially in this case, where both the polepiece and the coil have irregular profiles, and more meshes are required to define them.

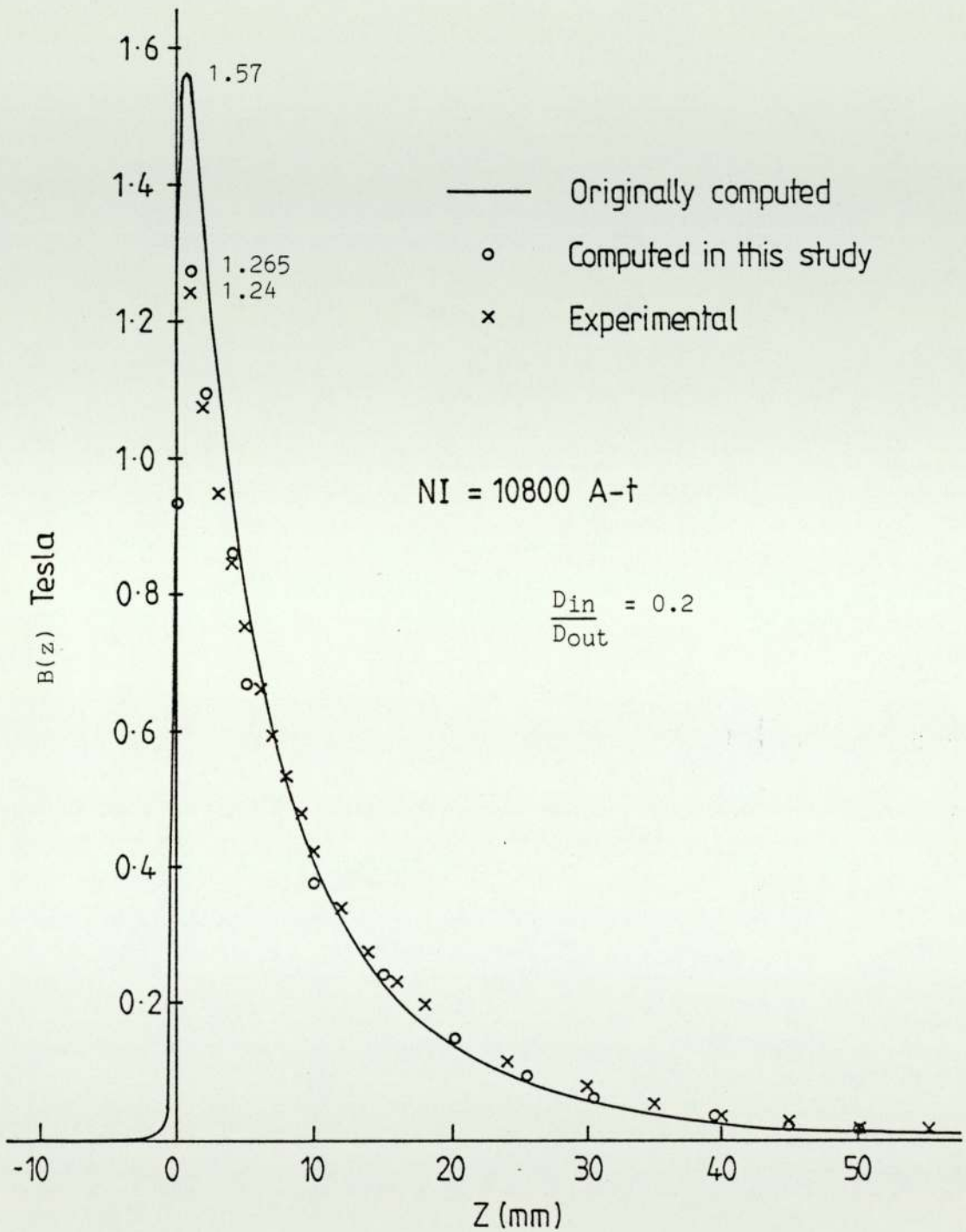


Figure 4.9 Axial field distribution for Christofides lens (figure 4.8). Comparison between experimentally determined, computed values of Christofides and recomputed values in this study.

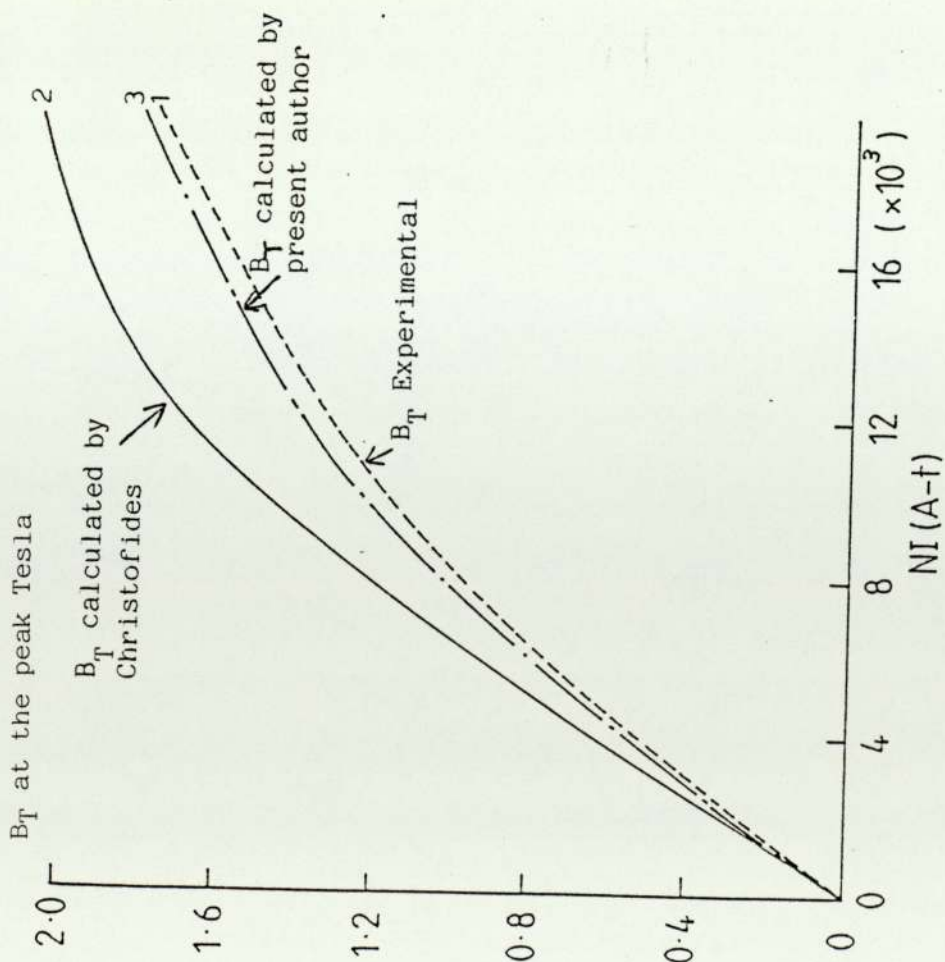


Figure 4.10a Comparison between the total field B_T at the peak (1) experimental (2) calculated by Christofides (1982) (3) calculated by present author

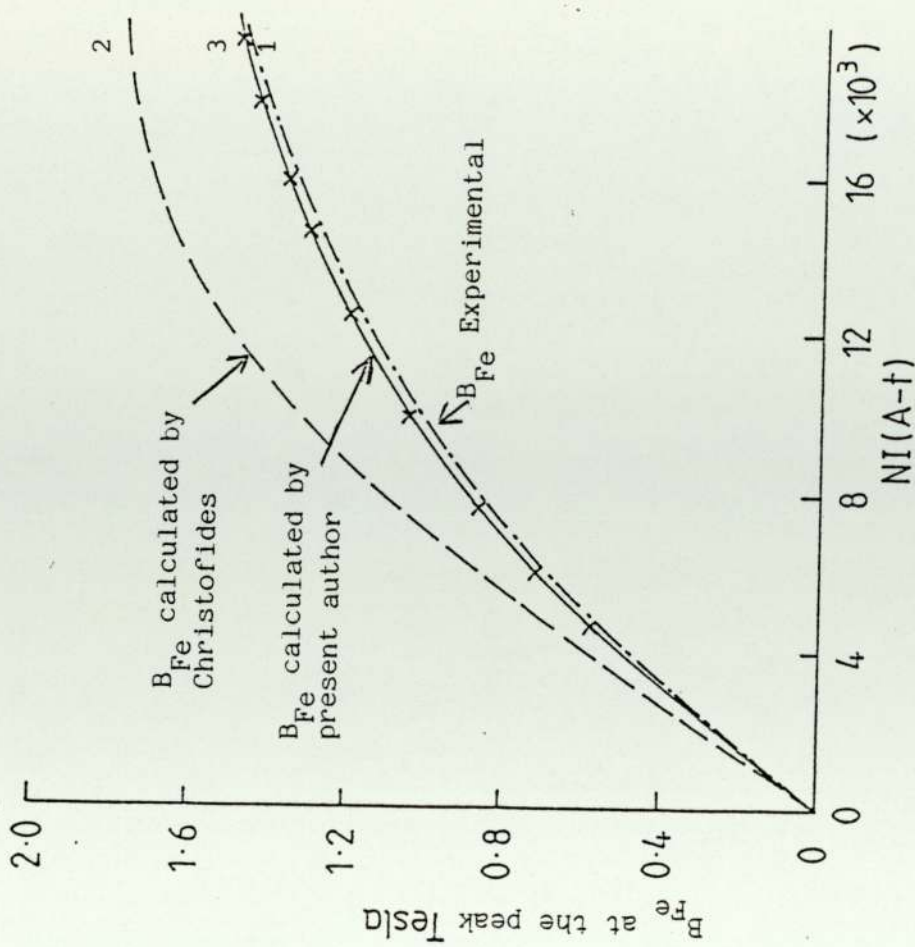


Figure 4.10b Comparison between (1) B_{Fe} at the peak experimental and (2) B_{Fe} coil calculated by Christofides and (3) by the present author

4.2.2 The Effect of Mesh Numbers

The effect of the number of meshes on the accuracy of the results was also studied, by the application of the FEM programs to the analysis of the same lens but with increasing mesh numbers, all other parameters being kept constant. The effect on the results was noticeable in all lens designs. However, the influence of number of meshes was more obvious in acute-angled pole faces and open structures, since more meshes are needed to define the pole face adequately in the former case, while in the latter case the boundary must be set as remote as possible from the coil to overcome boundary problems as explained in section (2.1). Open structures are particularly sensitive to the number of meshes employed.

As an example of the influence of mesh numbers, different programs were applied to the spherical single pole lens shown in figure 4.11 . The axial flux density was first computed with three programmes (Munro, Nasr and AMAG) for (25 x 50) meshes. It was noticed that at $Z = -34$, and $+0$, an unusual field shape appeared. It was therefore decided to run the AMAG program with 66 x 96 meshes which is not possible at the moment with the other programs. The same figure shows the resulting axial flux density distribution in which these anomalies disappear.

By plotting the peak flux density for the lens shown later in figure 4.29 for constant excitation against $1/n$, as shown in figure 4.12 where $1/n$ is reciprocal of the mesh numbers it is possible to extrapolate to an infinitely fine mesh. The results shown in this figure were obtained when the meshes were conveniently distributed between all the lens parts including the pole face and coil windings,

Output of:

- x 25 x 50 with M12, Vplin
one run and AMAG linear
- Vplin 4 - runs
- o 66 x 90 AMAG

$$\frac{D_{in}}{D_{out}} = 0$$

$$S = 26\text{mm}$$

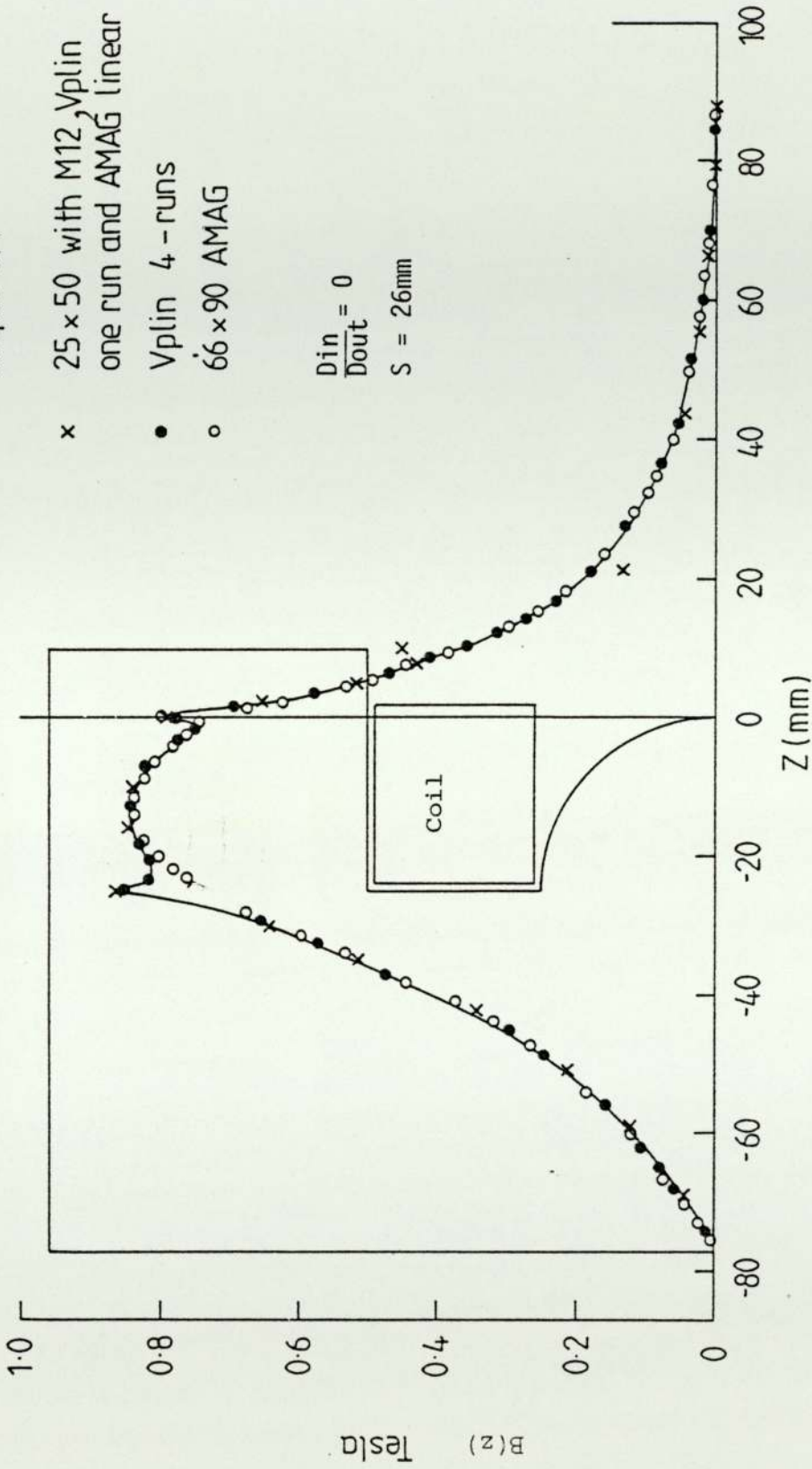


Figure 4.11

Spherical single pole lens under linear condition. Excitation of 10 000 A-t.
Coil of $26 \times 23\text{mm}^2$. (Munro, Nasr and AMAG programs).
Note the improvement at $Z = -34$ and $Z = 0$ with AMAG program with 66×90 meshes.
i.e the unusual field shape

avoiding abrupt steps as explained in section (3.1). However, when the mesh numbers were increased, without proper attention to their distribution, the accuracy still improves but not to the same extent. It seems therefore that the choice of mesh layout is as significant as the choice of mesh number.

A second example of the mesh number effect was demonstrated from the cleaver's double pole lens shown in figure 4.4 but without bore. The error in the peak flux density value for this lens, computed with (25 x 50) meshes, and an arbitrary but reasonable arrangement of the mesh distribution, was 30%. Without changing the mesh arrangement the error dropped to 4%, when the number of meshes was increased to (60 x 90) as shown in figure 4.12. When the mesh was optimised fig. 4.5 this error dropped to 0.8% for (25 x 50) meshes. It is shown in figure 4.12 also that using the step method always give good agreement with the expected value although slightly lower.

4.2.3 The Polepiece Shape Effect

The application of the FEM to various test lenses of constant gap width has indicated that, with the same mesh numbers and distribution, the accuracy of the results can change if the polepiece profile is changed, even for high permeability iron. An example is shown in figure 4.13 with four test lenses of constant gap width $S_g = 10$ mm but with different polepiece taper angle of 0° , 45° , 60° and 90° respectively. The permeability of the iron is high ($\mu_r = 5 \times 10^4$). The results, of maximum flux density values B_m at the air gap between the two polepieces shown in figure 4.14 indicate errors of between 0.3% and 1.8% according to the degree of the profile when compared to B_m value, obtained from equation 1.15, using the same optimised mesh

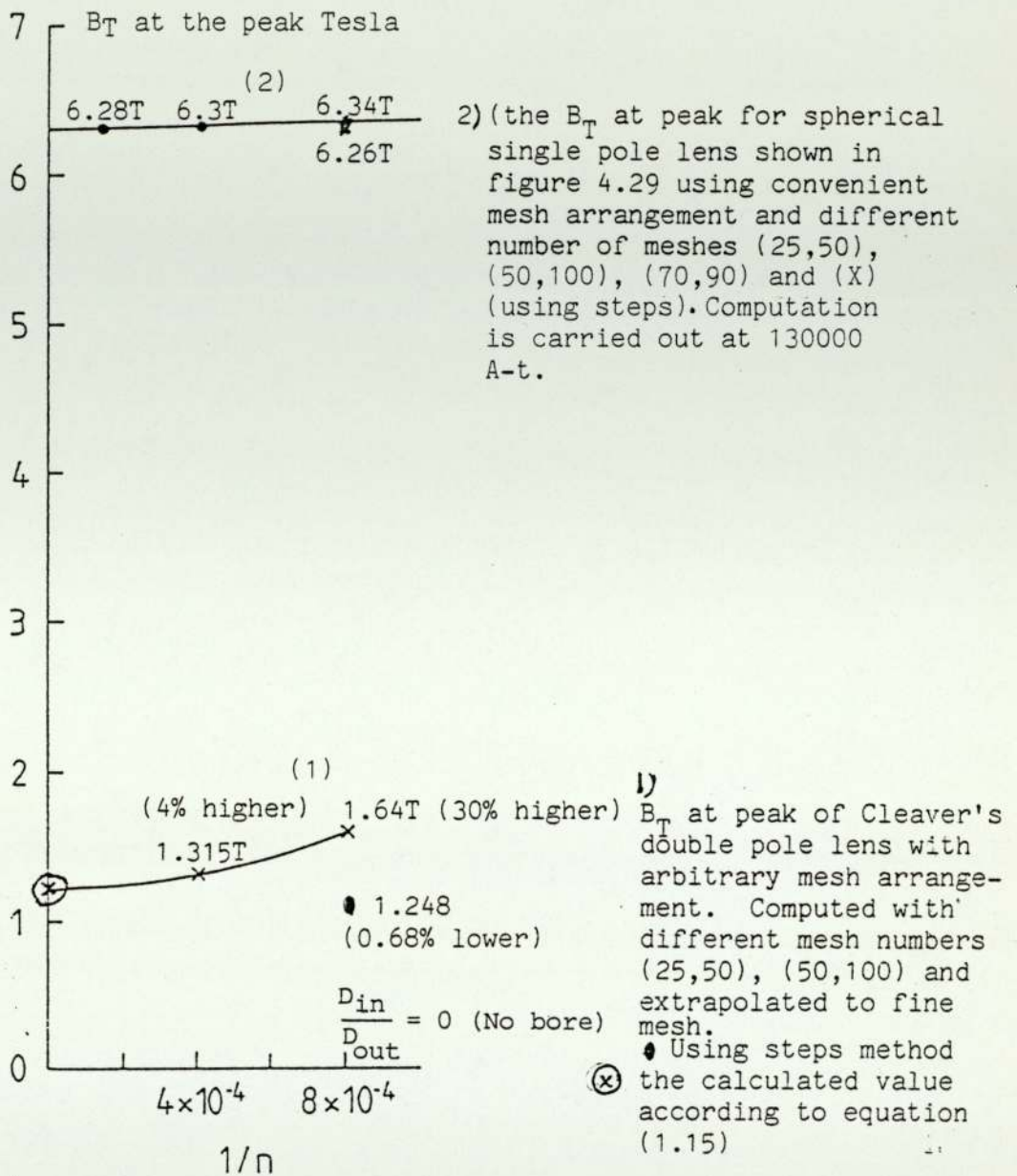


Figure 4.12

Variation of the peak axial flux density value with the reciprocal of the mesh numbers $1/n$

- 1) in double pole lens using arbitrary mesh arrangement
- 2) in single pole lens with convenient mesh arrangement

It can be noticed in the figure, that in the first case when the mesh arrangement is not correct there is higher error and it is improving with larger number of meshes. While in second case the error is low and the change is small with increasing the number of meshes.

B_m calculated according to equation 1.15

$$B_m = \frac{\mu_0 NI}{Sg} = 1.2566T$$

computed B_m values
 $0^\circ, B_m = 1.2526 \text{ T}$
 $45^\circ, B_m = 1.2746 \text{ T}$
 $60^\circ, B_m = 1.296 \text{ T}$
 $90^\circ, B_m = 1.264 \text{ T}$

$$NI = 10^4 \text{ A-t}$$

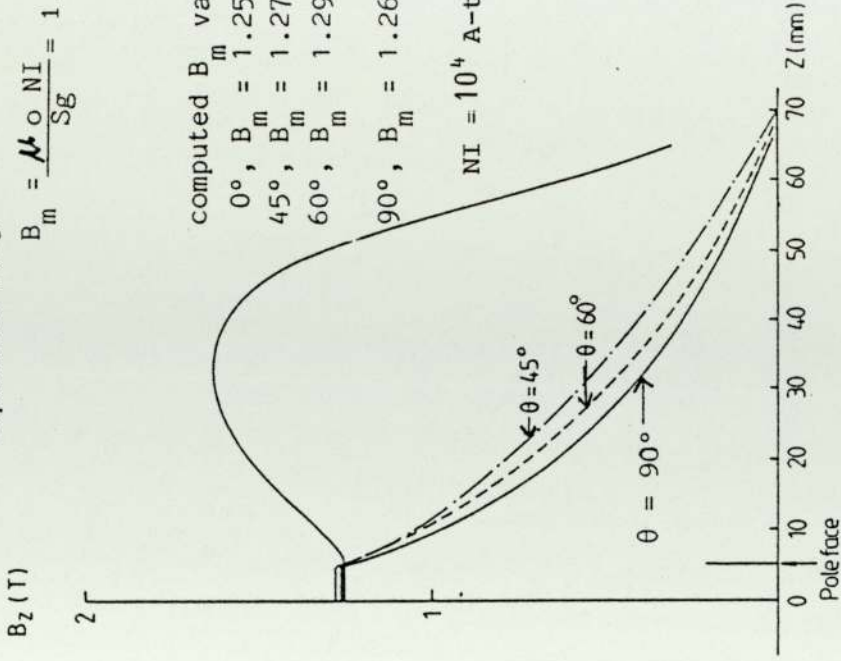


Figure 4.14 Axial flux density distribution of lenses shown in figure 4.13. Lenses excited by a flat thin coil under linear condition, same mesh distribution and number is used.

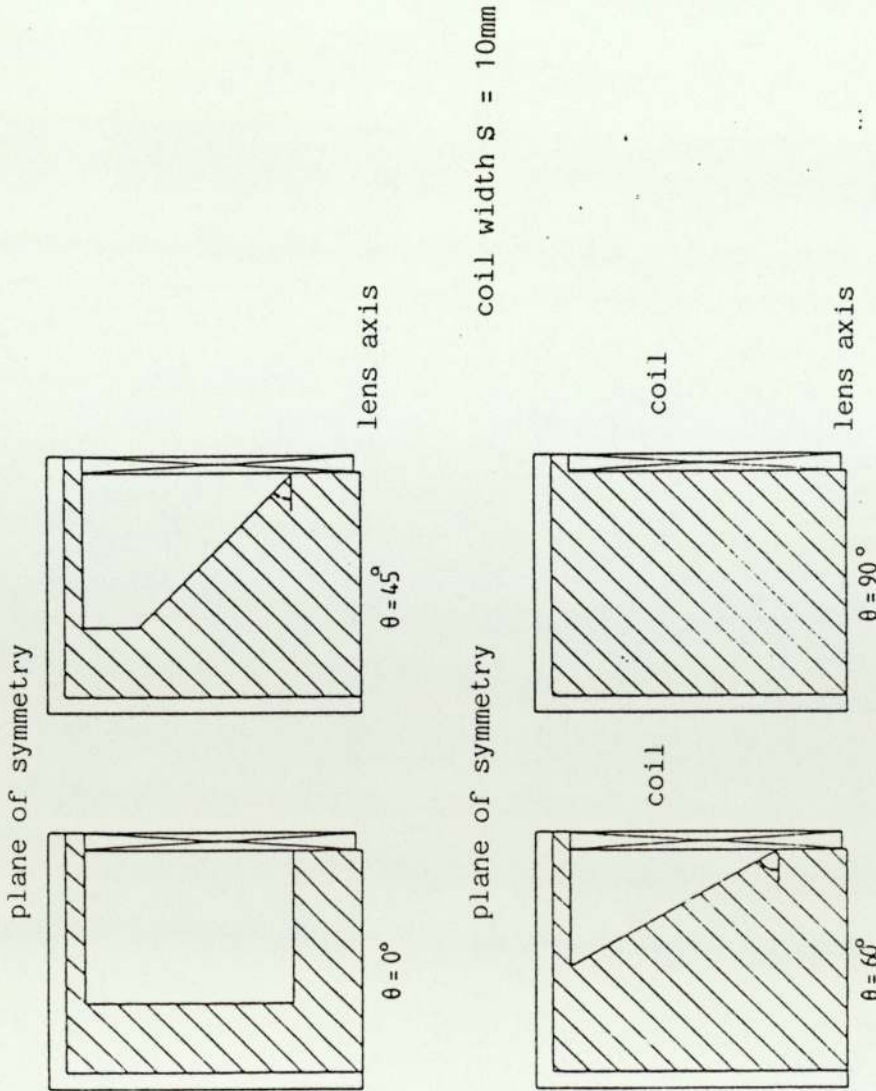


Figure 4.13 Symmetrical double polepiece of constant gap width ($Sg = 10\text{mm}$) with different polepiece taper angle θ .
 Permeability $\mu_r = 5 \times 10^4$
 Exciting coil placed between the polepieces

distribution and numbers. This suggests that with 45° and 60° taper angles larger errors in maximum flux density values B_m are expected when an arbitrary mesh distribution or insufficient mesh number are used.

4.2.4 The Boundary Effects

As explained in section (2.1), if the boundary is not chosen correctly, there may be loss in excitation leading to large errors in the axial field distribution. These errors can be reduced by setting the boundary at a place where the flux density is negligible. Alternatively one can place an iron sheet of infinite permeability close to the boundary. Note however that this may distort the field distribution near the iron sheet.

For reasonably accurate axial field distribution results with FEM, a useful rule of thumb is to set the boundary at a distance of about five times the mean coil diameter (D_m). This applies especially for iron free coils and also to single pole lenses under linear conditions and to all lenses under saturation conditions.

To show the effect of boundary setting and the number of meshes used, the axial flux density of a simple asymmetrical test lens consisting of a thin coil, shown in figure 4.15 backed by an annular iron ring of the same shape and size as the coil was computed with three different programs, M12, VPLIN and AMAG. Figure 4.16 shows the results. When the Z boundaries were at (-65 mm and 75 mm), the axial flux densities from the three programs agreed within 1%; however the loss in excitation with each program, with same mesh numbers (25 x 25), was about 8%. The boundary loss in excitation was reduced to

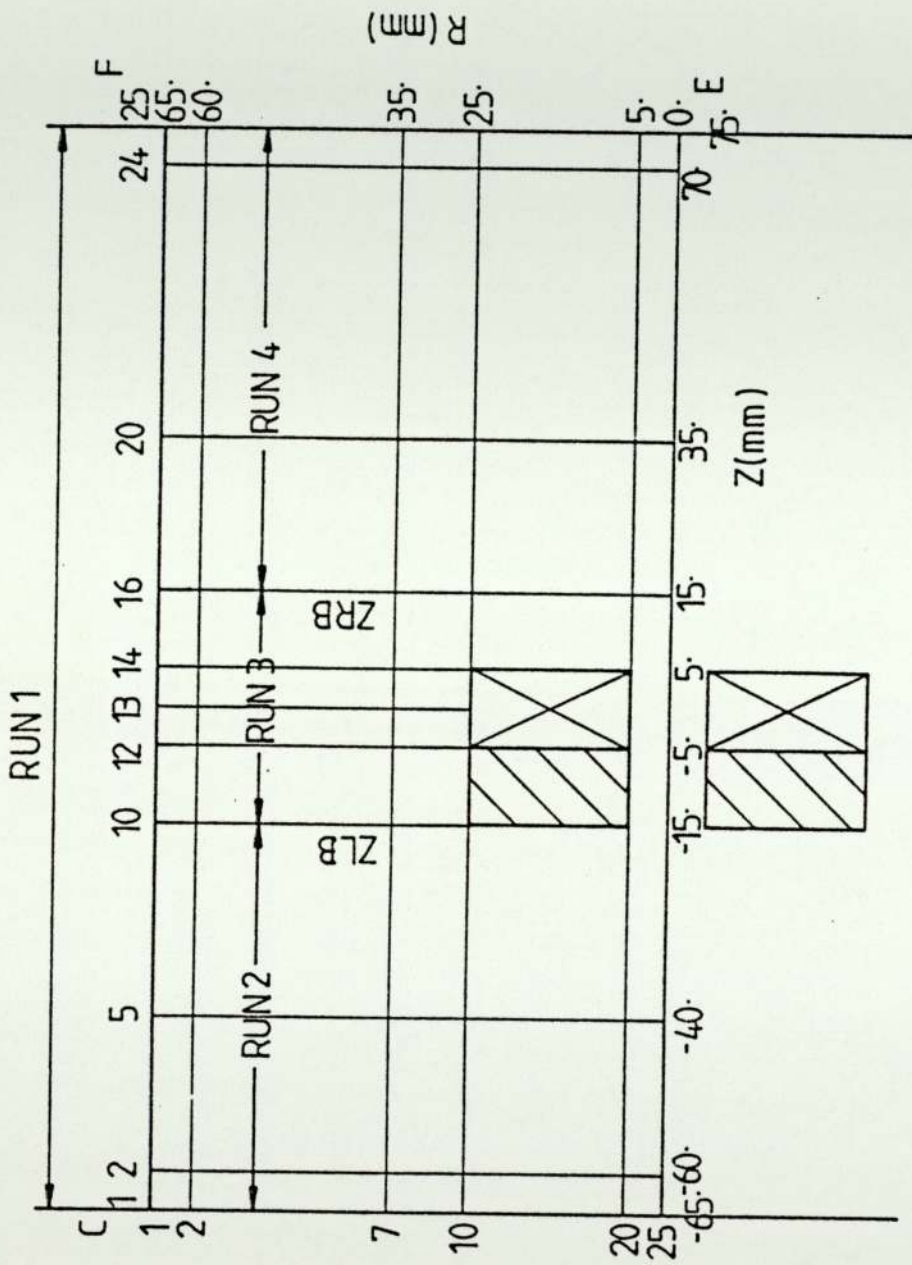


Figure 4.15 Simple asymmetrical test lens consisting of a coil and an iron ring. The figure shows an outer boundary, mesh point numbers and two inner boundaries for use with the VPLIN program

about 1% when the boundaries were set at (-100 and 150 mm), $\mu_r = 50,000$ or alternatively the open boundary was replaced by a 5 mm thick iron sheet of high permeability. When the mesh numbers were increased to (61 x 96) with the same Z boundary -65 and 75 mm, the loss in excitation due to the boundary remained at 8%, but the peak flux B_T density value was reduced by 7% (see figure 4.16). When the boundary was extended at five times the mean coil diameter i.e. at -100 and 150 mm, the loss in excitation was reduced to 1% when either (25 x 25) or (61 x 96) mesh arrangements were used. However, the corresponding peak flux density value was not affected. This means that a too-near boundary causes excitation loss, and substantially reduces the effects of the axial flux density distribution close to the boundary, but does not necessarily reduce the peak value. However insufficient mesh numbers do not of themselves cause a loss in excitation, but may well affect peak flux density values.

Another example of a lens, tested for boundary loss, is shown in figure 4.17. This lens was designed according to the idea of Huang (1981). It consists of an energising coil in the form of a long solenoid of rectangular cross-section, partly surrounded by a thick iron casing (A). Inside the coil are placed six field-shaping rings co-axial with the optical axis. Under saturation conditions a further external casing (dashed line) could be added. The axial field distribution, for the coil in free space (1) and the coil with rings only (3), were obtained. The loss in excitation in the absence of the iron casing was (21)%, when the Z boundary was set at +80 mm and the R boundary at 80 mm. To overcome the loss, the boundary had to be set at 260 mm i.e. five times the coil mean diameter, this required more meshes i.e. more computer memory store. The loss disappeared when the outer casing was placed in position. These results are shown in

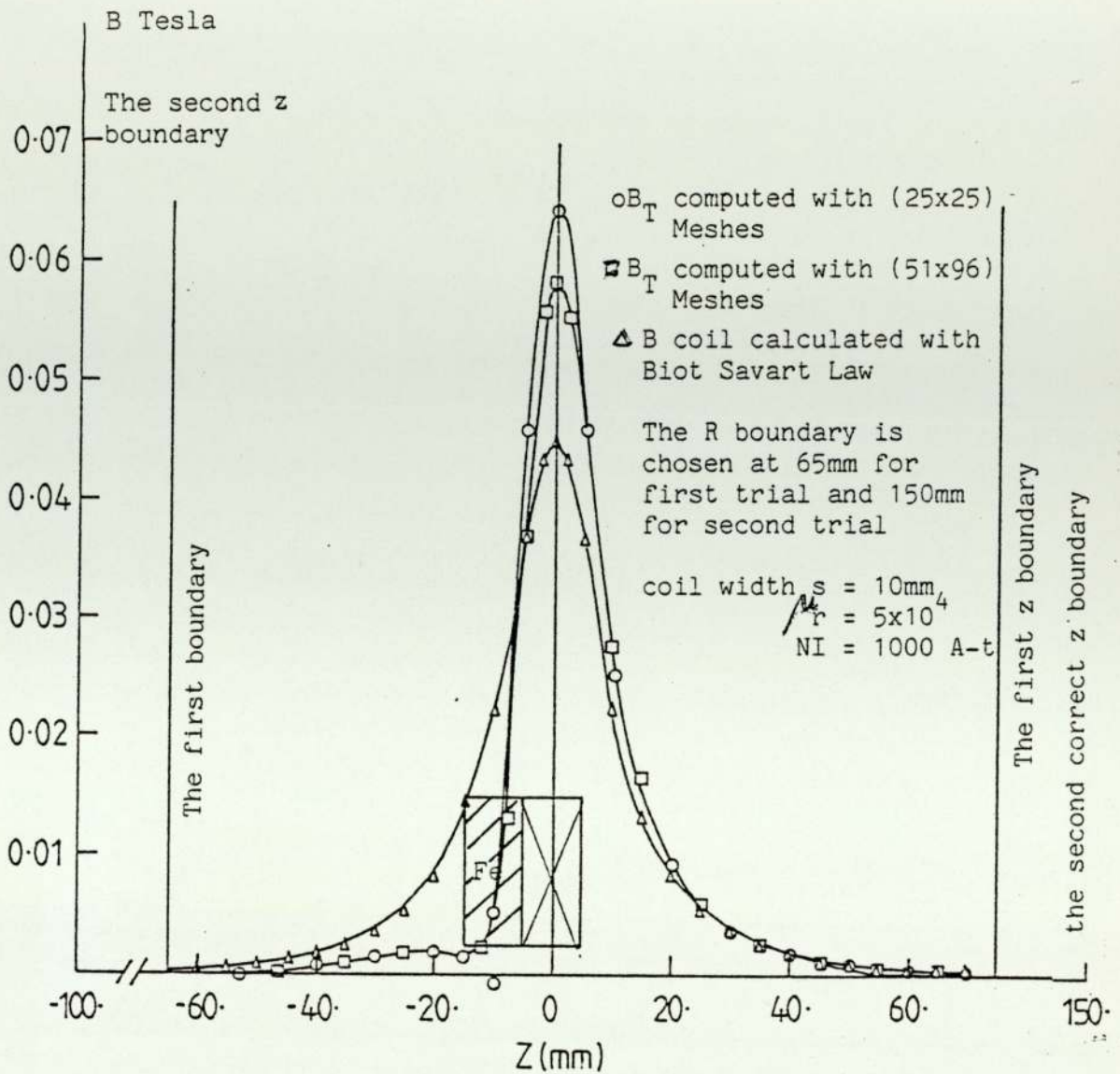


Figure 4.16

The total axial flux density distribution computed with (25x25) meshes using M_{12} , VPLIN, AMAG.

□ The total axial field distribution using AMAG (51x96) meshes on the asymmetrical test lens shown in figure 4.15 $S = 0.033$, D_m

Using the different boundary setting.

The first boundary -60 and 75mm cause 8% loss in excitation when either 25, 25 or 51, 96 meshes are used.

The second and correct boundary reduce the boundary loss in excitation to within 1%. The flux values near the boundary will be affected while the peak value will stand for either mesh number the same as it was for first boundary

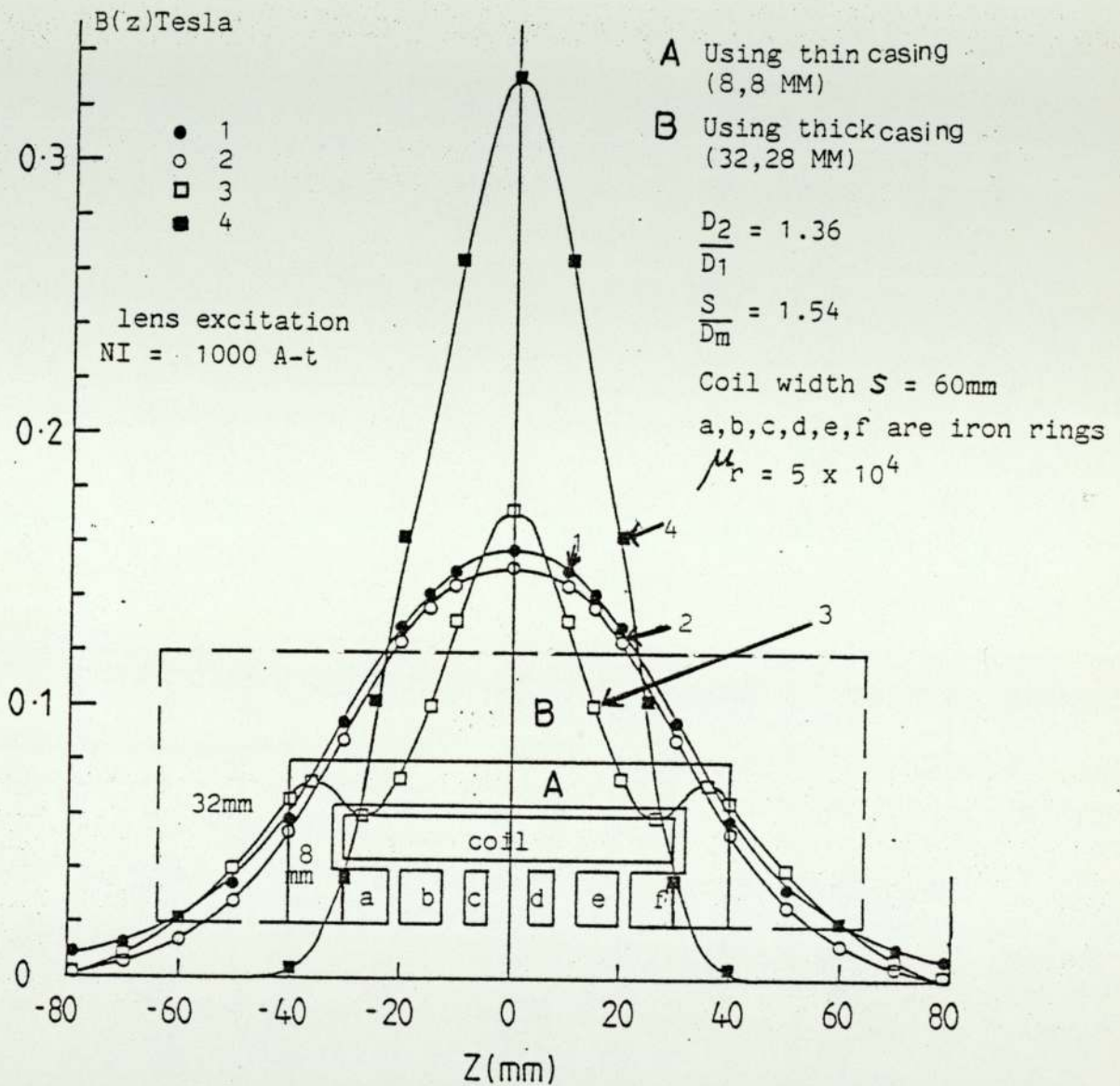


Figure 4.17

The axial field distribution. 1. $B(z)$ coil calculated with Biot Savart program with infinite boundary, 2. $B(z)$ coil calculated with AMAG program using finite boundary (80mm), 3. $B(z)$ for coil + iron rings with AMAG program using finite boundary (80mm) and finally 4. $B(z)$ for mini ring lens after surrounding the coil + iron rings with (A) 8mm thick iron casing and (B) (32,28mm) thick iron casing.

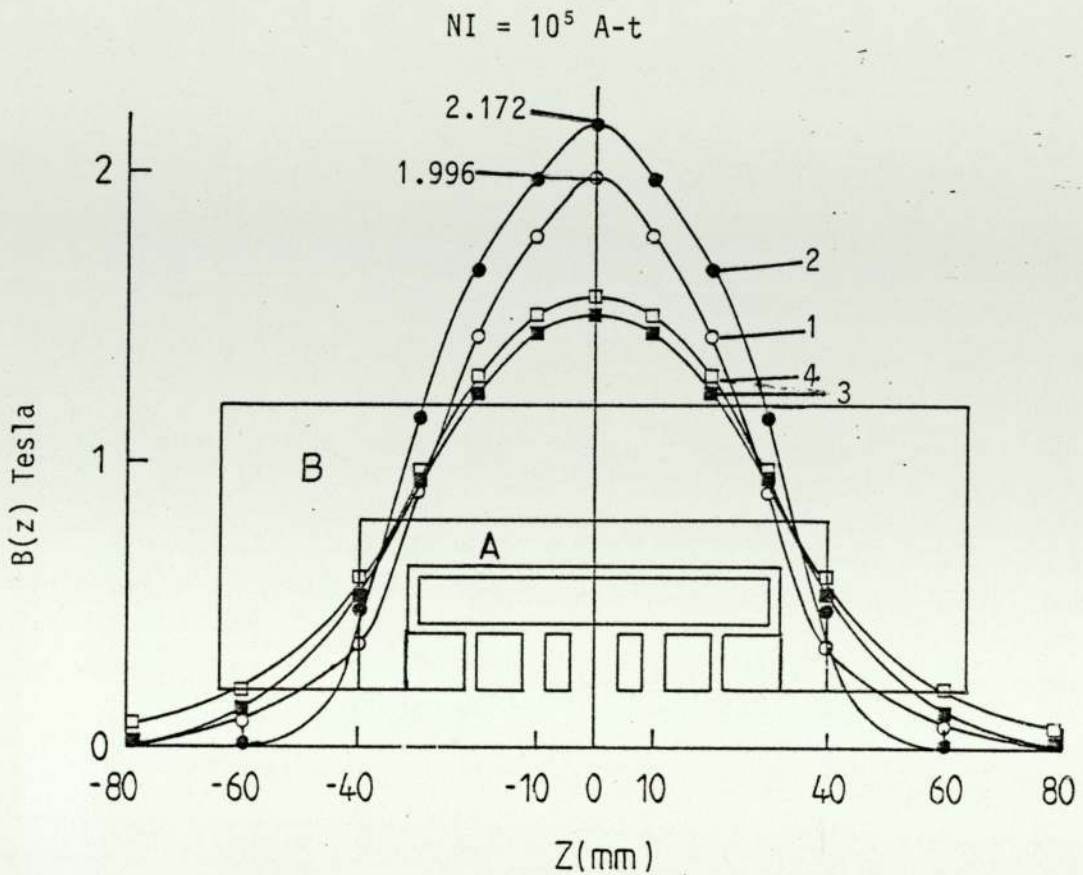


Figure 4.18

Axial flux density distribution in mini ring lens shown in Figure 4.17 under non linear condition 1. (o-o-o) with thin iron casing 8mm 2. (●-●-●) with thicker iron casing (32 from side and 28 from up) to prevent leakage.

Note

The difference between 1 and 2 is due to both boundary loss (7.4%) and leakage flux which have effect on the peak value equal to (8%) loss in 1.

3 (■-■-■) the axial flux density distribution of iron free coil computed as in previous cases 1 and 2 with 71×73 meshes using AMAG program.

4 (□-□-□) the axial flux density distribution of iron free coil calculated by Biot Savart law. The difference between 3 and 4, due to boundary loss is (14%) in 3.

figure 4.17. When the lens with the narrow casing (8 mm) was computed under saturation conditions, external leakage problems arose, therefore an extra casing (B) was added to overcome the leakage effects, as shown in figure 4.18.

4.3 Faults and Misinterpretations in Lens Design

The limitations of FEM, in magnetic lens design, have been set out in Section 4.2. However, it should be borne in mind that not all errors in FEM computation results are due to the FEM itself. Some of the errors are inherent in the lens design and have led some research workers into wrong conclusions. Prominent amongst factors causing such misleading conclusions is the influence of insufficient iron casing (shroud) thickness or external leakage effects, which in turn are influenced by the coil size and position.

4.3.1 External Leakage due to Insufficient Magnetic Circuit (Shroud) Thickness

External leakage can be significant in both single and double pole lenses under saturation conditions; where the excitation is high producing a correspondingly high lens flux. A portion of this flux will appear outside the iron casing if its thickness is not sufficient.

Examples of this kind of leakage effect are noticeable, with hindsight in the saturated single pole lenses studied by Al-khashab (1983). Figure 4.19 shows the recalculated $B(z)$ curves of the original spherical polepiece lens of Al-khashab (1983), with spherical polepiece and coil surrounding the polepiece. The figure shows that

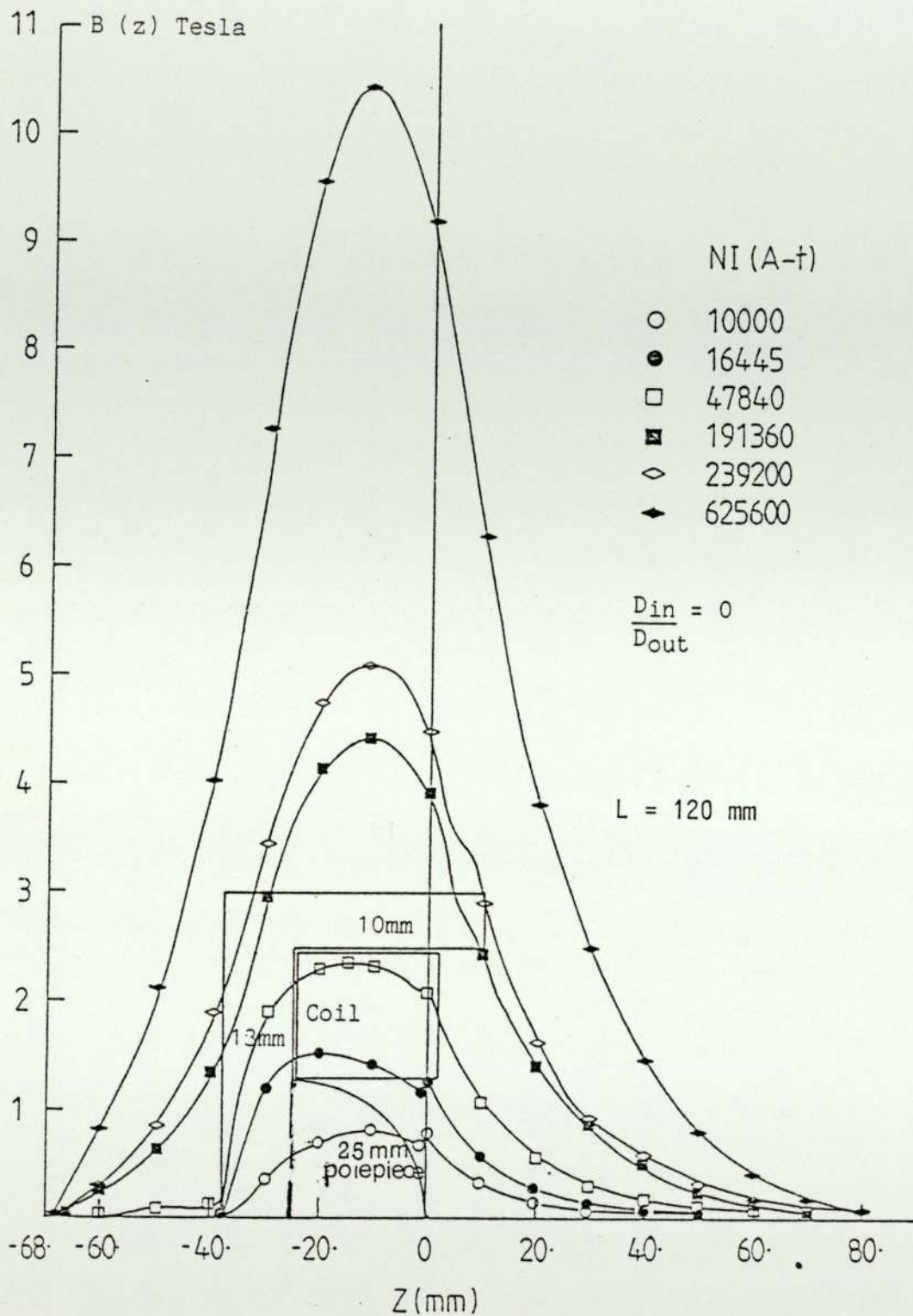


Figure 4.19

Recalculation of axial field distributions of the Al-Khashab's (1983) lens. i.e. Spherical single pole lens with coil surrounding the polepiece.

$$D_2/D_1 = 1.88, S/D_m = 0.347, s = 26 \text{ mm.}$$

Note: Appreciable external leakage occurs at excitations higher than 16445 A-t, i.e. at B_{pf} higher than 1.5 Tesla.

there is appreciable external leakage flux in the axial region between $Z = -38$ and $Z = -68$ mm for excitations greater than 16,000 A-t. The associated loss of amper-turns increases rapidly with increasing excitation amounts to some 32% at an excitation of 625,600 A-t, thereby reducing the polepiece flux density B_{pf} .

When the magnetic circuit is thickened as shown in figure 4.20, this loss is substantially reduced.

This figure shows the $B(z)$ curve of the redesigned spherical polepiece lens. As shown in this figure the external leakage is greatly reduced. At an excitation of 625,600 A-t, now a 7.5% increase in the B_{pf} value occurs.

If the magnetic circuit is further thickened as shown in figure 4.21, the external leakage is negligible, the B_{pf} value at an excitation of 625,600 A-t has increased by 15.8%.

Figure 4.22 summarizes these results. The total field B_T and the B_{Fe} values at the pole face are shown for different thickness of the shroud.

When the magnetic circuit thickness is equal or less than $R/2$ i.e. half the axial polepiece radius, appreciable external leakage flux occurs, this reduces the B_{Fe} value at the pole face and causes the progressive reduction of B_{Fe} .

This explains some of the curious results obtained by Al-khashab (1983). This external leakage effect is also noticeable in the single pole lens (Hermes) studied by Christofides (1982).

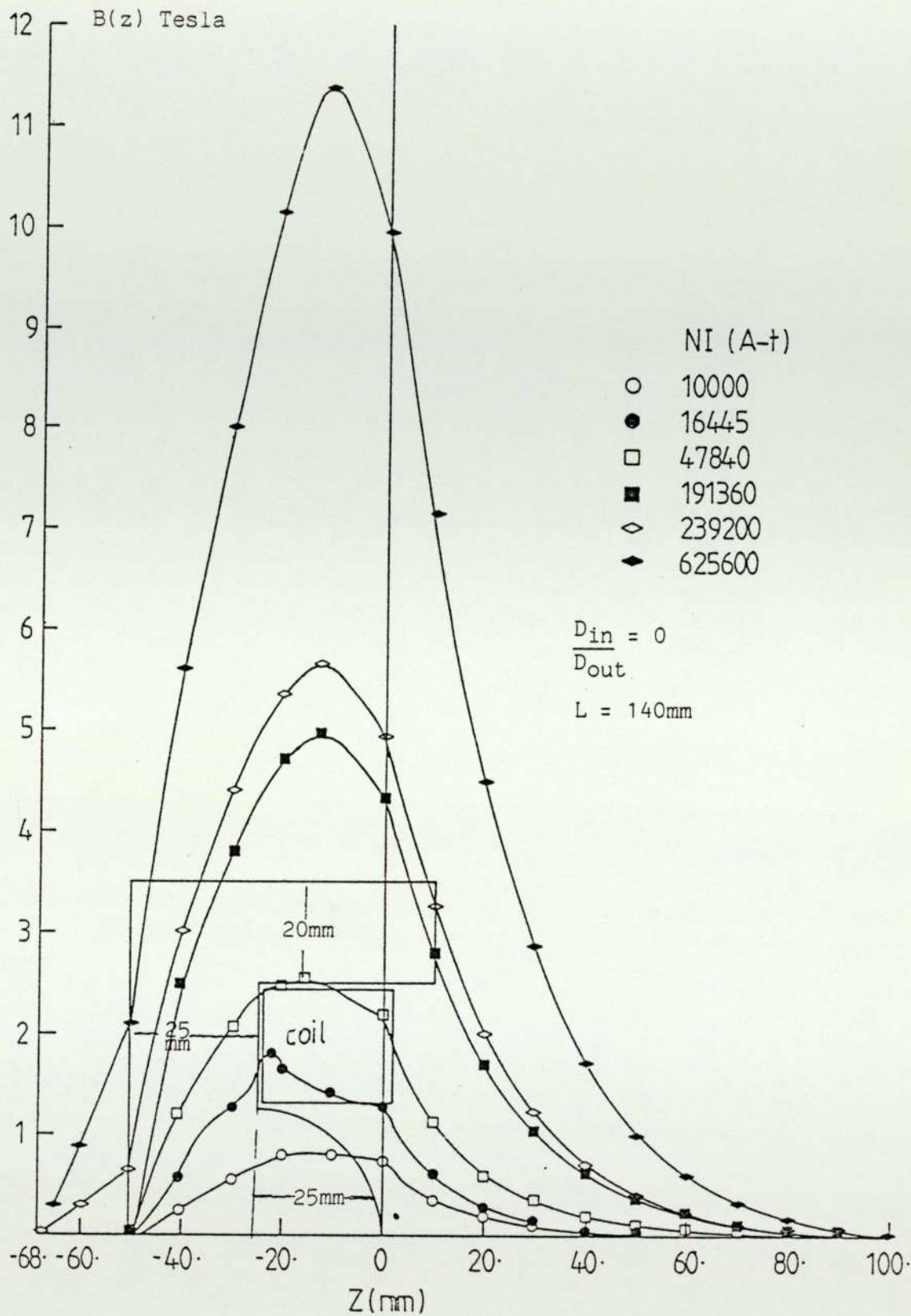


Figure 4.20

Variation of axial field distribution with excitation for spherical single pole lens shown above, with larger iron circuit than in figure 4.19. The external leakage occurs at excitation higher than 200,000 A-t i.e. pole face flux density (B_{pf}) higher than 4 Tesla.

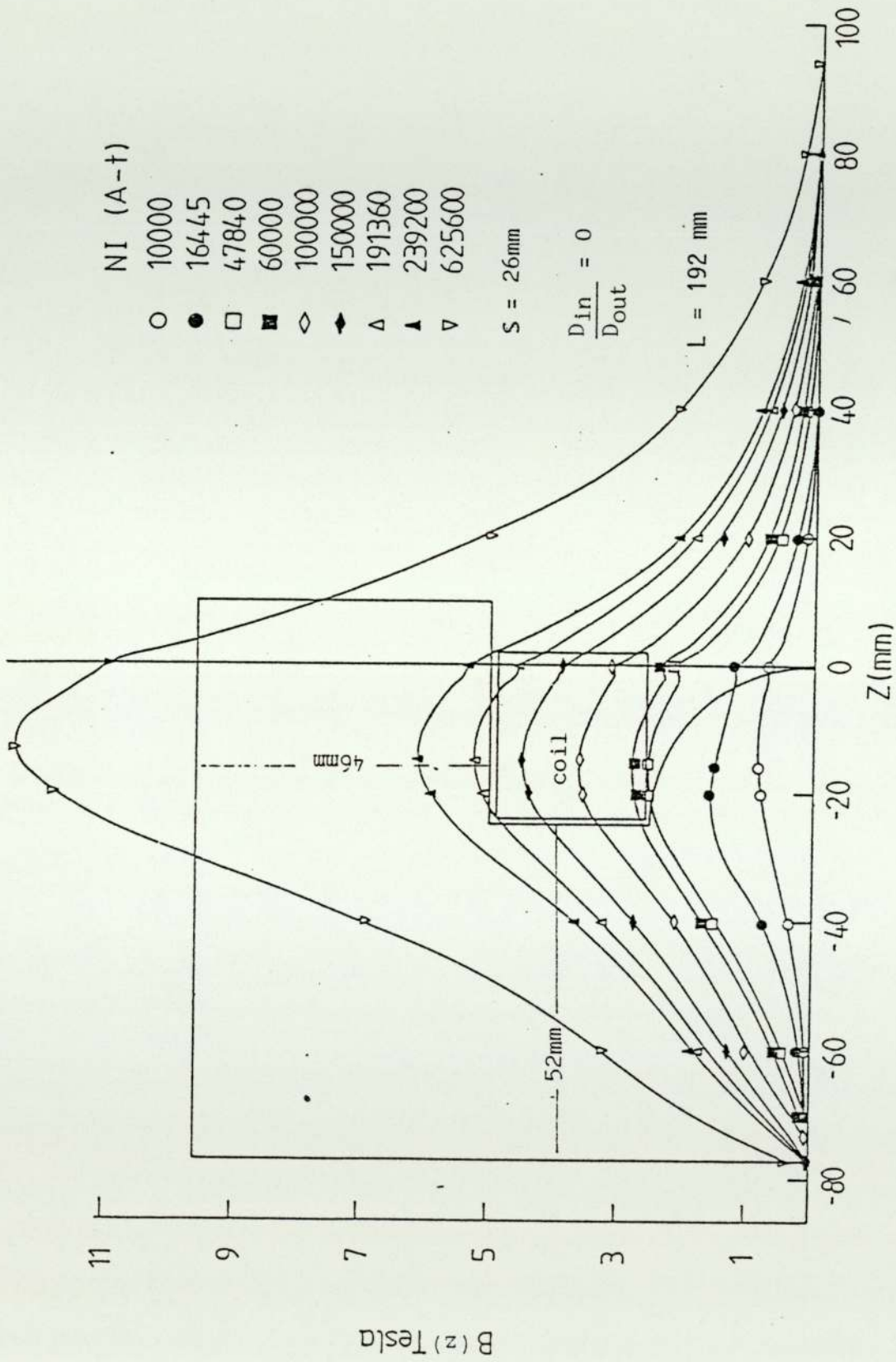
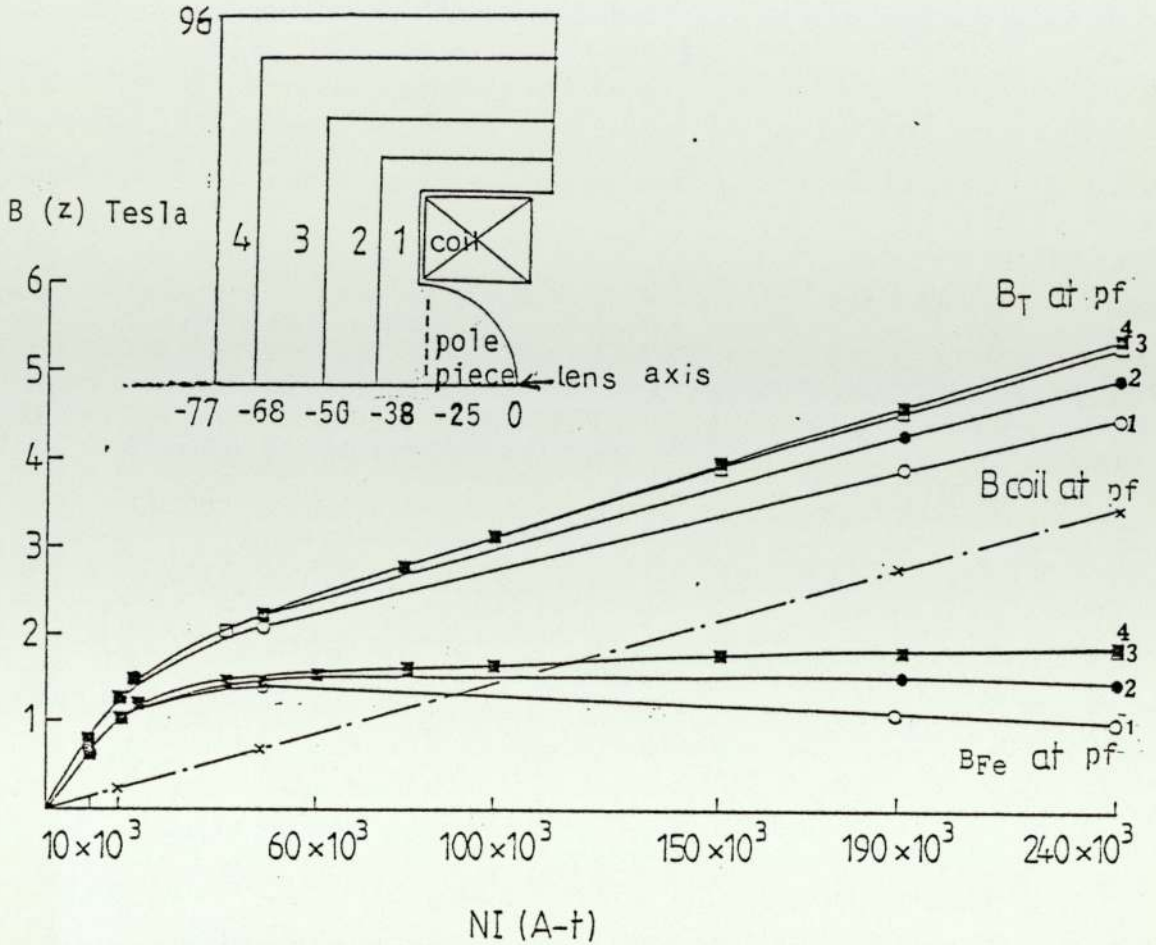


Figure 4.21 Axial flux density distribution for spherical single pole lens shown above at different lens excitation using $(26 \times 23 \text{ mm}^2)$ coil surrounding the polepiece lens. $(-24 \text{ to } 2 \text{ mm})$ after making the iron circuit large enough to prevent external leakage.



The B_T and B_{Fe} values at the pf

- 1 o Using original shrouds (13,10)
- 2 ● Using shrouds of thickness (25,20)
- 3 □ Using shrouds of thickness (43,35)
- 4 ■ Using shrouds of thickness (52,46)
- x B coil at pf with Biot Savart Law

Figure 4.22

The total axial flux density distribution and the B_{Fe} values ($B_T - B_{Fe}$) at the pole face tip of spherical single pole lens shown in Figure 4.19 at different lens excitation. (Calculated for four different thicknesses (1-4) of the lens shell).

Note The value of both B_T and B_{Fe} at the pole face increase with increasing shell thickness.

Figure 4.23 shows recalculated $B(z)$ curves of the lens with its original magnetic circuit (shroud); external leakage is noticeable at excitations higher than 1.5×10^4 A-t, i.e. at B_{pf} higher than 1.5 Tesla.

Figure 4.24 shows lens Hermes redesigned by the present writer, with a thicker magnetic circuit, it can be noticed from the same figure that there is no external leakage even up to 10^5 A-t.

There is also a useful increase in the total field at the pole face (B_{pf}) of 7% (for a lens excitation of 10^5 A-t) compared with B_{pf} with the original design of magnetic circuit.

The situation is summarized in figure 4.25 which shows the B_T and B_{Fe} at the pole face for different lens excitation for the original magnetic circuit (A) and with the thicker magnetic circuit (B).

It can be noticed from the figure that B_T and B_{Fe} are almost the same in the linear region up to 1.6×10^4 A-t; above this value external leakage starts to occur and tends to reduce B_T and B_{Fe} values, as indicated by their increasing values as the thicker magnetic circuit is made.

External leakage was also noticed in the double pole (test) lens, with rectangular section polepieces shown in figure 4.26 which shows the $B(z)$ curve at an excitation of 2×10^5 A-t when the lens is excited by (a) a short solenoid and (b) a long solenoid.

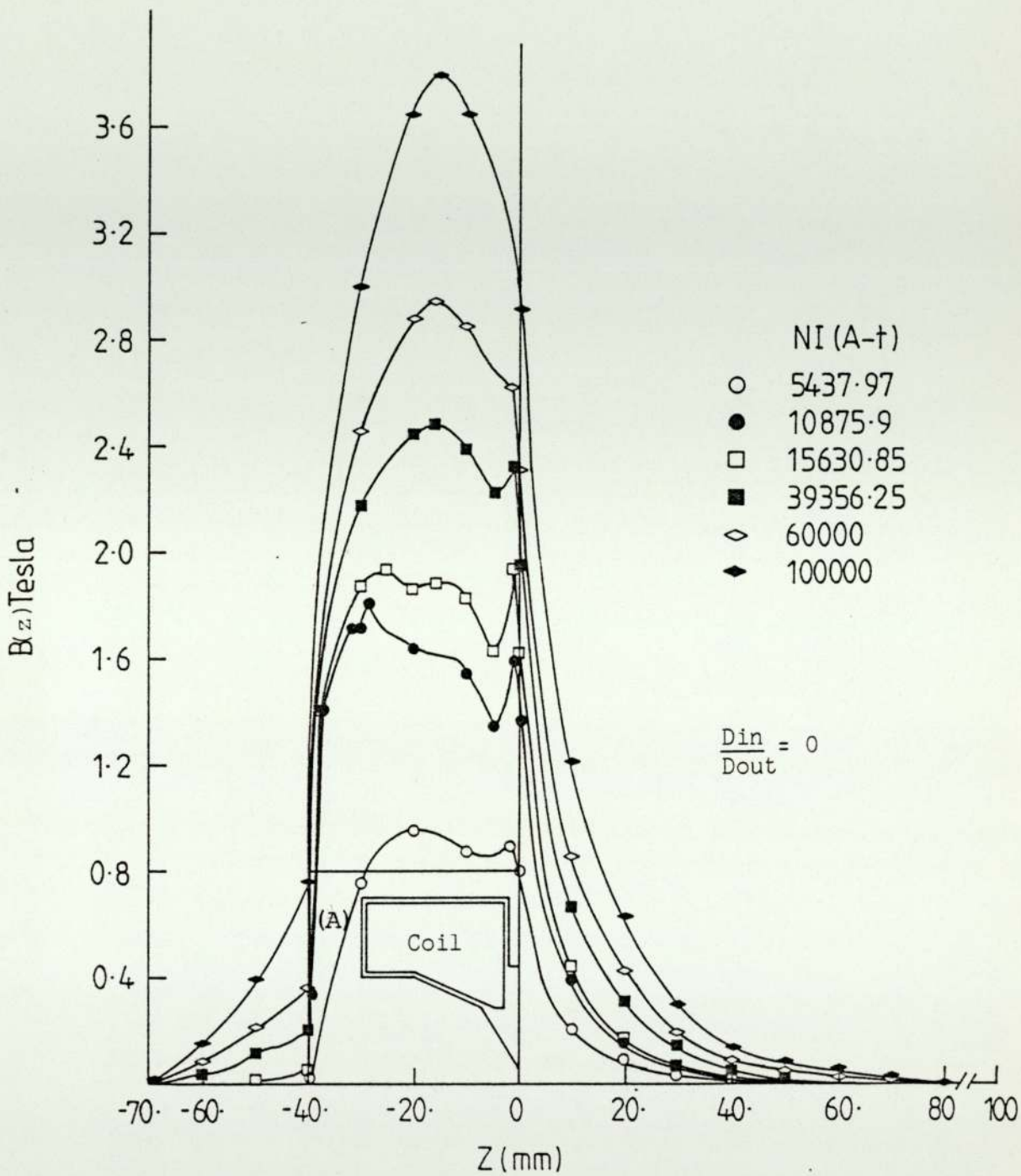


Figure 4.23 Recalculation of the variation of axial field distribution with lens excitation using the original magnetic circuit (A) (Christofides' (1982) zero bore lens Hermes). The external flux leakage is indicated at B_{pf} higher than 1.5 Tesla

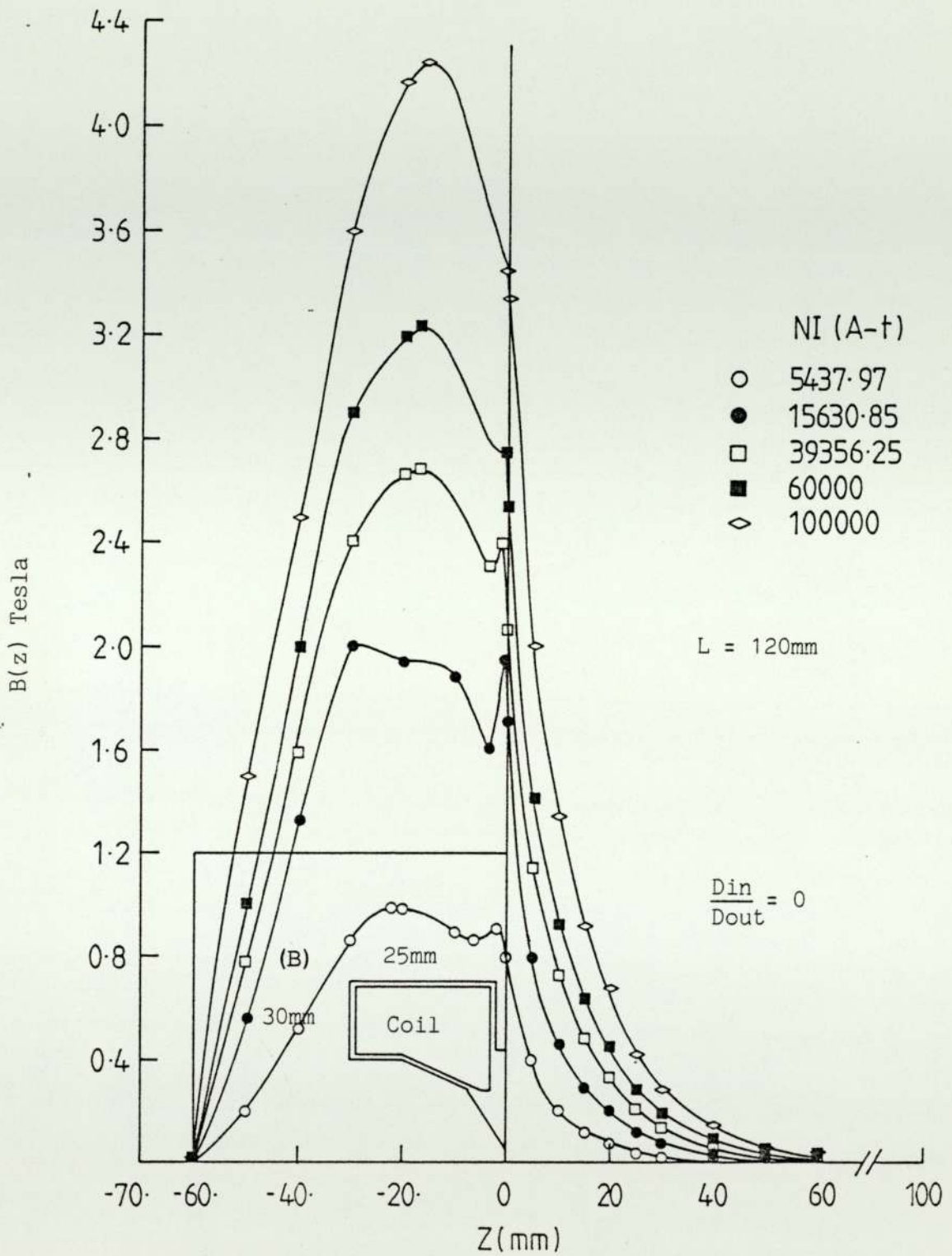


Figure 4.24 Variation of axial field distribution with lens excitation. Same lens of figure (4.23) recomputed with thicker magnetic circuit (B) designed to reduce external leakage.

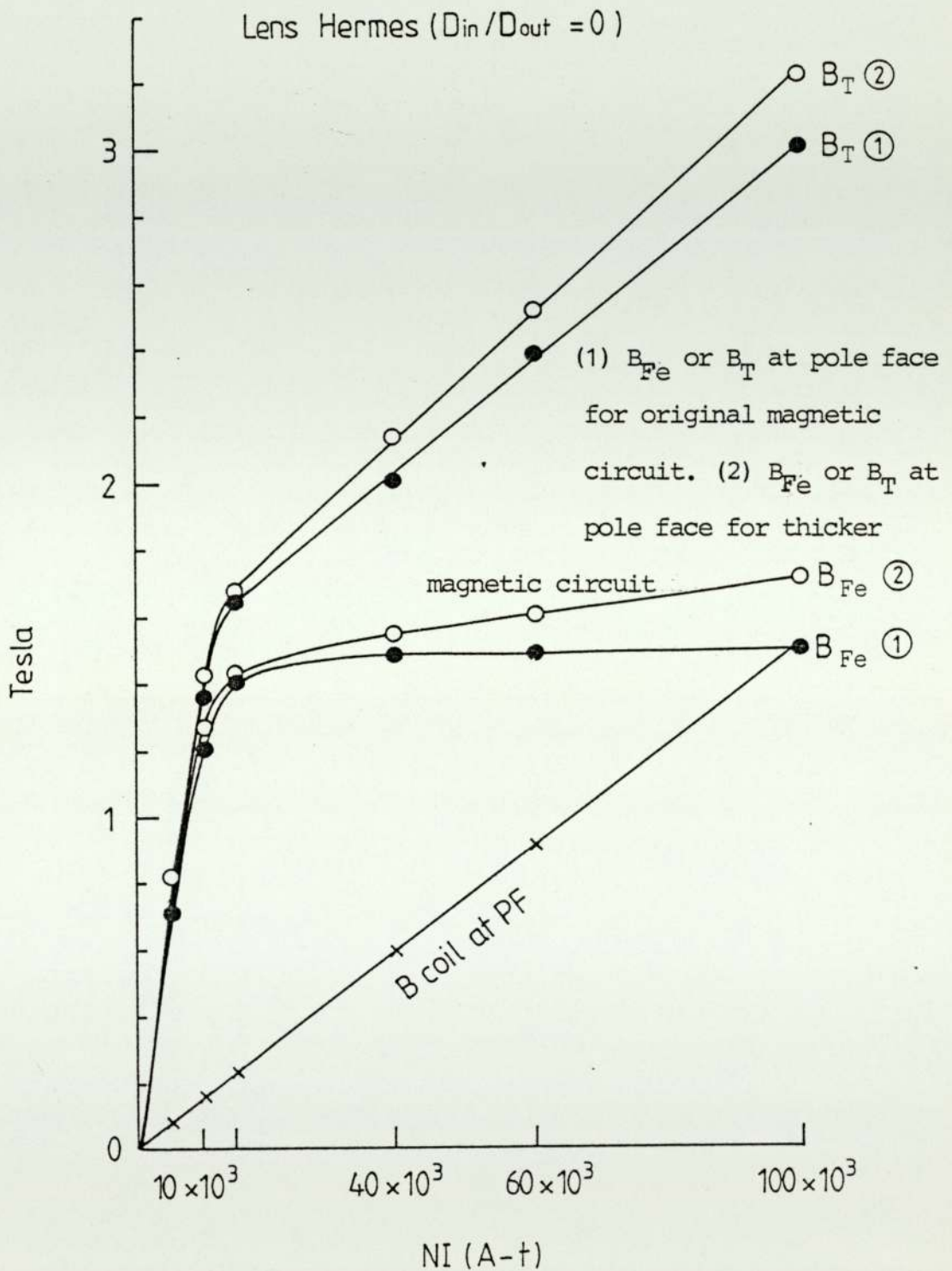
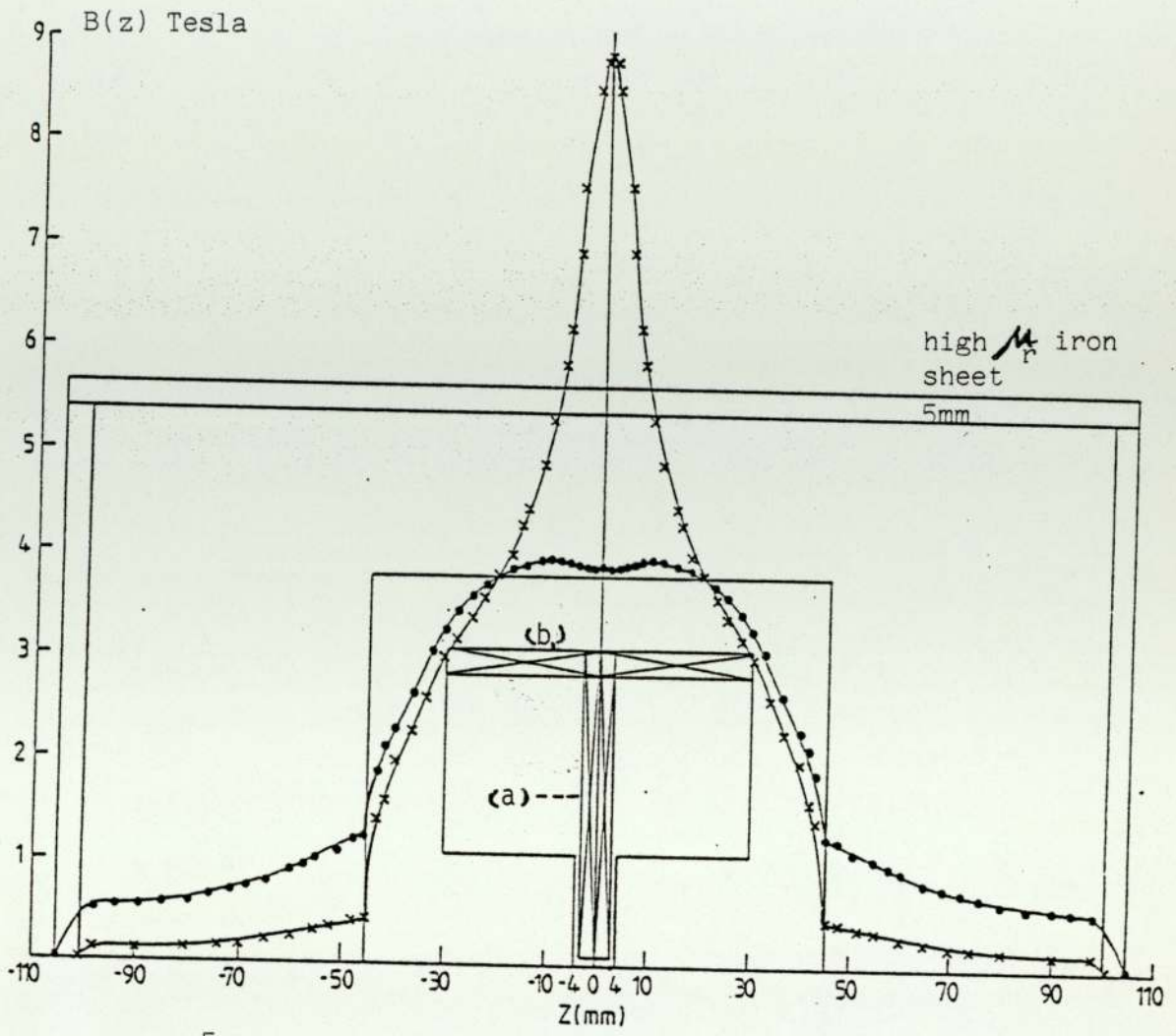


Figure 4.25 Variation of B_T and B_{Fe} at pole face with lens excitation for (A) original magnetic circuit; (B) thicker magnetic circuit, see Figure 4.23 and Figure 4.24 . B coil at pf is shown for reference.



$$NI = 2 \times 10^5 \text{ A-t}$$

$$\frac{D_{in}}{D_{out}} = 0$$

$$(b) \frac{D_2}{D_1} = 1.107$$

$$\frac{S}{D_m} = 0.508$$

$$S = 60 \text{ mm}$$

$$(a) \frac{D_2}{D_1} = 31$$

$$\frac{S}{D_m} = 0.094$$

$$S = 6 \text{ mm}$$

Figure 4.26

Axial flux density distribution of the rectangular double pole (test) lens shown above after surrounding the boundary with (5mm) high permeability iron sheet to overcome boundary loss in excitation (ooo for long solenoid (b) and xxx for short solenoid (a). Note the external flux leakage which is larger in the case of coil (b).

The lens itself is surrounded by a sheet of high permeability iron, in order to eliminate the effect of boundary loss.

External leakage can be noticed with both coils, but with the long solenoid the external leakage is much higher. Figure 4.27a shows a set of $B(z)$ curves at different lens excitation for the double polepiece lens shown in figure 4.28a, when the lens is excited by the short solenoid. Figure 4.27b shows the $B(z)$ curve at different lens excitation when the lens is excited by the long solenoid (b), using thick magnetic circuit to prevent leakage in both cases.

Figure 4.28b shows how thicker magnetic circuit can improve the B_{Fe} value at pole face especially when long solenoid is excited.

4.3.2 Influence of Coil Size and Position

The influence of coil size and position on external leakage can be illustrated from the two lenses studied by Al-khashab (1983). These are the lenses already discussed (see figure 4.19). The second lens studied by Al-khashab is shown in figure 4.29. This has an identical iron circuit; however it has a thin flat coil of 1 mm width placed 0.5 mm away from the pole tip.

Figure 4.29 shows that there is no significant loss in excitation and no appreciable leakage up to about 10^5 A-t.

Moreover the loss in excitation at 6.25×10^5 A-t is only 7% compared with the value of 32% mentioned previously (figure 4.19). This remarkable improvement in lens performance seems to be due to the fact that the thin coil in the vicinity of the polepiece produces a high

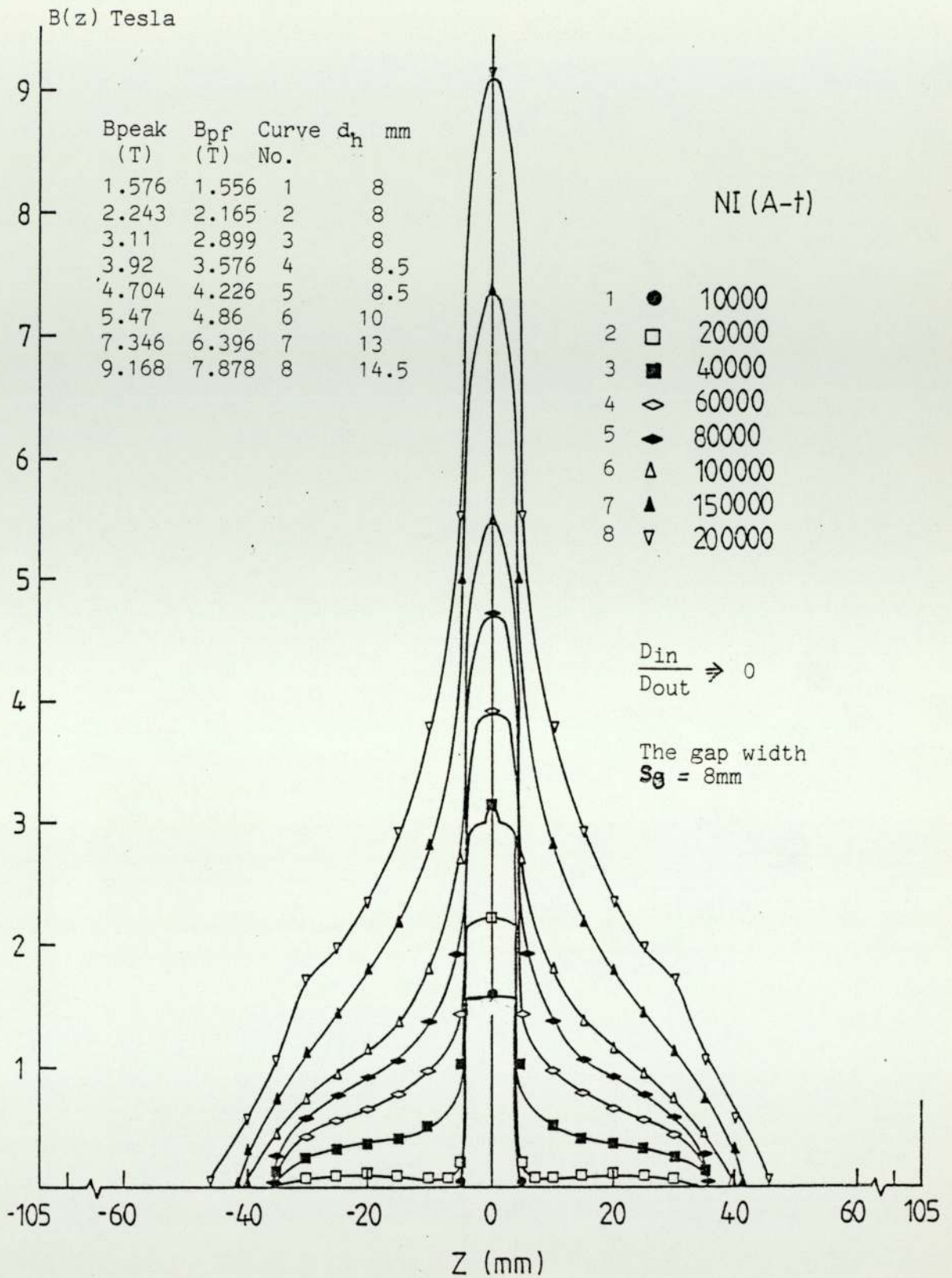


Figure 4.27a

Axial flux density distribution in rectangular double pole lens at different lens excitations with thin coil ($D_2/D_1 = 31$, $S/D_m = 0.094$) the coil position is -3 to 3 mm. The shrouds are very large (70mm, 50mm) i.e. there is no leakage up to (9) Tesla at the peak.

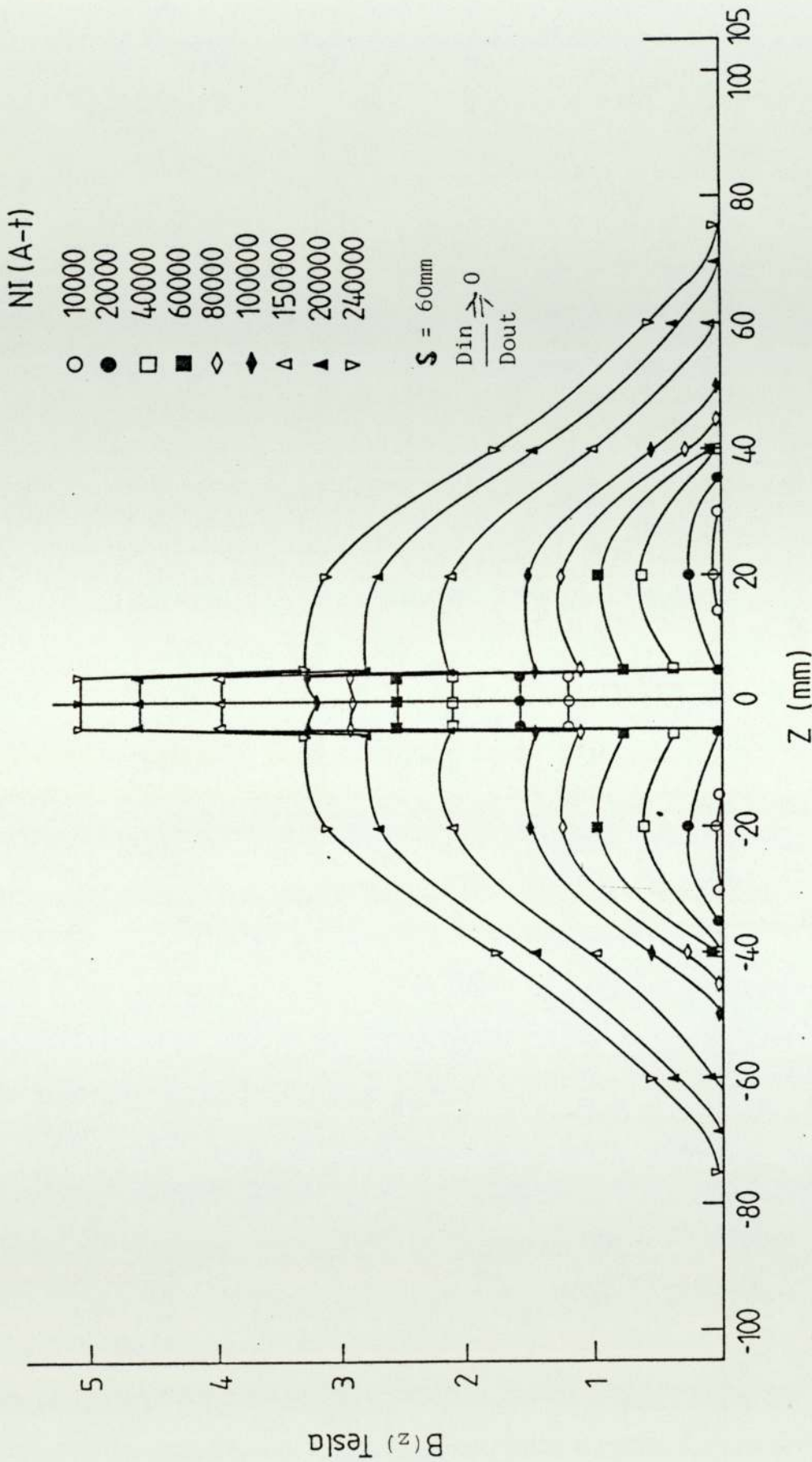


Figure 4.27b Axial flux density distribution for double pole test lens using sufficient shrouds (70,50mm) (i.e. no leakage) with long solenoid ($D_2/D_1 = 1.107$, $S/D_m = 0.508$) at different lens excitations.

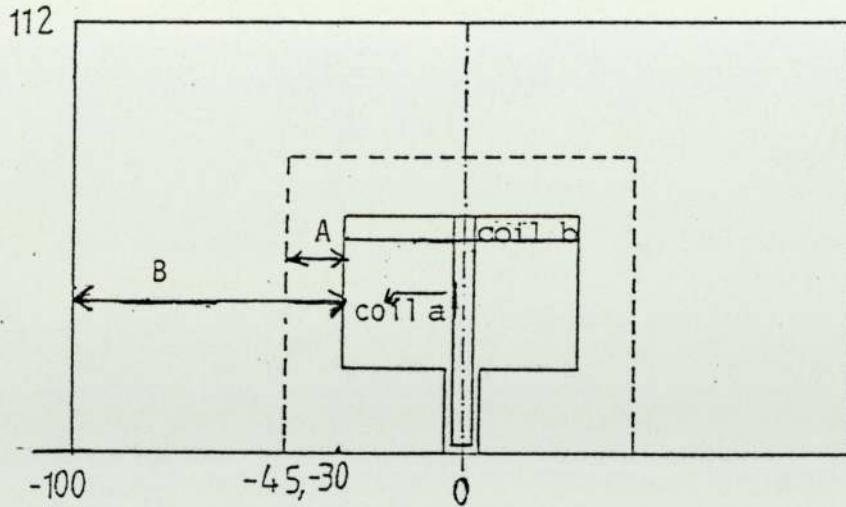


Figure 4.28a

Rectangular double pole test lens with thin magnetic circuit (A) and thick magnetic circuit (B). The lens exciting coils a and b have the same cross section.

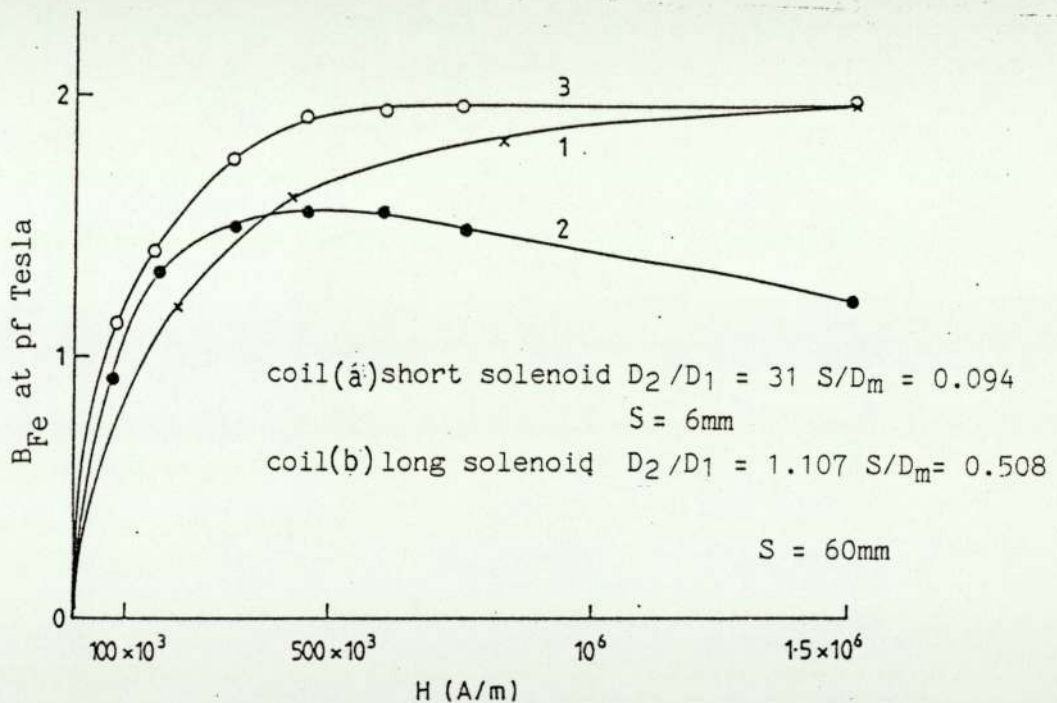


Figure 4.28b Variation of B_{Fe} at pole face with magnetic field strength (H) of double polepiece test lens shown above

- 1 xxx B_{Fe} value at pf when the lens is excited by coil (a) (short solenoid) using magnetic circuit thickness 15mm (A)
- 2 ••• B_{Fe} values when the lens is excited by coil (b) using previous magnetic circuit (A)
- 3 ooo B_{Fe} values when the lens is excited with coil (b) using thicker magnetic circuit (B)

Note: the change of B_{Fe} value for coil (b) when the magnetic circuit is thicker in 3

field in the lens gap but a low field strength in more distant parts of the magnetic circuit as revealed by the flux density distributions of figure 4.29. On the other hand, the coil shown in figure 4.19 produces a higher field strength in the body of the iron polepiece especially where it joins the backing plate of the lens, as indicated by the $B(z)$ curves in figure 4.19.

This means that for a given external leakage flux density a thicker backing plate will be needed for a thick coil surrounding the polepiece than for a thin coil placed near the polepiece tip. Thus the design of the iron casing is strongly influenced by the choice of coil position, when the polepiece operates at saturation flux densities. If the lens casing is not (sufficient) thick, premature saturation will occur in the casing itself, leading to anomalous behaviour of the magnetization of polepiece as mentioned previously (Figure 4.22).

4.4 Systematic Investigation of Possible Lens Designs

4.4.1 Important parameters of double pole lenses

An example of a double pole test lens is shown in figure 4.30. The lens has two coils (a and b) of the same cross-section, but of different shape and position. The lens has sufficiently thick shrouds to prevent external leakage. The lens is excited first with coil a (short solenoid of $S/D_m = 0.094$), placed between the two poles and secondly with coil b (long solenoid) ($S/D_m = 0.508$). The relevant set of $B(z)$ curves were shown previously (figs. 4.27a and b).

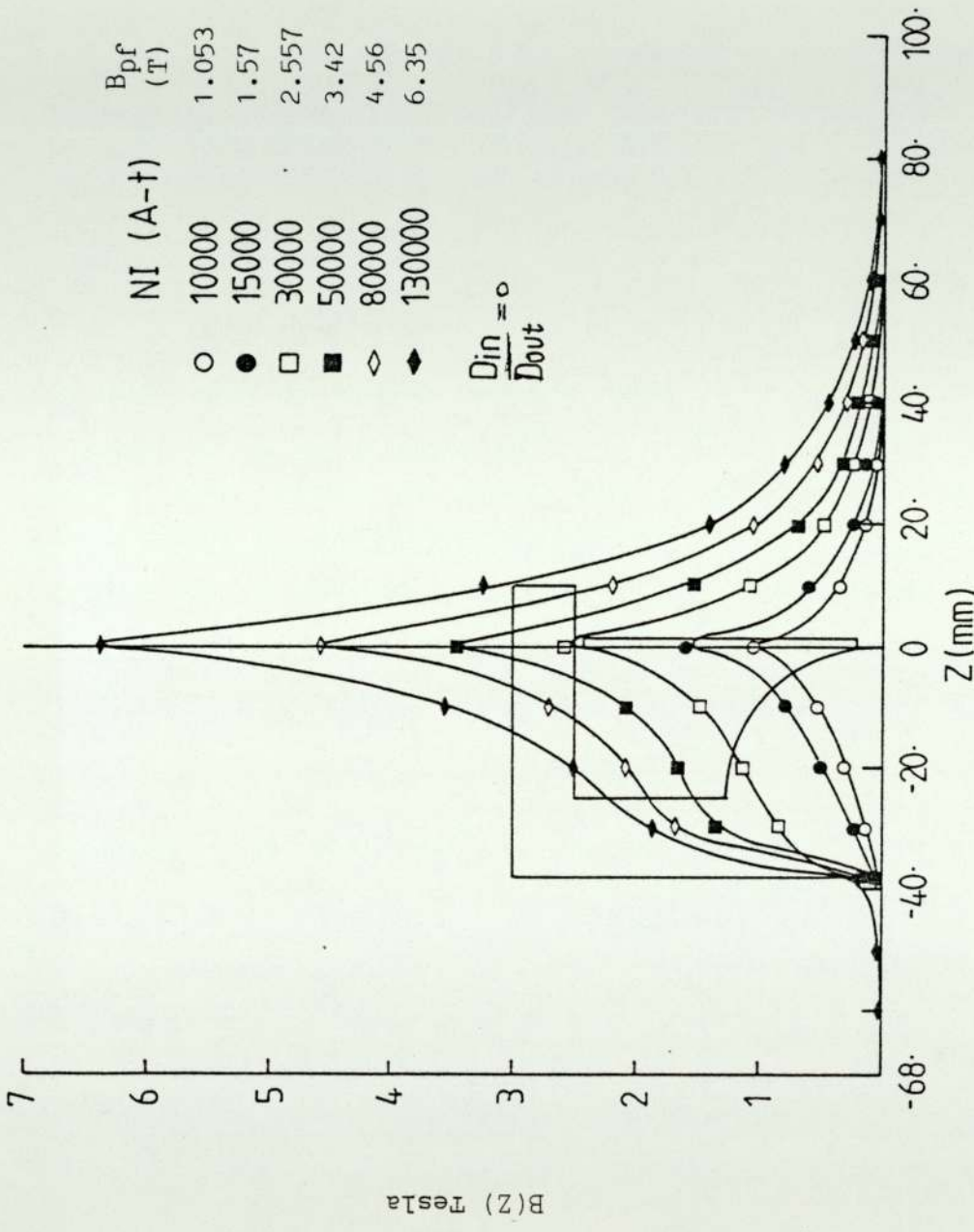


Figure 4.29 Recalculation of the axial flux density distribution for Al-Khashab (1983) spherical single pole lens at different lens excitations using coil of $\frac{S}{D_m} = 0.019$, $\frac{D_2}{D_1} = 12.89$, $S = 1\text{mm}$

Note the external leakage problems appear at 13×10^4 A-t, i.e at B_{pf} 6.35 Tesla

Figure 4.30 also shows the variation of the pole face tip magnetization B_{Fe} and the half width d_h as functions of the magnetic field strength (H).

Up to 7×10^5 A/m, the half width does not depend on the coil shape or position this means that the half-width is determined by the iron polepieces.

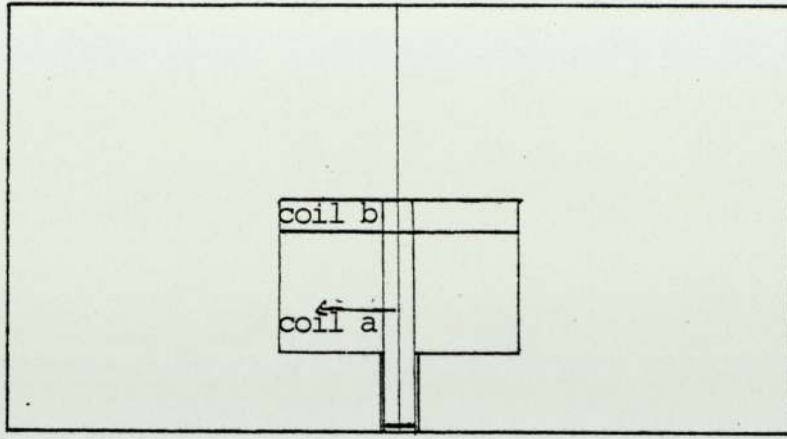
Above this excitation the half-width increases sharply when the long solenoid is excited. With the short solenoid the half-width does not increase with saturation since the half-width of this is much smaller than that of the long solenoid.

The B_{Fe} values for a given value of H are higher in case of the long solenoid; this means it is a better magnetiser for the pole face tip.

The relevant advantages and disadvantages of thick and thin coils are explained in the next section.

4.4.2 Important parameters in single pole lenses

In previous sections the importance of the lens casing of a single pole lens has been discussed. In the present section it is assumed that this aspect of the design has been taken care of. This means that the design of the exciting coils must now be considered in more detail. It must be borne in mind that the performance of any lens can be improved by making it smaller. This is particularly important in a single polepiece lens where the field produced by the coil itself plays a more important role than in the case of a double pole lens. Hence in the final design stage a decision has to be taken about the



b $60 \times 6\text{mm}^2$ ($D_2/D_1 = 1.107$, $S/D_m = 0.508$, $S = 60\text{mm}$)

a $6 \times 60\text{mm}^2$ ($D_2/D_1 = 31$, $S/D_m = 0.094$, $S = 6\text{mm}$)

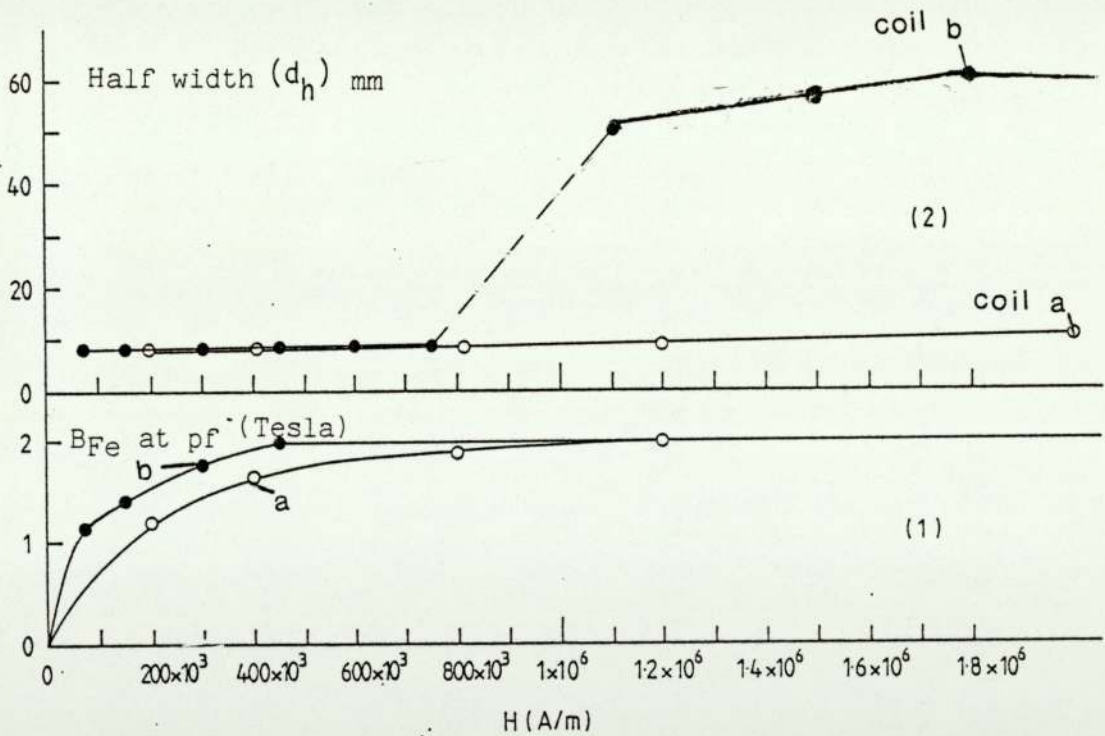
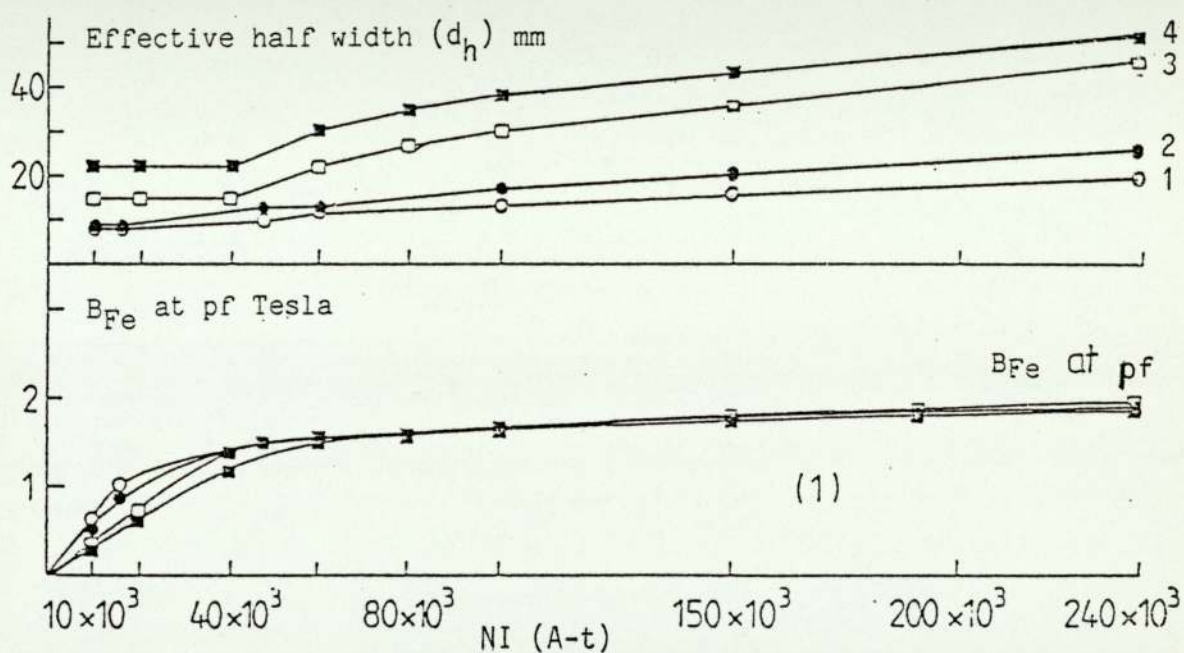
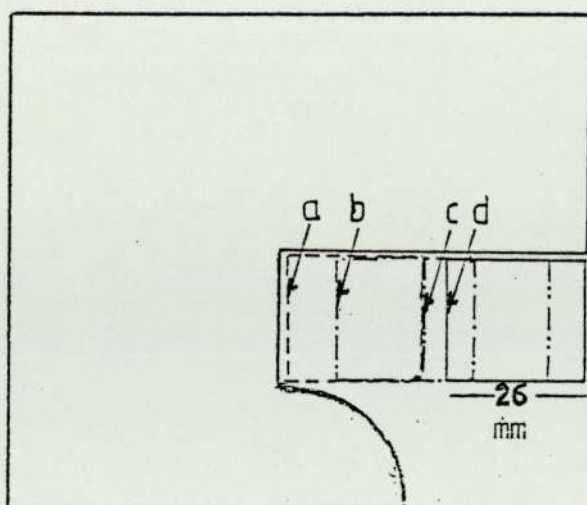


Figure 4.30 (1) Variation of the magnetization of the polepiece tip and (2) the variation of the half-width of rectangular double polepiece test lens as a function of magnetic field strength (H) excited:
 with **b** (●-●-●) long solenoid coil
a (○-○-○) short solenoid coil

maximum allowable current density in the windings. Hence in comparing different designs of lens, it is highly desirable to compare them at the same current density.

Figure 4.31 shows the results of a series of calculations on the single-pole lens already shown in Figure 4.21. The object of the calculations was to find the effect of coil positions on the magnetisation field B_{Fe} due to the iron at the pole face, and in particular to see under what conditions it reached the saturation value. The other important parameter is the half-width d_h . The results of this calculation are shown in Figure 4.31. The figure shows that when the coil face is in contact with the back plate of the lens (position a) the polepiece magnetisation is greatest, for a given value of NI . However, as saturation flux density is approached i.e. at higher excitations, the position of the coil is not important.

Concerning the half-width d_h , at low excitations and hence low iron polepiece magnetisation, the half width does not depend on the excitation. This is to be expected since in this region the field distribution is largely controlled by the iron polepiece. However the position of the coil does affect the half-width. The half-width is a minimum for coil position a. At low values of NI , the half-width is independent of excitation since it is strongly influenced by the iron circuit. However as the iron begins to approach saturation the half-width of the coil itself becomes important and finally dominates as the iron reaches its full saturation value. It might seem therefore that an ideal coil arrangement would be a thin coil placed near the pole tip of similar lens, as shown in Figure 4.32. This figure shows that for a given excitation, the thin coil is a slightly better

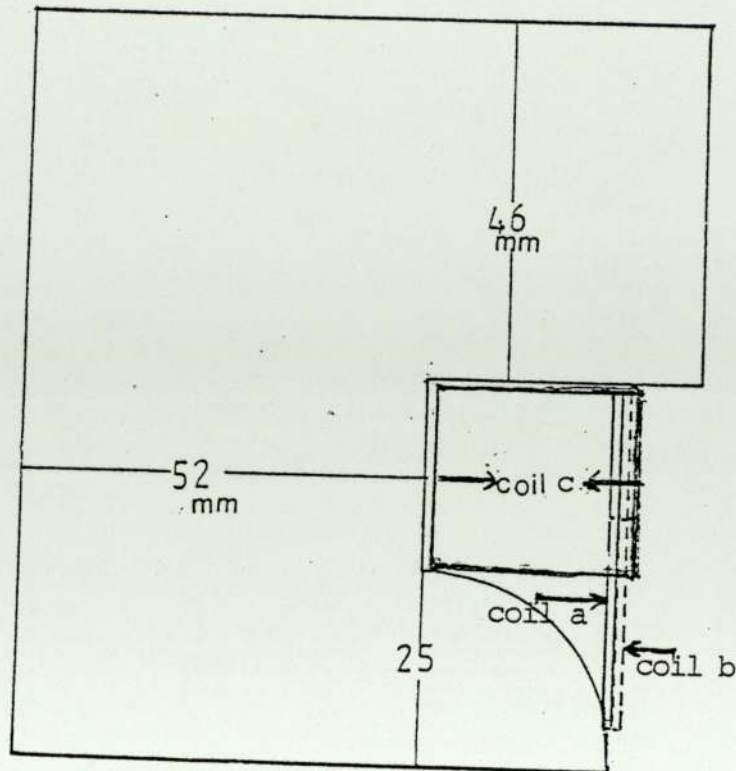


Rectangular coil 26mm in thickness
 $D_2/D_1 = 1.88$, $S/D_m = 0.347$

Coil face from lens end plate
 a) 1mm, b) 12mm, c) 27mm, d) 33mm.

1, 2, 3 & 4 are B_{Fe} or d_h , for coil position a, b, c & d respectively.

Figure 4.31 For coil position a - d as a function B_{Fe} at the pole face p_f and the axial field half width (d_h) with coil positions lens excitation in a spherical single pole lens. Full diagram shown in figure 4.21 .



coil c $D_2/D_1 = 1.88$ $S/D_m = 0.347$
 $S = 26$ mm

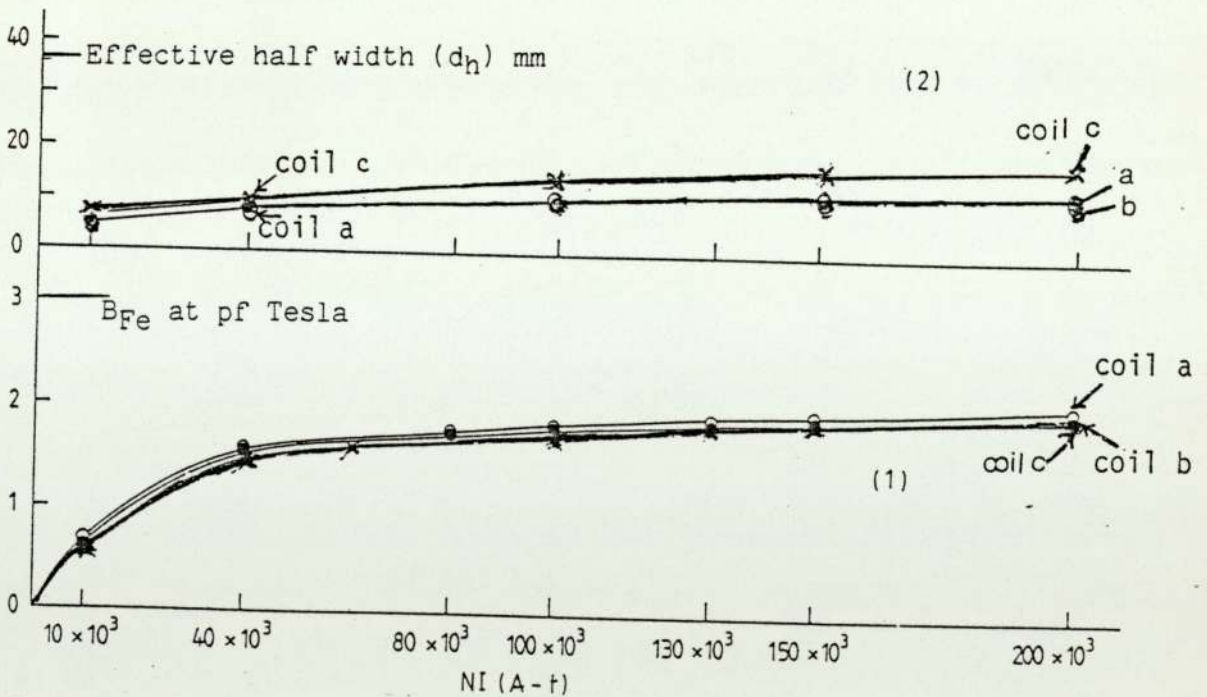


Figure 4.32

(1) Variation of the magnetization of polepiece tip and (2) the variation of the half-width of spherical single pole lens as a function of the lens excitation by thin coil ($D_2/D_1 = 9.8$, $S/D_m = 0.0185$).

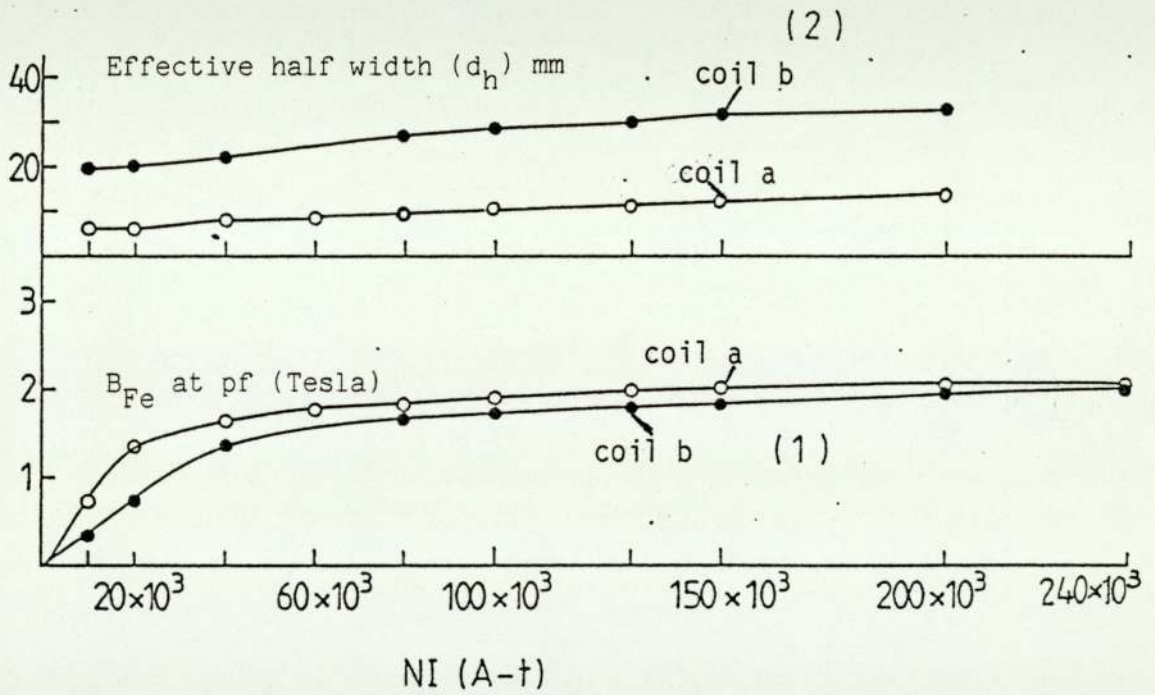
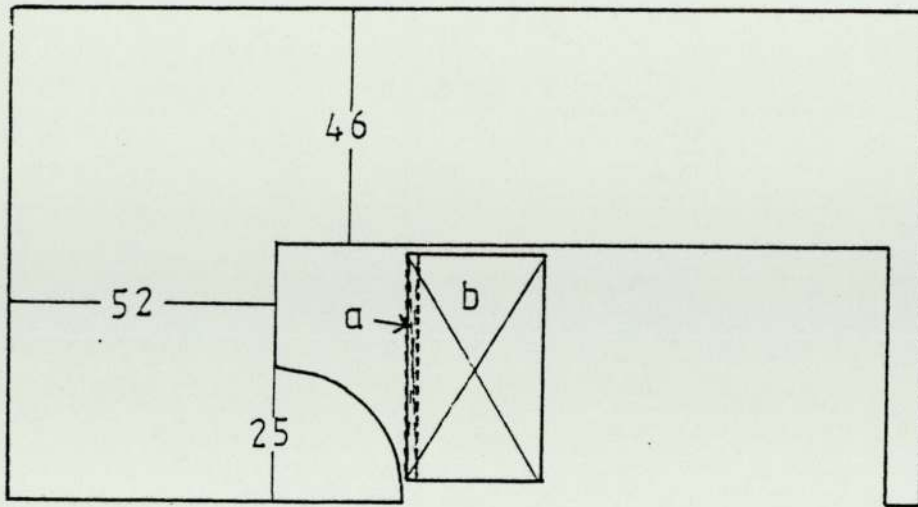
- a) (●-●-●) thin coil position (-0.5 to 0.5mm)
- b) (o-o-o) thin coil position = .5 to 1.5mm)
- c) (x-x-x) thick coil surrounding the polepiece

magnetiser i.e. B_{Fe} value at the pole tip is somewhat higher than with a thick coil. In addition the half-width (d_h) is also smaller and does not increase greatly at the polepiece saturation. However, other factors, such as the current density in the windings have not yet been taken into consideration, and these factors could be of decisive significance. Similar remarks also apply to the B_{Fe} and d_h values for the test lens shown in Figure 4.33, in which the coil a is a thin flat solenoid, and coil b is a much thicker solenoid of the same inner and outer diameter. The thin solenoid results in a significantly lower half-width and a stronger pole tip magnetisation for a given lens excitation.

Since in an electron lens operating at a given accelerating voltage, the excitation NI is specified in advance, rather than the field strength H , it appears that the thin flat solenoid of large outer to inner diameter is the ideal design for the exciting coil. The coil should ideally be in contact with the pole tip.

4.4.2.1 Comparison of B_{Fe} - H curves for single-pole lenses

In order to obtain an overview of the magnetic behaviour of a single-polepiece lens under well-defined magnetic conditions, figure 4.34 shows a single polepiece test lens with a spherical polepiece and completely surrounded by a substantial iron casing. The iron is a typical soft iron [B-H curve from Table 1.1 of Munro's Ph.D. thesis]. The thick iron casing in the polepiece region was designed to ensure negligible external leakage, so as to eliminate boundary errors in the calculation and also to eliminate anomalous magnetic behaviour (unwanted saturation effects) in the casing. The iron boundary that crosses the axis at a point remote from the polepiece was positioned



- a. Thin coil ($D_2/D_1 = 12.89$, $S/D_m = 0.019$) $s = 1\text{mm}$
 b. Large coil ($D_2/D_1 = 12.89$, $S/D_m = 0.99$) $s = 26\text{mm}$

Figure 4.33

Variation of (1) B_{Fe} values at pf and (2) half width with lens excitation of spherical single pole lens excited with different $\frac{S}{D_m}$ coils placed at same distance from the pole face.

sufficiently far away as not to influence the magnetisation of the polepiece itself.

In order to avoid computational difficulties caused by the presence of a bore, the axial flux densities were first calculated for the lens with zero bore. In presenting the results it was assumed that there was a bore of negligibly small diameter so that the calculated $B(z)$ values in the iron were simply divided by the relative permeability μ_r at the corresponding point on the axis. This means that the area under $B(z)$ curves in the figure is a measure of the ampere turns expended in the lens as a whole.

The maximum axial flux density in the axis on this series of calculations reached about 10 Tesla. The maximum flux density shown in Figure 4.34 is about 5.5 Tesla with the coil shown in the figure. Other distributions were obtained for a variety of coil arrangements. From these results it was possible to plot the B-H characteristics of the polepiece tip as shown in Figure 4.35. Here curve 1 is the magnetisation (B-H/H) curve of the soft iron of the lens. The other curves show the B/H curves of the pole tip with different coil arrangements stated in the figure. It can be seen that the best B/H curve is obtained for coils (2-5) completely surrounding the polepiece.

The coils (8-10) are thin flat solenoid types. This group does not produce such good B/H curves. However it should be remembered that coils in this position make a bigger contribution to the useful axial field distribution of the lens.

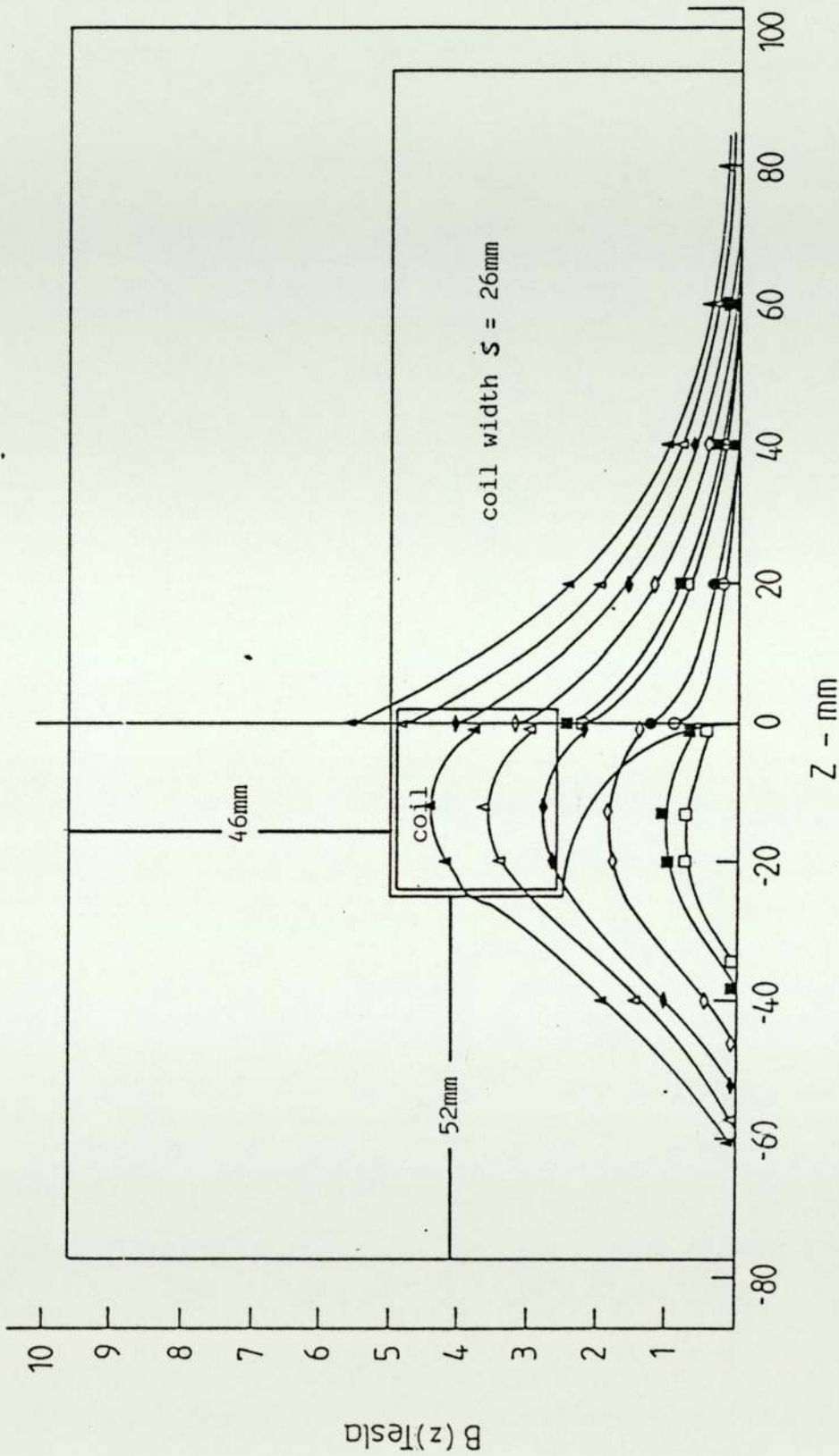


Figure 4.34 Axial flux density distribution for spherical single pole lens at different lens excitation with coil ($D_2/D_1 = 1.88$, $S/D_m = 0.347$) The lens is improved by very large shrouds and shielding from the open side (6 mm) ; $\frac{D_{in}}{D_{out}} \rightarrow 0$ (vanishingly small bore)
 NI :- \circ 10000, \bullet 16445, \square 47840, \blacksquare 60000, \diamond 100000,
 \blacklozenge 150000, \triangle 191360, \blacktriangle 239200. (A-t)

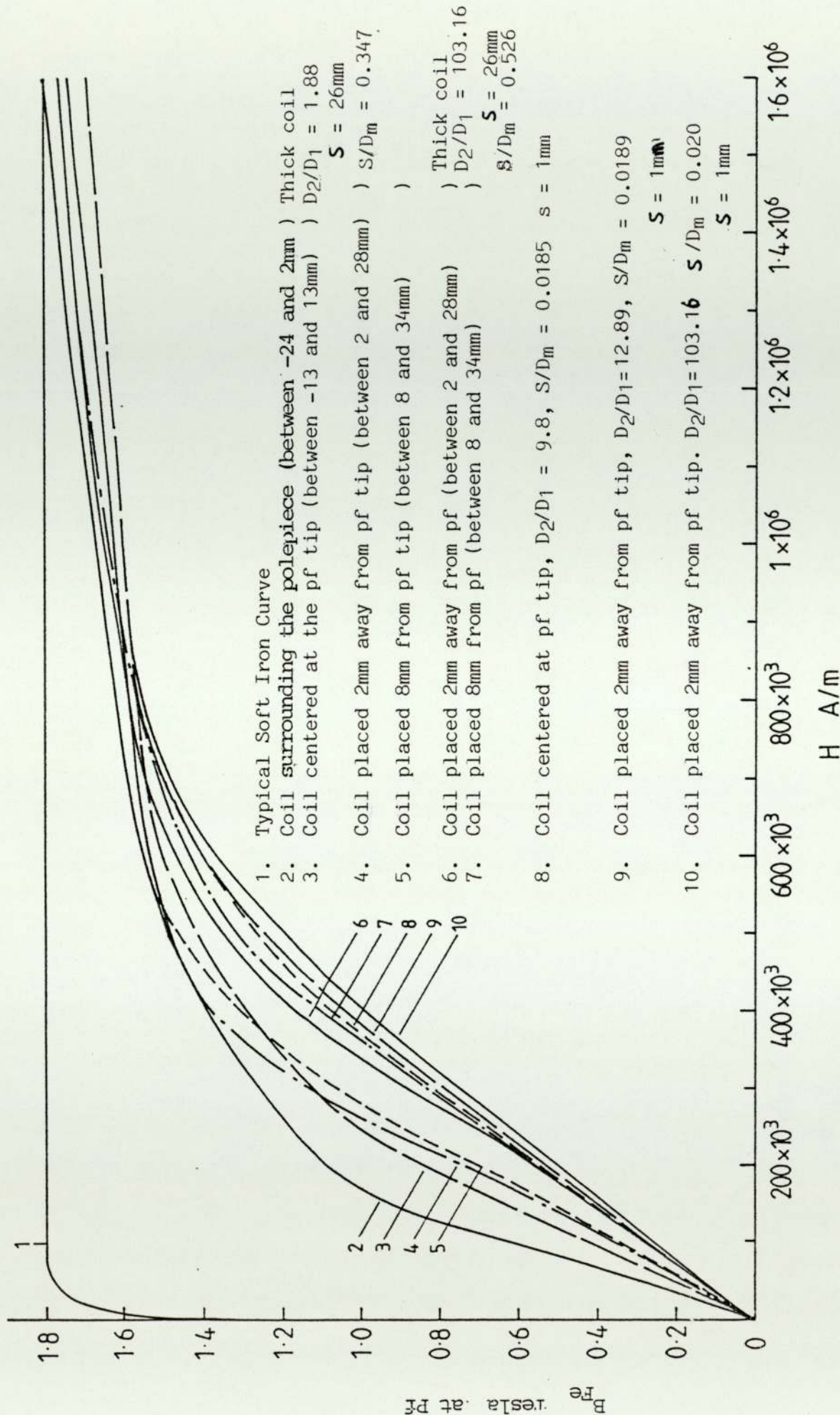


Figure 4.35 Variation of the B_{Fe} value at pf tip, as function of field strength (H A/m), with coil size and position, for the redesigned spherical polepiece lens, shown in figure 4.34

We can therefore conclude that the criterion of producing the best B/H curve at the pole-tip is not as critical a parameter as might be thought at first sight.

4.4.3 Effect of current density in lens windings

Since the thin flat coil in contact with the polepiece appears to be a favourable design, it is necessary to think about the effect of current density in the windings, since this increases rapidly as the coil is made thinner. If the current density is restricted, the main effect will be to make such a coil larger. The lens itself will be larger and so its focal properties and aberrations will also increase. This criterion will be relevant for double pole and single pole lenses. This is illustrated in Figure 4.36 which shows a double polepiece lens (1) with a thin flat solenoid placed between the polepieces of rectangular cross-section. The polepieces have a bore of negligible but not zero diameter. The axial flux density distribution is shown in the solid curve of Figure 4.36. The peak axial flux density is 7.34 Tesla and the half-width $d_h = 13$ mm.

If now a second coil in the form of a long solenoid of the same cross-sectional area is added (lens 2) and operating at the same current density the lens cross-section must clearly be reduced by a factor of two in order to maintain the same value of excitation NI. The resulting axial field distribution shown in Figure 4.36 is not significantly changed. A similar result is shown in Figure 4.37 for a single polepiece lens. The coils of lens (1) and lens (2) operate at the same excitation NI and the same current density. The relevant part of the field distribution i.e. for $Z > 0$ is nearly the same in both lenses. In fact the iron losses in lens (2) are somewhat greater

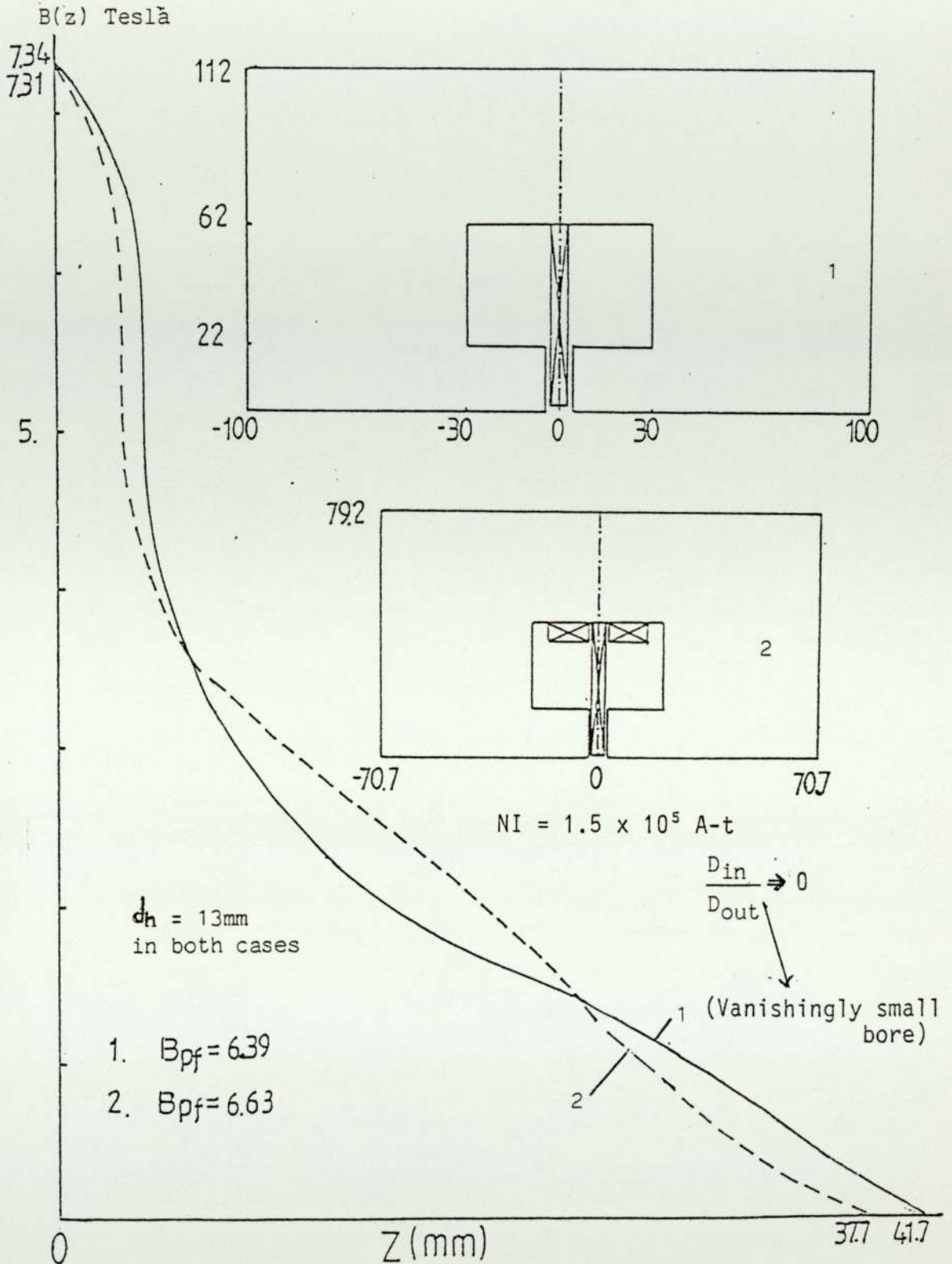


Figure 4.36 Comparison between the axial flux density distribution (keeping the current density constant) of rectangular double pole piece lens shown in figure 4.27a : excited with
 (1) Short solenoid placed in the gap between the two polepieces
 (2) Combination of short solenoid placed in the gap and two coils (of total area = 360 mm^2) as shown above. Note the cross-section of lens. (2) is half of lens (1). There is no significant difference in peak flux value or the half width between two cases.

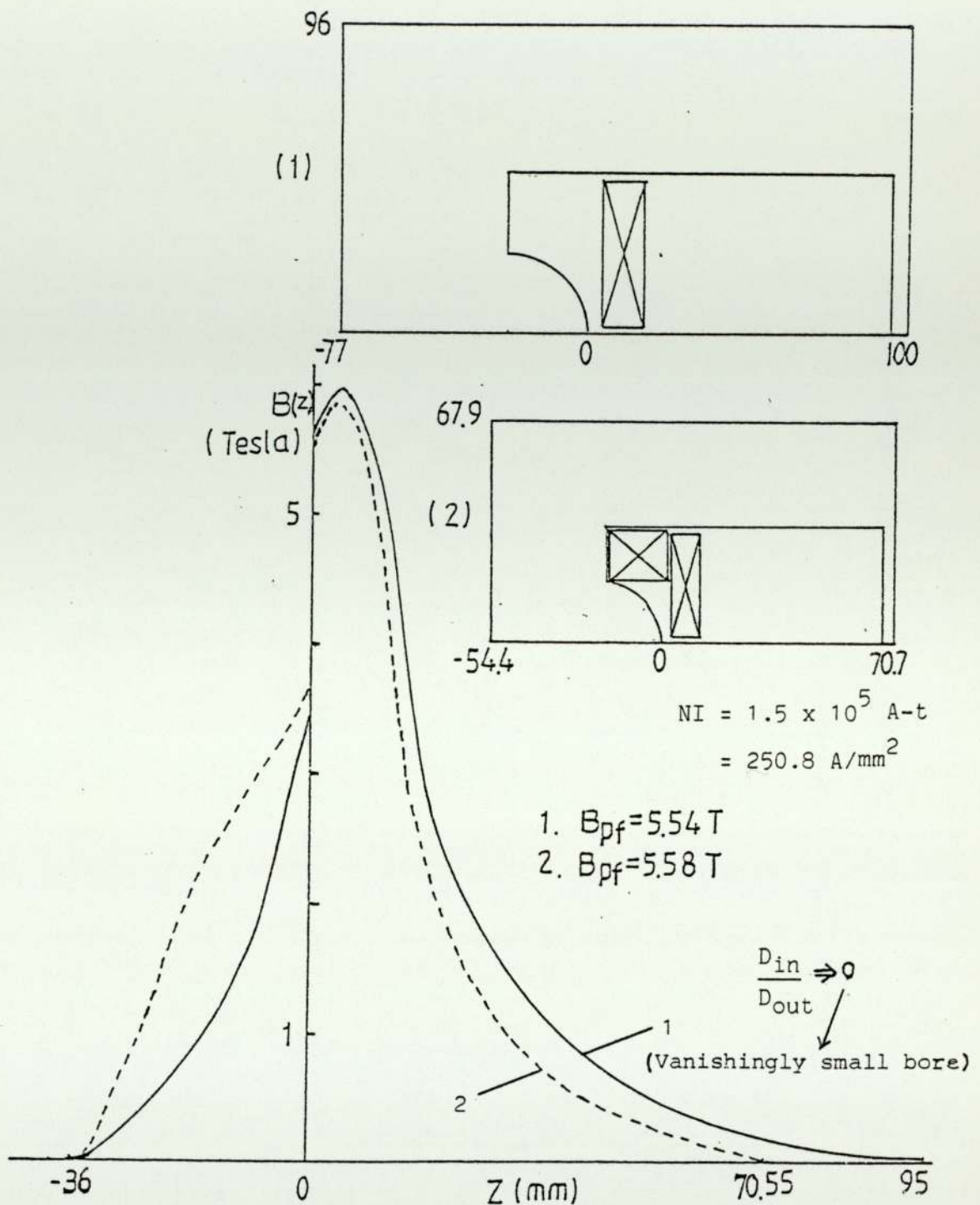


Figure 4.37

Comparison between the axial flux density distribution (keeping the current density constant) of the spherical single pole lens shown in figure 4.34 excited with (1) a coil ($D_2/D_1 = 24$).

$S/D_m = 0.26$, $s = 13\text{mm}$) placed outside the pole face (solid line)

(2) a combination of a thick coil surrounding the polepiece and a thin coil of the same cross section placed outside the polepiece (dotted line).

Note the cross-section of lens (2) is half that of lens (1).

Case 2 has a slightly lower peak and lower half-width than case 1.

than in lens 1. Thus if extra excitation were applied to lens 2, to bring the peak flux to that of lens 1, the resulting axial field distribution for $Z > 1$ would be approximately the same.

We can therefore conclude that the current density criterion is probably the most significant parameter in the design of saturated magnetic lenses.

CHAPTER FIVE

CONCLUSIONS AND DISCUSSION

The main purpose of the present investigation was to throw light on the application of the finite element method to the determination of the magnetic field distribution in magnetic electron lenses and especially to the development of criteria for judging the finally calculated results. Attention has been concentrated on two aspects of this subject; first the efficiency and limitation of existing programs and secondly on some unexpected lens design problems that arise when highly saturated polepieces are incorporated into the objective lens. These are partly connected with the programs themselves (boundary conditions) and partly with the electron optical design itself.

Munro's original programs are, justifiably, still very popular with research workers. The only subsequent programs which now seem to have achieved equal status are those of Nasr (1981) and Lencová (1984). The original program written by Nasr was unreliable for practical use but once the program errors were put right, it was possible to analyse it in detail. These two programs offer certain operational advantages which the present investigation has highlighted. It has been found extremely useful, for example to have a "second opinion" of doubtful output calculations during the present investigations. However, it may be concluded that, in the hands of experienced operators, no serious errors have been detected in any of these programs. However, if reliance is placed entirely in one program, the chances of making an undetectable error are greatly increased. Useful savings in computer memory can be achieved when Nasr's programs are used.

These programs are thus very convenient for small research laboratories where mini or micro computers are available, and computer time is not of the same importance as that of memory store. It is also possible to produce smooth axial field distributions of an initially obtained trial distribution at the early design stages.

The present investigation has confirmed previous work by Nasr on the importance of boundary settings and numbers of meshes. It would appear however, that many research workers have not paid enough attention to boundary problems in saturated lenses which produce high external leakage flux, in both conventional and unconventional lenses. It also seems that sufficient attention has not been paid in the past to the importance of mesh layout. It is a wise precaution to calculate a completely new type of lens with two different mesh layouts. Alternatively the number of meshes can be increased in a second calculation and the results extrapolated to zero mesh size.

This study has shown that single polepiece lenses, which have been computed under linear conditions with an adequate boundary setting, may exhibit large boundary loss under saturation conditions. This can be checked by calculating the flux density near the boundary. Conventional and double pole lenses usually have no boundary problems under linear conditions, since the high permeability iron casing on all sides of the lens will act as shielding for the lens field.

When such lenses are computed at high lens excitation (under saturation condition), there may be a large external field. If the boundary $A = 0$ is too close to the lens, this high external flux density will lead to an apparent loss of turns at the boundary.

This occurrence should draw the designers attention to faulty design of the lens casing. Some useful rules of thumb have emerged from this study; in iron-free coils, for example, the boundary should be set at a distance of about five times the mean coil diameter from the lens centre. In single pole lenses under linear condition, this is also appropriate for the open side, but less so on the side shielded by the magnetic circuit.

These rules also apply to a well designed magnetic lens under saturation conditions. Only if the lens is badly designed will the external flux values be very high resulting in loss of excitation at the boundary. The facility of calculating the excitation contributing to the axial flux distribution built into the Lencová program has proved to be an enormous advantage in designing new lenses.

In addition, the Lencová printout map of flux density distribution in the iron circuit is also a useful diagnostic aid in such cases, and is automatically available as part of the regular print-out. Another useful checking facility is the evaluation of the B_{Fe} values in the magnetic circuit. Since the magnetic circuit will not add any extra ampere-turns to that provided by the coil, this check can be made by calculating the B_{Fe} values as $(B_T - B_{coil})$. If the field computation has been made correctly, the integral $\int_{-\infty}^{\infty} B_{Fe} dz$ should be zero. A discrepancy in this quantity indicates some form of computational error. Figure 5.1 shows the total axial flux density distribution, the axial flux density of the coil calculated with the Biot program, and also the iron contribution to the field distribution $B_{Fe} = (B_T - B_{coil})$ for the rectangular single pole lens shown in figure 2.5. Here the lens is surrounded by a 5mm thick high permeability

iron sheet to prevent any boundary loss in excitation, also large number of meshes (69 x 90) were used to prevent any computational errors due to insufficient number of meshes.

In connection with the calculation of B_{coil} it may be remarked that the calculating of the axial flux density distribution by the Biot-Savart law is a very good starting point for any lens computation, especially for choosing the correct boundary. It is perhaps unfortunate that B_{coil} is not calculated routinely in any of the above programs. Appendix 2 lists a program Biot which can be used in connection with the above programs. It would therefore be useful to add Biot and a B_{Fe} facility to the existing programs.

A crucially important factor in FEM calculations is the choice of mesh distribution. This investigation has shown that different mesh arrangements set up even by experienced operators can sometimes lead to large discrepancies in the computed flux density values. For example, the initial coarse mesh layout must be chosen carefully, giving special attention not only to the polepiece gap region, but also to the complete polepiece and the coil. The mesh concentration must decrease gradually; sudden and abrupt changes must be avoided.

It is usually possible to find by trial and error a mesh layout that gives good agreement between experimental and calculated results even with limited mesh numbers. Experience shows that to optimise the mesh distribution for a new and unknown design, two or perhaps three different mesh layouts should be tried, especially if the number of meshes is restricted. The effect of changing mesh distribution is to alter the shape of the axial computed field

distribution, especially near the peak value. The effect of insufficient mesh numbers will almost certainly result in a change in the shape of the axial field distribution but possibly accompanied by an apparent loss of excitation. In all cases in this investigation, it was possible to find a mesh distribution that led to good agreement with experimental values. It is in any case advisable to check that the mesh distribution finally adopted is not sensitive to small variations. For example, one can extrapolate the calculated peak flux value for three limited mesh sizes to that for mesh of infinitely small size. The author is grateful to B. Lencová for this suggestion, (private communication), which has been found extremely helpful in checking for correct mesh layout.

Another conclusion of the investigation concerns the actual design of lenses. Although this was not the central issue of the investigation, it was realised that if one can be sure that all computational errors have been removed it would be possible to investigate difficult design questions concerning highly saturated magnetic electron lenses.

These include the effectiveness of the exciting coil in magnetising the pole face tip, the direct contribution of the coil itself to the field in the lens gap and the effect of a limiting coil current density on the maximum axial flux density for a given half-width that can be produced in a magnetic polepiece lens.

Concerning the magnetising of the polepiece, from the point of view of the relevant B/H curves of the iron polepiece tip, a coil surrounding the polepiece is superior to a thin flat coil placed in the gap. However, in electron optical systems, the total lens

excitation NI is fixed in advance. Under these conditions the B/NI curves are similar for both types of coils. From the point of view of the contribution of the coil to the field in the lens gap, a thin flat coil is superior to a coil surrounding the polepiece.

However, if we specify in advance the maximum current density in the coil the use of such a thin coil will mean that the size of the lens and hence the aberrations will increase compared with the use of a thicker coil surrounding the polepiece.

If a thick coil and a thin coil are incorporated in the lens at constant current density the overall size of the lens decrease. In a single pole lens as shown in Figure 4.37 the half width also decreases. Since the shape of the effective field distribution in the air gap space is not appreciably changed this leads to lower spherical aberration. On the other hand when different combined coils were used in a rectangular double pole lens at constant current density, although the size of the lens with combined coils is smaller as before, the spherical aberration for combined coils was always larger than that for a lens with a thin coil placed in the lens gap. This suggests that the best performance of a double polepiece lens can be obtained with short solenoid placed in the gap between two poles.

Spherical aberration characteristics of objective lenses with thin exciting coils placed in the air gap between two poles.

Figure 5.2 shows the variation of C_s with current density σ for four different lenses operating at 2000 Kv in the $Z = 0$ mode. Lens 1 is a

rectangular double polepiece test lens shown in Figure 4.36 computed with vanishingly small bore i.e $Sg/D = \infty$.

It can be seen from the Figure that the spherical aberration coefficient of this lens is very high at low current density. $C_s = 16.35$ mm at 1.1×10^3 A/cm². At higher current densities, the C_s value decreases sharply reaching $C_s = 1.39$ mm at 2.57×10^4 A/cm² as the pole tip reaches saturation ($B_{Fe} = 1.84$ T). The lens diameter decreases as σ increases; at the above current density the diameter is 145 mm, still a practical value. The dashed line in Figure 5.2 shows the C_s values for lens 1 but with $Sg/D = 2$. At a value of $\sigma = 1.1 \times 10^3$ A/cm² the C_s value is now 5.5 mm, compared with the previous 16.35 mm i.e a decrease in C_s value of 66% on changing the Sg/D ratio. This means that in double polepiece lens the Sg/D ratio will mainly influence the lens behaviour at low current density, while at high current density (polepiece saturated) this ratio will have only a minor influence on the spherical aberration.

Lens 2 is a rectangular double polepiece lens with $Sg/D = \infty$ also shown in Figure 5.2. Its design is similar to that of lens 1, but the axial length of the polepieces is shorter by a factor of 15/26 than those of lens 1. The computed C_s values for lens 2 at $\sigma = 1.1 \times 10^3$ is 6.5mm compared with 16.35mm for lens 1. At $\sigma = 2.57 \times 10^4$ A/cm² the (polepiece $B_{Fe} = 1.8T$) C_s value for lens 2 is 1.22 mm.

Lens 3 is a double spherical polepiece lens designed by the authors colleague H.C. Yin. The author is grateful to her for providing these unpublished results (private communication) for comparison purposes. The details of the lens are shown in the insert in

Figure 5.2. This lens has several important refinements. The pole piece have spherical ends that reduce the leakage flux compared with simple cylinders, and improve the shape of the axial field distribution. In addition the coil of lens 3 has a ratio D_2/D_1 (outer to inner diameter) of 58.5 compared with $D_2/D_1 = 21.0$ for lens 2. This means that the C_s values of lens 3 are consistently lower than those of lens 2. In both cases the C_s values decrease steadily as σ is increased. Further calculations also showed that at high values of σ , the effect of the lens bore is small.

Experience shows that log/log scale is the best, to compare the C_s behaviour of different lenses at any current density, since correct analysis can ^{be} made even for minor differences, which are confusing by ordinary comparison.

The main conclusion in this investigation is that computer aided design unassisted by experiment, can indeed be made successfully by applying FEM if the designers are aware of all the factors affecting the accuracy of the method and has enough experience to analyse the results correctly.

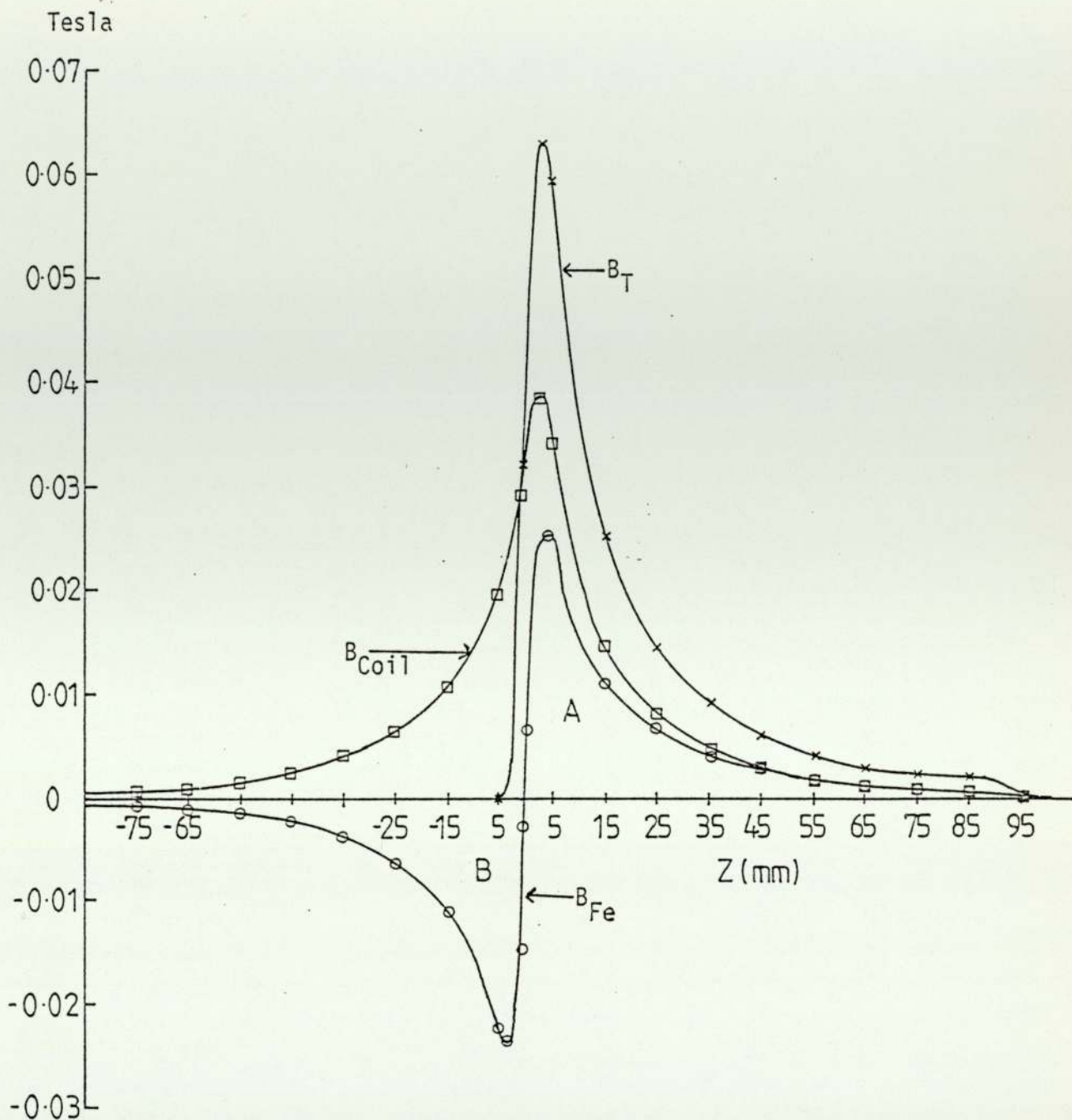


Figure 5.1

Contribution (B_{coil}) of the exciting coil and of the iron (B_{Fe}) to the total axial flux density B_T in the single polepiece lens shown in Fig. 2.5.

Note The positive and negative parts of the B_{Fe} curve balance within 1% indicating low computational error.

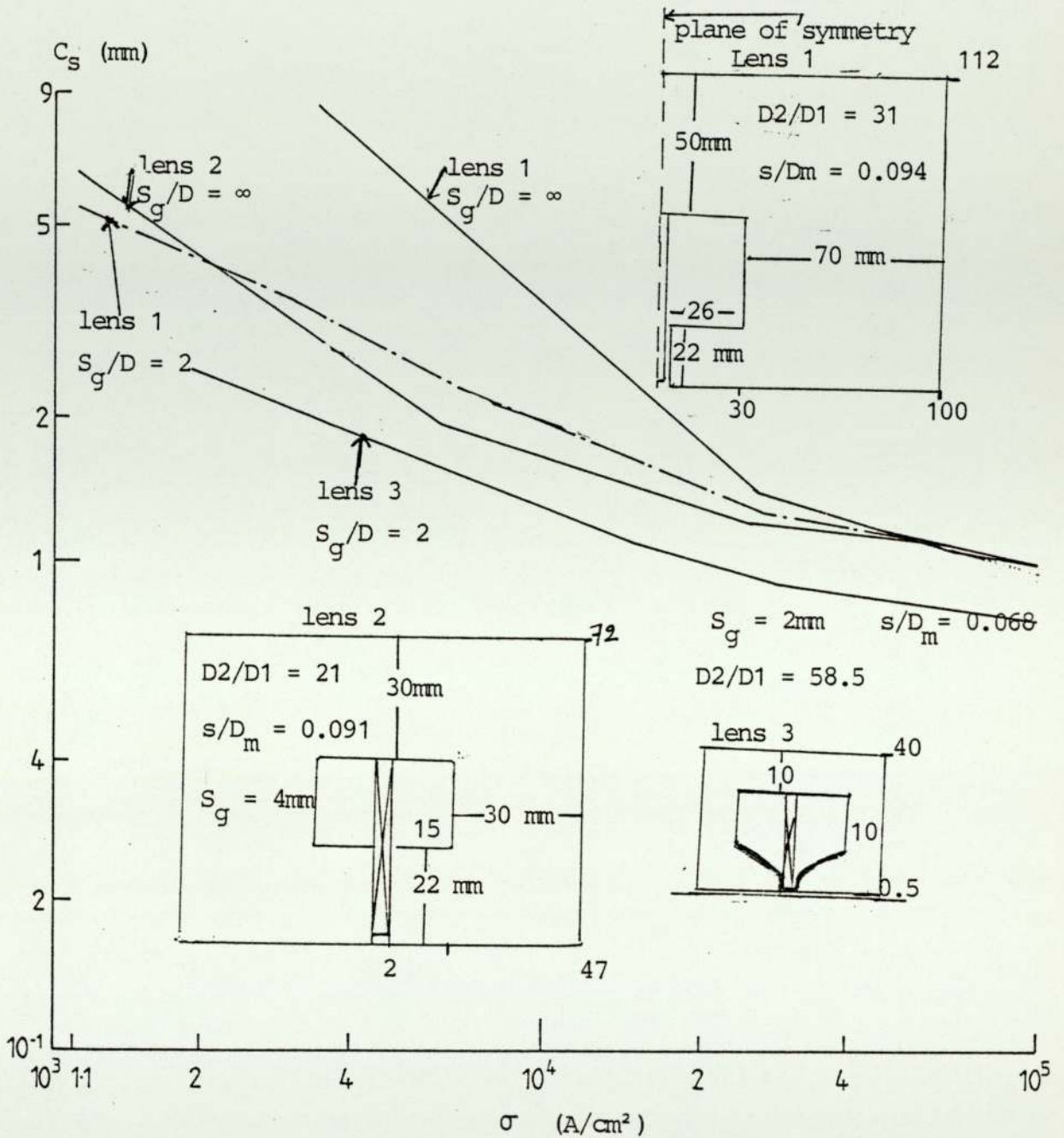


Figure 5.2

The variation of C_s with the current density for four different double pole lenses at 2000 KV at $Z = 0$ mode, log/log scale - lens 1 as shown above (quarter section) is a rectangular double pole test lens computed with $S_g/D = \infty$ and $S_g/D = 2$ (dashed line). Lens 2 is similar to lens 1, but with smaller axial polepiece radius with $S_g/D = \infty$. Lens 3 is a spherical double pole lens $S_g/D = 2$.

REFERENCES

- Al-Hilly, S.M. (1982), p.H.D. Thesis, The University of Aston in Birmingham.
- Al-Khashab, M.A.K. (1983), Ph.D. Thesis, The University of Aston in Birmingham.
- Ames, W.F. (1969), Numerical methods for Partial Differential Equations (Nelson, London, 1969).
- Bassett, R. and Mulvey, T. (1969), Zeitschrift Fur Angewandte Physik, 27, 1969, 142-145.
- Busch, H. (1926), Ann. Phys. (Leipzig) 4, 81, 974-993.
- Christofdes, S. (1982), Ph.D. Thesis, The University of Aston in Birmingham.
- Cleaver, J.R.A. Optik 49 (1978), 413-431.
- Cleaver, J.R.A. Inst. Phys. Conf. Ser. No. 52, 1980: Chapter 1.
- Cosslett, V.E. (1977), Proc. 5th Inst. Cong. High Voltage Electron Microscopy, Kyoto, ed. by T. Imura, H. Hashimoto (Japanese Soc. of Electron Microscopy, Tokyo, 1977), pp. 87-90.
- Craven, A.J. and Scott, C.P. (1985), The effect of systematic variation of the data in the Munro Programs on the predicted optical properties of a high excitation STEM objective lens. Inst.Phys.Conf. Series No.78 (EMAG 85) pp.105-108, 1985

Denegri, G.B., Molinari, G. and Viviani, A. (1976), 'A Generalized Finite Difference Method for the Computation of Electric and Magnetic Fields', Proc. COMPUMAG Conference on the Computation of Magnetic fields, Oxford 1976, p. 104. Ed. C.W. Trowbridge (Rutherford Laboratory, Didcot, Oxford 1976).

Forsythe, G.E. and Wasow, W.R. (1960), Finite Difference Methods for Partial Differential Equations. (Wiley, New York 1960).

Goddard, L.S. and Klemperer, O. (1944), 'Electron Ray Tracing Through Magnetic Lenses' Proc. Phys. Soc. No. 56, p. 378-396.

Hawkes, P.W. (1972), Electron Optics and Electron Microscopy, Taylor and Francis Limited, London.

Hill, R. and Smith, K.C.A. (1980), "Analysis of the single-pole lens by finite element computation", EMAG '79, Inst. Phys. Conf. Series (1980), Chapter 1, p. 49, Ed. T. Mulvey.

Hill, R. and Smith, K.C.A. (1982), The single pole lens as a scanning electron microscope objective scanning electron microscopy. 1982/II (Pages 465-471), Sem. Inc. AMF O'Hare (Chicago), II 60666, U.S.A.

Juma, S.M. and Mulvey, T., J. Phys. Sci. Instrum. Vol II, 1978, pp. 759-764.

Juma, S.M. and Faisal, A.D. J. Phys. Sci. Instrum. Vol. 14, 1981.

Kasper, E. and Lenz, F. (1980), 'Numerical Methods in Geometrical Electron Optics' in: Electron Microscopy 1980, Vol. 1, Seventh European Congress on Electron Microscopy, p. 10, Eds. P. Brederoo and G. Boom (Seventh European Congress on Electron Microscopy Foundation, Leiden 1980).

Kasper, E. (1982), "Magnetic Field Calculation and the Determination of Electron Trajectories". In magnetic electron lenses, p. 78 ed. P. Hawkes, Springer-Verlag, 1982.

Lefranc, G., Knappek, E. and Deitrich, I. Ultramicroscopy 10 (1982) 111-124, North Holland Publishing Co.

Lencová, B. in proc. VI Int. Conf. Magnet Technology, Bratislava (1977), 813-819.

Lencová, B. Computer Phys. Commun. 20 (1980), 127.

Lencová, B. and Lenc, M. Optik, 68 (1984), 37-60.

Lenz, F. (1982), "Properties of Electron Lenses", In magnetic electron lenses. Springer-Verlag, Berlin, Heidelberg, 1982.

Lepoole, J.B. and Mulvey, T. (1972), proc. 5th European Congress on Electron Microscopy, 148-149.

Marai, F.Z. and Mulvey, T., in "Electron Microscopy and Analysis" (Vanables, J. ed.), Academic Press, London, 1976.

Marai, F.Z. (1977), Ph.D. Thesis, The University of Aston in Birmingham.

Mulvey, T. and Wallington, M.J. (1969), J. Sci. Instrum. (J. Phys. E.) Sec. 2,2, 466-472.

Mulvey, T. and Newman, C.D. (1972), proc. 5th European Cong. Electron Microscopy, Manchester, Institute of Physics, London (1972), pp. 116-117.

Mulvey, T. (1974), Proc. Seventh Annual Scanning Electron Microscopy Symposium, Chicago, Illinois, U.S.A., pp. 43-49.

Mulvey, T. and Nasr, H. (1980a), "Limitations of the finite element method". EMAG 79, Inst. Phys. Conf. Series (1980), Chapter 1, p. 53, ed. T. Mulvey.

Mulvey, T. and Nasr, H. (1980b), "An improved finite element program for calculating the field distribution in magnetic lenses", in: Electron Microscopy 1980, Vol. 1, Seventh European Congress on Electron Microscopy, p. 64.

Mulvey, T. (1982), 10th International Congress on Electron Microscopy, Hamburg, August 17-24.

Munro, E. (1970), "Computer-aided design of magnetic electron lenses using the finite-element method", Microscopic Electronique 1970, Vol. II, Physique, p. 55.

Munro, E. (1971), Ph.D. Thesis, University of Cambridge.

Munro, E. In Image processing and computer aided design in electron optics, ed. P.W. Hawkes, Academic Press 1973.

Munro, E. (1975), A set of computer programs for calculating the properties of electron lenses. Department of Engineering, University of Cambridge.

Nasr, H.I.A. (1981), Ph.D. Thesis, University of Aston in Birmingham.

Newman, M.J., Trowbridge, C.W. and Turner, L.R. (1972), 'GFUN: An interactive program as an aid to magnet design', Proc. 4th Int. Conf. on Magnet Technology, Brookhaven, p. 117.

Pugh, E.M. and Pugh, E.W. (1970), Principles of Electricity and Magnetism, 2nd Edition, Addison-Wesley Publishing Company.

Shampine, L.F. and Allen, R.C. (1973), Numerical Computing: An Introduction, W.B. Saunders Company, London.

Silvester, P. and Charo, M.V.K. (1970), "Finite Element Solution of Saturable Magnetic Field Problems", I.E.E.E., PAS (1970), Vol. PAS-89, p. 1642.

Riecke, W.D. (1982), Practical Lens Design in Magnetic Electron Lenses, Springer Verlag, Berlin, Heidelberg, pp. 281-283.

Varga, R.S. (1962), Matrix Iterative Analysis (Prentice-Hall, Englewood Cliffs, New Jersey, 1962).

Yanaka, T. and Watanabe, M. (1966), Proc. 6th Int. Cong. Elect. Micros. Kyoto, Japan, 141-142.

Zienkewicz, O.C. and Cheung, Y.K. (1965), "Finite Elements in the Solution of Field Problems". The Engineer, Vol. 220, p. 507.

APPENDIX 1

TABLES

Table (3.1) General format of the data for program M12

	Data	Format
1)	Title	20A4
2)	N NSYM	(2I5)
3)	Blank line	
4)	J1 J2 J3.....Jn	(5x, nI5)
	I1 Z11 Z12 Z13.....Z1n	(I5, nF5.x)
	I2 Z21 Z22 Z23.....Z2n	(I5, nF5.x)
	I3 Z31 Z32 Z33.....Z3n	(I5, nF5.x)
	Im Zm1 Zm2 Zm3.....Zmn	(I5, nF5.x)
5)	Blank line	
6)	J1 J2 J3.....Jn	(5x, nI5)
	I1 R11 R12 R13.....R1n	(I5, nF5.x)
	I2 R21 R22 R23.....R2n	(I5, nF5.x)
	I3 R31 R32 R33.....R3n	(I5, nF5.x)
	Im Rm1 Rm2 Rm3.....Rmn	(I5, nF5.x)
7)	Blank line	
8)	JAl JB1 IA1 IB1 $A\mu r_1$	(4I5, F10.x)
	JAl JB2 IA2 IB2 $A\mu r_2$	(4I5, F10.x)
	JAn JBn IAn IBn $A\mu r_n$	(4I5, F10.x)
9)	Blank line	
10)	JC1 JD1 IC1 ID1 AJ1	(4I5, F10.x)
	JC2 JD2 IC2 ID2 AJ2	(4I5, F10.x)
	JCn JDn ICn IDn AJn	(4I5, F10.x)
11)	Blank line	

Explanation of symbols in Table 3.1

- 1) Title of up to 80 characters

- 2) N specifies what output is required (N=0 gives only the axial flux density distribution, N=1 gives also the flux value at each mesh point, N=2 gives the flux density values in the magnetic circuit as well). NSYM specifies whether the magnetic circuit is symmetric or asymmetric. NSYM=0 signifies it is asymmetric; while NSYM=1 is symmetric.

- 4 & 6) J1, J2, J3....Jn = mesh point numbers in the axial direction.
I1, I2, I3....In = mesh point numbers in the radial direction.
Zij = Z - coordinate values (millimeters).
RiJ = R - coordinate values (millimeters).

- 8) JAi, JBi, IAi, IBi = mesh point numbers defining a portion of magnetic circuit. μ_{ri} = relative permeability of that portion of magnetic circuit (dimensionless).

- 10) JCi, JDi, ICi, IDi = mesh point numbers defining a portion of coil winding, AJi = current density of that portion of coil winding (ampturns/sq.cm).

3, 5, 7, 9, 11 are blank lines.

Table (3.2) General format of the data for program M13

	Data	Format
1)	Title	20A4
2)	N NSYM	(2I5)
3)	Blank line	
4)	J1 J2 J3.....Jn	(5x, nI5)
	I1 Z11 Z12 Z13....Z1n	(I5, nF5.x)
	I2 Z21 Z22 Z23....Z2n	(I5, nF5.x)
	I3 Z31 Z32 Z33....Z3n	(I5, nF5.x)
	Im Zm1 Zm2 Zm3....Zmn	(I5, nF5.x)
5)	Blank line	
6)	J1 J2 J3.....Jn	(5x, nI5)
	I1 R11 R12 R13....R1n	(I5, nF5.x)
	I2 R21 R22 R23....R2n	(I5, nF5.x)
	I3 R31 R32 R33....R3n	(I5, nF5.x)
	Im Rm1 Rm2 Rm3....Rmn	(I5, nF5.x)
7)	Blank line	
8)	JA1 JB1 IA1 IB1 AN1	(4I5, F10.x)
	JA1 JB2 IA2 IB2 AN2	(4I5, F10.x)
	JAn JBn IAn IBn ANn	(4I5, F10.x)
9)	Blank line	
10)	JC1 JD1 IC1 ID1 AJ1	(4I5, F10.x)
	JC2 JD2 IC2 ID2 AJ2	(4I5, F10.x)
	JCn JDn ICn IDn AJn	(4I5, F10.x)
11)	Blank line	
12)	H1 B1	(2 F10.x)
	H2 B2	(2 F10.x)
	Hn Bn	(2 F10.x)

	Data	Format
13)	Blank line	
14)	H1 B1	(2 F10.x)
	H2 B2	(2 F10.x)
	Hn Bn	(2 F10.x)
15)	Blank line	

Explanation of symbols in Table 3.2

- 1) Title of up to 80 characters

- 2) N specifies what output is required (N=0 gives only the axial flux density distribution, N=1 gives the flux value at each mesh point, N=2 gives the flux density values in the magnetic circuit as well). NSYM specifies whether the magnetic circuit is symmetric or asymmetric. NSYM=0 signifies it is asymmetric; while NSYM=1 is symmetric.

- 4 & 6) J1, J2, J3....Jn = mesh point numbers in the axial direction.
I1, I2, I3....In = mesh point numbers in the radial direction.
Zij = Z - coordinate values (millimeters).
RiJ = R - coordinate values (millimeters).

- 8) JAi, JBi, IAi, IBi = mesh point numbers defining a portion of magnetic circuit. ANi = identification number of magnetic circuit material (1,2,3,4 or 5).

- 10) JCi, JDi, ICi, IDi = mesh point numbers defining a portion of coil winding; AJi = current density of that portion of coil winding (ampturns/sq.cm).

12) $H_1, H_2, H_3 \dots H_n$ = field strength values for magnetization curve (A/m). $B_1, B_2, B_3 \dots B_n$ = corresponding flux density values for magnetization curves (TESLA).

3, 5, 7, 9, 11, 13 are blank lines.

14) If another magnetization curve is requested then step 12 is repeated.

Table (3.3) General format of the data for program VPLIN

	Data	Format
1)	Title	20A4
2)	NSYM	I5
3)	NRI	4I5
4)	Blank Line	
5)	ZLB ZRB	2I5
6)	Blank Line	
7)	Title	20A4
8)	NBFE NFlux	2I5
9)	Blank Line	
10)	J1 J2 J3.....Jn	(5x, nI5)
	I1 Z11 Z12 Z13....Z1n	(I5, nF5.x)
	I2 Z21 Z22 Z23....Z2n	(I5, nF5.x)
	I3 Z31 Z32 Z33....Z3n	(I5, nF5.x)
	Im Zm1 Zm2 Zm3....Zmn	(I5, nF5.x)
11)	Blank Line	
12)	J1 J2 J3.....Jn	(5x, nI5)
	I1 R11 R12 R13....R1n	(I5, nF5.x)
	I2 R21 R22 R23....R2n	(I5, nF5.x)
	I3 R31 R32 R33....R3n	(I5, nF5.x)
	Im Rm1 Rm2 Rm3....Rmn	(I5, nF5.x)
13)	Blank Line	
14)	JAl JB1 IA1 IB1 Apr1	(4I5, F10.x)
	JA2 JB2 IA2 IB2 Apr1	(4I5, F10.x)
	JAn JBn IAn IBn Apr1	(4I5, F10.x)
15)	Blank Line	

	Data	Format
16)	JC1 JD1 IC1 ID1 AJ1	(4I5, F10.x)
	JC2 JD2 IC2 ID2 AJ2	(4I5, F10.x)
	JCn JDn ICn IDn AJn	(4I5, F10.x)
17)	Blank Line	
18)	Title	20 A4

Explanation of symbols in Table 3.3

- 1) Title of up to 80 characters
- 2) NSYM specifies whether the magnetic circuit is symmetric or asymmetric. NSYM=0 signifies it is asymmetric; while NSYM=1 is symmetric.
- 3) NR1 the number of runs to be performed.
- 5) ZLB, ZRB are the two inner boundaries.
- 7) Title of up to 80 characters is written for run 1.
- 8) NBFE, NFLUX are output of flux density in magnetic circuit and the flux values in every mesh point respectively, NBFE and NFLUX take values of 0 or 1, 0 = no and 1 = yes.
- 10 & 12) J1, J2, J3....Jn = mesh point numbers in the axial direction.
I1, I2, I3....In = mesh point numbers in the radial direction.
Zij = Z - coordinate values (millimeters)
Rij = R - coordinate values (millimeters)

14) J_{Ai} , J_{Bi} , I_{Ai} , I_{Bi} = mesh point numbers defining a portion of magnetic circuit, $A\mu r_1$ = relative permeability of that portion of magnetic circuit (dimensionless).

16) J_{Ci} , J_{Di} , I_{Ci} , I_{Di} = mesh point numbers defining a portion of coil winding, AJ_i = current density of that portion of coil winding (ampturns/sq.cm).

4, 6, 9, 11, 13, 15, 17 are blank lines.

18) If more than one run is requested then same steps from 7 to 17 are repeated for Run 2, Run 3 and Run 4.

Table (3.4) General format of the data for program VPSAT

	Data	Format
1)	Title	20A4
2)	NSYM NSAT	2I5
3)	NRI	4I5
4)	Blank Line	
5)	TB (IBM), TM (IBM)	(2 F 0.0)
	-999	End of Table
6)	Blank Line	
7)	ZLB ZRB	2I5
8)	Blank Line	
9)	Title	(20A4)
10)	NBFE N Flux	2I5
11)	Blank Line	
12)	J1 J2 J3.....Jn	(5x, nI5)
	I1 Z11 Z12 Z13....Z1n	(I5, nF5.x)
	I2 Z21 Z22 Z23....Z2n	(I5, nF5.x)
	I3 Z31 Z32 Z33....Z3n	(I5, nF5.x)
	Im Zm1 Zm2 Zm3....Zmn	(I5, nF5.x)
13)	Blank Line	
14)	J1 J2 J3.....Jn	(5x, nI5)
	I1 R11 R12 R13....R1n	(I5, nF5.x)
	I2 R21 R22 R23....R2n	(I5, nF5.x)
	I3 R31 R32 R33....R3n	(I5, nF5.x)
	Im Rm1 Rm2 Rm3....Rmn	(I5, nF5.x)
15)	Blank Line	

	Data	Format
16)	JAl JB1 IAl IB1 A _μ r1	(4I5, F10.x)
	JA2 JB2 IA2 IB2 A _μ r1	(4I5, F10.x)
	JAn JBn IAn IBn A _μ r1	(4I5, F10.x)
17)	Blank Line	
18)	JC1 JD1 IC1 ID1 AJ1	(4I5, F10.x)
	JC2 JD2 IC2 ID2 AJ2	(4I5, F10.x)
	JCn JDn ICn IDn AJn	(4I5, F10.x)
19)	Blank Line	
20)	If more than one run is requested then same steps from 9 to 19 are repeated for Run 2, Run 3 and Run 4.	

Explanation of symbols in Table 3.4

- 1) Title of up to 80 characters
- 2) NSYM specifies whether the magnetic circuit is symmetric or asymmetric. NSYM=0 signifies it is asymmetric; while NSYM=1 is symmetric. NSAT specifies whether the magnetic circuit is under linear or non-linear (saturation condition). NSAT=0 mean linear, and NSAT=1 mean saturation condition.
- 3) NR1 the number of runs to be performed.
- 5) Table representing typical relation of B and μ_r when computing saturation case. (i.e. NSAT=1) the table is ended with -999.
- 7) ZLB, ZRB are the two inner boundaries.

- 9) Title of up to 80 characters is written for Run 1.
- 10) NBFE, NFLUX are output of flux density in magnetic circuit and the flux values in every mesh point respectively. NBFE and NFLUX take values of 0 or 1, 0=NO and 1=YES.
- 12 & 14) J1, J2, J3.....Jn = mesh point numbers in the axial direction.
I1, I2, I3.....In = mesh point numbers in the radial direction.
Zij = Z - coordinate values (millimeters).
Rij = R - coordinate values (millimeters).
- 16) JAi, JBi, IAi, IBi = mesh point numbers defining a portion of magnetic circuit, μ_{ri} = relative permeability of that portion of magnetic circuit (dimensionless).
- 18) JCi, JDi, ICi, IDi = mesh point numbers defining a portion of coil winding, AJi = current density of that portion of coil winding (ampturns/sq.cm).

4, 6, 8, 11, 13, 15, 17, 19 are blank lines.

Table 3.5 General format of the data for program AMAG

	Data	Format
1)	Title	(20A4)
2)	NZ, NR, IM, IM1, ISYM, ICURR, IH1, IH2, IPRINT, IDISC	(20I4)
3)	IZ(1).....IZ(NZ)	(20I4)
4)	IR(1).....IR(NR)	(20I4)
5)	CZ (IZ)	(13 F6.0)
6)	CR (IR)	(13 F6.0)
7)	MM(2*I-1), MM (2*I), NM (2*I-1) NM (2*I), MI(I)	(5I4)
8)	CURR (I).....CURR (I CURR)	(13 F6.0)
9)	BM (I, 1), H (I, 1)	(12 F6.0)
10)		
11)	MAP MAT, MAPPSI, LISTIR, LISTED	(20I4)
12)	JMIN, JMAX, IMIN, IMAX	(20I4)

Explanation of symbols in table 3.5

1) The information about the lens is given which is printed as a heading.

2) This line contains a maximum of 20 integer numbers. The first two integers NZ and NR represent the numbers of the coarse mesh lines in Z and R direction respectively.

IM represents the number of areas specified as magnetic material or coil (maximum of 20). IMI specifies the number of magnetization curves (IMI=0 if there is no magnetic material in the lens or if standard magnetization curves

provided in program are used). A maximum of two magnetization curves can be used.

ISYM determines whether the lens is symmetric or not. ISYM>0 for symmetric lenses and ISYM=0 for asymmetric lenses. The symmetry plane, for program AMAG, coincides with the left hand boundary line i.e. for symmetrical lenses, the positive part only of the lens input data is given.

ICURR represents the current density numbers in the coil i.e. the numbers of excitations to be computed. For CURR=0, a linear approximation is done.

IH1 and IH2 are the numbers of points on the first and second magnetization curves when IMI>0.

IPRINT guides the output print. If IPRINT>0, the flux is printed. If IPRINT>2, the Z and R coordinates of the fine mesh are also printed.

IDISC guides flux density output. If IDISC>0 output of flux density on the axis is performed to the disc file.

- 3) This line indicates the coarse mesh lines in the Z direction (maximum of 20).
- 4) Same as above for the radial direction.
- 5) This line determines the Z coordinates of the coarse mesh in millimeters. If NZ>13, the coordinates will be in two lines.

- 6) Same as above for the Z coordinates.
- 7) The indices indicated limit the Ith region in the axial direction from left to right (MM), in the radial direction from top and bottom (NM), and the type of material (MI): 1 or 2 for iron, 3 for coil. Other regions are not specified.
- 8) This data line represents the current density in the excitation coil for the Ith lens excitation in A/mm². A maximum of 10 excitations are allowed. If ICURR=0, one number only is read.
- 9 & 10) These lines contain the magnetization curves data (when IMI>0). The first line (IHI) contains BM(I,1); H(I,1) values. The second curve data starts on a new line and contains BM(I,2); H(I,2) values. The flux density, BM, is in tesla and the field intensity, H, is in A/m.
- 11 & 12) The parameters in these lines are usually set to zero. If some of them have to be changed, then the respective values are inputed. If no output of material, PSI or iron flux density are desired; negative values are ascribed to them.

If LISTED>0, the listing of flux density is performed in the region bounded in the axial direction, by the line JMIN-1 from the left and the line JMAX from the right; and in the radial direction by IMIN-1 and IMIN from the top and bottom respectively.

APPENDIX 2

PROGRAM BIOT

```

C      CALCULATING THE AXIAL FLUX DENSITY DISTRIBUTION DUE TO THE CURRENT
C      WINDINGS IN THE COIL BY BIOT-SAVART LAW
PROGRAM LOOP1
REAL I,N
C      R1 =THE INNER RADIUS OF THE COIL IN METRES
R1=.002
C      R2 =THE OUTER RADIUS OF THE COIL IN METRES
R2=.062
C      A=0.5*COIL WIDTH
A=.003
C      I= THE CURRENT DENSITY
I=100.
C      THE NUMBER OF TURNS
N=100.
R0=(R1+R2)/2.
WRITE(2,44)
C      K REPRESENTS THE NUMBER OF Z POINTS REQUIRED (HERE IT STARTS FROM
C      1 AT THE CENTRE OF THE COIL AND IT END AT 250MM AT THE LAST POINT
DO 11 K=1,250
Z=.001*(FLOAT(K)-1.)
IF (Z.EQ.A) GOTO 11
ZP=Z+A
ZM=Z-A
THETA1=ATAN(ZP/R1)
THETA2=ATAN(ZP/R2)
THETA3=ATAN(ZM/R1)
THETA4=ATAN(ZM/R2)
C=I*N*1.256637*.000001
CF=C/(4.*A*(R2-R1))
X1=TAN(.5*THETA1)/TAN(.5*THETA2)
X2=TAN(.5*THETA3)/TAN(.5*THETA4)
BB=.5*C*R0*R0/(R0*R0+Z*Z)**1.5
B=CF*(ZP*ALOG(X1)-ZM*ALOG(X2))
Z1=Z*1000.
C      B IS THE AXIAL FLUX DENSITY DISTRIBUTION DUE TO CURRENT WINDINGS
C      OF A RECTANGULAR CROSS SECTION COIL
WRITE(2,30)Z1,B,BB
C      BB IS THE AXIAL FLUX DENSITY DISTRIBUTION DUE TO CURRENT WINDINGS
C      OF AN ARBITRARY SHAPE COIL (WHICH IS TAKEN AS THE TOTAL AXIAL FLUX
C      FROM SEVERAL LOOPS)
11 CONTINUE
STOP
C      THE OUTPUT FORMATS
30 FORMAT(1X,F10.5,5X,F14.5,5X,F14.5)
C      THE OUTPUT OF Z IN MM,AND B AND BB,IN TESLA
44 FORMAT(1X,' Z(MM) ', ' B(TESLA)', ' BB(TESLA) ')
END

```

APPENDIX 3

PROGRAM VPLIN

```

C      VPLIN PROGRAM
C      FINITE ELEMENT PROGRAM FOR COMPUTING AXIAL FLUX DENSITY
C      DISTRIBUTION AND VECTOR POTENTIAL THROUGHOUT THE MAGNET
C      -IC CIRCUIT OF USATURATED MAGNETIC LENSES
C      THE PRINCIPAL VARIABLES ARE DEFINED AS FOLLOWS:
C      Z(IM,JM)=Z-COORDINATES OF EACH MESH POINT
C      R(IM,JM)=R-COORDINATES OF EACH MESH POINT
C      IM=NUMBER OF MESH POINT IN THE R-DIRECTION
C      JM=NUMBER OF MESH POINT IN THE Z-DIRECTION
C      OTHER PROGRAMS PREVIOUS TO THIS PROGRAM UTILISE DIFFERE
C      -NT MESH NUMBERS DEPENDING ON THE COMPUTER MEMORY SIZE .
C      FOR SUCH PROGRAMS TYPICAL MESH POINTS NUMBERS ARE IN THE
C      ORDER OF (32,70) TO (40,80) WHEN UTILIZING LARGE COMPUTERS
C      FOR SMALLER COMPUTERS (20,40) TO (25,50) MESH POINTS ARE
C      USED IN MINI COMPUTERS THE NUMBERS ARE REDUCED TO (12,25) .
C      FOR SUCH PROGRAMS THE HIGHER THE MESH POINTS NUMBERS THE
C      MORE ACCURATE THE RESULTS ARE .
C      THIS NECESSITATES LARGE COMPUTERS FOR ACCURATE RESULTS.
C      THE PRESENT PROGRAM OVERCOMES THE INHERENT INACCURACIES
C      WHEN UTILISING MINI COMPUTERS BY INCREASING THE NUMBER
C      OF RUNS AS EXPLAINED LATER.
C      AMUR(IM,JM)=RELATIVE PERMEABILITY OF EACH QUADRILATERAL
C      AJ(IM,JM)=CURRENT DENSITY WITHIN EACH QUADRILATERAL
C      A(IM,JM)=NON ZERO ELEMENTS OF SYMMETRIC BAND MATRIX
C      C(IM,JM)=RIGHT HAND SIDE OF THE FINITE ELEMENTS EQUATIONS
C      V(IM,JM)=COMPUTED VECTOR POTENTIAL AT EACH MESH POINT
C      P(IM*JM,IM)=COEFFICIENTS OF THE FINITE ELEMENT EQUATIONS
C      AZLB(IM)=FIRST INNER BOUNDARY IN R-DIRECTION
C      AZRB(IM)=SECOND INNER BOUNDARY IN R-DIRECTION
C      NR=NUMBER OF RUNS DESIRED (1 TO 4)
C      TITLE(20) IS ANY TITLE UP TO 80 CHARACTERS
C      IJM=IM*JM
C      THE DIMENSION STATEMENTS ARE SET AS FOLLOWS :
C      COMMON/ONE/Z(IM,JM),R(IM,JM),AMUR(IM,JM),AJ(IM,JM)
C      COMMON/TWO/A(IJM),C(IJM),V(IM,JM),P(IJM,IM
C      DIMENSION AZLB(IM) , AZRB(IM) ,NR(4) ,TITLE(20)
C      ZZ (Z-COORDINATES OF AXIAL MESH POINTS)
C      ABZ(COMPUTED AXIAL FLUX DENSITY DISTRIBUTION)
C
      COMMON/ONE/  Z(25,50),R(25,50),AMUR(25,50),AJ(25,50)
      COMMON/TWO/  A(1250),C(1250),V(25,50),P(1250,25)
      DIMENSION AZLB(25),AZRB(25),NR(4),TITLE(20)
      DIMENSION ZZ(210),ABZ(210)
      IM=25
      JM=50
      IJM=IM*JM
      LBZ=JM*3
      X=0.
      DO 10 J=1,LBZ
      ZZ(J)=X
      ABZ(J)=X
10 CONTINUE
      LBZ=0
C      THE PROGRAM WILL READ THE FIRST LINE OF DATA WHICH

```

```

C   INDICATE WHETHER THE ENTIRE MESH IS SPECIFIED IN THE
C   DATA (I.E ASYMMETRIC CASE),OR THE PORTION OF THE MESH
C   IN THE NEGATIVE HALF PIECE ONLY IS SPECIFIED IN THE DATA
C   (SYMMETRIC CASE).
C   NSYM CAN TAKE VALUES OF 1 OR 0 ,0 INDICATES ASYMMETRY
      READ (1,1) NSYM1
C   WHILE 1 INDICATES SYMMETRY
      1 FORMAT (I5)
C   THE PROGRAM EXPECTS IN THE SECOND LINE OF DATA FOUR
C   INTEGERS WHICH WILL SPECIFY THE NUMBERS OF RUNS
C   REQUIRED TO BE PERFORMED
C   THESE ARE FROM 1 TO 4 .THUS FOR ONE RUN NR=1,0,0,0
C   FOR TWO RUNS NR=1,2,0,0 FOR THREE RUNS NR=1,2,3,0
C   FOR FOUR RUNS NR=1,2,3,4
      READ (1,2) (NR(I),I=1,4)
      2 FORMAT (4I5)
C   A BLANK LINE IS LEFT
      READ (1,1111)
C   FOR SYMMETRICAL CASE (NSYM=1),UP TO 3 RUNS ARE PERFORMED.
C   FOR ASYMMETRICAL CASE (NSYM=0),UP TO 4 RUNS ARE DONE
      IF (NSYM1.EQ.1) GOTO 20
      IF (NR(4).EQ.4) GOTO 24
20  IF (NR(3).EQ.3) GOTO 23
      IF (NR(2).EQ.2) GOTO 22
      IF (NR(1).EQ.1) GOTO 21
C   WARNING IF NUMBER OF RUNS HAVE NOT BEEN SPECIFIED THE
C   PROGRAM WILL STOP IN THIS CASE
      WRITE (2,3)
      3 FORMAT (1X,' RUNS NOT SPECIFIED')
      STOP
C   THE PROGRAM WILL NOTE THE NUMBER OF RUNS AND CONTINUE
C   DATA READING ACCORDINGLY
21  NRUN=1
      GOTO 25
22  NRUN=2
      GOTO 25
23  NRUN=3
      GOTO 25
24  NRUN=4
C   THE PROGRAM WILL NOW READ THE TWO INNER BOUNDARIES
25  READ (1,111) JLB,JRB
111  FORMAT (3I5)
C   ABLANK LINE IS LEFT
      READ (1,1111)
1111  FORMAT (1X)
C   DO LOOPS ACCORDING TO SPECIFIED NUMBER OF RUNS
      DO 112 IRUN=1,NRUN
      IF (IRUN.EQ.1) GOTO 2111
      IF (NR(IRUN).EQ.0) GOTO 112
C   READ ANY TITLE OF UP TO 80 CHARECTERS
2111  READ (1,1121) (TITLE(I),I=1,20)
1121  FORMAT (20A4)
C   THE OUTPUT IS SPECIFIED ACCORDING TO THE REQUIREMENTS
      READ (1,1122) NBF,NFLUX

```

```

1122 FORMAT (2I5)
C   A BLANK LINE IS LEFT
    READ (1,1111)
C   THE SUBROUTINE MESH ,READING AND SETTING AXIAL AND
C   RADIAL COORDINATS OF THE MAJOR MESH LINES NODES IS
C   CALLED TWICE, FOR Z AND R COORDINATES
    CALL MESH (Z, I1, J1, IM, JM)
    CALL MESH (R, I1, J1, IM, JM)
C   SET VARIOUS CONSTANTS
C   I1=NUMBER OF MESH-POINTS IN THE RADIAL DIRECTION
C   I2=I1-1=NUMBER OF QUADRILATERALS IN THE RADIAL
C   DIRECTION
C   J1=NUMBER OF MESH-POINTS IN THE AXIAL DIRECTION
C   J2=J1-1=NUMBER OF QUADRILATERALS IN THE AXIAL
C   I3, J3 ARE USED FOR FINDING NO. OF EQNS. TO BE SOLVED
    I2=I1-1
    I3=I1-2
    J2=J1-1
    J3=J1-2
C   DO LOOP TO SET OUTER BOUNDARY VECTOR POTENTIALS
C   TO ZERO FOR BOTH Z AND R DIRECTIONS
    DO 1124 J=1, JM
    DO 1124 I=1, IM
1124 V(I, J)=0.
C   THE SUBROUTINE AJMUR FOR READING THE DATA SPECIFYING
C   THE POSITION AND PERMEABILITY OF THE MAGNETIC CIRCUIT
C   IS CALLED
    CALL AJMUR (AMUR, AJ, I1, J1, IM, JM)
C   THE INITIAL LENS EXCITATION IS SET TO ZERO FOR ASYM
C   LENS
1123 ANI=0.
    NSYM=0
C   THE NEXT TWO STATEMENTS GUIDE THE PROGRAM TO EXECUTE
C   THE APPROPRIATE COMPUTATIONS FOR 1,2,3,4 RUNS
C   RESPECTIVELY
1126 IF (IRUN.EQ.1) GOTO 113
    IF (NR(IRUN)-3) 114, 115, 116
C   AN ITERATION COUNTER IS SET TO ZERO AND THE COORDINATES
C   THE MESH NODES IN Z AND R DIRECTIONS ARE SET BY LINEAR
C   INTERPOLATION
113 K1=0
    DO 130 J=1, J1
    DO 130 I=1, I1
    K1=K1+1
C   C(K1)=RIGHT HAND SIDE OF THE FINITE ELEMENTS EQUATION
    C(K1)=0.
130 A(K1)=0.
    NSYM=NSYM1
    GOTO 131
C   THE SAME PROCEDURE IS NOW REPEATED FOR RUN 2
114 K1=0
    K2=0
    DO 117 J=1, J1
    DO 117 I=1, I1

```

```

    K1=K1+1
    A(K1)=0.
    C(K1)=0.
C   THE DATA IS TESTED FOR TERMINATION
    IF (J.EQ.J1) GOTO 1171
    GOTO 117
1171 K2=K2+1
C   THE VECTOR POTENTIAL AT THE INNER BOUNDARY (AZLB)
C   IS STORED FOR RUN 2 FROM RUN 1
    A(K1)=AZLB(K2)
    V(I,J)=A(K1)
117 CONTINUE
C   THE PROGRAM IS NOW DIRECTED TO SET THE RELATIVE
C   PERMEABILITY OF THE FREE SPACE
    GOTO 131
115 K1=0
    K2=0
    K3=0
    IF (NRUN.EQ.3) NSYM=NSYM1
    DO 118 J=1,J1
    DO 118 I=1,I1
    K1=K1+1
    A(K1)=0.
    C(K1)=0.
    IF (J.EQ.1) GOTO 1151
    GOTO 1152
1151 K2=K2+1
    A(K1)=AZLB(K2)
    V(I,J)=A(K1)
C   THE DATA IS TESTED FOR SYMMETRY AND THE PROGRAM
C   DIRECTED ACCORDINGLY
1152 IF (NSYM.EQ.1) GOTO 118
    IF (J.EQ.J1) GOTO 1153
    GOTO 118
1153 K3=K3+1
C   THE COMPUTED VECTOR POTENTIAL AT THE SECOND INNER
C   BOUNDARY (AZRB) IS STORED
    A(K1)=AZRB(K3)
    V(I,J)=A(K1)
118 CONTINUE
    GOTO 131
C   THE PROCEDURE IS NOW REPEATED FOR RUN 4
116 K1=0
    K2=0
    DO 119 J=1,J1
    DO 119 I=1,I1
    K1=K1+1
    A(K1)=0.
    C(K1)=0.
    IF (J.EQ.1) GOTO 1191
    GOTO 119
1191 K2=K2+1
    A(K1)=AZRB(K2)
    V(I,J)=A(K1)

```

```

119 CONTINUE
C   THE VALUE OF FREE SPACE PERMEABILITY AMU0 IS SET
131 AMU0=1.2566371E-6
C   THE ARRAY WHICH HOLDS THE LEFT HAND COEFFICIENTS
C   OF THE EQUATIONS IS INITIALISED
      DO 1131 I=1,IJM
      DO 1131 J=1,IM
1131 P(I,J)=0.
      K=I2
      K1=0
C   THE DATA IS TESTED FOR SYMMETRY AND THE COORDINATES
C   ARE SET ACCORDINGLY
      IF (NSYM.EQ.1) GOTO 8
      J5=J3
      JS=0
C   IS=THE NUMBER OF EQNS TO BE SOLVED
      IS=I3*J3
      GOTO 9
8   J5=J2
      JS=J5
      IS=I3*J2
9   IT=IS-K
C   THE SUBROUTINE"PCLIN" WHICH SETS THE FINITE ELEMENT
C   COEFFICIENTS FOR EVERY QUADRILATERAL MESH AREA IS
C   CALLED
      CALL PCLIN(Z,R,AMUR,AJ,P,A,C,I1,J1,IM,JM,IJM,NSYM,ANI)
C   FOR SYMMETRICAL CASE ,THE LENS EXCITATION IS DOUBLED
      IF (NSYM.EQ.1) ANI=2.*ANI
C   SUBROUTINE "EQNS" IS CALLED ,THIS SUBROUTINE SOLVES
C   THE EQUATIONS BY GAUSSIAN ELIMINATION AND BACKWARD SUBSTITUTION
      A2=V(I3,J)
      B=(A1*R2*R2*R2-A2*R1*R1*R1)/(.5*R1*R2*(R2*R2-R1*R1))
C   THE OUTPUT OF Z-COORDINAT OF AXIAL MESH POINT AND
C   THE AXIAL FLUX DENSITY AT EACH MESH POINT IS WRITTEN
C   OUT
C   IF NUMBER OF RUNS IS MORE THAN 1,THE Z AND B OUTPUT
C   OF ALL THE RUNS IS OUTPUTED
      WRITE (2,95) Z1,B
      IF (IRUN.EQ.1) GOTO 94
      LBZ=LBZ+1
      ZZ(LBZ)=Z1
      ABZ(LBZ)=B
94 CONTINUE
C   FOR SYMMETRIC CASE,THE VALUES OF Z(MM) COORDINATES
C   AND B(TESLA) FOR POSITIVE HALF PLANE IS CALCULATED
      IF (NRUN.NE.1.OR.NSYM.EQ.0) GOTO 79
      DO 971 JJ=1,J2
      J=J2+1-JJ
      Z1=-Z(I1,J)*1000.
      R1=R(I2,J)
      R2=R(I3,J)
      A1=V(I2,J)
      A2=V(I3,J)
      B=(A1*R2*R2*R2-A2*R1*R1*R1)/(.5*R1*R2*(R2*R2-R1*R1))

```

```

        WRITE (2,95) Z1,B
971 CONTINUE
C   FOR 1 RUN OR 4 RUNS THE PROGRAM IS DIRECTED TO
C   WRITE THE EXCITATION.THIS ALSO HAPPENS IN CASE
C   OF SYMMETRY AND 3 RUNS
      79 IF (IRUN.EQ.1.OR.NR(IRUN).EQ.4) GOTO 941
        IF (NR(IRUN).EQ.3.AND.NSYM.EQ.1) GOTO 941
        IF (NR(IRUN).EQ.NR(IRUN-1)+1) LBZ=LBZ-1
      95 FORMAT (1X,F10.2,6X,F15.6)
C   THE LENS EXCITATION IS WRITTEN OUT
941 WRITE (2,96) ANI
      IF (IRUN.EQ.1) EXCIT=ANI
      96 FORMAT (1X/' EXCITATION GIVEN (NI) = ',F10.2,
+ ' AMPERETURNS'/)
C   IF FLUX DENSITY THROUGHTOUT THE MAGNETIC CIRCUIT
C   (NBFE) IS REQUIRED TO BE OUTPUTED,THE PROGRAM IS
C   DIRECTED TO ASUBROUTINE (BVALUES) TO DO SO
      IF (NBFE.EQ.0) GOTO 1102
      CALL BVALUES (Z,R,V,AMUR,I1,J1,IM,JM,NBFE)
C   IF FLUX VALUES AT EACH MESH POINT ARE REQUIRED,THE
C   PROGRAM IS DIRECTED TO ASUBROUTINE (FLUX) TO DO SO
1102 IF (NFLUX.EQ.0) GOTO 112
      CALL FLUX (V,I1,J1,IM,JM)
      112 CONTINUE
C   IF 1 RUN IS REQUIRED THE PROGRAM IS TERMINATED,OTHERWISE
C   TITLES ARE WRITTEN
      IF (NRUN.EQ.1) STOP
      WRITE(2,942)
      942 FORMAT (/1X,'TOTAL DISTRIBUTION FOR SPECIFIED REGION'/)
      WRITE (2,936)
      WRITE (2,9351)
C   THE Z COORDINATES OF MESH POINTS FOR SPECIFIED REGION
C   AND AXIAL FLUX DENSITY VALUES FOR THE SPECIFIED REGION
C   IS OUTPUTED
      DO 944 J=1,LBZ
        WRITE (2,95) ZZ(J),ABZ(J)
944 CONTINUE
C   FOR ASYMMETRIC CASE ,THE EXCITATION IS OUTPUTED.WHILE
C   FOR SYMMETRIC CASE ,THE Z AND B VALUES ARE CALCULATED
C   FOR POSITIVE HALF PLANE
      IF (NSYM.EQ.0) GOTO 946
      LBZ=LBZ-1
      DO 948 K=1,LBZ
        J=LBZ+1-K
        Z1=-ZZ(J)
        WRITE (2,95) Z1,ABZ(J)
948 CONTINUE
946 WRITE (2,96) EXCIT
      STOP
C   END OF THE MAIN PROGRAM
      END
C
C   SUBROUTINE (MESH) FOR SETTING COORDINATES OF EACH POINT ON THE
C   FINITE ELEMENT MESH

```

```

C   Z(IM,JM)=ARRAY OF COORDINATES TO BE SET
C   I1=NUMBER OF MESH POINTS IN THE RADIAL DIRECTION
C   J1=NUMBER OF MESH POINTS IN THE AXIAL DIRECTION
C   IM=MAXIMUM PERMISSIBLE VALUE OF I1
C   JM=MAXIMUM PERMISSIBLE VALUE OF J1
      SUBROUTINE MESH(Z,I1,J1,IM,JM)
      DIMENSION Z(IM,JM),TITLE(20)
      DIMENSION NC(15),NR(15),XA(15,15)
C   THE SUBROUTINE READS THE MESH-POINT NUMBERS IN AXIAL
C   DIRECTION
      READ (1,1)(NC(L),L=1,15)
1    FORMAT(5X,15I5)
      DO 2 L=1,15
      IF(NC(L).EQ.0)GOTO 3
2    CONTINUE
C   CALCULATE VALUES OF JJ AND J1
C   JJ=NUMBER OF COLUMNS OF COORDINATES SPECIFIED IN THE
C   DATA
C   J1=NUMBER OF MESH-POINTS IN THE AXIAL DIRECTION
      JJ=15
      GOTO 4
3    JJ=L-1
4    J1=NC(JJ)
C   READ THE COORDINATES VALUES
      DO 5 I=1,15
      READ(1,6)NR(I),(XA(I,J),J=1,JJ)
6    FORMAT(I5,15F5.0)
C   TEST FOR END OF DATA
      IF (NR(I).EQ.0)GOTO 7
5    CONTINUE
      GOTO 8
7    II=I-1
8    I1=NR(II)
C   SET COORDINATE VALUES BY LINEAR INTERPOLATION
      DO 9 I=2,II
      DO 9 J=2,JJ
      L1=NR(I-1)
      L2=NR(I)
      M1=NC(J-1)
      M2=NC(J)
      DO 9 LL=L1,L2
      DO 9 MM=M1,M2
      KL=L2-L1
      KM=M2-M1
      D1=(XA(I-1,J)-XA(I-1,J-1))/FLOAT(KM)
      D2=(XA(I,J)-XA(I,J-1))/FLOAT(KM)
      D1=D1*FLOAT(MM-M1)+XA(I-1,J-1)
      D2=D2*FLOAT(MM-M1)+XA(I,J-1)
9    Z(LL,MM)=(D2-D1)*FLOAT(LL-L1)/FLOAT(KL)+D1
C   THE COORDINATE VALUES WHICH HAVE BEEN SPECIFIED IN
C   MM ARE CONVERTED TO METRES
      DO 10 I=1,I1
      DO 10 J=1,J1
10   Z(I,J)=Z(I,J)/1000.

```

```

      RETURN
C   THE END OF SUBROUTINE MESH
      END
C
C   SUBROUTINE (AJMUR) FOR SETTING EACH ELEMENT OF THE ARRAY
C   AMUR(IM,JM) TO THE VALUE OF THE RELATIVE PERMEABILITY
C   OF CORRESPONDING QUADRILATERAL OF THE FINITE ELEMENT
C   MESH, AND EACH ELEMENT OF THE ARRAY AJ(IM,JM) TO THE VALUE
C   OF THE CURRENT DENSITY. AMUR(IM,JM)=RELATIVE PERMEABILITY
C   VALUES FOR EACH QUADRILATERAL.
C   AJ(IM,JM)=CURRENT DENSITY VALUES FOR EACH QUADRILATERAL
C   (IN AMP/TURNS/ SQUARE METRE)
C   IM=NUMBER OF QUADRILATERAL AREAS IN THE RADIAL DIRECTION
C   JM=NUMBER OF QUADRILATERAL AREAS IN THE AXIAL DIRECTION
C   SUBROUTINE AJMUR (AMUR,AJ,I1,J1,IM,JM)
C   DIMENSION AMUR(IM,JM),AJ(IM,JM)
C   INITIALISE ALL ELEMENTS OF AMUR TO 1. AND ALL ELEMENTS OF
C   AJ TO 0.
      DO 1 I=1,I1
      DO 1 J=1,J1
      AMUR(I,J)=1.
      AJ(I,J)=0.
      1 CONTINUE
C   READ VALUES OF JA,JB,IA,IB,XJ
C   JA=THE SMALLER MESH-POINT NUMBER IN THE AXIAL DIRECTION
C   JB=THE LARGER MESH-POINT NUMBER IN THE AXIAL DIRECTION
C   IA=THE SMALLER MESH-POINT NUMBER IN THE RADIAL DIRECTION
C   IB=THE LARGER MESH-POINT NUMBER IN THE RADIAL DIRECTION
C   XJ=THE RELATIVE PERMEABILITY OF THAT PORTION OF THE
C   MAGNETIC CIRCUIT (DIMENSIONLESS)
      2 READ (1,3) JA,JB,IA,IB,XJ
      3 FORMAT (4I5,F10.0)
C   TEST FOR END OF MAGNETIC CIRCUIT DATA
      IF (JA.EQ.0) GOTO 5
C   RESET APPROPRIATE ELEMENTS OF AMUR TO THE VALUE OF XJ
      IB1=IB-1
      JB1=JB-1
      DO 4 I=IA,IB1
      DO 4 J=JA,JB1
      4 AMUR(I,J)=XJ
C   GO TO 2 TO READ NEXT LINE OF MAGNETIC CIRCUIT DATA
      GOTO 2
C   READ NEXT LINE OF VALUES OF JA,JB,IA,IB,XJ,WHICH ARE
C   MESH-POINT NUMBERS SPECIFYING THE POSITION OF A PORTION OF
C   THE COIL WINDINGS AND THE CURRENT DENSITY IN THAT PORTION
C   JA=THE SMALLER MESH-POINT NUMBER IN THE AXIAL DIRECTION
C   JB=THE LARGER MESH-POINT NUMBER IN THE AXIAL DIRECTION
C   IA=THE SMALLER MESH-POINT NUMBER IN THE RADIAL DIRECTION
C   IB=THE LARGER MESH-POINT NUMBER IN THE RADIAL DIRECTION
C   XJ=THE CURRENT DENSITY IN THAT PORTION OF THE COIL WINDINGS
C   (XJ IS IN AMP/TURNS/SQUARE CM)
      5 READ (1,3) JA,JB,IA,IB,XJ
C   TEST FOR END OF DATA SPECIFYING COIL WINDINGS
      IF (JA.EQ.0) RETURN

```

```

C   RESET APPROPRIATE ELEMENTS OF AJ TO THE VALUE OF XJ
      IB1=IB-1
      JB1=JB-1
      DO 6 I=IA,IB1
      DO 6 J=JA,JB1
C   CNVERT CURRENT DENSITY XJ TO UNITS OF AMPTURNS/SQUARE
C   METRE
      6 AJ(I,J)=XJ*10000.
C   GO TO 5 TO READ NEXT LINE OF COIL WINDINGS DATA
      GOTO 5
C   TO 140
      IF (NN.GT.1) GOTO 140
      N3=0
      IC=I
      JC=J
      GOTO 141
140  IF (NN-3) 1402,1403,1404
1402 N3=6
      IC=I+1
      JC=J
      GOTO 141
1403 N3=12
      IC=I
      JC=J+1
      GOTO 141
1404 N3=18
      IC=I+1
      JC=J+1
C   DO LOOP FOR EACH THREE TRIANGULAR ELEMENTS
141  DO 16 N0=1,3
      N=N+1
      ND1=ND(NN)
      IF (N0.EQ.1) ND1=0
      IF (N0.EQ.3) N3=N3+1
C   SET Z AND R COORDINATES OF VERTICES OF TRIANGULAR
C   ELEMENTS
      N3=N3+1
      Z1=F(N3)

```

```

Z2=F(N3+1)
Z3=F(N3+2)
R1=G(N3)
R2=G(N3+1)
R3=G(N3+2)
C THE COEFFICIENTS OF NODAL EQUATIONS REPRESENTING
C THE VECTOR POTENTIAL OVER EACH ELEMENT ARE FOUND
  B1=R2-R3
  B2=R3-R1
  B3=R1-R2
  T1=Z3-Z2
  T2=Z1-Z3
  T3=Z2-Z1
C DET=DETERMINANT OF THE FINITE ELEMENTS TRIANGLE
  DET=B1*T2-B2*T1
  R0=(R1+R2+R3)/3.
  X=DET/(3.*R0)
  T1=T1+X
  T2=T2+X
  T3=T3+X
  X=R0/(2.*AMU0*AR(IC,JC)*DET)
  IF (N.EQ.2.OR.N.EQ.5.OR.N.EQ.8.OR.N.EQ.11) GOTO 162
  IF (N.EQ.3.OR.N.EQ.6.OR.N.EQ.9.OR.N.EQ.12) GOTO 163
161 D(M1)=(B2*B1+T2*T1)*X
  D(M1+1)=(B2*B2+T2*T2)*X
  D(M1+2)=(B2*B3+T2*T3)*X
  M1=M1+9
  GOTO 17
162 D(M2)=(B1*B1+T1*T1)*X
  D(M2+1)=(B1*B2+T1*T2)*X
  D(M2+2)=(B1*B3+T1*T3)*X
  M2=M2+9
  GOTO 17
163 D(M3)=(B3*B1+T3*T1)*X
  D(M3+1)=(B3*B2+T3*T2)*X
  D(M3+2)=(B3*B3+T3*T3)*X
  M3=M3+9
  17 ANI=ANI+.5*DET*AJ(IC,JC)*FLOAT(ND1)
  Q(N)=AJ(IC,JC)*R0*DET/6.
16 CONTINUE
14 CONTINUE
C SET FINITE ELEMENT COEFFICIENTS FOR QUADRILATERAL
C AREA TO OBTAIN NINE-POINT EQUATION FOR EACH NODE
  L=L+1
  L2=L2+1
  P(L,1)=0.
  P(L,2)=0.
  P(L,I3)=0.
  P(L,K)=0.
  P(L,I1)=0.
  P1=D(6)+D(7)
  P2=D(1)+D(8)+D(12)+D(14)
  P3=D(15)+D(16)
  P4=D(3)+D(5)

```

```

P5=D(2)+D(4)+D(9)+D(11)+D(13)+D(18)
P6=D(10)+D(17)
C(L)=Q(1)+Q(2)+Q(3)+Q(4)+Q(5)+Q(6)
Q1=P1*A(L2)
Q2=P2*A(L2+1)
Q3=P3*A(L2+2)
Q4=P4*A(L2+I1)
Q6=P6*A(L2+I1+2)
IF (J.EQ.JS) GOTO 18
P4=P4+D(19)+D(26)
    P5=P5+D(20)+D(22)+D(27)+D(29)+D(31)+D(36)
P6=P6+D(30)+D(32)
P7=D(24)+D(25)
P8=D(21)+D(23)+D(28)+D(35)
P9=D(33)+D(34)
C(L)=C(L)+Q(7)+Q(8)+Q(9)+Q(10)+Q(11)+Q(12)
Q7=P7*A(L2+2*I1)
Q8=P8*A(L2+2*I1+1)
Q9=P9*A(L2+2*I1+2)

```

```

C EACH NODAL EQUATION IS EXPRESSED IN TERMS OF THE VECTOR
C POTENTIAL AT THE NODE AND THE EIGHT NEIGHBOURING VECTOR
C POTENTIAL VALUES. THE RESULTING MATRIX IS SYMMETRICAL
C ABOUT THE DIAGONAL. HENCE ONLY THE COEFFICIENTS OF THE
C BANDED MATRIX IN THE UPPER TRIANGLE OF THE MATRIX NEED
C TO BE STORED. THE MATRIX EQUATION IS SOLVED BY GAUSSIAN
C ELIMINATION IN ANOTHER SUBROUTINE

```

```

18 IF (J.EQ.JS) GOTO 20
    IF (J.EQ.J5) GOTO 30
    IF (J.NE.1) GOTO 40
    IF (I.EQ.1) GOTO 50
    IF (I.EQ.I3) GOTO 60
    C(L)=C(L)-(Q1+Q2+Q3)
    P(L,1)=P5
    P(L,2)=P6
    P(L,I3)=P7
    P(L,K)=P8
    P(L,I1)=P9
    GOTO 11
50 C(L)=C(L)-(Q1+Q2+Q3+Q4+Q7)
    P(L,1)=P5
    P(L,2)=P6
    P(L,K)=P8
    P(L,I1)=P9
    GOTO 11
60 C(L)=C(L)-(Q1+Q2+Q3+Q6+Q9)
    P(L,1)=P5
    P(L,I3)=P7
    P(L,K)=P8
    GOTO 11
40 IF (I.EQ.1) GOTO 401
    IF (I.EQ.I3) GOTO 402
    P(L,1)=P5
    P(L,2)=P6
    P(L,I3)=P7

```

```

      P(L,K)=P8
      P(L,I1)=P9
      GOTO 11
401 C(L)=C(L)-(Q1+Q4+Q7)
      P(L,1)=P5
      P(L,2)=P6
      P(L,K)=P8
      P(L,I1)=P9
      GOTO 11
402 C(L)=C(L)-(Q3+Q6+Q9)
      P(L,1)=P5
      P(L,I3)=P7
      P(L,K)=P8
      GOTO 11
30 IF (I.EQ.1) GOTO 301
   IF (I.EQ.I3) GOTO 302
   C(L)=C(L)-(Q7+Q8+Q9)
   P(L,1)=P5
   P(L,2)=P6
   GOTO 11
301 C(L)=C(L)-(Q1+Q4+Q7+Q8+Q9)
      P(L,1)=P5
      P(L,2)=P6
      GOTO 11
302 C(L)=C(L)-(Q3+Q6+Q7+Q8+Q9)
      P(L,1)=P5
      GOTO 11
20 IF (I.EQ.1) GOTO 201
   IF (I.EQ.I3) GOTO 202
   P(L,1)=P5
   P(L,2)=P6
   GOTO 11
201 C(L)=C(L)-(Q1+Q4)
      P(L,1)=P5
      P(L,2)=P6
      GOTO 11
202 C(L)=C(L)-(Q3+Q6)
      P(L,1)=P5
11 CONTINUE
10 CONTINUE
   RETURN
C   THE END OF THIS SUBROUTINE
   END
C
C   SUBROUTINE (EQNS) FOR EQUATION SOLVING BY GAUSSIAN
C   ELIMINATION AND BACKWARD SUBSTITUTION
C   I1=NUMBER OF RADIAL NODES IN THE FINITE ELEMENT GRID
C   IS=NUMBER OF EQUATIONS TO BE SOLVED
C   C=ARRY WHICH HOLDS THE RIGHTHAND SIDE COEFFICIENTS OF
C   THE EQUATIONS
C   P=ARRY WHICH HOLDS THE LEFTHAND SIDE COEFFICIENTS OF
C   THE MATRIX EQUATION
      SUBROUTINE EQNS (C,IT,IS,P,I1,IM,IJM)
      DIMENSION C(IJM),P(IJM,IM)

```

```

C   SET VARIOUS CONSTANTS
      NC=I1
      IS1=IS-1
C   STEP 1-GAUSSIAN ELIMINATION
C   DO LOOP FOR EACH ROW OF BAND MATRIX
      DO 70 NT=1,IS1
        IF (NT.GT.IT) NC=IS-NT+1
C   DO LOOP FOR EACH COLUMN OF SUB-MATRIX
      DO 71 I=2,NC
        IC=NT+I-1
        RC=P(NT,I)/P(NT,1)
C   RESET APPROPRIATE ELEMENTS OF RIGHT-HAND SIDE
      C(IC)=C(IC)-RC*C(NT)
      II11=I1-I+1
C   DO LOOP FOR EACH ROW OF SUB-MATRIX
      DO 72 J=1,II11
C   RESET APPROPRIATE ELEMENT OF BAND MATRIX
      P(IC,J)=P(IC,J)-RC*P(NT,I+J-1)
72 CONTINUE
71 CONTINUE
70 CONTINUE
C   STEP 2-BACKWARD SUBSTITUTION
C   BACKWARD SUBSTITUTION FOR ROW IS
      C(IS)=C(IS)/P(IS,1)
C   DO LOOP FOR BACKWARD SUBSTITUTION FOR EACH ROW OF MATRIX
      IS1=IS-1
      DO 80 I=1,IS1
        II=IS-I
        NC=I1
        IF (II.GT.IT) NC=IS-II+1
        S=0.
C   DO LOOP FOR SUMMING PRODUCTS OF (APPROPRIATE ELEMENTS OF
C   C) * (APPROPRIATE ELEMENTS OF P)
      DO 81 J=2,NC
        JJ=NC+2-J
        S=S+P(II,JJ)*C(II+JJ-1)
81 CONTINUE
C   RESET APPROPRIATE ELEMENT OF C TO STORE THE SOLUTION
      C(II)=(C(II)-S)/P(II,1)
80 CONTINUE
      RETURN
C   END OF SUBROUTINE EQNS
      END

C
C   SUBROUTINE (VPOT) FOR COPYING THE SOLUTION OF THE
C   FINITE ELEMENT EQUATIONS INTO THE ARRAY V(IM,JM)
C   WHICH STORES THE COMPUTED VECTOR POTENTIAL AT EACH
C   MESH POINT .
C   THE VARIABLES ARE DEFINED IN THE MAIN PROGRAM
      SUBROUTINE VPOT (V,C,I2,IM,JM,IJM,J5)
      DIMENSION V(IM,JM),C(IJM)
      J6=J5+1
      L=0
      DO 1 J=2,J6

```

```

DO 2 I=2,I2
L=L+1
V(I,J)=C(L)
2 CONTINUE
1 CONTINUE
RETURN
C END OF SUBROUTINE VPOT
END

C
C SUBROUTINE (BVALUES) FOR CALCULATING THE FLUX DENSITY AT
C POINTS THROUGHOUT THE MAGNETIG CIRCUIT AND FOR WRITING OUT
C THE PEAK FLUX DENSITY.
C THE VARIABLES ARE DEFINED IN THE MAIN PROGRAM
SUBROUTINE BVALUES(Z,R,V,AMUR,I1,J1,IM,JM,NBFE)
DIMENSION Z(IM,JM),R(IM,JM),V(IM,JM),AMUR(IM,JM)
C INITIALIZE THE VALUE AND POSITION OF THE PEAK FLUX DENSITY
C IN THE MAGNETIC CIRCUIT
AMU0=1.2566371E-6
BMAX=0.
ZMAX=0.
RMAX=0.
C IF (FLUX DENSITY IN MAGNETIG CIRCUIT) IS REQUIRED AS
C OUTPUT,THE PROGRAM IS DIRECTED TO WRITE HEADING FOR THAT
IF (NBFE.EQ.1) WRITE (2,10)
10 FORMAT (/1X,'FLUX DENSITY VALUES IN MAGNETIC CIRCUIT'/)
C DO LOOPS FOR EVERY QUADRILATERAL AREA OF MESH
I2=I1-1
J2=J1-1
DO 1 J=1,J2
DO 1 I=1,I2
C TEST WHETHER THE QUADRILATERAL IS IN FREE SPACE OR IN
C THE MAGNETIC CIRCUIT
IF (AMUR(I,J).EQ.1) GOTO 1
C SET Z AND R COORDINATES AND VECTOR POTENTIAL VALUES AT
C CORNER POINTS OF QUADRILATERAL
Z1=Z(I,J)
Z2=Z(I+1,J)
Z3=Z(I+1,J+1)
Z4=Z(I,J+1)
R1=R(I,J)
R2=R(I+1,J)
R3=R(I+1,J+1)
R4=R(I,J+1)
V1=V(I,J)
V2=V(I+1,J)
V3=V(I+1,J+1)
V4=V(I,J+1)
C CALCULATE COORDINATES OF CENTRE POINT OF QUADRILATERAL
ZC=(Z1+Z2+Z3+Z4)*.25
RC=(R1+R2+R3+R4)*.25
C CALCULATE FLUX DENSITY COMPONENT BZ AND BR AT CENTRE
C POINT OF QUADRILATERAL
X1=(Z1-Z2)*R1*R2
X2=(Z1-Z3)*R1*R3

```

```

X3=(Z1-Z4)*R1*R4
X4=(Z2-Z3)*R2*R3
X5=(Z2-Z4)*R2*R4
X6=(Z3-Z4)*R3*R4
Y1=(R1-R2)*Z1*Z2
Y2=(R1-R3)*Z1*Z3
Y3=(R1-R4)*Z1*Z4
Y4=(R2-R3)*Z2*Z3
Y5=(R2-R4)*Z2*Z4
Y6=(R3-R4)*Z3*Z4
P1=X4-X5+X6
P2=-X2+X3-X6
P3=X1-X3+X5
P4=-X1+X2-X4
Q1=R1*Z2-Z1*R2
Q2=R1*Z3-Z1*R3
Q3=R1*Z4-Z1*R4
Q4=R2*Z3-Z2*R3
Q5=R2*Z4-Z2*R4
Q6=R3*Z4-Z3*R4
DET=Z1*P1+Z2*P2+Z3*P3+Z4*P4
F=V1*(-Z4*X4+Z3*X5-Z2*X6)+V2*(Z4*X2-Z3*X3+Z1*X6)
F=F+V3*(-Z4*X1+Z2*X3-Z1*X5)+V4*(Z3*X1-Z2*X2+Z1*X4)
G=V1*P1+V2*P2+V3*P3+V4*P4
H=V1*(-Y4+Y5-Y6)+V2*(Y2-Y3+Y6)+V3*(-Y1+Y3-Y5)+V4*(Y1-Y2+Y4)
AI=V1*(Q4-Q5+Q6)+V2*(-Q2+Q3-Q6)+V3*(Q1-Q3+Q5)+V4*(-Q1+Q2-Q4)
F=F/DET
G=G/DET
H=H/DET
AI=AI/DET
VC=F+G*ZC+H*RC+AI*ZC*RC
BZ=H+AI*ZC+VC/RC
BR=-G-AI*RC

```

```

C CALCULATE THE FLUX DENSITY B AT CENTRE POINT OF QUADRI-
C LATERAL

```

```

    B=SQRT(BZ*BZ+BR*BR)

```

```

C CNVERT COORDINATES OF MAX. FLUX DENSITY POSITION FROM
C METRES TO MM

```

```

    ZC=ZC*1000.

```

```

    RC=RC*1000.

```

```

C WRITE LOCATION AND VALUES OF AXIAL (BZ) AND RADIAL(BR)
C COMPONENTS OF THE FLUX DENSITY AND THE RESULTANT FLUX
C DENSITY THROUGHOUT THE MAGNETIC CIRCUIT

```

```

    IF (NBFE.EQ.1) WRITE(2,8) I,J,ZC,RC,BZ,BR,B

```

```

8 FORMAT (1X,2I5,2F15.3,3F15.6)

```

```

C TEST IF MAX. FLUX DENSITY HAS BEEN REACHED

```

```

    IF (B.LT.BMAX) GOTO 1

```

```

    BMAX=B

```

```

    ZMAX=ZC

```

```

    RMAX=RC

```

```

1 CONTINUE

```

```

C WRITE POSITION AND VALUES OF MAX. FLUX DENSITY IN THE
C MAGNETIC CIRCUIT

```

```

    WRITE(2,3)ZMAX,RMAX,BMAX

```

```

3 FORMAT(1X,'MAXIMAM FLUX DENSITY IN MAGNETIC CIRCUIT'//
+ 1X,2F10.5,F15.6,'(TESLA)')
RETURN
C END OF SUBROUTINE BVALUES
END

C
C SUBROUTINE (FLUX) FOR CONVERTING THE VALUES OF VECTOR
C POTENTIAL AT EACH MESH POINT TO THE CORESPONDING MAGNETIC
C FLUX VALUE V(I,J)=ARRAY WHICH HOLDS VALUES OF THE VECTOR
C POTENTIAL AT ENTRY TO THE ROUTINE AND WHICH HOLDS THE
C THE MAGNETIC FLUX VALUE AT EACH MESH POINT ON RETURN TO
C TO THE MAIN PROGRAM
SUBROUTINE FLUX (V,I1,J1,IM,JM)
DIMENSION V(IM,JM)
C SET VALUE 2.*PYE
PI=6.28318531
C CONVERT EACH ELEMENT OF V(IM,JM) FROM VECTOR POTENTIAL
C TO MAGNETIC FLUX VALUE AT EACH MESH POINT
DO 2 J=1,J1
DO 2 I=1,I1
V(I,J)=PI*V(I,J)
2 CONTINUE
C WRITE HEADING
WRITE (2,5)
5 FORMAT (/1X,'FLUX VALUES AT EACH MESH POINT'//)
C J,JF,JS ARE MESH POINT NUMBERS IN THE AXIAL DIRECTION
JS=1
JD=4
20 JF=JS+JD
WRITE (2,4) (J,J=JS,JF)
4 FORMAT (1X,5X,5I15)
C DO LOOP FOR WRITING MESH POINT NUMBERS IN THE RADIAL
C DIRECTION AND THE FLUX VALUES.
DO 6 I=1,I1
C I IS THE MESH POINT NUMBER IN THE RADIAL DIRECTION
WRITE (2,8) I,(V(I,J),J=JS,JF)
8 FORMAT (1X,I5,5E15.5)
6 CONTINUE
WRITE (2,10)
10 FORMAT (1X)
C TEST FOR END OF SET OF VALUES
IF (JF.EQ.J1) GOTO 12
JS=JF+1
IF ((JS+JD).GT.J1) JD=J1-JS
GOTO 20
12 WRITE (2,10)
RETURN
C END OF SUBROUTINE FLUX
END

```

APPENDIX 4

PROGRAM VPSAT

```

C     VPSAT PROGRAM
C     FINITE ELEMENT PROGRAM FOR COMPUTING AXIAL FLUX DENSITY
C     DISTRIBUTION AND VECTOR POTENTIAL THROUGHOUT THE MAGNET
C     -IC CIRCUIT OF SATURATED AND USATURATED MAGNETIC LENSES
C     THE PRINCIPAL VARIABLES ARE DEFINED AS FOLLOWS:
C     Z(IM,JM)=Z-COORDINATES OF EACH MESH POINT
C     R(IM,JM)=R-COORDINATES OF EACH MESH POINT
C     IM=NUMBER OF MESH POINT IN THE R-DIRECTION
C     JM=NUMBER OF MESH POINT IN THE Z-DIRECTION
C     OTHER PROGRAMS PREVIOUS TO THIS PROGRAM UTILISE DIFFERE
C     -NT MESH NUMBERS DEPENDING ON THE COMPUTER MEMORY SIZE .
C     FOR SUCH PROGRAMS TYPICAL MESH POINTS NUMBERS ARE IN THE
C     ORDER OF (32,70) TO (40,80) WHEN UTILIZING LARGE COMPUTERS
C     FOR SMALLER COMPUTERS (20,40) TO (25,50) MESH POINTS ARE
C     USED IN MINI COMPUTERS THE NUMBERS ARE REDUCED TO (12,25) .
C     FOR SUCH PROGRAMS THE HIGHER THE MESH POINTS NUMBERS THE
C     MORE ACCURATE THE RESULTS ARE .
C     THIS NECESSITATES LARGE COMPUTERS FOR ACCURATE RESULTS.
C     THE PRESENT PROGRAM OVERCOMES THE INHERENT INACCURACIES
C     WHEN UTILISING MINI COMPUTERS BY INCREASING THE NUMBER
C     OF RUNS AS EXPLAINED LATER AMUR(IM,JM)=RELATIVE PERMEAB
C     -ILITY OF EACH QUADRILATERAL
C     AJ(IM,JM)=CURRENT DENSITY WITHIN EACH QUADRILATERAL
C     A(IM,JM)=NON ZERO ELEMENTS OF SYMMETRIC BAND MATRIX
C     C(IM,JM)=RIGHT HAND SIDE OF THE FINITE ELEMENTS EQUATIONS
C     V(IM,JM)=COMPUTED VECTOR POTENTIAL AT EACH MESH POINT
C     P(IM*JM,IM)=COEFFICIENTS OF THE FINITE ELEMENT EQUATIONS
C     AZLB(IM)=FIRST INNER BOUNDARY IN R-DIRECTION
C     AZRB(IM)=SECOND INNER BOUNDARY IN R-DIRECTION
C     NR=NUMBER OF RUNS DESIRED (1 TO 4)
C     TITLE(20) IS ANY TITLE UP TO 80 CHARACTERS
C     IJM=IM*JM
C     NSAT=THE SATURATION CONDITON .NSAT TAKES THE VALUE OF 0
C     FOR UNSATURATED LENSE AND 1 FOR SATURATED LENSE I.E THE
C     PROGRAM WILL FUNCTION FOR BOTH LINEAR AND NONLINEAR
C     CONDITIONS
C     TB(IBM),TM(IBM) REPRESENT TABLE OF TYPICAL RELATION
C     BETWEEN FLUX DENSITY AND RELATIVE PERMEABILITY .
C     THE DIMENSION STATEMENTS ARE SET AS FOLLOWS :
C     COMMON/ONE/Z(IM,JM),R(IM,JM),AMUR(IM,JM),AJ(IM,JM)
C     COMMON/TWO/A(IJM),C(IJM),V(IM,JM),ZR1(IM,JM),TMUR(IM,JM)
C     COMMON/THREE/ P(IJM,IM)
C     DIMENSION AZLB(IM) , AZRB(IM) ,NR(4) ,TITLE(20)
C     COMMON TB(IBM) ,TM(IBM) ,IBM ,NSAT
C     ZZ (Z-COORDINATES OF AXIAL MESH POINTS)
C     ABZ(COMPUTED AXIAL FLUX DENSITY DISTRIBUTION)
C
C
C     COMMON/ONE/  Z(25,50),R(25,50),AMUR(25,50),AJ(25,50)
C     COMMON/TWO/  A(1250),C(1250),V(25,50),ZR1(25,50),TMUR(25,50)
C     COMMON/THREE/  P(1250,25)
C     DIMENSION AZLB(25),AZRB(25),NR(4),TITLE(20)
C     COMMON TB(100),TM(100),IBM,NSAT
C     DIMENSION ZZ(210),ABZ(210)

```

```

IM=25
JM=50
IJM=IM*JM
LBZ=JM*3
X=0.
DO 10 J=1, LBZ
  ZZ(J)=X
  ABZ(J)=X
10 CONTINUE
  LBZ=0
C THE PROGRAM WILL READ THE FIRST LINE OF DATA WHICH
C CONSIST OF TWO INTEGERS THE FIRST INDICATE WHETHER
C THE ENTIRE MESH IS SPECIFIED IN THE DATA I.E ASYMM
C -ETRIC CASE ,OR THE PORTION OF THE MESH IN THE NEG
C -ATIVE HALF OF THE LENS IS SPECFIED (SYMMETRIC
C -CASE)
C THE SECOND INTEGER IDICATE WHETHER THE MAGNETIC
C STRUCTURE IS UNDER LINEAR (UNSATURATED) OR NON
C LINEAR (SATURATED) CONDITION .
C NSYM CAN TAKE VALUES OF 1 OR 0 . 1 INDICATES
C SYMMETRY
  READ (1,1) NSYM1, NSAT
  1 FORMAT (2I5)
C THE PROGRAM EXPECTS IN THE SECOND LINE OF DATA
C FOUR INTEGERS WHICH WILL SPECIFY THE NUMBER OF
C REQUIRED TO BE PERFORMED (FROM 1 TO 4). THUS FOR
C ONE RUN NR=1,0,0,0, FOR TWO RUNS NR=1,2,0,0, FOR
C THREE RUNS NR=1,2,3,0, AND FINALL FOR FOUR RUNS
C NR=1,2,3,4,
  READ (1,2) (NR(I), I=1,4)
  2 FORMAT (4I5)
C A BLANK LINE IS LEFT
  READ (1,1111)
C FOR SYMMETRICAL CASE (NSYM1=1), UP TO 3 RUNS ARE
C PERFORMED. FOR ASYMMETRIC CASE (NSYM1=0) UP TO FOUR
C RUNS ARE DONE
  IF (NSYM1.EQ.1) GOTO 20
  IF (NR(4).EQ.4) GOTO 24
20 IF (NR(3).EQ.3) GOTO 23
  IF (NR(2).EQ.2) GOTO 22
  IF (NR(1).EQ.1) GOTO 21
C WARNING IF NUMBER OF RUNS HAVE NOT BEEN SPECIFIED
C THE PROGRAM WILL STOP IN THIS CASE
  WRITE (2,3)
  3 FORMAT (1X, ' RUNS NOT SPECIFIED')
  STOP
21 NRUN=1
  GOTO 25
22 NRUN=2
  GOTO 25
23 NRUN=3
  GOTO 25
24 NRUN=4
C THE PROGRAM WILL TEST WHETHER THE LENS IS UNDER

```

```

C   LINEAR CONDITION (NSAT=0) OR UNDER SATURATION. IF
C   NSAT=0 THE PROGRAM IS DIRECTED TO READ THE TWO
C   INNER BOUNDARIES (JLB,JRB).OTHERWISE(SATURATION
C   CONDITIONS) THE PROGRAM WILL READ ATABLE OF TYPICAL
C   RELATION BETWEEN FLUX DENSITY AND RELATIVE PERMEA
C   -BILITY OF THE MAGNETIG MATERIAL.

    25 IF (NSAT.EQ.0) GOTO 4
      IBM=0
    98 IBM=IBM+1
      READ(1,100)TB(IBM),TM(IBM)
    100 FORMAT(2F10.0)
C   THE PROGRAM WILL TEST FOR END OF TABLE
      IF (TM(IBM).EQ.(-999.)) GOTO 1001
      GOTO 98
    1001 IBM=IBM-1
C   FOR FLUX DENSITY VALUES NOT SPECIFIED IN TABLE
C   AFACOR IS CALCULATED WHICH IS USED FOR DERIVING
C   RELATIVE PERMEABILTY
      AMAG=TB(IBM)*(1.-1./TM(IBM))
C   A BLANK LINE IS LEFT
C   THE VALUES OF TWO INNER BOUNDARIES ARE READ
      READ (1,1111)
    4 READ (1,111) JLB,JRB
    111 FORMAT (2I5)
C   A BLANK LINE IS LEFT
      READ (1,1111)
    1111 FORMAT (1X)
C   INITIALISE NUMBER OF COMPLETED ITERATIONS TO ZERO
      NIT=0
C   DO LOOPS ACORDING TO SPECIFIED NUMBER OF RUNS
      DO 112 IRUN=1,NRUN
        IF (IRUN.EQ.1) GOTO 2111
        IF (NR(IRUN).EQ.0) GOTO 112
C   READ ANY TITLE UP TO 80 CHARACTERS
    2111 READ (1,1121) (TITLE(I),I=1,20)
    1121 FORMAT (20A4)
C   THE OUTPUT IS SPECIFIED ACCORDING TO REQUIREMENTS
      READ (1,1122) NBF,E,NFLUX
    1122 FORMAT (2I5)
C   A BLANK LINE IS LEFT
      READ (1,1111)
C   THE SUBROUTINE MESH ,FOR READING AND SETTING AXIAL
C   AND RADIAL COORDINATES OF THE MAJOR MESH LINES
C   THE SUBROUTINE IS CALLED TWICE,FOR Z AND R COORDINATES
      CALL MESH (Z,I1,J1,IM,JM)
      CALL MESH (R,I1,J1,IM,JM)
C   SET VARIOUS CONSTANTS
C   I1=NUMBER OF MESHES IN THE RADIAL DIRECTION
C   I2=I1-1 =NUMBER OF QUADRILATERALS IN THE RADIAL
C   J1=NUMBER OF MESH-POINTS IN THE AXIAL DIRECTION
C   J2=J1-1 =NUMBER OF QUADRILATERALS IN THE AXIAL
C   DIRECTION
      I2=I1-1

```

```

      I3=I1-2
      J2=J1-1
      J3=J1-2
C   DO LOOP TO SET OUTER BOUNDARY VECTOR POTENTIALS
C   TO ZERO FOR BOTH Z AND R DIRECTIONS
      DO 1124 J=1,JM
      DO 1124 I=1,IM
1124 V(I,J)=0.
C   THE SUBROUTINE READING THE DATA SPECIFYING THE POSITION
C   AND PERMEABILITY OF THE MAGNETIC CIRCUIT IS CALLED
      CALL AJMUR (AMUR,AJ,I1,J1,IM,JM,MS,MC)
C   THE DATA IS TESTED FOR SATURATION AND SUBROUTINE
C   SETMUR IS CALLED
      IF (IRUN.EQ.1.OR.NSAT.EQ.0.OR.MS.EQ.0) GOTO 1123
      CALL SETMUR (Z,AMUR,ZR1,TMUR,I2,J2,IM,JM)
C   THE INITIAL LENS EXCITATION(AMPERTURNS) IS SET TO
C   ZERO FOR ASYMMETRIC LENS
1123 ANI=0.
      NSYM=0
C   THE NEXT TWO STATEMENTS GUIDE THE PROGRAM TO
C   EXECUTE THE APPROPRIATE COMPUTATIONS FOR 1,2,3,4
C   RUNS RESPECTIVELY
1126 IF (IRUN.EQ.1) GOTO 113
      IF (NR(IRUN)-3)      114,115,116
C   AN ITERATION COUNTER IS SET TO ZERO AND THE COORDINATES
C   OF THE MESH NODES IN Z AND R DIRECTIONS ARE SET BY
C   LINEAR INTERPOLATION
113 K1=0
      DO 130 J=1,J1
      DO 130 I=1,I1
      K1=K1+1
C   THE RIGHT HAND SIDE OF THE FINITE ELEMENTS EQUATION
C   IS SET
      C(K1)=0.
130 CONTINUE
      K1=0
C   THE DATA IS TESTED FOR LINEARITY AND THE PROGRAM IS
C   DIRECTED ACCORDINGLY
      IF (NIT.GT.0) GOTO 1304
C   FOR LINEAR CASE THE COORDINATES OF THE MESH NODES
C   IN Z AND R DIRECTION ARE SET BY LINEAR INTERPOLATION
C   IN Z AND R DIRECTIONS ARE SET BY LINEAR INTERPOLATION
      DO 1302 J=1,J1
      DO 1302 I=1,I1
      K1=K1+1
      A(K1)=0.
1302 CONTINUE
1304 NSYM=NSYM1
      GOTO 131
114 K1=0
      K2=0
      DO 117 J=1,J1
      DO 117 I=1,I1
      K1=K1+1

```

```

A(K1)=0.
C(K1)=0.
IF (J.EQ.J1) GOTO 1171
GOTO 117
1171 K2=K2+1
C THE VECTOR POTENTIAL AT FIRST INNER BOUNDARY IS STORED FOR
C RUN2 FROM RUN1
A(K1)=AZLB(K2)
V(I,J)=A(K1)
117 CONTINUE
GOTO 131
115 K1=0
K2=0
K3=0
C UP TO THREE RUNS CAN BE DONE FOR SYMMETRIC CASES
IF (NRUN.EQ.3) NSYM=NSYM1
DO 118 J=1,J1
DO 118 I=1,I1
K1=K1+1
A(K1)=0.
C(K1)=0.
IF (J.EQ.1) GOTO 1151
GOTO 1152
1151 K2=K2+1
C THE VECTOR POTENTIAL AT THE INNER BOUNDARIES ARE
C STORED FOR LATER USE IN OTHER RUNS
A(K1)=AZLB(K2)
V(I,J)=A(K1)
1152 IF (NSYM.EQ.1) GOTO 118
IF (J.EQ.J1) GOTO 1153
GOTO 118
1153 K3=K3+1
C THE VECTOR POTENTIAL IN SECOND INNER BOUNDARY IS STORED FOR
C RUN3 AND RUN4
A(K1)=AZRB(K3)
V(I,J)=A(K1)
118 CONTINUE
GOTO 131
116 K1=0
K2=0
NSYM=NSYM1
DO 119 J=1,J1
DO 119 I=1,I1
K1=K1+1
A(K1)=0.
C(K1)=0.
IF (J.EQ.1) GOTO 1191
GOTO 119
1191 K2=K2+1
A(K1)=AZRB(K2)
V(I,J)=A(K1)
119 CONTINUE
C THE RELATIVE PERMEABILITY OF FREE SPACE IS SETED
131 AMU0=1.2566371E-6

```

```

DO 1131 I=1,IJM
DO 1131 J=1,IM
1131 P(I,J)=0.
K=I2
K1=0
IF (NSYM.EQ.1) GOTO 8
J5=J3
JS=0
IS=I3*J3
GOTO 9
8 J5=J2
JS=J5
IS=I3*J2
9 IT=IS-K
NM=NSYM
C IF ONLY ONE RUN IS REQUESTED THEAND IN SATURATION CASE
C THE PROGRAM IS DIRECTED ACORDINGLY
C IF (IRUN.EQ.1.AND.NSAT.EQ.1.AND.MS.GT.0) GOTO 82
C IN CASE OF UNSATURATION THE PROGRAM WILL CALL SUBROUTINE
C PCLIN OTHERWISE (SATURATION) PCSAT IS CALLED
C CALL PCLIN(Z,R,AMUR,AJ,P,A,C,I1,J1,IM,JM,IJM,NM,ANI)
C GOTO 84
82 CALL PCSAT(Z,R,V,AMUR,AJ,P,A,C,AMAG,I1,J1,IM,JM,IJM,NM,ANI)
C FOR SYMMETRIC LENSES ,TO TAKE ACCOUNT OF THE FACT THAT
C ONLY HALF OF THE COIL IS SPECIFIED IN THE DATA, THE
C EXCITATION IS DOUBLED
84 IF (NSYM.EQ.1) ANI=2.*ANI
C SUBROUTINE "EQNS" IS CALLED . THIS SUBROUTINE SOLVES
C EQUATIONS BY GAUSSIAN ELIMINATION AND BACKWARD SUBST-
C -ITUTION
C CALL EQNS (C,IT,IS,P,I1,IM,IJM)
C SUBROUTINE "VPLUSDV" IS CALLED . THIS SUBROUTINE ADDS
C THE COMPUTED CHANGES IN THE MESH-POINT POTENTIALS TO
C CURRENT POTENTIAL VALUES TO OBTAIN AN IMPROVED APPRO-
C -XIMATION TO THE TRUE POTENTIAL DISTRIBUTION AND TEST
C WHETHER CONVERGENCE HAS BEEN ACHIEVED
93 CALL VPLUSDV (V,C,I2,IM,JM,IJM,J5,VMAX,DVMAX,NTEST)
C FOR RUN NUMERS GREATER THAN 1 AND LINEAR CONDITION,
C THE PROGRAM IS DIRECTED TO WRITE OUTPUT TITLES.
C OTHERWISE IT WILL STORE THE VECTOR POTENTIAL OF INNER
C BOUNDARIES
C IF (IRUN.GT.1.OR.NSAT.EQ.0.OR.MS.EQ.0) GOTO 931
C L1=J3
C IF (NSYM.EQ.1) L1=J2
C L=I2
C K1=0
C DO 842 J=1,L1
C L=L+2
C DO 842 I=1,I3
C L=L+1
C K1=K1+1
C A(L)=V(I+1,J+1)
842 CONTINUE
NIT=NIT+1

```

```

C   WRITE TITLES IN CASE OF SATURATION WHEN NUMBER OF
C   ITERATIONS IS MORE THAN 1

      IF (NIT.EQ.1) WRITE(2,222)
222  FORMAT (1X,'ITERATIONS',5X,'MAX VECTOR',5X,'MAX CHANGE IN'
      -/1X,'COMPLETED ',5X,'POTENTIAL ',4X,'VECTOR POTENTIAL'/)
      WRITE (2,1125) NIT,VMAX,DVMAX
1125 FORMAT (1X,I5,5X,E15.5,3X,E15.5)
C   TEST WHETHER CONVERGENCE HAS BEEN ACHIEVED IF SO
C   THE TITLES ARE WRITTEN.OTHERWISE MORE ITERATIONS
C   ARE PERFORMED
      IF (NTEST.EQ.1) GOTO 930
      GOTO 1123
930  WRITE (2,9301)
9301 FORMAT (/1X,'CONVERGENCE ACHIEVED'/)
931  IF (IRUN.GT.1) GOTO 934
      DO 932 I=1,I1
C   THE VECTOR POTENTIAL IN FIRST INNER BOUNDARY IS STORED
      AZLB(I)=V(I,JLB)
      IF (NSYM.EQ.1) GOTO 932
C   THE VECTOR POTENTIAL IN SECOND INNER BOUNDARY IS STORED
      AZRB(I)=V(I,JRB)
932  CONTINUE
C   WRITE TITELS
934  WRITE (2,935) (TITLE(I),I=1,20)
935  FORMAT (/1X,20A4/)
      WRITE (2,936)
936  FORMAT (/1X,'AXIAL FLUX DENSITY DISTRIBUTION'/)
      WRITE (2,9351)
C   FOR EACH MESH-POINT ON THE AXIS WRITE THE Z-COORDINATES
C   OF AXIAL MESH-PT(IN MM) AND AXIAL FLUX DENSITY AT MESH-
C   POINT (IN TESLAS)
9351 FORMAT (1X,'Z (MILLIMETRES)          B (TESLAS)'/)

      DO 94 J=1,J1
      Z1=Z(I1,J)*1000.
      R1=R(I2,J)
      R2=R(I3,J)
      A1=V(I2,J)
      A2=V(I3,J)
C   THE AXIAL FLUX DENSITY IS CALCULATED
      B=(A1*R2*R2*R2-A2*R1*R1*R1)/(.5*R1*R2*(R2*R2-R1*R1))
      WRITE (2,95) Z1,B
C   IF ONLY ONE RUN IS REQUIRED THEN
      IF (IRUN.EQ.1) GOTO 94
      LBZ=LBZ+1
      ZZ(LBZ)=Z1
      ABZ(LBZ)=B
94  CONTINUE
C   IF NUMBER OF RUNS IS MORE THAN 1,THE Z AND B OUTPUTED
      IF (NRUN.NE.1.OR.NSYM.EQ.0) GOTO 79
      DO 971 JJ=1,J2
      J=J2+1-JJ
      Z1=-Z(I1,J)*1000.

```

```

R1=R(I2,J)
R2=R(I3,J)
A1=V(I2,J)
A2=V(I3,J)
B=(A1*R2*R2*R2-A2*R1*R1*R1)/(.5*R1*R2*(R2*R2-R1*R1))
WRITE (2,95) Z1,B
971 CONTINUE
C FOR SYMMETRIC CASE THE VALUES OF Z(MM)COORDINATES AND
C B(AXIAL FLUX DENSITY) FOR THE POSITIVE HALF PLANE IS
C CALCULATED
79 IF (IRUN.EQ.1.OR.NR(IRUN).EQ.4) GOTO 941
C FOR 1 RUN OR 4 RUNS THE PROGRAM IS DIRECTED TO WRITE
C THE LENS EXCITATION . THIS ALSO HAPPENS IN CASE OF
C SYMMETRY AND 3 RUNS
IF (NR(IRUN).EQ.3.AND.NSYM.EQ.1) GOTO 941
IF (NR(IRUN).EQ.NR(IRUN-1)+1) LBZ=LBZ-1
95 FORMAT (1X,F10.2,6X,F15.6)
C LENS EXCITATION IS WRITEN OUT
941 WRITE (2,96) ANI
IF (IRUN.EQ.1) EXCIT=ANI
96 FORMAT (1X/' EXCITATION GIVEN (NI) = ',F10.2,
+ ' AMPERETURNS'/)
IF (MS.EQ.0) GOTO 112
IR=IRUN
C THE PROGRAM IS DIRECTED TO SUBROUTINE "BVALUES"
CALL BVALUES (Z,R,V,AMUR,AMAG,I1,J1,IM,JM,NSAT,NBFE,IR)
IF (NSAT.EQ.0.OR.IRUN.GT.1) GOTO 1102
C IN CASE OF SATURATION (NON LINEAR) SUBROUTINE "TRZRMU"
C IS CALLED
CALL TRZRMU (Z,AMUR,ZR1,TMUR,I1,J1,IM,JM)
C IF FLUX VALUES AT EACH MESH POINT ARE NOT REQUIRED
C THE PROGRAM IS
1102 IF (NFLUX.EQ.0) GOTO 112
C IF FLUX VALUES AT EACH MESH POINT ARE REQUIRED,THE
C PROGRAM IS DIRECTED TO SUBROUTINE "FLUX"
CALL FLUX (V,R,I1,J1,IM,JM)
112 CONTINUE
C IF ONLY ONE RUN IS REQUIRED ,THE PROGRAM WILL STOP
C OTHERWISE IT IS DIRECTED TO OUTPUT THE TOTAL AXIAL
C FLUX DENSITY DISTRIBUTION FOR THE SPECIFIED REGION
IF (NRUN.EQ.1) STOP
WRITE(2,942)
942 FORMAT (/1X,'TOTAL DISTRIBUTION FOR SPECIFIED REGION'/)
WRITE (2,936)
WRITE (2,9351)
DO 944 J=1,LBZ
WRITE (2,95) ZZ(J),ABZ(J)
944 CONTINUE
C IN SYMMETRIC CASE THE Z AND B VALUES FOR THE POSITIVE
C HALF ARE OUTPUTED
IF (NSYM.EQ.0) GOTO 946
LBZ=LBZ-1
DO 948 K=1,LBZ
J=LBZ+1-K

```

```

      Z1=-ZZ(J)
      WRITE (2,95) Z1,ABZ(J)
948 CONTINUE
C   THE LENS EXCITATION IS OUTPUTED (IN AMPERTURNS)
946 WRITE (2,96) EXCIT
C   THE MAIN PROGRAM ENDS
      STOP
      END

C
C   SUBROUTINE (MESH) FOR SETTING COORDINATES OF EACH POINT ON THE
C   FINITE ELEMENT MESH
C   Z(IM,JM)=ARRAY OF COORDINATES TO BE SET
C   I1=NUMBER OF MESH POINTS IN THE RADIAL DIRECTION
C   J1=NUMBER OF MESH POINTS IN THE AXIAL DIRECTION
C   IM=MAXIMUM PERMISSIBLE VALUE OF I1
C   JM=MAXIMUM PERMISSIBLE VALUE OF J1
      SUBROUTINE MESH(Z,I1,J1,IM,JM)
      DIMENSION Z(IM,JM),TITLE(20)
      DIMENSION NC(15),NR(15),XA(15,15)
C   THE SUBROUTINE READS THE MESH-POINT NUMBERS IN AXIAL
C   DIRECTION
      READ (1,1)(NC(L),L=1,15)
1   FORMAT(5X,15I5)
      DO 2 L=1,15
      IF(NC(L).EQ.0)GOTO 3
2   CONTINUE
C   CALCULATE VALUES OF JJ AND J1
C   JJ=NUMBER OF COLUMNS OF COORDINATES SPECIFIED IN THE
C   J1=NUMBER OF MESH-POINTS IN THE AXIAL DIRECTION
      JJ=15
      GOTO 4
3   JJ=L-1
4   J1=NC(JJ)
C   READ THE COORDINATES VALUES
      DO 5 I=1,15
      READ(1,6)NR(I),(XA(I,J),J=1,JJ)
6   FORMAT(I5,15F5.0)
C   TEST FOR END OF DATA
      IF (NR(I).EQ.0)GOTO 7
5   CONTINUE
      GOTO 8
7   II=I-1
8   I1=NR(II)
C   SET COORDINATE VALUES BY LINEAR INTERPOLATION
      DO 9 I=2,I1
      DO 9 J=2,J1
      L1=NR(I-1)
      L2=NR(I)
      M1=NC(J-1)
      M2=NC(J)
      DO 9 LL=L1,L2
      DO 9 MM=M1,M2
      KL=L2-L1
      KM=M2-M1

```

```

      D1=(XA(I-1,J)-XA(I-1,J-1))/FLOAT(KM)
      D2=(XA(I,J)-XA(I,J-1))/FLOAT(KM)
      D1=D1*FLOAT(MM-M1)+XA(I-1,J-1)
      D2=D2*FLOAT(MM-M1)+XA(I,J-1)
9    Z(LL,MM)=(D2-D1)*FLOAT(LL-L1)/FLOAT(KL)+D1
C    THE COORDINATE VALUES WHICH HAVE BEEN SPECIFIED IN
C    MM ARE CONVERTED TO METRES
      DO 10 I=1,I1
      DO 10 J=1,J1
10   Z(I,J)=Z(I,J)/1000.
      RETURN
C    THE END OF SUBROUTINE MESH
      END

C
C    SUBROUTINE (AJMUR) FOR SETTING EACH ELEMENT OF THE ARRY
C    AMUR(IM,JM) TO THE VALUE OF THE RELATIVE PERMEABILITY
C    OF CORRESPONDING QUADRILATERAL OF THE FINITE ELEMENT
C    MESH, AND EACH ELEMENT OF THE ARRY AJ(IM,JM) TO THE VALUE
C    OF THE CURRENT DENSITY. AMUR(IM,JM)=RELATIVE PERMEABILITY
C    VALUES FOR EACH QUADRILATERAL.
C    AJ(IM,JM)=CURRENT DENSITY VALUES FOR EACH QUADRILATERAL
C    (IN AMP/TURNS/ SQUARE METER)
C    IM=NUMBER OF QUADRELATERAL AREAS IN THE RADIAL DIRECCION
C    JM=NUMBER OF QUADRELATERAL AREAS IN THE AXIAL DIRECTION
      SUBROUTINE AJMUR (AMUR,AJ,I1,J1,IM,JM,MS,MC)
      DIMENSION AMUR(IM,JM),AJ(IM,JM)
C    INITIALISE ALL ELEMENTS OF AMUR TO 1. AND ALL ELEMENTS OF
C    AJ TO 0.
      DO 1 I=1,I1
      DO 1 J=1,J1
      AMUR(I,J)=1.
      AJ(I,J)=0.
1    CONTINUE
      MS=0
C    READ VALUES OF JA,JB,IA,IB,XJ
C    JA=THE SMALLER MESH-POINT NUMBER IN THE AXIAL DIRECTION
C    JB=THE LARGER MESH-POINT NUMBER IN THE AXIAL DIRECTION
C    IA=THE SMALLER MESH-POINT NUMBER IN THE RADIAL DIRECTION
C    IB=THE LARGER MESH-POINT NUMBER IN THE RADIAL DIRECTION
C    XJ=THE RELATIVE PERMEABILITY OF THAT PORTION OF THE
C    MAGNETIC CIRCUIT (DIMENSIONLESS)
2    READ (1,3) JA,JB,IA,IB,XJ
3    FORMAT (4I5,F10.0)
C    TEST FOR END OF MAGNETIC CIRCUIT DATA
      IF (JA.EQ.0) GOTO 5
C    RESET APPROPRIATE ELEMENTS OF AMUR TO THE VALUE OF XJ
      IB1=IB-1
      JB1=JB-1
      DO 4 I=IA,IB1
      DO 4 J=JA,JB1
4    AMUR(I,J)=XJ
      MS=MS+1
C    GO TO 2 TO READ NEXT LINE OF MAGNETIC CIRCUIT DATA
      GOTO 2

```

```

5 MC=0
C READ NEXT LINE OF VALUES OF JA,JB,IA,IB,XJ,WHICH ARE
C MESH-POINT NUMBERS SPECIFYING THE POSITION OF APORTION OF
C THE COIL WINDINGS
C JA=THE SMALLER MESH-POINT NUMBER IN THE AXIAL DIRECTION
C JB=THE LARGER MESH-POINT NUMBER IN THE AXIAL DIRECTION
C IA=THE SMALLER MESH-POINT NUMBER IN THE RADIAL DIRECTION
C IB=THE LARGER MESH-POINT NUMBER IN THE RADIAL DIRECTION
C XJ=THE CURRENT DENSITY IN THAT PORTION OF THE COIL WINDINGS
C (XJ IS IN AMPTURNS/SQUARE CM)
6 READ (1,3) JA,JB,IA,IB,XJ
C TEST FOR END OF DATA SPECIFYING COIL WINDINGS
  IF (JA.EQ.0) RETURN
C RESET APPROPRIATE ELEMENTS OF AJ TO THE VALUE OF XJ
  IB1=IB-1
  JB1=JB-1
  DO 7 I=IA,IB1
  DO 7 J=JA,JB1
C CONVERT CURRENT DENSITY XJ TO UNITS OF AMPTURNS/SQUARE
C METRE
7 AJ(I,J)=XJ*10000.
  MC=MC+1
C GO TO 6 TO READ NEXT LINE OF COIL WINDINGS DATA
  GOTO 6
  END

C
C SUBROUTINE (PCLIN) FOR SETTING THE FINITE ELEMENT COEFFICIENTS
C F AND G FOR EVERY QUADRILATERAL AREA OF THE FINITE ELEMENT
C MESH
C Z(IM,JM)=Z-COORDINATES OF EVERY MESH-POINT
C R(IM,JM)=R-COORDINATES OF EVERY MESH-POINT
C AJ(IM,JM)=CURRENT DENSITY OF EVERY QUADRILATERAL
C AR(IM,JM)RELATIVE PERMEABILITY OF EVERY QUADRILATERAL
C F(24) FINITE ELEMENT F-COEFFICIENTS FOR EVERY QUADRILATERAL
C G(24)=FINITE ELEMENT G-COEFFICIENTS FOR EVERY QUADRILATERAL
C I1=NUMBER OF MESH-POINTS IN THE R-DIRECTION
C J1=NUMBER OF MESH-POINTS IN THE Z-DIRECTION
  SUBROUTINE PCLIN(Z,R,AR,AJ,P,A,C,I1,J1,IM,JM,IJM,NM,ANI)
  DIMENSION Z(IM,JM),R(IM,JM),C(IJM),P(IJM,IM)
  DIMENSION AR(IM,JM),AJ(IM,JM),A(IJM)
  DIMENSION F(24),G(24)
  DIMENSION D(36),Q(12),ND(4)
C SET AMUO=PERMEABILITY OF FREE SPACE (IN HENRY.METRE)
  AMUO=1.2566371E-6
  I2=I1-1
  I3=I1-2
  J2=J1-1
  J3=J1-2
  K=I2
C THE DATA IS TESTED FOR SYMMETRY
  IF (NM.EQ.1) GOTO 8
  J5=J3
  JS=0
C IS=NUMBER OF FINITE ELEMENT EQUATIONS TO BE SOLVED

```

```

      IS=I3*J3
      GOTO 9
8 J5=J2
  JS=J5
  IS=I3*J2
C SET VARIOUS CONSTANTS
9 IT=IS-K
  NC=4
  L=0
  L2=-2
C DO LOOPS FOR EVERY QUADRILATRAL AREA OF MESH
  DO 10 J=1,J5
    L2=L2+2
    DO 11 I=1,I3
C SET Z AND R COORDINATES OF CORNER POINTS OF QUADRILATRAL
  F(1)=Z(I+1,J)
  F(2)=Z(I+1,J+1)
  F(3)=Z(I,J+1)
  F(4)=Z(I,J)
  F(5)=F(1)
  F(6)=F(2)
  F(7)=Z(I+2,J+1)
  F(8)=F(2)
  F(9)=F(1)
  F(10)=Z(I+2,J)
  F(11)=F(7)
  F(12)=F(8)
  F(13)=F(3)
  F(14)=F(2)
  F(17)=F(3)
  F(18)=F(2)
  F(20)=F(2)
  F(21)=F(7)
  F(24)=F(2)
  G(1)=R(I+1,J)
  G(2)=R(I+1,J+1)
  G(3)=R(I,J+1)
  G(4)=R(I,J)
  G(5)=G(1)
  G(6)=G(2)
  G(7)=R(I+2,J+1)
  G(8)=G(2)
  G(9)=G(1)
  G(10)=R(I+2,J)
  G(11)=G(7)
  G(12)=G(8)
  G(13)=G(3)
  G(14)=G(2)
  G(17)=G(3)
  G(18)=G(2)
  G(20)=G(2)
  G(21)=G(7)
  G(24)=G(2)
C TEST FOR ASYMMETRY

```

```

IF (J.EQ.J5) GOTO 12
F(15)=Z(I+1,J+2)
F(16)=Z(I,J+2)
F(19)=F(15)
F(22)=Z(I+2,J+2)
F(23)=F(15)
G(15)=R(I+1,J+2)
G(16)=R(I,J+2)
G(19)=G(15)
G(22)=R(I+2,J+2)
G(23)=G(15)
GOTO 13
12 NC=2
13 M1=1
M2=4
M3=7
C INITIALIASATION FOR NUMBER OF RUNS
DO 121 NN=1,NC
121 ND(NN)=0
C SETTING REFERENCE NUMBERS FOR THE RUNS FROM 1 TO 4
IF (I.EQ.I3.AND.J.EQ.J5) GOTO 1211
IF (J.EQ.J5) GOTO 1212
IF (I.EQ.I3) GOTO 1213
ND(1)=1
GOTO 1214
1211 DO 122 NN=1,4
122 ND(NN)=1
GOTO 1214
1212 ND(1)=1
ND(3)=1
GOTO 1214
1213 ND(1)=1
ND(2)=1
1214 N=0
C DO LOOP CALCULATING Z,R AND FINITE ELEMENT COEFFICIENTS
C ACCORDING TO RUN NUMBERS FROM 1 TO 4
DO 14 NN=1,NC
C IF NUMBER OF RUNS IS GREATER THAN 1 THE PROGRAM IS DIRECTED
C TO 140
IF (NN.GT.1) GOTO 140
N3=0
IC=I
JC=J
GOTO 141
140 IF (NN-3) 1402,1403,1404
1402 N3=6
IC=I+1
JC=J
GOTO 141
1403 N3=12
IC=I
JC=J+1
GOTO 141

```

```

1404 N3=18
      IC=I+1
      JC=J+1
C   DO LOOP FOR EACH THREE TRIANGULAR ELEMENTS
141 DO 16 N0=1,3
      N=N+1
      ND1=ND(NN)
      IF (N0.EQ.1) ND1=0
      IF (N0.EQ.3) N3=N3+1
C   SET Z AND R COORDINATES OF VERTICES OF TRIANGULAR
C   ELEMENTS
      N3=N3+1
      Z1=F(N3)
      Z2=F(N3+1)
      Z3=F(N3+2)
      R1=G(N3)
      R2=G(N3+1)
      R3=G(N3+2)
C   THE COEFFICIENTS OF NODAL EQUATIONS REPRESENTING
C   THE VECTOR POTENTIAL OVER EACH ELEMENT ARE FOUND
      B1=R2-R3
      B2=R3-R1
      B3=R1-R2
      T1=Z3-Z2
      T2=Z1-Z3
      T3=Z2-Z1
C   DET=DETERMINANT OF THE FINITE ELEMENTS TRIANGLE
      DET=B1*T2-B2*T1
      R0=(R1+R2+R3)/3.
      X=DET/(3.*R0)
      T1=T1+X
      T2=T2+X
      T3=T3+X
      X=R0/(2.*AMU0*AR(IC,JC)*DET)
      IF (N.EQ.2.OR.N.EQ.5.OR.N.EQ.8.OR.N.EQ.11) GOTO 162
      IF (N.EQ.3.OR.N.EQ.6.OR.N.EQ.9.OR.N.EQ.12) GOTO 163
161 D(M1)=(B2*B1+T2*T1)*X
      D(M1+1)=(B2*B2+T2*T2)*X
      D(M1+2)=(B2*B3+T2*T3)*X
      M1=M1+9
      GOTO 17
162 D(M2)=(B1*B1+T1*T1)*X
      D(M2+1)=(B1*B2+T1*T2)*X
      D(M2+2)=(B1*B3+T1*T3)*X
      M2=M2+9
      GOTO 17
163 D(M3)=(B3*B1+T3*T1)*X
      D(M3+1)=(B3*B2+T3*T2)*X
      D(M3+2)=(B3*B3+T3*T3)*X
      M3=M3+9
17 ANI=ANI+.5*DET*AJ(IC,JC)*FLOAT(ND1)
      Q(N)=AJ(IC,JC)*R0*DET/6.
16 CONTINUE
14 CONTINUE

```

C SET FINITE ELEMENT COEFFICIENTS FOR QUADRILATERAL
C AREA TO OBTAIN NINE-POINT EQUATION FOR EACH NODE

L=L+1
L2=L2+1
P(L,1)=0.
P(L,2)=0.
P(L,I3)=0.
P(L,K)=0.
P(L,I1)=0.
P1=D(6)+D(7)
P2=D(1)+D(8)+D(12)+D(14)
P3=D(15)+D(16)
P4=D(3)+D(5)
P5=D(2)+D(4)+D(9)+D(11)+D(13)+D(18)
P6=D(10)+D(17)
C(L)=Q(1)+Q(2)+Q(3)+Q(4)+Q(5)+Q(6)
Q1=P1*A(L2)
Q2=P2*A(L2+1)
Q3=P3*A(L2+2)
Q4=P4*A(L2+I1)
Q6=P6*A(L2+I1+2)
IF (J.EQ.JS) GOTO 18
P4=P4+D(19)+D(26)
P5=P5+D(20)+D(22)+D(27)+D(29)+D(31)+D(36)
P6=P6+D(30)+D(32)
P7=D(24)+D(25)
P8=D(21)+D(23)+D(28)+D(35)
P9=D(33)+D(34)
C(L)=C(L)+Q(7)+Q(8)+Q(9)+Q(10)+Q(11)+Q(12)
Q7=P7*A(L2+2*I1)
Q8=P8*A(L2+2*I1+1)
Q9=P9*A(L2+2*I1+2)

C EACH NODAL EQUATION IS EXPRESSED IN TERMS OF THE VECTOR
C POTENTIAL AT THE NODE AND THE EIGHT NEIGHBOURING VECTOR
C POTENTIAL VALUES. THE RESULTING MATRIX IS SYMMETRICAL
C ABOUT THE DIAGONAL. HENCE ONLY THE COEFFICIENTS OF THE
C BANDED MATRIX IN THE UPPER TRIANGLE OF THE MATRIX NEED
C TO BE STORED. THE MATRIX EQUATION IS SOLVED BY GAUSSIAN
C ELIMINATION IN ANOTHER SUBROUTINE

18 IF (J.EQ.JS) GOTO 20
IF (J.EQ.J5) GOTO 30
IF (J.NE.1) GOTO 40
IF (I.EQ.1) GOTO 50
IF (I.EQ.I3) GOTO 60
C(L)=C(L)-(Q1+Q2+Q3)
P(L,1)=P5
P(L,2)=P6
P(L,I3)=P7
P(L,K)=P8
P(L,I1)=P9
GOTO 11
50 C(L)=C(L)-(Q1+Q2+Q3+Q4+Q7)
P(L,1)=P5
P(L,2)=P6

```

P(L,K)=P8
P(L,I1)=P9
GOTO 11
60 C(L)=C(L)-(Q1+Q2+Q3+Q6+Q9)
P(L,1)=P5
P(L,I3)=P7
P(L,K)=P8
GOTO 11
40 IF (I.EQ.1) GOTO 401
IF (I.EQ.I3) GOTO 402
P(L,1)=P5
P(L,2)=P6
P(L,I3)=P7
P(L,K)=P8
P(L,I1)=P9
GOTO 11
401 C(L)=C(L)-(Q1+Q4+Q7)
P(L,1)=P5
P(L,2)=P6
P(L,K)=P8
P(L,I1)=P9
GOTO 11
402 C(L)=C(L)-(Q3+Q6+Q9)
P(L,1)=P5
P(L,I3)=P7
P(L,K)=P8
GOTO 11
30 IF (I.EQ.1) GOTO 301
IF (I.EQ.I3) GOTO 302
C(L)=C(L)-(Q7+Q8+Q9)
P(L,1)=P5
P(L,2)=P6
GOTO 11
301 C(L)=C(L)-(Q1+Q4+Q7+Q8+Q9)
P(L,1)=P5
P(L,2)=P6
GOTO 11
302 C(L)=C(L)-(Q3+Q6+Q7+Q8+Q9)
P(L,1)=P5
GOTO 11
20 IF (I.EQ.1) GOTO 201
IF (I.EQ.I3) GOTO 202
P(L,1)=P5
P(L,2)=P6
GOTO 11
201 C(L)=C(L)-(Q1+Q4)
P(L,1)=P5
P(L,2)=P6
GOTO 11
202 C(L)=C(L)-(Q3+Q6)
P(L,1)=P5
11 CONTINUE
10 CONTINUE
RETURN

```

```

C THE END OF THIS SUBROUTINE
  END
C
C SUBROUTINE (PCSAT) FOR DERIVATION OF NODAL EQUATIONS FOR
C AXIAL FLUX DENSITY DISTRIBUTION THROUGHOUT THE MAGNETIC
C CIRCUIT OF SATURATED MAGNETIC LENSES.
C THE NODAL EQUATIONS WHICH ARE NON-LINEAR ARE SOLVED
C BY NEWTON-RAPHSON ITERATION AND THE MATRIX EQUATION
C IS SOLVED BY GAUSSIAN ELIMINATION.
C Z(IM,JM)=Z-COORDINATES OF EVERY MESH POINT
C R(IM,JM)=R-COORDINATES OF EVERY MESH POINT
C I1=NUMBER OF MESH POINTS IN THE RADIAL DIRECTION
C J1=NUMBER OF MESH POINTS IN THE AXIAL DIRECTION
C AMAG=FACTOR FOR DERIVING RELATIVE PERMEABILITY
C AR(IM,JM)=RELATIVE PERMEABILITY AT EVERY
C QUADRILATERAL
C F(24)=FINITE ELEMENT F-COEFFICIENTS FOR EVERY
C QUADRILATERAL
C G(24)=FINITE ELEMENT G-COEFFICIENTS FOR EVERY
C QUADRILATERAL
  SUBROUTINE PCSAT(Z,R,V,AR,AJ,P,A,C,AMAG,I1,J1,IM,JM,IJM,NM,ANI)
  DIMENSION Z(IM,JM),R(IM,JM),C(IJM),P(IJM,IM)
  DIMENSION AR(IM,JM),AJ(IM,JM),A(IJM),V(IM,JM)
  DIMENSION F(24),G(24),VP(24)
  DIMENSION D(36),Q(12),ND(4)
  COMMON TB(100),TM(100),IBM,NSAT
C SET AMU0=PERMEABILITY OF FREE SPACE (IN HENRY/METRE)
  AMU0=1.2566371E-6
C INITIALISE VECTOR POTENTIAL VALUES AT VERTICES OF
C THE TRIANGULAR ELEMENT
C DMU IS THE INCREMENTAL PERMEABILITY
  A1=0.
  A2=0.
  A3=0.
  TMU=1.
  DMU=0.
C I2=NUMBER OF QUADRILATERALS IN THE RADIAL DIRECTION
C J2=NUMBER OF QUADRILATERALS IN THE AXIAL DIRECTION
C I3,J3 ARE USED FOR FINDING NO. OF EQNS. TO BE SOLVED
  I2=I1-1
  I3=I1-2
  J2=J1-1
  J3=J1-2
  K=I2
C THE DATA IS TESTED FOR SYMMETRY
  IF (NM.EQ.1) GOTO 8
  J5=J3
  JS=0
C IS=NUMBER OF FINITE ELEMENT EQNS. TO BE SOLVED
  IS=I3*J3
  GOTO 9
8 J5=J2
  JS=J5
  IS=I3*J2

```

```

9 IT=IS-K
  NC=4
  L=0
  L2=-2
C DO LOOPS FOR EVERY QUADRILATERAL AREA OF MESH
  DO 10 J=1,J5
    L2=L2+2
    DO 11 I=1,I3
C SET Z AND R COORDINATES OF VERTICES AND THE VECTOR
C POTENTIAL VALUES AT EACH POINT OF THE QUADRILATERAL
C I=NUMBER OF RADIAL NODES
C J=NUMBER OF AXIAL NODES
  F(1)=Z(I+1,J)
  F(2)=Z(I+1,J+1)
  F(3)=Z(I,J+1)
  F(4)=Z(I,J)
  F(5)=F(1)
  F(6)=F(2)
  F(7)=Z(I+2,J+1)
  F(8)=F(2)
  F(9)=F(1)
  F(10)=Z(I+2,J)
  F(11)=F(7)
  F(12)=F(8)
  F(13)=F(3)
  F(14)=F(2)
  F(17)=F(3)
  F(18)=F(2)
  F(20)=F(2)
  F(21)=F(7)
  F(24)=F(2)
  G(1)=R(I+1,J)
  G(2)=R(I+1,J+1)
  G(3)=R(I,J+1)
  G(4)=R(I,J)
  G(5)=G(1)
  G(6)=G(2)
  G(7)=R(I+2,J+1)
  G(8)=G(2)
  G(9)=G(1)
  G(10)=R(I+2,J)
  G(11)=G(7)
  G(12)=G(8)
  G(13)=G(3)
  G(14)=G(2)
  G(17)=G(3)
  G(18)=G(2)
  G(20)=G(2)
  G(21)=G(7)
  G(24)=G(2)
  VP(1)=V(I+1,J)
  VP(2)=V(I+1,J+1)
  VP(3)=V(I,J+1)
  VP(4)=V(I,J)

```

```

VP(5)=VP(1)
VP(6)=VP(2)
VP(7)=V(I+2,J+1)
VP(8)=VP(2)
VP(9)=VP(1)
VP(10)=V(I+2,J)
VP(11)=VP(7)
VP(12)=VP(8)
VP(13)=VP(3)
VP(14)=VP(2)
VP(17)=VP(3)
VP(18)=VP(2)
VP(20)=VP(2)
VP(21)=VP(7)
VP(24)=VP(2)
IF (J.EQ.J5) GOTO 12
F(15)=Z(I+1,J+2)
F(16)=Z(I,J+2)
F(19)=F(15)
F(22)=Z(I+2,J+2)
F(23)=F(15)
G(15)=R(I+1,J+2)
G(16)=R(I,J+2)
G(19)=G(15)
G(22)=R(I+2,J+2)
G(23)=G(15)
VP(15)=V(I+1,J+2)
VP(16)=V(I,J+2)
VP(19)=VP(15)
VP(22)=V(I+2,J+2)
VP(23)=VP(15)
GOTO 13
12 NC=2
13 M1=1
M2=4
M3=7
DO 121 NN=1,NC
121 ND(NN)=0
IF (I.EQ.I3.AND.J.EQ.J5) GOTO 1211
IF (J.EQ.J5) GOTO 1212
IF (I.EQ.I3) GOTO 1213
ND(1)=1
GOTO 1214
C SETTING REFERENCE NUMBERS FOR THE RUNS FROM 1 TO 4
1211 DO 122 NN=1,4
122 ND(NN)=1
GOTO 1214
1212 ND(1)=1
ND(3)=1
GOTO 1214
1213 ND(1)=1
ND(2)=1
1214 N=0
C DO LOOP CALCULATING Z,R AND FINITE ELEMENT COEFFICIENTS

```

```

C   ACCORDING TO RUN NUMBERS FROM 1 TO 4
    DO 14 NN=1,NC
    IF (NN.GT.1) GOTO 140
    N3=0
    IC=I
    JC=J
    GOTO 141
140 IF (NN-3) 1402,1403,1404
1402 N3=6
    IC=I+1
    JC=J
    GOTO 141
1403 N3=12
    IC=I
    JC=J+1
    GOTO 141
1404 N3=18
    IC=I+1
    JC=J+1
C   DO LOOP FOR EACH THREE TRIANGULAR ELEMENTS
141 DO 16 N0=1,3
    N=N+1
    ND1=ND(NN)
    IF (N0.EQ.1) ND1=0
    IF (N0.EQ.3) N3=N3+1
    N3=N3+1
C   SET Z AND R COORDINATES OF VERTICES OF TRIANGULAR
C   ELEMENTS
    Z1=F(N3)
    Z2=F(N3+1)
    Z3=F(N3+2)
    R1=G(N3)
    R2=G(N3+1)
    R3=G(N3+2)
    V1=VP(N3)
    V2=VP(N3+1)
    V3=VP(N3+2)
    B1=R2-R3
    B2=R3-R1
    B3=R1-R2
    T1=Z3-Z2
    T2=Z1-Z3
    T3=Z2-Z1
C   DET=DETERMINANT OF THE FINITE ELEMENTS TRIANGLE=2*AREA
    DET=B1*T2-B2*T1
C   R0=VALUE OF R AT THE CENTROID
    R0=(R1+R2+R3)/3.
    X=1./(3.*R0)
    B1=-B1/DET
    B2=-B2/DET
    B3=-B3/DET
    T1=T1/DET+X
    T2=T2/DET+X
    T3=T3/DET+X

```

```

C THE FLUX DENSITY AT EACH TRIANGLE IS CALCULATED
C BR=RADIAL COMPONENT OF MAGNETIC FLUX DENSITY
C BZ=AXIAL COMPONENT OF MAGNETIC FLUX DENSITY
C B=MAGNETIG FLUX DENSITY
  BR=B1*V1+B2*V2+B3*V3
  BZ=T1*V1+T2*V2+T3*V3
  B=SQRT(BR*BR+BZ*BZ)
  A1=B1*BR+T1*BZ
  A2=B2*BR+T2*BZ
  A3=B3*BR+T3*BZ
C TMU=THE RELATIVE PERMEABILITY OF FREE SPACE
C DMU=THE INCREMENTAL PERMEABILITY
  TMU=1.
  DMU=0.
C IF THE FINITE ELEMENT TRIANGLE IS IN THE FREE SPACE
C THE PROGRAM IS DIRECTED TO 15
  IF (AR(IC,JC).EQ.1.) GOTO 15
C IF THE FINITE ELEMENT TRIANGLE IS PART OF MAGNETIC
C CIRCUIT THE MAGNETISATION CURVE OF THE MAGNETIC MATERIAL
C MUST BE ACCOUNTED (ATABLE OF MR AND B MUST BE CONSIDERED)
  IF (NSAT.EQ.1) GOTO 70
  TMU=AR(IC,JC)
  GOTO 15
C THE PROGRAM IS DIRECTED ACORDING TO THE OCCURANCE OF
C THE CALCULATED VALUE OF B WITH RESPECT TO THE GIVEN
C VALUES OF B,MR IN THE TABLE
70 IB=0
160 IB=IB+1
C IF THE CALCULATED B IS LARGER THAN THE MAXMIUM B
C GIVEN IN THE TABLE THE PROGRAM IS DIRECTED TO
C 80 TO CALCULATE DMU
  IF (IB.GE.IBM.OR.B.GT.TB(IBM)) GOTO 80
C IF B CALCULATED VALUE LIES IN THE LINEAR PART OF
C THE MAGNETIG CURVE THE PROGRAM IS DIRECTED TO CALCULATE DMU
  IF (B.LE.TB(IB+1).AND.B.GE.TB(IB)) GOTO 1602
C THE PROGRAM IS DIRECTED TO RECOGNISE THE FIRST AND
C FURTHER NON LINEAR PARTS OF THE MAGNETIG CURVE
  GOTO 160
1602 ZM=TB(IB+1)-B
  ZL=B-TB(IB)
  TMU=TM(IB)+(TM(IB+1)-TM(IB))/(ZM+ZL)*ZL
C IF B CALCULATED=0. THE PROGRAM IS DIRECTED TO 15
  IF (B.EQ.0.) GOTO 15
  DMU=(TM(IB)-TM(IB+1))/(TB(IB)-TB(IB+1))
  DMU=DMU/(B*TMU)
  GOTO 15
80 TMU=B/(B-AMAG)
  IF (B.EQ.0.) GOTO 15
  DMU=(1.0001*B/(1.0001*B-AMAG)-TMU)/B*10000.
  DMU=DMU/(B*TMU)
15 X=R0*DET/(TMU*AMU0)
  AJD=AJ(IC,JC)/3.*TMU*AMU0
C SETTING NINE POINT NON LINEAR EQUATION TO BE SOLVED
C WITH NEWTON ITERATION

```

```

IF (N.EQ.2.OR.N.EQ.5.OR.N.EQ.8.OR.N.EQ.11) GOTO 162
IF (N.EQ.3.OR.N.EQ.6.OR.N.EQ.9.OR.N.EQ.12) GOTO 163
161 D(M1)=(B2*B1+T2*T1-A2*A1*DMU)*X
D(M1+1)=(B2*B2+T2*T2-A2*A2*DMU)*X
D(M1+2)=(B2*B3+T2*T3-A2*A3*DMU)*X
Q(N)=(AJD-A2)*X
M1=M1+9
GOTO 17
162 D(M2)=(B1*B1+T1*T1-A1*A1*DMU)*X
D(M2+1)=(B1*B2+T1*T2-A1*A2*DMU)*X
D(M2+2)=(B1*B3+T1*T3-A1*A3*DMU)*X
Q(N)=(AJD-A1)*X
M2=M2+9
GOTO 17
163 D(M3)=(B3*B1+T3*T1-A3*A1*DMU)*X
D(M3+1)=(B3*B2+T3*T2-A3*A2*DMU)*X
D(M3+2)=(B3*B3+T3*T3-A3*A3*DMU)*X
Q(N)=(AJD-A3)*X
M3=M3+9
17 ANI=ANI+.5*DET*AJ(IC,JC)*FLOAT(ND1)
16 CONTINUE
14 CONTINUE
L=L+1
L2=L2+1
C SETTING THE VECTOR POTENTIAL IN THE AXIS AND THE BOUDARIES
C TO 0.
P(L,1)=0.
P(L,2)=0.
P(L,I3)=0.
P(L,K)=0.
P(L,I1)=0.
C STORING THE NON ZERO VECTOR POTENTIALS
P1=D(6)+D(7)
P2=D(1)+D(8)+D(12)+D(14)
P3=D(15)+D(16)
P4=D(3)+D(5)
P5=D(2)+D(4)+D(9)+D(11)+D(13)+D(18)
P6=D(10)+D(17)
C(L)=Q(1)+Q(2)+Q(3)+Q(4)+Q(5)+Q(6)
Q1=P1*A(L2)
Q2=P2*A(L2+1)
Q3=P3*A(L2+2)
Q4=P4*A(L2+I1)
Q6=P6*A(L2+I1+2)
IF (J.EQ.JS) GOTO 18
P4=P4+D(19)+D(26)
P5=P5+D(20)+D(22)+D(27)+D(29)+D(31)+D(36)
P6=P6+D(30)+D(32)
P7=D(24)+D(25)
P8=D(21)+D(23)+D(28)+D(35)
P9=D(33)+D(34)
C(L)=C(L)+Q(7)+Q(8)+Q(9)+Q(10)+Q(11)+Q(12)
Q7=P7*A(L2+2*I1)
Q8=P8*A(L2+2*I1+1)

```

```

Q9=P9*A(L2+2*I1+2)
18 IF (J.EQ.J5) GOTO 20
   IF (J.EQ.J5) GOTO 30
   IF (J.NE.1) GOTO 40
   IF (I.EQ.1) GOTO 50
   IF (I.EQ.I3) GOTO 60
   C(L)=C(L)-(Q1+Q2+Q3)
   P(L,1)=P5
   P(L,2)=P6
   P(L,I3)=P7
   P(L,K)=P8
   P(L,I1)=P9
   GOTO 11
50 C(L)=C(L)-(Q1+Q2+Q3+Q4+Q7)
   P(L,1)=P5
   P(L,2)=P6
   P(L,K)=P8
   P(L,I1)=P9
   GOTO 11
60 C(L)=C(L)-(Q1+Q2+Q3+Q6+Q9)
   P(L,1)=P5
   P(L,I3)=P7
   P(L,K)=P8
   GOTO 11
40 IF (I.EQ.1) GOTO 401
   IF (I.EQ.I3) GOTO 402
   P(L,1)=P5
   P(L,2)=P6
   P(L,I3)=P7
   P(L,K)=P8
   P(L,I1)=P9
   GOTO 11
401 C(L)=C(L)-(Q1+Q4+Q7)
   P(L,1)=P5
   P(L,2)=P6
   P(L,K)=P8
   P(L,I1)=P9
   GOTO 11
402 C(L)=C(L)-(Q3+Q6+Q9)
   P(L,1)=P5
   P(L,I3)=P7
   P(L,K)=P8
   GOTO 11
30 IF (I.EQ.1) GOTO 301
   IF (I.EQ.I3) GOTO 302
   C(L)=C(L)-(Q7+Q8+Q9)
   P(L,1)=P5
   P(L,2)=P6
   GOTO 11
301 C(L)=C(L)-(Q1+Q4+Q7+Q8+Q9)
   P(L,1)=P5
   P(L,2)=P6
   GOTO 11
302 C(L)=C(L)-(Q3+Q6+Q7+Q8+Q9)

```

```

    P(L,1)=P5
    GOTO 11
20 IF (I.EQ.1) GOTO 201
   IF (I.EQ.I3) GOTO 202
   P(L,1)=P5
   P(L,2)=P6
   GOTO 11
201 C(L)=C(L)-(Q1+Q4)
    P(L,1)=P5
    P(L,2)=P6
    GOTO 11
202 C(L)=C(L)-(Q3+Q6)
    P(L,1)=P5
11 CONTINUE
10 CONTINUE
   RETURN
C   THE END OF PCSAT SUBROUTINE WHICH IS DEALING WITH SATURATION
C   CASE
   END
C
C   SUBROUTINE (EQNS) FOR EQUATION SOLVING BY GAUSSIAN ELIMINATION
C   AND BACKWARD SUBSTITUTION
C   I1=NUMBER OF RADIAL NODES IN THE FINITE ELEMENT GRID
C   IS=NUMBER OF EQUATIONS TO BE SOLVED
C   C=ARRAY WHICH HOLDS THE RIGHTHAND SIDE COEFFICIENTS OF
C   THE EQUATIONS
C   P=ARRAY WHICH HOLDS THE LEFTHAND SIDE COEFFICIENTS OF
C   THE MATRIX EQUATION
   SUBROUTINE EQNS (C,IT,IS,P,I1,IM,IJM)
   DIMENSION C(IJM),P(IJM,IM)
C   SET VARIOUS CONSTANTS
   NC=I1
   IS1=IS-1
C   STEP 1-GAUSSIAN ELIMINATION
C   DO LOOP FOR EACH ROW OF BAND MATRIX
   DO 70 NT=1,IS1
     IF (NT.GT.IT) NC=IS-NT+1
C   DO LOOP FOR EACH COLUMN OF SUB-MATRIX
     DO 71 I=2,NC
       IC=NT+I-1
       RC=P(NT,I)/P(NT,1)
C   RESET APPROPRIATE ELEMENTS OF RIGHT-HAND SIDE
       C(IC)=C(IC)-RC*C(NT)
       II11=I1-I+1
C   DO LOOP FOR EACH ROW OF SUB-MATRIX
     DO 72 J=1,II11
C   RESET APPROPRIATE ELEMENT OF BAND MATRIX
       P(IC,J)=P(IC,J)-RC*P(NT,I+J-1)
72 CONTINUE
71 CONTINUE
70 CONTINUE
C   STEP 2-BACKWARD SUBSTITUTION
C   BACKWARD SUBSTITUTION FOR ROW IS
   C(IS)=C(IS)/P(IS,1)

```

```

C DO LOOP FOR BACKWARD SUBSTITUTION FOR EACH ROW OF MATRIX
  IS1=IS-1
  DO 80 I=1,IS1
    II=IS-I
    NC=I1
    IF (II.GT.IT) NC=IS-II+1
    S=0.
C DO LOOP FOR SUMMING PRODUCTS OF (APPROPRIATE ELEMENTS OF
C C) * (APPROPRIATE ELEMENTS OF P)
  DO 81 J=2,NC
    JJ=NC+2-J
    S=S+P(II,JJ)*C(II+JJ-1)
81 CONTINUE
C RESET APPROPRIATE ELEMENT OF C TO STORE THE SOLUTION
  C(II)=(C(II)-S)/P(II,1)
80 CONTINUE
  RETURN
C END OF SUBROUTINE EQNS
  END

C
C SUBROUTINE (VPLUSDV) TO SET ALIMIT TO THE CYCLE OF ITERATION
C PROCESS THIS LIMIT IS DETERMINED WHEN THE VALUE OF THE
C DIFFERENCE IN VECTOR POTENTIAL BETWEEN TWO CONSECUTIVE
C ITERATIONS IS WITHIN ACERTAIN ACCURACY LIMIT
C
  SUBROUTINE VPLUSDV (V,C,I2,IM,JM,IJM,J5,X1,Y1,NTEST)
  DIMENSION V(IM,JM),C(IJM)
C NTEST IS INITALIZED TO ZERO
  NTEST=0
C X1=THE ABSOLUTE VALUE OF THE MAXIMUM VECTOR POTENTIAL
C IN ANY MATERIAL AFTER THE NTH NEWTON'S ITERATION.
  X1=0.
C Y1=THE MAXIMUM CHANGE IN VECTOR POTENTIAL
  Y1=0.
  J6=J5+1
  L=0
  DO 1 J=2,J6
    DO 2 I=2,I2
      L=L+1
      IF (ABS(C(L)).GT.Y1) Y1=ABS(C(L))
      V(I,J)=V(I,J)+C(L)
      IF (ABS(V(I,J)).GT.X1) X1=ABS(V(I,J))
2 CONTINUE
1 CONTINUE
C ERR=THE LARGEST PERMISSIBLE CHANGE IN ANY MATERIAL
  ERR=.001*X1
C NTEST=THE LIMIT WHERE THE ITERATION PROCESS IS REACHED
C I.E NTEST=1 WHEN Y1 IS LESS THAN ERR.
  IF (Y1.LE.ERR) NTEST=1
  RETURN
C THE END OF SUBROUTINE VPLUSDV
  END

C
C SUBROUTINE (BVALUES) FOR CALCULATING THE FLUX DENSITY AT POINTS

```

```

C THROUGHOUT THE MAGNETIG CIRCUIT AND FOR WRITING OUT THE
C PEAK FLUX DENSITY.
  SUBROUTINE BVALUES(Z,R,V,AMUR,AMAG,I1,J1,IM,JM,NSAT,NBFE,IR)
  DIMENSION Z(IM,JM),R(IM,JM),V(IM,JM),AMUR(IM,JM)
  COMMON TB(100),TM(100),IBM
C INITIALIZE THE VALUE OF RELATIVE PERMEABILITY IN FREE
C SPACE
  AMU0=1.2566371E-6
C INITIALIZE THE VALUE AND POSITION OF THE PEAK FLUX DENSITY
C IN THE MAGNETIG CIRCUIT
  BMAX=0.
  ZMAX=0.
  RMAX=0.
C IF NBFE (FLUX DENSITY IN MAGNETIC CIRCUIT) IS REQUIRED AS
C OUTPUT,THE PROGRAM IS DIRECTED TO WRITE HEADING
  IF (NBFE.EQ.1) WRITE (2,10)
10 FORMAT (/1X,'FLUX DENSITY VALUES IN MAGNETIC CIRCUIT'/)
C DO LOOP FOR EVERY QUADRILATERAL AREA OF MESH
  I2=I1-1
  J2=J1-1
C DO LOOPS FOR EVERY QUADRILATERAL AREA OF MESH
  DO 1 J=1,J2
  DO 1 I=1,I2
C TEST WHETHER THE QUADRILATERAL IS IN FREE SPACE OR IN THE
C MAGNETIG CIRCUIT
  IF (AMUR(I,J).EQ.1) GOTO 1
C SET Z AND R COORDINATES AND VECTOR POTENTIAL VALUES AT
C CORNER POINTS OF QUADRILATERAL
  Z1=Z(I,J)
  Z2=Z(I+1,J)
  Z3=Z(I+1,J+1)
  Z4=Z(I,J+1)
  R1=R(I,J)
  R2=R(I+1,J)
  R3=R(I+1,J+1)
  R4=R(I,J+1)
  V1=V(I,J)
  V2=V(I+1,J)
  V3=V(I+1,J+1)
  V4=V(I,J+1)
C CALCULATE COORDINATES OF CENTRE POINT OF QUADRILATERAL
  ZC=(Z1+Z2+Z3+Z4)*.25
  RC=(R1+R2+R3+R4)*.25
C CALCULATE FLUX DENSITY COMPONENT BZ AND BR AT CENTRE POINT
C OF QUADRILATERAL
  X1=(Z1-Z2)*R1*R2
  X2=(Z1-Z3)*R1*R3
  X3=(Z1-Z4)*R1*R4
  X4=(Z2-Z3)*R2*R3
  X5=(Z2-Z4)*R2*R4
  X6=(Z3-Z4)*R3*R4
  Y1=(R1-R2)*Z1*Z2
  Y2=(R1-R3)*Z1*Z3
  Y3=(R1-R4)*Z1*Z4

```

```

Y4=(R2-R3)*Z2*Z3
Y5=(R2-R4)*Z2*Z4
Y6=(R3-R4)*Z3*Z4
P1=X4-X5+X6
P2=-X2+X3-X6
P3=X1-X3+X5
P4=-X1+X2-X4
Q1=R1*Z2-Z1*R2
Q2=R1*Z3-Z1*R3
Q3=R1*Z4-Z1*R4
Q4=R2*Z3-Z2*R3
Q5=R2*Z4-Z2*R4
Q6=R3*Z4-Z3*R4
DET=Z1*P1+Z2*P2+Z3*P3+Z4*P4
F=V1*(-Z4*X4+Z3*X5-Z2*X6)+V2*(Z4*X2-Z3*X3+Z1*X6)
F=F+V3*(-Z4*X1+Z2*X3-Z1*X5)+V4*(Z3*X1-Z2*X2+Z1*X4)
G=V1*P1+V2*P2+V3*P3+V4*P4
H=V1*(-Y4+Y5-Y6)+V2*(Y2-Y3+Y6)+V3*(-Y1+Y3-Y5)+V4*(Y1-Y2+Y4)
AI=V1*(Q4-Q5+Q6)+V2*(-Q2+Q3-Q6)+V3*(Q1-Q3+Q5)+V4*(-Q1+Q2-Q4)
F=F/DET
G=G/DET
H=H/DET
AI=AI/DET
VC=F+G*ZC+H*RC+AI*ZC*RC
BZ=H+AI*ZC+VC/RC
BR=-G-AI*RC
C  CALCULATE FLUX DENSITY B AT CENTRE POINT OF QUADRILATERAL
    B=SQRT(BZ*BZ+BR*BR)
C  CONVERT COORDINATES OF MAXIMUM FLUX DENSITY POSITION FROM
C  METRES TO MM
    ZC=ZC*1000.
    RC=RC*1000.
C  WRITE LOCATION AND VALUES OF AXIAL (BZ) AND RADIAL (BR)
C  COMPONENTS OF THE FLUX DENSITY AND THE RESULTANT FLUX
C  DENSITY THROUGHOUT THE MAGNETIC CIRCUIT
    IF (NSAT.EQ.0.OR.IR.GT.1) GOTO 7
    IB=0
4  IB=IB+1
C  IF THE COPUTED FLUX DENSITY IS GREATER THAN THE FINAL
C  VALUE PRESENT IN THE B,MUR TABLE THE PROGRAM IS DIRECTED
C  ACCORDINGLY
    IF (IB.GE.IBM.OR.B.GT.TB(IBM)) GOTO 5
C  IF THE COMPUTED FLUX DENSITY IS AT THE LINEAR PART OF
C  THE MAGNETIC CURVE (B,MUR) TABLE THE PROGRAM IS DIRECTED
C  ACCORDING TO THAT
    IF (B.LE.TB(IBM+1).AND.B.GE.TB(IBM)) GOTO 6
    GOTO 4
6  ZM=TB(IBM+1)-B
    ZL=B-TB(IBM)
    AMUR(I,J)=TM(IBM)+(TM(IBM+1)-TM(IBM))/(ZM+ZL)*ZL
    GOTO 7
5  AMUR(I,J)=B/(B-AMAG)
C  TEST IF MAXIMUM FLUX DENSITY HAS BEEN REACHED
7  IF (B.LT.BMAX) GOTO 11

```

```

      BMAX=B
      ZMAX=ZC
      RMAX=RC
C   IF NBF=1 IN THE DATA INPUT THE PROGRAM IS DIRECTED
C   TO WRITE THE HEADINGS (I,J,ZC,RC,BZ,BR,B)ACORDING
C   TO THE REQUIRED FORMAT
11  IF (NBF.EQ.1) WRITE(2,8) I,J,ZC,RC,BZ,BR,B,AMUR(I,J)
      8 FORMAT (1X,2I5,2F15.3,4F15.6)
      1 CONTINUE
C   WRITE THE VALUES AND POSITION OF MAXIMUM FLUX DENSITY
C   IN THE MAGNETIG CIRCUIT ACORDING TO THE REQUIRED FORMAT
      WRITE(2,3)ZMAX,RMAX,BMAX
      3 FORMAT(1X,'MAXIMAM FLUX DENSITY IN MAGNETIC CIRCUIT'//
+ 1X,2F10.5,F15.6,'(TESLA)')
      RETURN
C   THE END OF SUBROUTINE BVALUES
      END

C
C   SUBROUTINE (TRZRMU) TO TRANSFER THE CORECTED RELATIVE
C   PERMEABILITY WHICH HAVE BEEN CALCULATED IN SUBROUTINE
C   PCSAT FOR THE MESH NODES INTO THE Z ,R COORDINATES
      SUBROUTINE TRZRMU (Z,AMUR,ZR1,TMUR,I1,J1,IM,JM)
      DIMENSION Z(IM,JM),AMUR(IM,JM),ZR1(IM,JM),TMUR(IM,JM)
      I2=I1-1
      J2=J1-1
      DO 2 J=1,J1
      DO 2 I=1,I1
      2 ZR1(I,J)=Z(I,J)
      DO 4 J=1,J2
      DO 4 I=1,I2
      4 TMUR(I,J)=AMUR(I,J)
      RETURN
C   END OF SUBROUTINE TRZMU
      END

C
C   SUBROUTINE (SETMUR) FOR SETTING THE RELATIVE PERMEABILITY
C   AFTER CORECTING ACORDING TO THE GIVEN VALUES IN THE B,MUR
C   TABLE WHICH IS GIVEN WITH THE DATA INPUT
C   AND SETTING THE POSITION OF THE MAGNETIC MATERIAL
      SUBROUTINE SETMUR (Z,AMUR,ZR1,TMUR,I2,J2,IM,JM)
      DIMENSION Z(IM,JM),AMUR(IM,JM),ZR1(IM,JM),TMUR(IM,JM)
      II=1
      JJ=1
      I=II
      J=JJ
      6 IF (AMUR(II,JJ).EQ.1.) GOTO 2
      Z1=Z(II,JJ)
      10 X1=ZR1(I,J)
      X2=ZR1(I,J+1)
      IF (Z1.GE.X1.AND.Z1.LE.X2) GOTO 8
      12 J=J+1
      GOTO 10
      8 IF (TMUR(I,J).EQ.1.) GOTO 12
      AMUR(II,JJ)=TMUR(I,J)

```

```

2 JJ=JJ+1
  IF (JJ.GT.J2) GOTO 4
  GOTO 6
4 II=II+1
  I=II
  IF (II.GT.I2) RETURN
  JJ=1
  J=JJ
  GOTO 6
C END OF SUBROUTINE SETMUR
  END

C
C SUBROUTINE (FLUX) FOR CONVERTING THE VALUES OF VECTOR POTENTIAL
C AT EACH MESH POINT TO THE CORRESPONDING MAGNETIC FLUX
C VALUE
C V(I,J)=ARRAY WHICH HOLDS VALUES OF THE VECTOR POTENTIAL
C AT ENTRY TO THE ROUTINE AND WHICH HOLDS THE MAGNETIC FLUX
C VALUE AT EACH MESH POINT ON RETURN TO THE MAIN PROGRAM
  SUBROUTINE FLUX (V,R,I1,J1,IM,JM)
  DIMENSION V(IM,JM),R(IM,JM)
C SET VALUE 2.*PYE
  TPI=6.28318531
C CONVERT EACH ELEMENT OF V(IM,JM) FROM VECTOR POTENTIAL
C TO MAGNETIC FLUX VALUE AT EACH MESH POINT
  DO 2 J=1,J1
  DO 2 I=1,I1
  V(I,J)=TPI*R(I,J)*V(I,J)
  2 CONTINUE
C WRITE HEADING FOR THE FLUX VALUES AT EACH MESH POINT
  WRITE (2,5)
  5 FORMAT (/1X,'FLUX VALUES AT EACH MESH POINT'/)
C J,JF,JS ARE MESH POINT NUMBERS IN THE AXIAL DIRECTION
  JS=1
  JD=4
20 JF=JS+JD
  WRITE (2,4) (J,J=JS,JF)
  4 FORMAT (1X,5X,5I15)
C DO LOOP FOR WRITING MESH POINT NUMBERS IN THE RADIAL
C DIRECTION AND THE FLUX VALUES AT EACH MESH
C I=THE MESH POINT NUMBER IN THE RADIAL DIRECTION
  DO 6 I=1,I1
  WRITE (2,8) I,(V(I,J),J=JS,JF)
  8 FORMAT (1X,I5,5E15.5)
  6 CONTINUE
  WRITE (2,10)
10 FORMAT (1X)
C TEST FOR END OF SET OF VALUES
  IF (JF.EQ.J1) GOTO 12
  JS=JF+1
  IF ((JS+JD).GT.J1) JD=J1-JS
  GOTO 20
C LEAVE BLANK LINE
12 WRITE (2,10)
  RETURN
  END

```

APPENDIX 5

PROGRAM AMAG

C PROGRAM AMAG
SAUF77.E

C
C FINITE ELEMENT PROGRAM FOR COMPUTING VECTOR POTENTIAL AND AXIAL
C FLUX DENSITY DISTRIBUTION THROUGHOUT THE MAGNETIC CIRCUIT OF
C UNSATURATED AND SATURATED MAGNETIC LENSES.

C THE PRINCIPAL VARIABLES ARE DEFINED AS FOLLOWS:

C U=VECTOR POTENTIAL AT THE MESH POINTS INCLUDING THE BOUNDARY
C MESH POINTS U(IRZ)

C IRZ=TOTAL NUMBER OF POINTS IN THE MESH INCLUDING THE BOUNDARY
C POINTS (IRZ=I1*J1)

C I1,J1=ARE NUMBER OF MESH POINTS IN THE MESH IN RADIAL AND
C AXIAL DIRECTION RESPECTIVELY (I1=IR(NR) J1=IZ(NZ))

C B,P,P1,P2,P3,P4 -ARE RIGHT HAND SIDE AND THE COEFFICIENTS OF
C THE SYSTEM OF LINEAR EQUATIONS (B(IS),P(IS),P1(IS),P2(IS),
C P3(IS),P4(IS) WHERE (IS) IS THE TOTAL NUMBER OF POINTS WITH
C UNKNOWN POTENTIAL ,(IS=I2*J2)

C I2,J2 - NUMBER OF MESH POINTS WITH UNKNOWN POTENTIAL IN RADIAL

C AND AXIAL DIRECTION ,RESPECTIVELY (I2=I1-2 , J2=J1-2+ISYM)

C R,Z - R AND Z COORDINATES OF MESH POINTS , MAXIMUM OF 6500
C MESH POINTS ALLOWED

C OZ(J1) Z-COORDINATES OF THE AXIAL MESH POINTS

C BM,H - FLUX DENSITY IN TESLA AND THE CORRESPONDING FIELD

C INTENSITY IN A/M ON THE MAGNETIZATION CURVES,MAXIMUM OF TWO

C CURVES EACH OF 20 VALUES FOR BM,H CAN BE USED

C PSI - VECTOR WHERE EITHER FLUX IS STORED OR USED AS AUXILIARY VECTOR
C PSI(IRZ)

C D,D1,D2,D3,D4 - COEFFICIENTS OF THE APPROXIMATELY DECOMPOSED
C MATRIX ,DIMENSION IS

C MAT(IRZ) - VECTOR STORING THE MATERIALS OF THE SMALL QUADRILATERALS

C
C
C
C COMPUTATION OF VECTOR POTENTIAL IN ROTATIONALLY SYMMETRIC ELECTRON LENSES
C BY FINITE ELEMENT METHOD AS INTRODUCED BY E. MUNRO
C AUTHOR: B. LENCOVA, INST. SCI. INSTRUM., BRNO, CZECHOSLOVAKIA

C IMPLICIT REAL*12 (A-H,O-Z)

C INTEGER INFORM(20),MAT(6500),IBH(2)

C DIMENSION U(6500),B(6000),P(6000),P1(6000),P2(6000),P3(6000),

C * P4(6000),R(6500),Z(6500),OZ(120),BM(20,2),H(20,2),

C * X(6000),PSI(6500),Q(6000),Y(6001),RR(6000),

C * S(6000),D(6000),D1(6000),D2(6000),D3(6000),D4(6000)

C
C TWO DIFFERENT MAGNETIZATION CURVES DEFINING THE MAGNETIC MATERIAL
C CAN BE USED THE FOLLOWING LINES GIVE SOFT IRON MAGNETIZATION CURVE
C AND PERMENDUR THE FOLLOWING TABLES ARE OF STANDARD SOFT IRON AND
C PERMENDUR

C EACH TABLE HAVE MAXIMUM OF 20 VALUES FOR EACH BM AND H
C COMMON

C */BLDAT/IM,IMI,ISYM,IH(2),MM(40),NM(40),MI(20),NP,ICURR,CURR(10)

C */BLCOOR/NZ,NR,IZ(20),IR(20),CZ(400),CR(400)

```

*/BLU/U /BLARZ/R,Z,PSI /BLCOEF/B,P,P1,P2,P3,P4
*/BLAUX1/D,D1,D2,D3,D4 /BLAUX2/Q,RR,S,X,Y
*/BPARAM/I2,J2,IS,I1,J1,IRZ

```

```

C
C TWO DIFFERENT MAGNETISATION CURVES CAN BE USED BY THE PROGRAM
C EACH WITH MAXIMUM OF 20 POINTS ,THESE POINTS REPRESENTS THE
C FIELD INTENSITY IN A/M ,AND THE FLUX DENSITY IN TESLA
C THE FOLLOWING TABLE CONTAIN STANDARD MAGNETISATION CURVES OF
C BOTH SOFT IRON ,AND PERMENDUR .

```

```

DATA MAPMAT,MAPPSI,LISTIR,LISTFD,NIT,TOL/0,0,0,0,150,1D-9/,
* LETZ,LETR/1HZ,1HR/,PI/3.14159265358979D0/,IBH/20,20/,
* BM/1.09D0,1.17D0,1.22D0,1.26D0,1.29D0,1.345D0,1.385D0,1.455D0,
* 1.49D0,1.525D0,1.555D0,1.58D0,1.6D0,1.63D0,1.655D0,1.75D0,
* 1.83D0,1.9D0,1.955D0,1.99D0,1D0,1.13D0,1.21D0,1.345D0,1.45D0,
* 1.545D0,1.63D0,1.695D0,1.755D0,1.805D0,1.87D0,1.92D0,2D0,
* 2.065D0,2.125D0,2.19D0,2.25D0,2.3D0,2.39D0,2.48D0/,
* H/35D1,4D2,45D1,5D2,55D1,65D1,75D1,1D3,12D2,15D2,2D3,25D2,3D3,
* 4D3,5D3,1D4,15D3,2D4,25D3,3D4,6D2,75D1,105D1,16D2,215D1,27D2,
* 32D2,36D2,4D3,44D2,5D3,55D2,65D2,75D2,85D2,1D4,12D3,14D3,2D4,3D4/

```

```

C THE PROGRAM WILL CALL DIFFERENT SUBROUTINES
C CALL OF NOUFLO=ICL COMMAND TO PREVENT UNDERFLOW IN AICCG!
C CALL NOUFLO

```

```

C INPUT OF DATA
C WRITE(6,104)
C CALL AINPUT(INFORM,IPRINT,IDISC,MAPMAT,MAPPSI,LISTIR,LISTFD,
* JMIN,JMAX,IMIN,IMAX,LETZ,LETR,PI,BM,H,IBH)

```

```

C COMPUTATION OF COORDINATES, MAPPING OF MATERIALS
C I=NR*NZ
C CALL AMESH(IRZ,NZ,NR,IZ,IR,I,CZ,CR,R,Z)
C I=2*IM
C CALL AMATER(IRZ,MAPMAT,IM,I,I1,J1,MM,NM,MI,MAT)
C IF(IPRINT.LT.2)GOTO 1
C WRITE(6,105)LETZ
C CALL APRINT(Z,I1,J1,-1,IRZ)
C WRITE(6,105)LETR
C CALL APRINT(R,I1,J1,-1,IRZ)

```

```

C
1 WRITE(6,110)CURR(1)
MULVEY=0
DO 2 I=1,J1
IE=I*I1
IF(I.GT.1.AND.(MAT(IE).EQ.1.OR.MAT(IE).EQ.2))MULVEY=1
2 OZ(I)=Z(IE)
DO 3 I=1,IRZ
3 U(I)=0
ISTEP=0
GOTO 4

```

```

C COMPUTATION OF AN APPROXIMATION ISTEP (ISTEP=0 FOR LINEAR APPROX.)
C 5 WRITE(6,113)ISTEP
4 CALL ACOEF(ISTEP,MAT,AUX,PI,AREA,BM,H,B,P,P1,P2,P3,P4,R,Z,U)
IF(ISTEP.EQ.0)WRITE(6,117)AREA

```

```

IF(ICURR.GT.0)WRITE(6,108)AUX
C
C SOLUTION OF THE MATRIX EQUATION BY ICCG METHOD
IE=0
I=IS+1
CALL AICCG(NIT,IE,I,I2,IS,TOL,
* P,P1,P2,P3,P4,B,D,D1,D2,D3,D4,X,Q,RR,S,Y)
IF((IE.EQ.0).OR.(IE.EQ.2))GOTO 6
WRITE(6,115)
STOP 1

C
C SOLUTION INTO POTENTIAL, EVALUATION OF AXIAL FLUX DENSITY AND ITS
CORRECTION
6 CALL ACORR(ISTEP,ISYM,I1,J1,IRZ,I2,J2,IS,AUX,U,R,B,D,D1,D2)
IF(AUX.LT.3.)GOTO 7
ISTEP=ISTEP+1
C TEST ON MAXIMUM OF 7 APPROXIMATIONS ALLOWED
IF(ISTEP.LE.7)GOTO 5
WRITE(6,114)
STOP 7
C END OF LOOP FOR VECTOR POTENTIAL COMPUTATION
C
C FINAL PRINTS: EXCITATION AS AXIAL INTEGRAL OF B(Z), FLUX (NOT IF
C IPRINT(0),
C AXIAL FLUX DENSITY, OUTPUT ON DISC
7 IF(MULVEY.GT.0)CALL AMULV(J1,I1,IRZ,ISTEP,MAT,PI,IH,BM,H,D2)
CALL ALINEI(ISYM,J1,IRZ,PSIMAX,PI,R,D2,OZ,U,PSI)
IF(IPRINT.LT.1)GOTO 8
WRITE(6,111)
CALL APRINT(PSI,I1,J1,ISTEP,IRZ)
8 WRITE(6,100)INFORM,ISYM
WRITE(6,109)(OZ(I),D1(I),D2(I),I=1,J1)
IF(MULVEY.GT.0)WRITE(6,116)
IF(IDISC.LE.0)GOTO 10
IF(ISTEP.NE.0)GOTO 9
WRITE(10,101)INFORM,J1
WRITE(10,102)(OZ(I),I=1,J1)
9 WRITE(10,103)(D2(I),I=1,J1)

C
C MAP OF PSI (IN 30 LEVELS) AND FLUX DENSITY IN IRON OR ITS LISTING
10 IF(MAPPSI.LT.0)GOTO 12
AUX=3333D-5*PSIMAX
DO 11 I=1,30
11 D3(I)=I*AUX
WRITE(6,106)
CALL AMAP3D(I1,J1,IRZ,30,D3,PSI)
12 IF(IMI.EQ.0)GOTO 15
IF(LISTIR.LT.0)GOTO 13
WRITE(6,107)
CALL AFLUXD(I1,J1,IRZ,IMIN,IMAX,JMIN,JMAX,1,
* MAT,R,Z,U,PSI,D4)
13 IF(LISTFD.EQ.0)GOTO 14
CALL AFLUXD(I1,J1,IRZ,IMIN,IMAX,JMIN,JMAX,0,
* MAT,R,Z,U,PSI,D4)

```

```

C
C      ++++++*****+++++   FURTHER EXCITATION?
14 IF(ISTEP.GT.0)GOTO 15
   IF(ICURR.EQ.0)STOP
   GOTO 17
C
C      NEW CURRENT DENSITY IN THE COIL
15 NP=NP+1
   IF(NP.GT.ICURR)STOP
   AUX=CURR(NP)/CURR(NP-1)
   IF(AUX.LE.0.0)STOP 2
C      VECTOR POTENTIAL IS SLIGHTLY INCREASED BEFORE THE NEXT EXCITATION
   AUX=0.5*(1.+AUX)
   DO 16 I=1,IRZ
16 U(I)=AUX*U(I)
17 ISTEP=1
   AUX=AREA*CURR(NP)
   WRITE(6,112)CURR(NP),AUX
   GOTO 5
C
100 FORMAT(/////5X,'CASE=',2X,20A3//11X,'INPUT FOR TRAJECTORY',
* ' CALCULATIONS -- SYMMETRY PARAMETER=',I2//11X,'Z (MM)',15X,
* ' B(Z) (TESLA)'/27X,'FROM 1ST LINE',7X,'FROM 2 LINES'//)
101 FORMAT(20A3/I4)
102 FORMAT(5F16.9)
103 FORMAT(1P5E16.8)
104 FORMAT(////10X,'VECTOR POTENTIAL COMPUTATION * A=0 ON BOUNDARY'
*      /10X,'PROGRAM AMAG --- VERSION SEPTEMBER 1984 *****'//)
105 FORMAT(//10X,'COORDINATES OF MESH LINES ',1A1//)
106 FORMAT(/////2X,20('*'),2X,'MAP OF FLUX (MICROWEBER)')
107 FORMAT(/////2X,20('*'),2X,'MAP OF IRON FLUX DENSITY (TESLA)')
108 FORMAT(//10X,'+++++ SUM OF RESIDUALS =',1PE11.4)
109 FORMAT(0PF18.6,1P2E20.6)
110 FORMAT(////10X,'LINEAR APPROXIMATION'//10X,'CURRENT DENSITY IN ',
*      ' COIL=',1PE10.3,' A/MM**2')
111 FORMAT(//////////10X,'FLUX ** MICROWEBER'//)
112 FORMAT(/////10X,'NONLINEAR COMPUTATION'//10X,
*      'CURRENT DENSITY IN EXCIT. COIL =',1PE12.3,' A/MM**2'/
*      10X,'LENS EXCITATION',0PF15.3,' A-TURNS'//)
113 FORMAT(//2X,'*****++++*','I5,'. APPROXIMATION')
114 FORMAT(10X,'EXCEEDED 7 APPROXIMATIONS ALLOWED!!!!')
115 FORMAT(//10X,'IE = +1, CONVERGENCE IN ICCG-METHOD NOT REACHED')
116 FORMAT(//2X,20('*'),2X,'B(Z) FROM 2 LINES CORRECTED FOR'
*      ', PERMEABILITY OF IRON ON THE AXIS')
117 FORMAT(10X,'AREA OF EXCITATION COIL',F10.3,' MM**2')
C
C      END
C
C      SUBROUTINE AINPUT(INFORM, IPRINT, IDISC, MAPMAT, MAPPSI, LISTIR, LISTFD,
*
*      JMIN, JMAX, IMIN, IMAX, LETZ, LETR, PI, BM, H, IBH)
C
C      INPUT OF DATA FOR AMAG
C      IMPLICIT REAL*12 (A-H, O-Z)
C      DIMENSION INFORM(20), BM(20, 2), H(20, 2), IBH(2)

```

```

C      COMMON
      */BLDAT/IM,IMI,ISYM,IH(2),MM(40),NM(40),MI(20),NP,ICURR,CURR(10)
      */BLCOORD/NZ,NR,IZ(20),IR(20),CZ(400),CR(400)
      */BPARAM/I2,J2,IS,I1,J1,IRZ
C
C      ***** INPUT + PRINT OF THE COARSE MESH AND INDICES
      READ(5,100)INFORM
      WRITE(6,101)INFORM
      READ(5,102)NZ,NR,IM,IMI,ISYM,ICURR,IH1,IH2,IPRINT,IDISC
      READ(5,102)(IZ(J),J=1,NZ)
      READ(5,102)(IR(J),J=1,NR)
      J2=NR*NZ
      DO 3 J=1,NR
3     READ(5,103)(CZ(I),I=J,J2,NR)
      DO 4 J=1,NR
4     READ(5,103)(CR(I),I=J,J2,NR)
      WRITE(6,104)LETZ,(IZ(J),J=1,NZ)
      DO 5 J=1,NR
5     WRITE(6,105)IR(J),(CZ(I),I=J,J2,NR)
      WRITE(6,104)LETR,(IZ(J),J=1,NZ)
      DO 6 J=1,NR
6     WRITE(6,105)IR(J),(CR(I),I=J,J2,NR)
C
C      INPUT OF REGIONS WITH NONZERO MATERIAL, CURRENT DENSITY IN THE COIL
      IF(IM.EQ.0.OR.IM.GT.20)STOP 20
      J=0
      DO 7 I=1,IM
      READ(5,102)MM(2*I-1),MM(2*I),NM(2*I-1),NM(2*I),MI(I)
      IF((MI(I).LT.3).AND.(MI(I).GT.J))J=MI(I)
7     CONTINUE
      WRITE(6,106)(MM(2*I-1),MM(2*I),NM(2*I-1),NM(2*I),MI(I),I=1,IM)
      IF(ICURR.GT.10)STOP 10
      IF(ICURR.EQ.0)THEN
      READ(5,999)CURR(1)
      WRITE(6,107)ICURR,CURR(1)
      ELSE
      READ(5,999)(CURR(I),I=1,ICURR)
      WRITE(6,107)ICURR,(CURR(I),I=1,ICURR)
      ENDIF
C
C      INPUT OF MAGNETIZATION CURVES
C      IF IMI=0 STANDARD SOFT IRON AND PERMENDUR CURVES ARE USED IN IRON PARTS
      IF(IMI.GT.0)GOTO 8
      IF(J.EQ.0)GOTO 12
      IH(1)=IBH(1)
      IF(J.EQ.2)IH(2)=IBH(2)
      IMI=J
      WRITE(6,112)
      IF(J.EQ.2)WRITE(6,113)
      GOTO 12
8     IH(1)=IH1
      IF(IMI.GT.1)IH(2)=IH2
      DO 9 I=1,IMI

```

```

      J=IH(I)
9    READ(5,114)(BM(K,I),H(K,I),K=1,J)
      WRITE(6,115)
      DO 11 I=1,IMI
      K=IH(I)
      DO 10 J=1,K
      B1=25D5/PI*BM(J,I)/H(J,I)
10   WRITE(6,116)J,H(J,I),BM(J,I),B1
11   WRITE(6,117)
12   READ(5,102,END=13)MAPMAT,MAPPSI,LISTIR,LISTFD
      IF(LISTFD.GT.0)READ(5,102)JMIN,JMAX,IMIN,IMAX
C
13  NP=1
      J1=IZ(NZ)
      I1=IR(NR)
      J2=J1-2
      IF(ISYM.LT.0)ISYM=0
      IF(ISYM.GT.0)ISYM=1
      IF(ISYM.EQ.1)J2=J1-1
      I2=I1-2
      IS=I2*J2
      IRZ=I1*J1
      WRITE(6,108)I1,J1,IRZ,I2,J2,IS
      WRITE(6,109)MAPMAT,MAPPSI,LISTIR,LISTFD,IDISC
      IF(LISTFD.GT.0)WRITE(6,110)JMIN,JMAX,IMIN,IMAX
C
      TEST ON MAXIMUM DIMENSIONS ALLOWED
      IF(IS.GT.6000)STOP 6000
      IF(IRZ.GT.6500)STOP 6500
      IF(J1.GT.120)STOP 120
C
C
      TEST, IF THERE ARE POSITIVE AREAS IN THE COARSE MESH ONLY
      DO 14 J=2,NZ
      DO 14 I=2,NR
      K=(J-1)*NR+I
      L=K-NR
      A1=(CR(K)-CR(L-1))*(CZ(L)-CZ(L-1))-(CR(L-1)-CR(L))*(CZ(L-1)-CZ(K))
      A2=(CR(L-1)-CR(K))*(CZ(K-1)-CZ(K))-(CR(K)-CR(K-1))*(CZ(K)-CZ(L-1))
      A3=(CR(L)-CR(K-1))*(CZ(L-1)-CZ(K-1))-(CR(K-1)-CR(L-1))*(CZ(K-1)
      *
      -CZ(L))
      A4=(CR(K-1)-CR(L))*(CZ(K)-CZ(L))-(CR(L)-CR(K))*(CZ(L)-CZ(K-1))
      IF(A1.LE.0D0.OR.A2.LE.0D0.OR.A3.LE.0D0.OR.A4.LE.0D0)GOTO 15
14  CONTINUE
      RETURN
15  WRITE(6,111)I,J,A1,A2,A3,A4
      STOP 15
C
100  FORMAT(20A3)
101  FORMAT(////1X,93('*')/1X,'INFORMATION: ',20A3/1X,93('*')//)
102  FORMAT(20I4)
103  FORMAT(13F6.0)
999  FORMAT(10F8.0)
104  FORMAT(//2X,'INPUT COORDINATES ',A1//(5X,12I10))
105  FORMAT(I3,2X,12F10.3,(/5X,8F10.3))
106  FORMAT(//2X,'LINES LIMITING POSITION OF IRON(MAT.'

```

```

* , ' 1 AND 2) AND COIL(MAT. 3)'/2X, 'IN Z FROM-TO', 3X,
* 'IN R FROM-TO', 3X, 'TYPE OF MATERIAL'/(2(I9, I4), I8))
107 FORMAT(//2X, 'NUMBER OF EXCITATIONS COMPUTED:', I2/
* 2X, 'EXCITATION CURRENT DENSITY IN A/MM**2:', 1P4E16.6/
* 8X, 6E16.6)
108 FORMAT(//2X, '** PARAMETERS OF THE MESH: I1=', I3, ', J1=', I3,
*, IRZ=', I5/2X, '++ OF F.E.M. SYSTEM: I2=', I3, ', J2=', I3,
*, IS=', I5)
109 FORMAT(2X, '** FURTHER PARAMETERS: MAPMAT=', I2, ', MAPPSI=', I2,
* ', LLSTIR=', I2, ', LISTFD=', I2, ', IDISC=', I2)
110 FORMAT(5X, 'MAPPING OF FLUX DENSITY: IN Z FROM J=', I3, ' TO J=', I3,
* ', IN R FROM I=', I3, ' TO I=', I3)
111 FORMAT(' ERROR DETECTED IN THE COARSE MESH: FOR I=', I2,
* ', J=', I2, ' ARE THE AREAS', 1P4E10.2)
112 FORMAT(//2X, 'MAGNET. CURVE 1: SOFT IRON(STANDARD)')
113 FORMAT(2X, 'MAGNET. CURVE 2: PERMENDUR(STANDARD)')
114 FORMAT(12F6.0)
115 FORMAT(//2X, 'MAGNETIZATION CURVE: '/' J', 10X, 'H (A/M)', 5X,
* 'B (TESLA)', 5X, 'MI RELATIVE'//)
116 FORMAT(I4, F14.1, F14.3, F14.1)
117 FORMAT('/' *****'/)

```

C

END

C

SUBROUTINE AMESH(IRZ, NZ, NR, IZ, IR, IDIM, CZ, CR, R, Z)

C

C

FROM THE COARSE MESH FORMS THE FINE MESH OF R AND Z COORDINATES
REAL*12 R(IRZ), Z(IRZ), CR(IDIM), CZ(IDIM), Z1, Z2, R1, R2, DK, DK1, DL, DL1
INTEGER IZ(NZ), IR(NR)

C

```

I2=1
DO 1 J=2, NZ
K1=IZ(J)-IZ(J-1)
DK=K1
IF(J.EQ.NZ)K1=K1+1
DO 1 K=1, K1
DO 1 I=2, NR
IA=(J-2)*NR+I-1
ID=IA+NR
DK1=K-1
Z1=CZ(IA)+(CZ(ID)-CZ(IA))*DK1/DK
R1=CR(IA)+(CR(ID)-CR(IA))*DK1/DK
Z2=CZ(IA+1)+(CZ(ID+1)-CZ(IA+1))*DK1/DK
R2=CR(IA+1)+(CR(ID+1)-CR(IA+1))*DK1/DK
L1=IR(I)-IR(I-1)
DL=L1
IF(I.EQ.NR)L1=L1+1
DO 1 L=1, L1
DL1=L-1
Z(I2)=Z1+(Z2-Z1)*DL1/DL
R(I2)=R1+(R2-R1)*DL1/DL
I2=I2+1

```

1 CONTINUE

C

```

RETURN
END
C
SUBROUTINE AMATER(IRZ,MAPMAT,IM,IM2,I1,J1,MM,NM,MI,MAT)
C
C INTO THE VECTOR MAT THE MATERIAL OF EACH QUADRILLATERAL WILL BE GIVEN
C FOR MAPMAT>=0 A 2D MATERIAL DISTRIBUTION IN THE MESH IS PRINTED
C
DIMENSION MM(IM2),NM(IM2),MI(IM),MAT(IRZ)
C
C IN VECTOR MAT ARE I AND J INDICES OF THE LOWER RIGHT-HAND CORNER OF
C QUADRIL.
C DO 1 I=1,IRZ
1 MAT(I)=0
DO 2 J=2,J1
DO 2 I=2,I1
DO 2 K=1,IM
IF(((J.GT.MM(2*K-1)).AND.(J.LE.MM(2*K))).AND.
* ((I.GT.NM(2*K-1)).AND.(I.LE.NM(2*K))))MAT((J-1)*I1+I)=MI(K)
2 CONTINUE
IF(MAPMAT.LT.0)RETURN
C
C PRINT OF MAT
C WRITE(6,100)(I,I=5,J1,5)
100 FORMAT(////1X,10('*'),' DISTRIBUTION OF MATERIALS IN MESH'//
* 10X,'INDEX J'/1X,'INDEX I',I7,23I5)
C
DO 3 I=2,I1
WRITE(6,102)I,(MAT((J-1)*I1+I),J=2,J1)
3 CONTINUE
102 FORMAT(I8,' -',120I1)
C
RETURN
END
C
SUBROUTINE ACOEF(ISTEP,MAT,SUM,PI,AREA,BM,H,B,P,P1,P2,P3,P4,R,Z,U)
C
C EVALUATES THE COEFFICIENTS OF THE F.E.M. EQUATIONS IN LINEAR/NONLINEAR
CASE
IMPLICIT REAL*12 (A-H,O-Z)
DIMENSION U(IRZ),B(IS),P(IS),P1(IS),P2(IS),P3(IS),P4(IS),
* R(IRZ),Z(IRZ),F(24),Q(12),MAT(IRZ),BM(20,2),H(20,2)
C
COMMON /BPARAM/I2,J2,IS,I1,J1,IRZ
*/BLDAT/IM,IMI,ISYM,IH(2),MM(40),NM(40),MI(20),NP,ICURR,CURR(10)
C
DO 1 I=1,IS
P(I)=0.
P1(I)=0.
P2(I)=0.
P3(I)=0.
P4(I)=0.
1 B(I)=0.0
IF(ISTEP.EQ.0)AREA=0.

```

```

C     RELATIVE PERMEABILITY IS USED
      RMIV=PI*4D-7
C
C     COMPUTATION OF COEFFICIENTS
      L1=1
      IF(ISYM.EQ.0)L1=3-I1
      DO 3 J=2,J1
      DO 4 I=2,I1
      IK=(J-1)*I1+I
      IMIV=MAT(IK)
      ICOIL=0
      IF(IMIV.LT.3)GOTO 2
      ICOIL=NP
      IMIV=0
C
C     2 IA=(J-1)*I1+I
      IB=IA-1
      IC=IB-I1
      ID=IC+1
C
      CALL ATRIAN(IMIV,ICOIL,ISTEP,0,0,AR1,R(ID),R(IA),R(IC),Z(ID),
*     Z(IA),Z(IC),U(ID),U(IA),U(IC),RMIV,BM,H,IH,F,Q,CURR(NP))
      CALL ATRIAN(IMIV,ICOIL,ISTEP,6,3,AR2,R(IB),R(IC),R(IA),Z(IB),
*     Z(IC),Z(IA),U(IB),U(IC),U(IA),RMIV,BM,H,IH,F,Q,CURR(NP))
      CALL ATRIAN(IMIV,ICOIL,ISTEP,12,6,AR3,R(IC),R(ID),R(IB),Z(IC),
*     Z(ID),Z(IB),U(IC),U(ID),U(IB),RMIV,BM,H,IH,F,Q,CURR(NP))
      CALL ATRIAN(IMIV,ICOIL,ISTEP,18,9,AR4,R(IA),R(IB),R(ID),Z(IA),
*     Z(IB),Z(ID),U(IA),U(IB),U(ID),RMIV,BM,H,IH,F,Q,CURR(NP))
      IF(ISTEP.EQ.0.AND.ICOIL.GT.0)AREA=AREA+(AR1+AR2+AR3+AR4)/4.
C
C     SUBSTITUTION INTO B, P...P4
      IF(ISYM.EQ.0.AND.J.EQ.2)GOTO 6
      IF(I.EQ.I1)GOTO 5
C     LOWER LEFT-HAND VERTEX OF THE QUADRILATERAL
      IK=L1
      B(IK)=B(IK)+Q(1)+Q(8)+Q(12)
      P(IK)=P(IK)+F(1)+F(16)+F(24)
      P2(IK)=P2(IK)+F(17)+F(23)
      P3(IK)=P3(IK)+F(2)+F(21)
C     5 IF(I.EQ.2)GOTO 6
C     UPPER LEFT-HAND VERTEX
      IK=L1-1
      B(IK)=B(IK)+Q(3)+Q(5)+Q(7)
      P(IK)=P(IK)+F(6)+F(10)+F(13)
      P1(IK)=P1(IK)+F(3)+F(14)
      P3(IK)=P3(IK)+F(8)+F(15)
      P4(IK)=P4(IK)+F(5)+F(11)
C     6 IF(J.EQ.J1)GOTO 4
      IF(I.EQ.I1)GOTO 7
C     LOWER RIGHT-HAND VERTEX
      IK=L1+I2
      B(IK)=B(IK)+Q(2)+Q(6)+Q(10)
      P(IK)=P(IK)+F(4)+F(12)+F(19)
C     7 IF(I.EQ.2)GOTO 4

```

```

C   UPPER RIGHT-HAND VERTEX
      IK=L1+I2-1
      B(IK)=B(IK)+Q(4)+Q(9)+Q(11)
      P(IK)=P(IK)+F(7)+F(18)+F(22)
      P1(IK)=P1(IK)+F(9)+F(20)
C
4   L1=L1+1
3   L1=L1-1
      IF(ISTEP.EQ.0.AND.ISYM.GT.0)AREA=2.*AREA
C   *****
C   A=0 ON THE BOUNDARY (SOME COEFFICIENTS MUST BE PUT EQUAL TO ZERO)
      DO 8 I=1,J2
      IK=(I-1)*I2+1
      P2(IK)=0.0
      IK=I*I2
      P1(IK)=0.0
8   P4(IK)=0.0
C
      DO 9 I=1,I2
      IK=IS+1-I
      P2(IK)=0.0
      P3(IK)=0.0
9   P4(IK)=0.0
C
C   SUM OF RIGHT-HAND SIDES - AN INDICATION OF THE VALUE OF RESIDUALS
      SUM=0.
      DO 10 I=1,IS
10  SUM=SUM+ABS(B(I))
C
      RETURN
      END
C
      SUBROUTINE ATRIAN(IMIV,ICOIL,ISTEP,IK,IL,AR,R1,R2,R3,Z1,Z2,Z3,
*   U1,U2,U3,RMIV,BM,H,IH,F,Q,CURR)
C
      REAL*12 BM(20,2),H(20,2),F(24),Q(12),CURR,RST,AR,BR,BZ,BC,H1,
*   H2,H3,R1,R2,R3,Z1,Z2,Z3,B1,B2,B3,C1,C2,C3,RMI,RMI1,RMIV
*   ,AUX,U1,U2,U3,PK
      DIMENSION IH(2)
C
      B1=R2-R3
      B2=R3-R1
      B3=R1-R2
      RST=R1+R2+R3
      C1=Z3-Z2
      C2=Z1-Z3
      AR=B1*C2-B2*C1
      AUX=AR/RST
      C1=C1+AUX
      C2=C2+AUX
      C3=Z2-Z1+AUX
C
      RMI=1.0

```

```

RMI1=0.0
IF (IMIV.GT.0)RMI=H(1,IMIV)/BM(1,IMIV)*RMIV
IF (ISTEP.EQ.0)GOTO 3
C
BR=- (B1*U1+B2*U2+B3*U3)/AR
BZ=(C1*U1+C2*U2+C3*U3)/AR
BC=SQRT(BR**2+BZ**2)
H1=-B1*BR+C1*BZ
H2=-B2*BR+C2*BZ
H3=-B3*BR+C3*BZ
IF (IMIV.EQ.0)GOTO 3
IF (BC.LE.BM(1,IMIV))GOTO 3
C
EVALUATION OF RELATIVE PERMEABILITY IN IRON
IP=IH(IMIV)
RMI1=1.
1 IF (BC.GT.BM(IP,IMIV))GOTO 2
RMI1=(H(IP,IMIV)-H(IP-1,IMIV))/(BM(IP,IMIV)-BM(IP-1,IMIV))*RMIV
IP=IP-1
GOTO 1
2 RMI=RMI1+(H(IP,IMIV)*RMIV-RMI1*BM(IP,IMIV))/BC
C
3 PK=RST*RMI/AR
F(IK+1)=PK*(B1*B1+C1*C1)
F(IK+2)=PK*(B1*B2+C1*C2)
F(IK+3)=PK*(B1*B3+C1*C3)
F(IK+4)=PK*(B2*B2+C2*C2)
F(IK+5)=PK*(B2*B3+C2*C3)
F(IK+6)=PK*(B3*B3+C3*C3)
C
IF (ICOIL.GT.0)GOTO 4
Q(IL+1)=0.0
Q(IL+2)=0.0
Q(IL+3)=0.0
GOTO 5
C
4 PK=25D1*AR*CURRE*RMIV
Q(IL+1)=PK*(RST+R1)
Q(IL+2)=PK*(RST+R2)
Q(IL+3)=PK*(RST+R3)
C
5 IF (ISTEP.EQ.0)GOTO 6
PK=-RST*RMI
Q(IL+1)=Q(IL+1)+PK*H1
Q(IL+2)=Q(IL+2)+PK*H2
Q(IL+3)=Q(IL+3)+PK*H3
C
6 IF (RMI1.EQ.0.0)RETURN
PK=(RMI1-RMI)*RST/(AR*BC**2)
F(IK+1)=F(IK+1)+PK*H1*H1
F(IK+2)=F(IK+2)+PK*H1*H2
F(IK+3)=F(IK+3)+PK*H1*H3
F(IK+4)=F(IK+4)+PK*H2*H2
F(IK+5)=F(IK+5)+PK*H2*H3
F(IK+6)=F(IK+6)+PK*H3*H3

```

```

C      RETURN
      END
C
C      SUBROUTINE ACORR(ISTEP, ISYM, I1, J1, IRZ, I2, J2, IS, AUX,
*                               U, R, B, RELCOR, D1, D2)
C
C      REAL*12 AUX, RELCOR(J2), D1(J1), D2(J1), B(IS), U(IRZ), R(IRZ)
C
C      SOLUTION IN B SUBSTITUTED INTO VECTOR POTENTIAL U
      AUX=0.
      IK=I1-1
      IF(ISYM.GT.0) IK=-1
      DO 1 J=1, J2
      IK=IK+2
      DO 2 I=1, I2
      IL=I2*(J-1)+I
      IK=IK+1
2     U(IK)=U(IK)+B(IL)
      IF(ISTEP.EQ.0) GOTO 1
C      EVALUATION OF RELATIVE CORRECTION TO B(Z) ON THE AXIS
      RELCOR(J)=1.
      IF(U(IK).NE.0) RELCOR(J)=-B(IL)/U(IK)
C      IF U<0, ONLY ONE THIRD OF THE CORRECTION IS CONSIDERED!!!
      IF(U(IK).LT.0) RELCOR(J)=RELCOR(J)/3.
      AUX=AUX+ABS(RELCOR(J))
1     CONTINUE
      AUX=AUX/J2*100.
C
C      COMPUTATION OF AXIAL FLUX DENSITY (FROM 1 OR 2 MESH LINES)
      IK=I1-1
      DO 3 I=1, J1
      D1(I)=2.*U(IK)/R(IK)
      D2(I)=2.*(U(IK)*R(IK-1)**3-U(IK-1)*R(IK)**3)/
*           (R(IK)*R(IK-1)*(R(IK-1)**2-R(IK)**2))
3     IK=IK+1
C
C      PRINT OF THE CORRECTIONS
      IF(ISTEP.EQ.0) GOTO 4
      WRITE(6, 103) AUX
      WRITE(6, 100) (RELCOR(I), I=1, J2)
      IF(AUX.GE.3.) GOTO 4
      WRITE(6, 101) (D2(I), I=1, J1)
C
101  FORMAT(///10X, 'AXIAL FLUX DENSITY FROM 2ND LINE (TESLA)'//
*           (1X, 10F11.6))
100  FORMAT(///10X, 'RELATIVE CORRECTION OF B(Z)'//(10F12.6))
103  FORMAT(/10X, 'AVERAGE CORRECTION OF B(Z) =', F10.5, ' %')
C
4     RETURN
      END
C
      SUBROUTINE APRINT(X, I1, J1, N, L)
      REAL*12 X(L)

```

```

C      SUBROUTINE FOR PRINTING A VECTOR X WITH DIMENSION L=I1*J1
C      TOGETHER J1 COLUMNS, I1 LINES (MAX. 10 ITEMS ON A LINE)
C      FORMAT ACCORDING TO N: FOR N<0 IN F FORMAT, N>0 EXPONENTIAL FORM
C      - TO PRINT COORDINATES, POTENTIAL AND FLUX DENSITIES
      DO 1 J=1,J1,10
      I3=(J-1)*I1+1
      I4=I3-1+10*I1
      IF(I4.GT.L)I4=L
      IF(N.GE.0)GOTO 3
      DO 2 I=1,I1
      WRITE(6,102)(X(K),K=I3,I4,I1)
2     I3=I3+1
      GOTO 1
3     DO 4 I=1,I1
      WRITE(6,101)(X(K),K=I3,I4,I1)
4     I3=I3+1
1     WRITE(6,103)
C
101  FORMAT(1X,1P10E12.5)
102  FORMAT(1X,10F12.5)
103  FORMAT(//)
C
      RETURN
      END
C
      SUBROUTINE AMULV(J1,I1,IRZ,ISTEP,MAT,PI,IH,BM,H,B)
C
C      DIVIDES VALUE OF AXIAL FLUX DENSITY BY RELATIVE PERMEABILITY OF IRON
C      INTEGER MAT(IRZ),IH(2)
C      REAL*12 B(J1),BM(20,2),H(20,2),BC,PI,RMIL,RMIL,RMIR,RMIV
C
      RMIV=4D-7*PI
      RMIR=2.
      DO 4 I=2,J1
      RMIL=RMIR
      RMIR=1.
      IMIV=MAT(I*I1)
      IF(IMIV.GE.3)IMIV=0
      IF(IMIV.EQ.0)GOTO 3
      BC=0.5*B(I)+B(I-1)/RMIL
      RMIR=H(1,IMIV)/BM(1,IMIV)*RMIV
      IF((BC.LE.BM(1,IMIV)).OR.(ISTEP.EQ.0))GOTO 3
      IP=IH(IMIV)
      RMIL=1.
1     IF(BC.GT.BM(IP,IMIV))GOTO 2
      RMIL=(H(IP,IMIV)-H(IP-1,IMIV))/(BM(IP,IMIV)-BM(IP-1,IMIV))*RMIV
      IP=IP-1
      GOTO 1
2     RMIR=RMIL+(H(IP,IMIV)*RMIV-RMIL*BM(IP,IMIV))/BC
C
3     IF(I.NE.2)GOTO 5
      RMIL=RMIR
      B(1)=B(1)*RMIL/2.
5     B(I)=B(I)*RMIR/2.

```

```

      B(I-1)=B(I-1)*(1.+RMIR/RMIL)
4 CONTINUE
C
      RETURN
      END
C
      SUBROUTINE ALINEI( ISYM, J1, IRZ, PSIMAX, PI, R, BZ, OZ, U, PSI)
C
C     CALCULATES INTEGRAL OF BZ ON AXIS DIVIDED BY MUO BY TRAPEZ. RULE
C     EVALUATES THE FLUX PSI=2*PI*U*R AND FINDS PSIMAX
C     REAL*12 R(IRZ), OZ(J1), U(IRZ), PSI(IRZ), BZ(J1), PSIMAX, SUM, PI
C
      SUM=0.
      DO 1 J=2, J1
1     SUM=SUM+(BZ(J)+BZ(J-1))*(OZ(J)-OZ(J-1))
      SUM=25D2*SUM/PI
      IF( ISYM.EQ.0) SUM=SUM/2D0
C
      WRITE(6, 10) SUM
10  FORMAT(////10X, '***** EXCITATION (INTEGRAL OF AXIAL FLUX',
* ' DENSITY): ', 1PE14.6, ' A-TURNS'//)
C
      PSIMAX=0.
      DO 2 J=1, IRZ
      PSI(J)=2.*PI*R(J)*U(J)
      IF(ABS(PSI(J)).LT.PSIMAX)GOTO 2
      PSIMAX=ABS(PSI(J))
      I=J
2 CONTINUE
C
      J=I/(IRZ/J1)+1
      I=I-(J-1)*(IRZ/J1)
      WRITE(6, 11) PSIMAX, I, J
11  FORMAT(10X, '+++++ MAXIMUM VALUE OF FLUX =', 1PE16.6,
* ' MICROWEBER AT I=', I3, ', J=', I3//)
C
      RETURN
      END
C
      SUBROUTINE AMAP3D(I1, J1, IRZ, NLEVEL, XF, FIELD)
C
C     3D MAP IN NLEVEL LEVELS OF GIVEN VECTOR FIELD
C     - TO MAP THE FLUX OR FLUX DENSITY DISTRIBUTION
C     DIMENSION LETTER(39), LINE(120)
C     REAL*12 XF(NLEVEL), FIELD(IRZ)
C     DATA LETTER/1H, 1H0, 1H1, 1H2, 1H3, 1H4, 1H5, 1H6, 1H7, 1H8, 1H9, 1HA, 1HB,
* 1HC, 1HD, 1HE, 1HF, 1HG, 1HH, 1HI, 1HJ, 1HK, 1HL, 1HM, 1HN, 1HO, 1HP, 1HQ,
* 1HR, 1HS, 1HT, 1HU, 1HV, 1HW, 1HX, 1HY, 1HZ, 1H-, 1H!/
C
C     PRINT OF FIRST 3 LINES OF THE MAP
      DO 1 I=1, J1
      LINE(I)=LETTER(38)
      IF(MOD(I, 5).EQ.0) LINE(I)=LETTER(39)
1 CONTINUE

```

```

WRITE(6,100)(I,I=5,J1,5)
WRITE(6,101)(LINE(I),I=1,J1)
100 FORMAT(20X,'INDEX J'/' INDEX I ',24I5)
101 FORMAT(10X,120A1)
C
C PRINT OF I1 LINES OF THE MAP
LINE(1)=LETTER(1)
DO 3 I=1,I1
DO 2 J=1,J1
LINE(J)=LETTER(1)
DO 2 K=1,NLEVEL
INDEX=(J-1)*I1+I
IF(FIELD(INDEX).GT.XF(K))LINE(J)=LETTER(K+1)
2 CONTINUE
K=LETTER(39)
IF(MOD(I,5).EQ.0)K=LETTER(38)
3 WRITE(6,102)I,K,(LINE(J),J=1,J1),K
102 FORMAT(I9,122A1)
C
C PRINT OF FINAL LINE
DO 4 I=1,J1
LINE(I)=LETTER(38)
IF(MOD(I,5).EQ.0)LINE(I)=LETTER(39)
4 CONTINUE
WRITE(6,101)(LINE(I),I=1,J1)
C
C PRINT OF DESCRIPTION
WRITE(6,103)
103 FORMAT(/2X,'MEANING OF LETTERS:')
K=(NLEVEL+4)/5
DO 5 I=1,K
L=5*I
IF(L.GT.NLEVEL)L=NLEVEL
L1=5*(I-1)+1
WRITE(6,104)(LETTER(J),XF(J),J=L1,L),LETTER(L+1)
5 CONTINUE
104 FORMAT(2X,5(' ',1A1,' '<','F12.2,5X,'<'),' ',1A1,' ')
C
RETURN
END
C
SUBROUTINE AFLUXD(I1,J1,IRZ,IMIN,IMAX,JMIN,JMAX,MAPIR,MAT,
* R,Z,U,BB,XZ)
C
C ++++++ PRINT OF FLUX DENSITY IN IRON OR GIVEN REGION
C ***** MAPIR=1 - ONLY IRON
C * * * * * MAPIR=0 - FLUX DENSITY FROM IMIN TO IMAX, JMIN TO JMAX
IMPLICIT REAL*12 (A-H,O-Z)
REAL*12 R(IRZ),Z(IRZ),U(IRZ),BB(IRZ),XZ(36)
INTEGER S,MAT(IRZ)
C
DO 1 I=1,IRZ
1 BB(I)=-1.
C

```

```

IJK=1
JMI=JMIN
JMA=JMAX
IMI=IMIN
IMA=IMAX
IF(MAPIR.EQ.0)GOTO 2
JMI=2
JMA=J1
IMI=2
IMA=I1
C
C THE COMPUTATION OF FLUX DENSITY
2 BMAX=0.
  BMIN=1E50
  IF(IMI.LT.2)IMI=2
  IF(IMA.GT.I1)IMA=I1
  IF(JMI.LT.2)JMI=2
  IF(JMA.GT.J1)JMA=J1
C
C *****
DO 3 J=JMI,JMA
DO 3 I=IMI,IMA
IA=(J-1)*I1+I
IMIV=MAT(IA)
IF(((IMIV.EQ.0).OR.(IMIV.EQ.3)).AND.(MAPIR.GT.0))GOTO 3
C IA,IB,IC,ID - INDICES OF QUADRILATERAL'S VERTICES IN R-Z MESH
  IB=IA-1
  IC=IB-I1
  ID=IC+1
  S=1
  G=0.0
4 GO TO (5,6,7,8,9),S
C TRIANGLES T1, T2, T3 AND T4
5 IK1=ID
  IK2=IA
  IK3=IC
  S=2
  GOTO 10
6 IK1=IB
  IK2=IC
  IK3=IA
  S=3
  GOTO 10
7 IK1=IC
  IK2=ID
  IK3=IB
  S=4
  GOTO 10
8 IK1=IA
  IK2=IB
  IK3=ID
  S=5
C
10 R1=R(IK1)

```

```

R2=R(IK2)
R3=R(IK3)
Z1=Z(IK1)
Z2=Z(IK2)
Z3=Z(IK3)
U1=U(IK1)
U2=U(IK2)
U3=U(IK3)
B1=R2-R3
B2=R3-R1
B3=R1-R2
RST=R1+R2+R3
C1=Z3-Z2
C2=Z1-Z3
AR=B1*C2-B2*C1
XY=AR/RST
C1=C1+XY
C2=C2+XY
C3=Z2-Z1+XY
BR=-(B1*U1+B2*U2+B3*U3)/AR
BZ=(C1*U1+C2*U2+C3*U3)/AR
BC=SQRT(BR**2+BZ**2)
G=G+0.25*BC
GOTO 4

```

C

```

9 IF((ABS(G)-BMAX).LT.0.)GOTO 11
  BMAX=ABS(G)
  IBMAX=(J-2)*I1+I
11 IF((BMIN-ABS(G)).LT.0.)GOTO 12
  BMIN=ABS(G)
  IBMIN=(J-2)*I1+I
12 IF(MAPIR.EQ.0)GOTO 13
  BB((J-2)*I1+I)=G
  GOTO 3
13 BB(IJK)=G
  IJK=IJK+1
3 CONTINUE

```

C

C

```

*****
IF(MAPIR.EQ.0)WRITE(6,100)IMI,IMA,JMI,JMA
J=IBMAX/I1+2
I=IBMIN/I1+2
IBMAX=IBMAX-(J-2)*I1
IBMIN=IBMIN-(I-2)*I1
WRITE(6,101)BMAX,J,IBMAX,BMIN,I,IBMIN
101 FORMAT(/,10X,'BMAX=',1PE11.4,' TESLA FOR J=',I3,' AND I=',
* I3/10X,'BMIN=',E11.4,' TESLA FOR J=',I3,' AND I=',I3/)
IF(MAPIR.EQ.0)GOTO 16

```

C

C 3D PLOT OF IRON FLUX DENSITY IN .1 TESLA STEPS (1<BMAX<3.6 T) OR IN 30 LEVELS

```

XY=0.1
NZ=BMAX/XY+1
IF((NZ.LE.36).AND.(NZ.GT.10))GOTO 14

```

```

      NZ=30
      XY=BMAX/NZ
14 DO 15 I=1,NZ
15 XZ(I)=XY*(I-1)
      CALL AMAP3D(I1,J1,IRZ,NZ,XZ,BB)
      RETURN
C
C PRINT OF FLUX DENSITY IN GIVEN REGION
16 I=IMA-IMI+1
      J=JMA-JMI+1
100 FORMAT(////10X,'FLUX DENSITY DISTRIBUTION FROM I=',I4,' TO I=',
* I4/32X,'AND FROM J=',I4,' TO J=',I4)
      IK=I*J
      CALL APRINT(BB,I,J,-1,IK)
C
      RETURN
      END
C
      SUBROUTINE AICCG(NIT,IE,IS1,I2,IS,EPS,
* P,P1,P2,P3,P4,B,D,D1,D2,D3,D4,X,Q,R,S,Y)
C
C SUBROUTINE FOR THE SOLUTION OF THE F.E.M. SYSTEM OF LINEAR EQUATIONS
C BY ICCG METHOD (ALSO PRECONDITIONED CONJUG. GRAD. METHOD)
C
      REAL*12 X(IS),B(IS),P(IS),P1(IS),P2(IS),P3(IS),P4(IS),
* D(IS),D1(IS),D2(IS),D3(IS),D4(IS),Q(IS),R(IS),S(IS),Y(IS1),
* EPS,TOL,XMAX,DXMAX,SPROD,AA,BB
C
C APPROXIMATE CHOLESKI DECOMPOSITION
      CALL ADECOM(IS,I2,P,P1,P2,P3,P4,D,D1,D2,D3,D4)
C
C INITIAL CONDITIONS: X=0 - SOLUTION
C R=B - RESIDUALS
C S=Y=APPR.INVERSE*R - AUX. VECTORS
C Q=MATRIX*Y
C
      DO 1 I=1,IS
      X(I)=0.
      R(I)=B(I)
1 CONTINUE
      Y(IS1)=0.
      CALL ASOLVE(I2,IS,D,D1,D2,D3,D4,R,Y)
      NCYCLE=-1
      CALL AMULTI(Q,P,P1,P2,P3,P4,Y,I2,IS,IS1)
      SPROD=0.
      DO 2 I=1,IS
      S(I)=Y(I)
2 SPROD=SPROD+R(I)*S(I)
C
C ALGORITHM OF THE ICCG METHOD ACCORDING TO J.A.MEIJERINK&H.A.VAN DER VORST
C MATHEMATICS OF COMPUTATION 31(JAN.1977),148-162
C *** FOR I-TH STEP: AA=(R,S)/(Y,Q)
C X=X+AA*Y
C R=R-AA*Q

```

```

C          NEW S: S=APPROX.INVERSE*R
C          BB=(R,S NEW)/(R,S OLD)
C          Y=S+BB*Y
C
C          MAXIMUM NIT STEPS ALLOWED, ACCURACY REQUIRED DXMAX<TOL=EPS*XMAX
C          (FOR EPS=10**(-N) ABOUT N-2 DIGITS VALID)
3 NCYCLE=NCYCLE+1
  CALL ACYCLE(I2,IS,IS1,DXMAX,XMAX,SPROD,AA,BB,
  *          Q,P,P1,P2,P3,P4,Y,X,R,S,D,D1,D2,D3,D4)
  IF(NCYCLE.GE.NIT)GOTO 4
  TOL=EPS*XMAX
  IF(TOL.GT.DXMAX)GOTO 5
  GOTO 3
C
C          CONVERGENCE NOT OBTAINED IN NIT ITERATIONS (IF THE ACCURACY IS ONLY 10
C          TIMES WORSE THAN REQUIRED BY EPS, RESULTS USED FOR FURTHER COMPUTATION,
C          OTHERWISE THE COMPUTATION STOPS!)
4 IE=1
  TOL=10.*ABS(EPS*XMAX)
  IF(TOL.GT.DXMAX)IE=2
  WRITE(6,104)NIT,EPS,TOL,DXMAX,XMAX,IE
104 FORMAT(///10X,'NIT=',I4,' STEPS OF ICCG, EPS=',1PE13.3/
  *10X,'TOL=',E14.5,', DXMAX=',E14.5,', XMAX=',E14.5,', IE=',I2//)
  GOTO 6
C
C          CONVERGENCE OBTAINED WITH REQUIRED ACCURACY
5 WRITE(6,103)EPS,NCYCLE,NIT
103 FORMAT(/10X,'*** ICCG REACHED THE ACCURACY',1PE9.1,
  *' IN STEP ',I4,' FROM',I4,' ALLOWED')
C
C          AFTER RETURN: SOLUTION IN B
C          ORIGINAL RIGHT-HAND SIDES IN Q
6 DO 7 I=1,IS
  Q(I)=B(I)
7 B(I)=X(I)
C
C          RETURN
C          END
C
C          SUBROUTINE ADECOM(IS,I2,P,P1,P2,P3,P4,D,D1,D2,D3,D4)
C
C          APPROXIMATE DECOMPOSITION OF THE FINITE ELEMENT MATRIX
REAL*12 P(IS),P1(IS),P2(IS),P3(IS),P4(IS),D(IS),D1(IS),D2(IS),
*          D3(IS),D4(IS),SUM
C
C          P,P1,... - THE COEFFICIENTS OF THE F.E.M. MATRIX
C          D,D1,... - THE COEFFICIENTS OF THE APPROX.DECOMPOSED UPPER TRIANG. MATRIX
C
C          FIRST I2 LINES (I2 - THE WIDTH OF THE BAND)
D(1)=1D0/SQRT(P(1))
D1(1)=P1(1)*D(1)
D2(1)=P2(1)*D(1)
D3(1)=P3(1)*D(1)
D4(1)=P4(1)*D(1)

```

```

DO 1 I=2, I2
D(I)=1D0/SQRT(ABS(P(I)-D1(I-1)**2))
D1(I)=P1(I)*D(I)
D4(I)=P4(I)*D(I)
D3(I)=(P3(I)-D1(I-1)*D4(I-1))*D(I)
D2(I)=(P2(I)-D3(I-1)*D1(I-1))*D(I)
1 CONTINUE
C LINE I2+1
D(I2+1)=1D0/SQRT(ABS(P(I2+1)-D1(I2)**2-D3(1)**2-D2(2)**2))
D1(I2+1)=(P1(I2+1)-D3(1)*D4(1)-D3(2)*D2(2))*D(I2+1)
D4(I2+1)=P4(I2+1)*D(I2+1)
D3(I2+1)=(P3(I2+1)-D1(I2)*D4(I2))*D(I2+1)
D2(I2+1)=(P2(I2+1)-D3(I2)*D1(I2))*D(I2+1)
C
C THE REST LINES -- I2+2 TO IS
J=I2+2
DO 2 I=J, IS
IK=I-I2
SUM=D1(I-1)**2+D2(IK+1)**2+D3(IK)**2+D4(IK-1)**2
D(I)=1D0/SQRT(ABS(P(I)-SUM))
D1(I)=(P1(I)-D3(IK)*D4(IK)-D3(IK+1)*D2(IK+1))*D(I)
D2(I)=(P2(I)-D3(I-1)*D1(I-1))*D(I)
D3(I)=(P3(I)-D1(I-1)*D4(I-1))*D(I)
D4(I)=P4(I)*D(I)
2 CONTINUE
C
C RETURN
C END
C
C SUBROUTINE ACYCLE(I2, IS, IS1, DXMAX, XMAX,
*   SPROD, A, B, Q, P, P1, P2, P3, P4, Y, X, R, S, D, D1, D2, D3, D4)
C
C PERFORMS ONE STEP OF ICCG METHOD
C REAL*12 Q(IS), P1(IS), P2(IS), P3(IS), P4(IS), X(IS), R(IS), Y(IS1),
*   P(IS), S(IS), D(IS), D1(IS), D2(IS), D3(IS), D4(IS), A, B, SPROD,
*   DXMAX, XMAX, AUX
C
C MAKE VECTOR Q
C CALL AMULTI(Q, P, P1, P2, P3, P4, Y, I2, IS, IS1)
C MAKE A
C AUX=0.
C DO 1 I=1, IS
1 AUX=AUX+Q(I)*Y(I)
C WRITE (13, *) SPROD, AUX
C A=SPROD/AUX
C
C FIND MAXIMUM CORRECTION TO X, NEW R AND X
C DXMAX=0.
C XMAX=0.
C DO 2 I=1, IS
C AUX=A*Y(I)
C X(I)=X(I)+AUX
C AUX=ABS(AUX)
C IF(AUX.GT.DXMAX)DXMAX=AUX

```

```

AUX=ABS(X(I))
IF(AUX.GT.XMAX)XMAX=AUX
R(I)=R(I)-A*Q(I)
2 CONTINUE
C
C MAKE NEW S
CALL ASOLVE(I2,IS,D,D1,D2,D3,D4,R,S)
AUX=0.
DO 3 I=1,IS
3 AUX=AUX+R(I)*S(I)
C
C MAKE B
B=AUX/SPROD
DO 4 I=1,IS
4 Y(I)=S(I)+B*Y(I)
SPROD=AUX
C
RETURN
END
C
SUBROUTINE AMULTI(B,P,P1,P2,P3,P4,D,I2,IS,IS1)
C
C PERFORMS MULTIPLICATION OF VECTOR D
C BY THE F.E.M. MATRIX WITH COEFFICIENTS STORED IN P,P1 ... P4
C ***** I.E. B=MATRIX*D
C
REAL*12 B(IS),D(IS1),P(IS),P1(IS),P2(IS),P3(IS),P4(IS),SUM
C
B(1)=P(1)*D(1)+P1(1)*D(2)+P3(1)*D(I2+1)+P4(1)*D(I2+2)
DO 5 I=2,IS
SUM=P1(I-1)*D(I-1)
IL=I-I2-1
IK=I+I2
IF(IL)3,2,1
1 SUM=SUM+P4(IL)*D(IL)
2 SUM=SUM+P2(IL+2)*D(IL+2)+P3(IL+1)*D(IL+1)
IF(IK.GT.IS)GOTO 4
3 SUM=SUM+P2(I)*D(IK-1)+P3(I)*D(IK)+P4(I)*D(IK+1)
4 B(I)=P(I)*D(I)+SUM+P1(I)*D(I+1)
5 CONTINUE
C
RETURN
END
C
SUBROUTINE ASOLVE(I2,IS,D,D1,D2,D3,D4,P,V)
C
C APPROXIMATE SOLUTION FOR ICCG
C V=(L*LTRANS)**-1*P
REAL*12 D(IS),D1(IS),D2(IS),D3(IS),D4(IS),P(IS),V(IS),SUM
C
FORWARD SUBSTITUTION *****
C LINES 1 TO I2+1
V(1)=P(1)*D(1)
DO 1 I=2,I2

```

```

1 V(I)=(P(I)-D1(I-1)*V(I-1))*D(I)
  IK=I2+1
  V(IK)=(P(IK)-D1(I2)*V(I2)-D3(1)*V(1)-D2(2)*V(2))*D(IK)
C
  J=I2+2
  DO 2 I=J, IS
    IK=I-I2
    SUM=D2(IK+1)*V(IK+1)+D4(IK-1)*V(IK-1)+D3(IK)*V(IK)
2 V(I)=(P(I)-D1(I-1)*V(I-1)-SUM)*D(I)
C
C   BACKWARD SUBSTITUTION *****
C                                     LINES IS TO IS-I2-1
  V(IS)=V(IS)*D(IS)
  DO 3 N=2, I2
    I=IS+1-N
3 V(I)=(V(I)-D1(I)*V(I+1))*D(I)
  I=IS-I2
  V(I)=(V(I)-D1(I)*V(I+1)-D3(I)*V(IS)-D2(I)*V(IS-1))*D(I)
  J=IS-I2-1
  DO 4 N=1, J
    I=J+1-N
    IK=I+I2
    SUM=D2(I)*V(IK-1)+D3(I)*V(IK)+D4(I)*V(IK+1)
4 V(I)=(V(I)-D1(I)*V(I+1)-SUM)*D(I)
C
  RETURN
  END

```